NUREG/CR-4829
UCID-20733
Vol. 2

Shipping Container Response to Severe Highway and Railway Accident Conditions

Appendices

Prepared by L. E. Fischer, C. K. Chou, M. A. Gerhard, C. Y. Kimura,
R. W. Martin, R. W. Mensing, M. E. Mount, M. C. Witte

Lawrence Livermore National Laboratory

**Prepared for
U.S. Nuclear Regulatory
Commission**

Reprinted October 1988

NUREG/CR-4829
UCID-20733
Vol. 2
RT

Shipping Container Response to Severe Highway and Railway Accident Conditions

Appendices

Manuscript Completed: April 1986
Date Published: February 1987

Prepared by
L. E. Fischer, C. K. Chou, M. A. Gerhard, C. Y. Kimura,
R. W. Martin, R. W. Mensing, M. E. Mount, M. C. Witte

Lawrence Livermore National Laboratory
7000 East Avenue
Livermore, CA 94550

Prepared for
Division of Reactor System Safety
Office of Nuclear Regulatory Research
U.S. Nuclear Regulatory Commission
Washington, DC 20555
NRC FIN A0397

ABSTRACT

This report describes a study performed by the Lawrence Livermore National Laboratory to evaluate the level of safety provided under severe accident conditions during the shipment of spent fuel from nuclear power reactors. The evaluation is performed using data from real accident histories and using representative truck and rail cask models that likely meet 10 CFR 71 regulations. The responses of the representative casks are calculated for structural and thermal loads generated by severe highway and railway accident conditions. The cask responses are compared with those responses calculated for the 10 CFR 71 hypothetical accident conditions. By comparing the responses it is determined that most highway and railway accident conditions fall within the 10 CFR 71 hypothetical accident conditions. For those accidents that have higher responses, the probabilities and potential radiation exposures of the accidents are compared with those identified by the assessments made in the "Final Environmental Statement on the Transportation of Radioactive Material by Air and other Modes," NUREG-0170. Based on this comparison, it is concluded that the radiological risks from spent fuel under severe highway and railway accident conditions as derived in this study are less than risks previously estimated in the NUREG-0170 document.

TABLE OF CONTENTS

	Page
1. INTRODUCTION	1-1
1.1 Background	1-1
1.2 Regulations and Past Assessments	1-4
1.2.1 Title 10, Code of Federal Regulations, Part 71	1-4
1.2.2 Transportation of Radioactive Material - Environmental Statement (NUREG-0170)	1-7
1.3 Objective and Approach	1-9
2. ACCIDENT RATES, ACCIDENT SCENARIOS, AND LOADING PARAMETER DISTRIBUTIONS	2-1
2.1 Introduction	2-1
2.2 Highway Accident Rates	2-3
2.3 Railway Accident Rates	2-3
2.4 Accident Loading Data Requirements	2-4
2.5 Highway Accident Loading Parameters	2-10
2.5.1 Mechanical Loading Parameters	2-10
2.5.1.1 Accident Scenarios and Object Hardness	2-10
2.5.1.1.1 Collision Accident Hardness Data	2-11
2.5.1.1.2 Non-Collision Accident Hardness Data	2-14
2.5.1.2 Impact Velocity	2-17
2.5.1.2.1 Cask Velocity	2-17
2.5.1.2.2 Impact Angle	2-21
2.5.1.3 Cask Orientation	2-23
2.5.2 Thermal Loading Parameters	2-24
2.5.2.1 Accident Scenarios and Fire Frequency	2-24
2.5.2.2 Fire Duration	2-26
2.5.2.3 Flame Temperature	2-26
2.5.2.4 Fire Location	2-27
2.6 Railway Accident Loading Parameters	2-27
2.6.1 Mechanical Loading Parameters	2-27

TABLE OF CONTENTS (continued)

Page

2.6.1.1 Accident Scenarios and Object Hardness 2-28
2.6.1.2 Impact Velocity 2-30
2.6.1.2.1 Cask Velocity 2-31
2.6.1.2.2 Impact Angle 2-34
2.6.1.3 Cask Orientation 2-34
2.6.2 Thermal Loading Parameters 2-34
2.6.2.1 Accident Scenarios and Fire Frequency 2-35
2.6.2.2 Fire Duration 2-35
2.6.2.3 Flame Temperature 2-35
2.6.2.4 Fire Location 2-37

3. SELECTION OF REPRESENTATIVE SPENT FUEL CASKS FOR EVALUATION 3-1
3.1 Introduction 3-1
3.2 Cask Functions and Design Features 3-2
3.3 Cask Design Features Important to Safety 3-5
3.3.1 Containment 3-5
3.3.2 Radiation Shielding 3-8
3.3.3 Subcriticality Assurance 3-8
3.4 Selection of Cask Shielding Material 3-11
3.5 Definition of Representative Cask Designs 3-14
3.5.1 Shielding Features 3-14
3.5.2 Containment Features 3-15
3.5.3 Subcriticality Assurance Features 3-17
3.5.4 Damage-Mitigating Features 3-17
3.5.5 Representative Cask Design Description 3-18
3.6 Margins of Safety 3-19

4. REPRESENTATIVE CASK RESPONSE STATES, LEVELS, AND REGIONS 4-1
4.1 Introduction 4-1
4.2 Response States and Levels for Mechanical Loads 4-2

TABLE OF CONTENTS (continued)

Page

4.2.1 Structural Response Level, S_1 4-4
4.2.2 Structural Response Level, S_2 4-4
4.2.3 Structural Response Level, S_3 4-6
4.2.4 Application of Response States and Levels 4-6
4.3 Response States and Levels for Thermal Loads 4-7
4.3.1 Thermal Response Level, T_1 4-9
4.3.2 Thermal Response Level, T_2 4-11
4.3.3 Thermal Response Level, T_3 4-11
4.3.4 Thermal Response Level, T_4 4-12
4.3.5 Application of Response States and Levels 4-12
4.4 Cask Response Regions 4-14

5. PROBABILITY ANALYSIS 5-1
5.1 Introduction 5-1
5.2 Probabilistic Inputs 5-4
5.2.1 Mechanical Loading Parameter Distributions 5-5
5.2.1.1 Object Hardness Distributions 5-5
5.2.1.2 Impact Velocity Distributions 5-5
5.2.1.2.1 Cask Velocity 5-5
5.2.1.2.2 Impact Angle 5-9
5.2.1.3 Cask Orientation Distributions 5-11
5.2.2 Thermal Loading Parameter Distributions 5-13
5.2.2.1 Fire Duration Distributions 5-13
5.2.2.2 Flame Temperature Distributions 5-15
5.2.2.3 Fire Location Distributions 5-18
5.3 Probability Calculation 5-20

6. FIRST-STAGE SCREENING ANALYSIS 6-1
6.1 Introduction 6-1
6.2 Structural Response Analysis 6-7

TABLE OF CONTENTS (continued)

Page

6.2.1 Cask Response Analysis for Highway Accidents 6-15
6.2.1.1 Response to Minor Accidents..... 6-15
6.2.1.2 Response to Other Accidents 6-16
6.2.1.2.1 Response for Impacts with Unyielding Surfaces 6-18
6.2.1.2.2 Response for Real Objects 6-18
6.2.2 Cask Response Analysis for Railway Accidents 6-21
6.2.2.1 Response to Minor Accidents..... 6-23
6.2.2.2 Response to Other Accidents 6-25
6.2.2.2.1 Response for Impacts with Unyielding Surfaces 6-25
6.2.2.2.2 Response for Real Objects 6-27
6.2.3 Discussion of Structural Analysis Results..... 6-31
6.3 Thermal Response Analysis 6-32
6.3.1 Cask Response Analysis for Highway Fire Accidents..... 6-36
6.3.2 Cask Response Analysis for Railway Fire Accidents..... 6-39
6.3.3 Discussion of Thermal Analysis Results..... 6-43
6.4 Accident Screening Analysis..... 6-45

7. SECOND-STAGE SCREENING ANALYSIS 7-1
7.1 Introduction 7-1
7.2 Structural Response Analysis 7-3
7.2.1 Cask Response Analysis for Highway Accidents 7-4
7.2.1.1 Endwise Impacts 7-5
7.2.1.2 Sidewise Impacts 7-8
7.2.1.3 Impact Response Summary 7-8
7.2.2 Cask Response Analysis for Railway Accidents 7-12
7.2.2.1 Endwise Impacts 7-12
7.2.2.2 Sidewise Impacts 7-14
7.2.2.3 Impact Response Summary 7-14

TABLE OF CONTENTS (continued)

Page

7.2.3 Discussion of Structural Analysis Results 7-14
7.3 Thermal Response Analysis 7-18
7.3.1 Cask Response Analysis for Highway Fire Accidents 7-19
7.3.2 Cask Response Analysis for Railway Fire Accidents 7-21
7.3.3 Discussion of Thermal Analysis Results 7-22
7.4 Accident Screening Analysis 7-24

8. POTENTIAL RADIOLOGICAL SIGNIFICANCE OF TRANSPORTATION ACCIDENTS 8-1
8.1 Introduction 8-1
8.2 Description of Spent Fuel 8-1
8.3 Measures of Radiological Significance 8-3
8.4 Estimates of Radiological Hazards 8-7
8.4.1 Potential Radioactive Material Releases to the Environment ... 8-7
8.4.2 Potential Radiation Increases from Shielding Reduction..... 8-12
8.5 Radiological Effect Estimates for Response Regions 8-18

9. RESULTS AND CONCLUSIONS 9-1
9.1 Introduction 9-1
9.2 Results 9-2
9.2.1 First-Stage Screening 9-2
9.2.2 Second-Stage Screening 9-4
9.2.3 Comparison with Previous Risk Assessments: NUREG-0170 9-6
9.2.4 Estimated Responses for Sample Severe Accidents 9-15
9.2.4.1 Caldecott Tunnel Fire 9-15
9.2.4.2 I-80 Bridge Accident 9-16
9.2.4.3 Livingston Train Fire 9-17
9.2.4.4 Derailment into the Alabama River 9-18
9.3 Uncertainties 9-19
9.3.1 Uncertainty in Cask Response 9-20
9.3.1.1 Selection of Representative Cask Designs 9-20
9.3.1.2 Definition of Accident Loads 9-21

TABLE OF CONTENTS (continued)

Page

9.3.1.3 Computer Code Applications and Modeling 9-21
9.3.2 Uncertainty in Estimating an Accident's Potential Radiological Hazard 9-23
9.3.2.1 Radioactive Releases from Fuel Rods 9-23
9.3.2.2 Radioactive Releases from Casks 9-24
9.3.2.3 Reduction in Radiation Shielding 9-24
9.3.2.4 Reduction in Subcriticality Control 9-24
9.3.3 Uncertainty in Probability Models 9-25
9.3.3.1 Accident Statistics 9-25
9.3.3.2 Surveys of Structures and Features 9-26
9.3.3.3 Past Analysis and Models 9-26
9.3.3.4 Engineering Judgment 9-27
9.3.4 Overall Statement of Uncertainty 9-27
9.4 Conclusions 9-27

REFERENCES R-1

APPENDIX A: Severe Accident Data A-1
APPENDIX B: Truck Accident Data B-1
APPENDIX C: Railroad Accident Data C-1
APPENDIX D: Highway Survey Data and Bridge Column Properties D-1
APPENDIX E: Structural Analysis E-1
APPENDIX F: Thermal Analysis F-1
APPENDIX G: Probability Estimation Techniques G-1
APPENDIX H: Benchmarking for Computer Codes used in Impact Analysis H-1

LIST OF FIGURES

1-1 Schematic of a typical spent fuel cask 1-6
1-2 Two-stage screening process used in evaluating the regulations 1-11
1-3 Schematic representation of the report 1-13

2-1 Three impact loading parameters considered in the response analysis for impacts on surfaces 2-7
2-2 Three impact loading parameters considered in the response analysis for impacts with objects such as train sills 2-8
2-3 Truck collision accident scenarios and their percent probabilities 2-12
2-4 Truck non-collision accident scenarios and their percent probabilities 2-13
2-5 Train accident scenarios 2-29

3-1 Spent fuel cask features important to safety 3-4
3-2 Typical closure designs for spent fuel casks 3-7
3-3 Typical cask penetration subsystems 3-9
3-4 Preliminary truck cask designs with three types of gamma shielding, used for quasi-static loading response studies only 3-12
3-5 Preliminary rail cask designs with three types of gamma shielding, used for quasi-static loading response studies only 3-13
3-6 Representative truck cask design used for dynamic structural and thermal response studies 3-20
3-7 Representative rail cask design used for dynamic structural and thermal response studies 3-21
3-8 Force-deflection characteristics of the limiter design as a function of cask orientation at impact 3-22

LIST OF FIGURES (continued)

Page

4-1 Schematic representation of cask response state for mechanical load 4-5
4-2 Schematic representation of cask structural response for various surface hardness and impact velocities 4-8
4-3 Schematic representation of cask response state for thermal loads 4-10
4-4 Schematic representation of cask response for various fire locations and fire durations 4-13
4-5 Matrix of cask response regions for combined mechanical and thermal loads 4-15

5-1 Effect of cask orientation on the strain-impact velocity relationship for a truck cask impacting an unyielding object 5-2
5-2 Effect of flame temperature and fire location on lead-temperature-time relationship for a truck cask 5-3
5-3 Distribution of vehicle velocities adjusted for braking 5-7
5-4 Flow Chart of TASP computer code 5-32

6-1 Identification of first-stage screening 6-2
6-2 Methods of analysis used in cask response determinations 6-5
6-3 Three impact loading parameters considered in the response analysis for impacts on surfaces 6-8
6-4 Three impact loading parameters considered in the response analysis for impacts with objects such as train sills 6-10
6-5 Equivalent damage technique 6-13
6-6 Strain versus impact velocity and cask orientation for the representative truck cask impacting an unyielding surface 6-19
6-7 Impact force for a rigid truck cask dropped endwise onto real surfaces 6-20

LIST OF FIGURES (continued)

		Page
6-8	Rail car coupler override of spent fuel cask car	6-24
6-9	Strain versus impact velocity and cask orientation for the representative rail cask impacting an unyielding surface	6-28
6-10	Impact force versus impact velocity for a rigid rail cask dropped endwise onto real surfaces	6-29
6-11	Comparison of an engulfing hypothetical fire and a real fire	6-34
6-12	Representative truck cask temperature response to a hypothetical 1475°F (equivalent to a real 1700°F) fire versus fire duration	6-37
6-13	Heat flux versus fire duration for the representative truck cask exposed to the regulatory 1475° fire	6-38
6-14	Average heat flux factor versus temperature for the representative truck cask	6-40
6-15	Heat load factor for real fire versus location of representative truck cask	6-41
6-16	Representative rail cask temperature response to a hypothetical 1475°F (equivalent to a real 1700°F) fire versus fire duration	6-42
6-17	Heat load factor for real fire versus location of representative rail cask	6-44
7-1	Second-stage screening analysis relationship with response regions	7-2
7-2	Example showing strain response of the representative truck cask for 45 mph endwise impact on an unyielding surface (2-D model with impact limiters) without any truck cab crushing included	7-6
7-3	Response of the representative truck cask to endwise impacts on an unyielding surface (2-D model with impact limiters and cab crush)	7-7

LIST OF FIGURES (continued)

Page

7-4 Example showing strain response of the representative truck cask for 60 mph sidewise impact on soil (2-D model without limiters) with strain exceeding the 2% (S_2) limit 7-9

7-5 Response of the representative truck cask to sidewise impacts on various surfaces 7-10

7-6 Response of the representative rail cask to endwise impacts on an unyielding surface (2-D model with impact limiters and railcar crush) 7-13

7-7 Response of the representative rail cask to sidewise impacts on various surfaces 7-15

7-8 Representative truck cask temperature response to a hypothetical 1475°F (equivalent to a real 1700°F) fire versus fire duration 7-20

7-9 Representative rail cask temperature response to a hypothetical 1475°F (equivalent to a real 1700°F) fire versus fire duration 7-23

7-10 Fraction of truck accidents that could result in responses within each response region, assuming an accident occurs 7-25

7-11 Fraction of rail accidents that could result in responses within each response region, assuming an accident occurs 7-26

8-1 PWR fuel bundle 8-4

8-2 Three mechanisms required to establish a radioactive material release path 8-8

8-3 Percentage of fuel rods breached as a function of force for endwise impacts 8-9

8-4 Percentage of fuel rods breached per fuel assembly in each cask response region 8-11

8-5 Lead voiding due to lead slump resulting from endwise impact of cask 8-15

LIST OF FIGURES (continued)

Page

8-6 Lead voiding due to high thermal loads and lead melting 8-17
8-7 Radiological hazards estimated for response regions for a representative truck cask 8-19
8-8 Radiological hazards estimated for response regions for a representative rail cask 8-20

9-1 Two-stage screening process in the 20 response regions 9-5
9-2 Probability-hazard estimates in curies for the 20 truck cask response regions 9-8
9-3 Probability-hazard estimates in curies for the 20 rail cask response regions 9-9

LIST OF TABLES

		Page
1.1	Correlation of NUREG-0170 Accident Fractional Occurrence and Radiological Hazards as a Function of Accident Severity	1-8
2.1	Accident Loads and Loading Parameters	2-5
2.2	Fractional Occurrence of Surface Types below Bridges on Interstate 80 from Davis, California to Nevada Border	2-15
2.3	Distribution of Velocities for Trucks/Semitrailers Involved in Fatal and Injury Accidents in California, 1958-1967	2-19
2.4	Distribution of Bridge Heights along Interstate 5 through Orange and Los Angeles Counties, California	2-20
2.5	Train Velocity Distribution for Rail-Highway Grade-Crossing Accident/Incidents Involving Motor Vehicles, 1975-1982	2-22
2.6	Frequency of Fire for Truck Accident Types	2-25
2.7	Railroad Accident Velocity Distribution, Collisions, Main Line, 1979-1982	2-32
2.8	Railroad Accident Velocity Distribution, Derailments, Main Line, 1979-1982	2-33
2.9	Train-Fire Accident Types	2-36
5.1	Cumulative Cask Velocity Distributions for Highway Analysis	5-8
5.2	Cumulative Cask Velocity Distributions for Railway Analysis	5-10
5.3	Cumulative Impact Angle Distributions	5-12
5.4	Cumulative Cask Orientation Angle Distributions	5-14
5.5	Cumulative Fire Duration Distributions for Truck Cask Analysis	5-16
5.6	Cumulative Fire Duration Distributions for Rail Cask Analysis	5-17
5.7	Cumulative Flame Temperature Distribution	5-19
5.8	Cumulative Fire Location Distributions	5-21
5.9	Probability Inputs for Highway Analysis	5-25
5.10	Heat Flux Factors for Flame Temperatures (Engulfing Fire)	5-28
5.11	Probability Inputs for Railway Analysis	5-31

LIST OF TABLES (continued)

Page

6.1 Material Parameters Selected for Real Surfaces 6-14
6.2 Evaluation of Quasi-Static Force for Minor Highway Accidents 6-17
6.3 Impact Velocities Required to Reach the 0.2% Strain (S_1) Level for Objects Impacted in Highway Accidents 6-22
6.4 Evaluation Summary of Minor Railway Accidents 6-26
6.5 Impact Velocities Required to Reach the 0.2% Strain (S_1) Level for Objects Impacted in Railway Accidents 6-30

7.1 Impact Velocities Required to Attain 2% (S_2) and 30% (S_3) Strain Levels for Objects Impacted in Highway Accidents 7-11
7.2 Impact Velocities Required to Attain 2% (S_2) and 30% (S_3) Strain Levels for Objects Impacted in Railway Accidents 7-16

8.1 PWR Fuel Assembly Decay Heat and Radioactivity 8-2
8.2 10 CFR 71 Release Limits for Radioisotopes..... 8-6
8.3 Material Release Fractions from Breached Fuel Rods Occurring over 1 Week Following Rod Burst 8-13
8.4 Gamma Dose Summary for Lead Slump in a Rail Cask for Impacts on Closure Region 8-16

9.1 Comparative Measure of Risk/Accident for Spent Fuel Shipment by Truck 9-12
9.2 Comparison of Release Risk/Accident for Spent Fuel Shipment by Rail 9-13

PREFACE

This report describes a study conducted to estimate the responses of spent fuel casks to severe highway and railway accident conditions and to assess the level of safety provided to the public during the shipment of spent fuel. The study was performed by the Lawrence Livermore National Laboratory for the U.S. Nuclear Regulatory Commission (NRC), Office of Nuclear Regulatory Research.

This report is divided into two volumes: Volume I, the main report, describes the study, the technical approach, the study results, and conclusions; and Volume II, the Appendixes, provide supporting accident data and engineering calculations. This report has been reviewed by the Denver Research Institute at the University of Denver under a separate contract to the NRC as the peer review. A companion summary report entitled "Transporting Spent Fuel-Protection Provided Against Severe Highway and Railway Accidents" (NUREG/BR-0111) has been prepared by the NRC for wide distribution to federal agencies, local governments, and interested citizens.

Commercial spent fuel shipments are regulated by both the Department of Transportation (DOT) and the NRC. The NRC evaluates and certifies the design, manufacture, operation, and maintenance of spent fuel casks, whereas the DOT regulates the vehicles and drivers which transport the spent fuel.

Current NRC regulations require spent fuel casks to meet certain performance standards. The performance standards include normal and hypothetical accident conditions which a cask must be capable of withstanding without exceeding established acceptance criteria that

(1) limit the release of radioactive material from the cask,
(2) limit the radiation levels external to the cask, and
(3) assure that the spent fuel remains subcritical.

This study evaluates the possible mechanical and thermal loads generated by actual and potential truck and railroad transportation accidents. The magnitudes of the loads from accidents are compared with the loads implied from the hypothetical accident conditions. The frequency of the accidents that can produce defined levels of mechanical and thermal loads are developed from the accident data base. Using this information, it is determined that

for certain broad classes of accidents, spent fuel casks provide essentially complete protection against radiological hazards. For extremely severe accidents--those which could impose loads on the cask greater than those implied by the hypothetical accident conditions--the likelihood and magnitude of any radiological hazards are conservatively estimated. The radiological risk is then estimated and compared with risk estimates previously used by the NRC in judging the adequacy of its regulations.

The results of this study depend primarily on the quality of the cask response models, the radiation release models, and the probability models and distributions used in the analysis. Models for cask responses, radioactive releases, and distributions for the accident parameters are new developments based on current computer codes, limited test data on radioactive releases, and limited historical accident data. The results are derived using representative spent fuel casks which use design principles and materials that have been used in casks currently licensed by the NRC. The representative casks are assumed to have been designed, manufactured, operated, and maintained in accordance with national codes and standards (or equivalent) which have adequate margins of safety embedded in them. The results of this study are limited to spent fuel casks designed and fabricated under current technologies and operated under current regulations. New designs using alternative design principles and materials, or changes to regulations such as the imposition of a 75 mph national speed limit, could affect the results and conclusions of this study.

This study does not consider the effects which human factors can have on the cask design, manufacture, operation, and maintenance. If further study is conducted, human factors should be considered because they can contribute to the overall risk in each phase of transporting spent fuel.

L. E. Fischer

ACKNOWLEDGEMENTS

The authors wish to acknowledge the technical contributions made to this report by R. C. Chun, L. L. George, T. E. McKone, and M. W. Schwartz of Lawrence Livermore National Laboratory. The authors wish to thank G. E. Cummings of Lawrence Livermore National Laboratory for his report review and comments. The authors also wish to thank J. R. Cook, W. R. Lahs, and W. H. Lake of the U.S. Nuclear Regulatory Commission for their support and comments during the research and preparation of this report. Many thanks to N. J. Barnes and E. A. Sturmer for report preparation and D. Bowden for report editing.

In addition, the authors would particularly like to thank the following organizations for providing information and counsel which were used in preparing this report:

Anatech International Corporation
Association of American Railroads
Bureau of Motor Carrier Safety
California Department of Transportation
Central Electricity Generating Board, England
Denver Research Institute
Department of California Highway Patrol
Electric Power Research Institute
Engineering Computer Corporation
Federal Highway Administration
Federal Railroad Administration
Health and Safety Executive, England
Los Alamos National Laboratory
National Fire Protection Association
Oak Ridge National Laboratory
Ridihalgh, Eggers and Associates, Inc.
Sandia National Laboratories
Southern Pacific Transportation Company

APPENDIX A

List of Tables

		Page
A.1	Caldecott Tunnel Fire Data Summary Sheet	A-4
A.2	I-80 Bridge Accident Data Summary Sheet	A-7
A.3	Livingston Train Fire Data Summary Sheet	A-10
A.4	Alabama River Derailment Data Summary Sheet	A-14
A.5	Rail-Highway Grade-Crossing Accidents	A-17
A.6	Truck Accidents	A-22
A.7	Train Accidents	A-35

APPENDIX A
Severe Accident Data

A.1 Introduction

Under the first phase of the Nuclear Regulatory Commission Transportation Model Study Program, Ridihalgh, Eggers and Associates (REA) reviewed hundreds of severe highway and railway accident reports for the period from 1961 to 1981.[A.1] Information on selected accidents was recorded onto a set of specially formatted data summary sheets. In this study, the severe accident data base was expanded to cover additional accidents in the 1980 - 1983 period. The accident data compiled by REA was reviewed to sort out the information related to structural and thermal loading conditions. This appendix describes the process used to select severe accidents and presents sample data summary sheets for four severe accidents. Also summarized are all of the selected severe accidents with some of their more important loading parameters.

A.2 Data Summary Sheets

A literature search reported over 100,000 truck and train accidents in the period from 1961 to 1983. Approximately 335 accidents were selected for the period 1961 to 1981,and 60 accidents were selected for the period 1981 to 1983. These accidents were judged to contain accident information that could be useful in assessing high physical loading conditions. All accidents had to involve either a truck or a train to be included in the selection process.

In general, the information contained in the accident reports was more related to public safety issues and the loss of life and property rather than to the physical loading conditions that occurred during an accident. For example, a severe accident typically reported could involve a truck and several cars resulting in a high loss of property and life, but could have occurred at moderate velocities (less than 45 mph) and loading conditions that could have been relatively high to the cars (40,000-150,000 pounds), but relatively low to the truck. On the other hand, a runaway truck could hit a bridge abutment at high speed (greater than 80 mph) which could result in high

loads (greater than 400,000 pounds), but never be included in a detailed national report because the loss of life and property would not be high, and the event would be so rare that it was not a public safety issue. All the compiled accident data were reviewed and the more important loading parameters that an accident can generate on a shipping container involved in such an accident are identified. Tables A.1 to A.4 present the data summary sheets for four typical severe accidents with high physical loading conditions.

The first data summary sheet, Table A.1, provides information on a truck-fire accident in the Caldecott Tunnel near Oakland, California, in April 1982. The accident involved a gasoline truck-trailer, an automobile, and a bus. A fire resulting from approximately 8,800 gallons of gasoline had a peak flame temperature of 1900°F. Although the fire lasted 2 hours and 42 minutes according to the records, the peak flame temperature was estimated to have occurred for at least 20 minutes but not for the entire fire duration.

Table A.2 summarizes a truck-bridge accident, where in March 1981, a truck-tractor-trailer was struck by a pickup while on an overpass bridge on Interstate I-80 near San Francisco, California. The truck-tractor-trailer veered into the bridge railing, broke through the railing and fell 64 feet to the soil surface below.

Table A.3 provides information on a train fire accident, where on September 28, 1982, 43 railroad cars derailed near Livingston, Louisiana. Following the derailment, a fire started to burn various materials which included plastic pellets, vinyl chloride, and petroleum products. The fire which covered a wide area was allowed to burn for several days because of the toxic chemicals and explosions involved. A railroad car carrying motor fuel anti-knock compound (tetra-ethyl lead) exploded about 19 hours after the derailment. A second thermally induced explosion occurred on October 1, 82 hours after the derailment, involving a car carring vinyl chloride. The fire cooled down sufficiently on the fifth day to permit fire-fighting operations. Six cars carring chloride materials were purposely detonated on October 11 to dispose of the remaining unvented materials within them.

Finally, Table A.4 summarizes a train-bridge accident, where on January 19, 1979, a train derailed off a bridge into the Alabama River near Hunter, Alabama. One of the rail cars was carrying a pipe which struck the bridge and caused the derailment. Five rail cars fell into the river 75 feet below.

A.3 Severe Accident Summary Tables

Using the severe accident data summary sheets as input, tables were prepared summarizing each of the selected severe accidents to highlight the information related to loading magnitudes. Three different tables were prepared: Truck-Train Grade Crossing Accidents, Table A.5; Truck Accidents, Table A.6; and Rail Accidents, Table A.7.

Each accident is identified by its location (name of state and city) and is listed by its location in alphabetical order. For each accident the following information is provided: report source, date of accident, type of accident, number of vehicles involved, the velocity prior to the accident, the height of any fall involved, any object struck, and the duration of any fire involved. In some cases, the information was not stated on the data summary sheets and an NS is entered in the corresponding column.

A.4 Reference

A.1 P. Eggers, Severe Rail and Truck Accidents: Toward a Definition of Bounding Environment for Transportation Packages, U.S. Nuclear Regulatory Commission, Washington, DC, NUREG/CR-3499, October 1983.

Table A.1
Caldecott Tunnel Fire Data Summary Sheet

1.0 ACCIDENT IDENTIFICATION

1.01 Date of Accident: April 7, 1982
1.02 Time of Accident: 0012
1.03 Rail, Highway or Both: Highway
1.04 Location: Caldecott Tunnel near Oakland, California
1.05 Railroad and/or Trucking Co. Involved: Armour Oil Company
1.06 Accident Report No.: NTSB/HAR-83/01, PB83-916201
1.07 Source: NTSB
1.08 Title: HIGHWAY ACCIDENT REPORT - Multiple Vehicle Collisions and Fire Caldecott Tunnel near Oakland, California April 7, 1982
1.09 Location of Document: REA
1.10 Location of Additional Information: NTSB
1.11 No. of Drawings/Photos: 16

2.0 ACCIDENT EVENT DATA

2.01 Initiating Event (derail, skid, overturn, explosion, collision, head to tail, head to head, tail to tail, head to side, fall): Head to tail collision
2.02 Cause: Intoxicated driver operating car, inattention of truck driver, excessive speed of bus
2.03 Number of Vehicles Involved: 1 truck and trailer, 1 car, 1 bus
2.04 Speed of Impact: Car stopped, truck 45 mph, bus 55 mph
2.05 Distance of Fall: Not applicable (N/A)
2.06 Weather Conditions: Clear
2.07 Ambient Temperature: $50^{o}F$
2.08 Distance Traveled from Impact Point: Truck about 536 ft., bus about 2,175 ft
2.09 Description of Vehicles Involved: Cargo tank truck with full trailer and 5,400 gallon aluminum cargo tank, Grumman Flexible 53-passenger bus, Honda Accord
2.10 Adjacent Structures or Natural Formations: Caldecott Tunnel
2.11 Description of Cargo Involved in Accident: 8,800 gallons of gasoline, bus had no passengers
2.12 Elevation of Vehicles at Time of Accident: Highway through tunnel
2.13 Description of Surface Impacted: Truck to car, bus to car, bus to truck trailer, bus to highway support pier, car to tunnel wall

3.0 SEQUENCE OF EVENTS

3.01 Description of First Event: Honda car struck curb and stopped at left edge of roadway one-third of way through tunnel
3.02 Description of Second Event: Left front tire of tank trailer struck right rear corner of Honda

3.03 Description of Third Event: Bus changed lanes and struck Honda and right front of the bus struck left side of the tank trailer

3.04 Description of Fourth Event: Trailer rolled over on right side and tank truck stops upright, gasoline spills

3.05 Description of Additional Events: Bus climbed left curb, traveled out of tunnel and impacted highway support pier. Gasoline spilled from trailer ignites.

3.06 Summary of Sequence of Events: N/A

4.0 POST ACCIDENT EVENT DATA

4.1 POST ACCIDENT EVENT DATA

4.1.01 Truck or Rail Car No. 1: Truck completely destroyed by fire, only remaining parts of cargo tank shell material included a 70 in by 96 in bottom sheet section from the rear compartment of the tank truck and a 40 in by 21 ft section from the right side of the trailer tank. Left safety cable broken, main leaf springs deformed and separated from spring shackle.

4.1.02 Truck or Rail Car No. 2: Bus center front components displaced 17 ft rearward, front axle beam bent 6 inches rearward with axle and suspension attachment devices displaced and destroyed. Forward entrance door separated, forward front door post and hinge bar displaced 17 feet rearward.

4.1.03 Truck or Rail Car No. 3: Honda destroyed by fire.

4.1.04 Truck or Rail Car No. 4: N/A

4.1.05 Additional Trucks or Rail Cars Damaged: Tractor and utility semitrailer (beer truck), Ford pickup, Toyota pickup and Pontiac Phoenix sedan in tunnel incurred extensive fire damage but were not involved in collision.

4.1.06 Evidence of Crushing: N/A

4.1.07 Evidence of Impact: Left front tire of tank trailer struck right rear corner of Honda, Honda impacted tunnel wall, left front bumper of bus struck rear bumper of Honda, right front of bus struck left side of tank trailer, bus impacted highway support pier

4.1.08 Evidence of Falling: N/A

4.1.09 Evidence of Puncture: N/A

4.1.10 Evidence of Bending/Deformation of Support Members: Front axle beam of bus bent 6 inches

4.1.11 Evidence of Tearing Structural Members: N/A

4.1.12 Evidence of Projectiles Distance Traveled, Size/Weight of Projectile: N/A

4.1.13 Other Evidence of Severe Structural Damage: Tank truck and trailer tank destroyed, Honda destroyed, bus heavily damaged

4.2 THERMAL/EXPLOSION DAMAGE DATA

4.2.01 Type of Fire(s) and Fuel(s) Involved and Amounts: 8,800 gallons of gasoline

4.2.02 Duration of Fire(s): 2 hours and 42 minutes
4.2.03 Evidence of Thermal Damage (e.g., melting, sagging or weakening): All low melting point and combustible material consumed by fire, only 2 sections of cargo tank shell material remained, examination of copper wires, aluminum casting, plastic parts, glass, glazed tile and concrete spalling provided a temperature determination in tunnel
4.2.04 Materials which Showed Evidence of Thermal Damage: Aluminum cargo tank
4.2.05 Evidence of Torch or Plume Fire: N/A
4.2.06 Evidence of Rocketing: N/A
4.2.07 Evidence of Explosions: Loud explosions were heard, lights went out, tiles fell from wall, final explosion shook building
4.2.08 No. of Vehicles Affected by Fires, Explosions: 1 cargo tank truck and tank trailer, 1 bus, 2 automobiles, 1 beer truck, 2 pickup trucks
4.2.09 Approximate Area Covered by Flames: 1,900 ft of tunnel
4.2.10 Evidence of Burial/Duration: N/A

4.3 LEAK OR SPILL DATA

4.3.01 Substance(s) Leaked or Spilled: Gasoline
4.3.02 Hazards/Damage Generated by Leakage/Spill: Fire
4.3.03 Amount Leaked or Spilled: 8,800 gallons
4.3.04 Area Contaminated by Spill: N/A

5.0 MISCELLANEOUS OTHER DATA

Fire produced temperature reaching 1900^{o}F and remained that high for at least 20 minutes. Photos of damaged vehicles included in report.

6.0 KEYWORD SUMMARY OF REPORT

Table A.2
I-80 Bridge Accident Data Summary Sheet

1.0 ACCIDENT IDENTIFICATION

1.01 Date of Accident: March 1981
1.03 Rail, Highway or Both: Highway
1.04 Location: I-80, San Francisco Bay
1.05 Railroad and/or Trucking Co. Involved: Thomas M. Bonnell Tractor/trailer
George A. Burris Pickup
1.07 Source: San Jose, California
1.08 Title: N/P Clipping
1.09 Location of Document: REA
1.10 Location of Additional Information: NTSB, BMCS, CHP
1.11 No. of Drawings/Photos: 1

2.0 ACCIDENT EVENT DATA

2.01 Initiating Event (derail, skid, overturn, explosion, collision, head to tail, head to head, tail to tail, head to side, fall): Collision and loss of control
2.02 Cause: Not applicable (N/A)
2.04 Speed of Impact: 55 mph
2.05 Distance of Fall: 64 feet
2.09 Description of Vehicles Involved: Commercial Tractor/trailer, pickup truck
2.10 Adjacent Structures of Natural Formations: East Bay overpass
2.11 Description of Cargo Involved in Accident: N/A
2.12 Elevation of Vehicles at Time of Accident: On bridge roadway
2.13 Description of Surface Impacted: Tractor/trailer to pickup, tractor/trailer to concrete barrier, tractor/trailer to gravel and earth

3.0 SEQUENCE OF EVENTS

3.01 Description of First Event: Pickup truck veered in front of the tractor/trailer
3.02 Description of Second Event: Tractor/trailer then struck the pickup and then itself. Tractor/trailer veered off the overpass, vaulted a concrete barrier and railing, and fell 64 feet.

4.0 POST ACCIDENT EVENT DATA

4.1 POST ACCIDENT EVENT DATA

4.1.01 Truck or Rail Car No. 1: Tractor/trailer was demolished
4.1.02 Truck or Rail Car No. 2: Pickup truck was damaged
4.1.05 Additional Trucks or Rail Cars Damaged: 73 feet of rail and 12 feet of concrete barrier was torn out of bridge

4.1.06 Evidence of Crushing: N/A
4.1.07 Evidence of Impact: Tractor/trailer collided first with pickup truck then with bridge barrier and finally with earth
4.1.08 Evidence of Falling: 64 feet from bridge to earth
4.1.09 Evidence of Puncture: N/A
4.1.10 Evidence of Bending/Deformation of Support Members: N/A
4.1.11 Evidence of Tearing Structural Members: N/A
4.1.12 Evidence of Projectiles Distance Traveled, Size/Weight of Projectile: None
4.1.13 Other Evidence of Severe Structural Damage: N/A

4.2 THERMAL/EXPLOSION DAMAGE DATA

4.2.01 Type of Fire(s) and Fuel(s) Involved and Amounts: None
4.2.05 Evidence of Torch or Plume Fire: None
4.2.06 Evidence of Rocketing: None
4.2.07 Evidence of Explosions: None

4.3 LEAK OR SPILL DATA

4.3.01 Substance(s) leaked or spilled: N/A

5.0 MISCELLANEOUS OTHER DATA

6.0 KEYWORD SUMMARY OF REPORT

6.01 Vehicle Class (R = rail, T = truck, C = rail & truck): T
6.02 Speed of Impact: 55 mph
6.03 Falling Distance: 64 feet
6.05 Impacting Object (I1 = locomotive, I2 = coupler, I3 = sill, I4 = axle, I5 = bar stock, I6 = plate stock, I7 = I-beam, I9 = rail, I10 = forging/casting, I11 = tractor, I12 = trailer, I13 = no evidence of impacted object, I14 = caboose, I15 = other): I11 I12
6.06 Object Impacted (01 = locomotive, 02 = nox car, 03 = tank car, 04 = coal car, 05 = tractor, 06 = trailer, 07 = cargo, 08 = cask, 09 = structural concrete, 010 = building, 011 = bridge, 012 = automobile, 013 = no evidence of impacted object, 014 = caboose, 015 = other): 011 015
6.08 Fire Duration: 0 minutes
6.09 Torch Duration: 0 minutes
6.10 Rocketing Distance: 0 feet
6.11 Weight of Rocketed Object: 0 pounds
6.12 Burial Event (B1 = evidence of burial larger than 24 hours, B2 = evidence of burial shorter than 24 hours, B3 = no evidence of burial): B3
6.13 Ambient Temperature: $0^{o}F$
6.16 Number of Fatalities: 0
6.17 Vehicle Type Involved in Accident (V1 = unit train, V2 = passenger train, V3 = mixed train cargo, V4 = tractor trailer, V5 = tandem trailer, V6 = unit truck, V7 = other): V4

6.18 Cargo Type Involved in Accident (Z1 = flammable, Z2 = explosive, Z3 = toxic, Z4 = ordnance, Z5 = radioactive, Z6 = other): Z6

Table A.3
Livingston Train Fire Data Summary Sheet

1.0 ACCIDENT INFORMATION

1.01 Date of Accident: September 28, 1982
1.02 Time of Accident: 0512
1.03 Rail, Highway or Both: Rail
1.04 Location: Livingston, Lousiana
1.05 Railroad and/or Trucking Co. Involved: Illinois Central Gulf Railroad
1.06 Accident Report No.: NTSB/RAR-83/05, PB83-916305
1.07 Source: NTSB
1.08 Title: RAILROAD ACCIDENT REPORT - Derailment of Illinois Central Gulf Railroad Freight Train Extra 9629 East (GS-2-28) and Release of Hazardous Materials at Livingston, Louisiana, September 28, 1982
1.09 Location of Document: REA
1.10 Location of Additional Information: NTSB
1.11 No. of Drawings/Photos: 11

2.0 ACCIDENT EVENT DATA

2.01 Initiating Event (derail, skid, overturn, explosion, collision, head to tail, head to head, tail to tail, head to side, fall): Derail
2.02 Cause: Disengagement of air hose coupling, excessive buff force, placement of empty cars in train profile
2.03 Number of Vehicles Involved: 1 train
2.04 Speed of Impact: 40 mph
2.05 Distance of Fall: Not applicable (N/A)
2.06 Weather Conditions: Clear
2.07 Ambient Temperature: 57°F
2.08 Distance Traveled from Impact Point: N/A
2.09 Description of Vehicles Involved: Extra 9629 East consisting of 3 locomotive units, 84 loaded cars, 16 empty cars and a caboose, 29 cars were tank cars loaded with hazardous materials and 5 tank cars with flammable petroleum products
2.10 Adjacent Structures or Natural Formations: Small community with buildings and pine groves surrounding tracks
2.11 Description of Cargo Involved in Accident: Plastic pellets, petroleum products, vinyl chloride, chemical products, styrene monomer, motor fuel anti-knock compound, toluene diisocyanate, phosphoric acid, hydrofluosilicic acid, sodium hydroxide, perchloroethylene, ethylene glycol
2.12 Elevation of Vehicles at Time of Accident: Railroad bed 47 foot above sea level
2.13 Description of Surface Impacted: Gondola car to gondola car, tank car to railroad bed

3.0 SEQUENCE OF EVENTS

3.01 Description of First Event: Train arrives Livingston and bottoms out at 2 crossings. Train went into emergency braking, automatic brake put into emergency position and throttle placed in ? position

3.02 Description of Second Event: 43 cars derail breaching 2 cars loaded with vinyl chloride

3.03 Description of Third Event: Leaking vinyl chloride gas ignites creating fireball exceeding 100 ft south and 150 ft north.

3.04 Description of Fourth Event: Explosion occurs and numerous fires break out

3.05 Description of Additional Events: Evacuation of area begun, hazardous materials unit notified and begin work. Next day tank car containing anti-knock compound explodes and rockets. September 30 fires intensify and vinyl chloride begins venting. October 1 vinyl chloride car explodes and rockets. October 4 styrene monomer re-ignites. October 5 styrene burns off and burning oil cars extinguished. October 10 and 11 vinyl chloride cars detonated. October 12 residents allowed to return. October 16 last derailed cars removed from accident site.

3.06 Summary of Sequence of Events: N/A

4.0 POST ACCIDENT EVENT DATA

4.1 POST ACCIDENT EVENT DATA

4.1.01 Truck or Rail Car No. 1: 19th and 20th cars detached from their trucks. 20th car had a vertical crease the full height

4.1.02 Truck or Rail Car No. 2: 3 tank cars loaded with petroleum products separated from their trucks and heavily damaged. 1 of these was breached.

4.1.03 Truck or Rail Car No. 3: Next 15 cars separated from their trucks and were damaged beyond economical repair

4.1.04 Truck or Rail Car No. 4: Next 18 cars were tank cars loaded with chemical products and were heavily damaged. 16 were punctured or breached.

4.1.05 Additional Trucks or Rail Cars Damaged: 5 cars had minor damage, 13 more cars separated from trucks, 15 tank cars had bottom outlet extensions sheared off

4.1.06 Evidence of Crushing: N/A

4.1.07 Evidence of Impact: Vertical crease full height of gondola car, tank cars overturned, several cars destroyed by impact

4.1.08 Evidence of Falling: N/A

4.1.09 Evidence of Puncture: 20 tank cars punctured or breached, shell punctures in car containing perchloroethylene

4.1.10 Evidence of Bending/Deformations of Support Members: 36 cars destroyed by crushing impacts during derailment or by post-accident fires

4.1.11 Evidence of Tearing Structural Members: 33 tank cars separated from trucks and many breached

4.1.12 Evidence of Projectiles Distance Traveled, Size/Weight of Projectile: Shell of tank car carrying anti-knock compound propelled about 80 ft north and its tank head about 25 ft south and most of its tub portion rocketed 425 ft north. Large section of steel outer insulating jacket found about 80 ft away. Other parts found 1,500 ft south

4.1.13 Other Evidence of Severe Structural Damage: 36 cars destroyed either by crushing impacts during the derailment or by post-accident fires, explosions, and demolition. Empty gondola car had vertical separation of bolster center plates.

4.2 THERMAL/EXPLOSION DAMAGE DATA

4.2.01 Type of Fire(s) and Fuel(s) Involved and Amounts: Vinyl chloride 163,043 gallons, styrene monomer 28,145 gallons, motor fuel anti-knock compound (tetra-Ethyl lead) 5,666 gallons, toluene diisocyanate 2,259 gallons. Fires also fed by plastic pellets

4.2.02 Duration of Fire(s): 8 days

4.2.03 Evidence of Thermal Damage (e.g., melting, sagging or weakening): 2 thermally induced explosions

4.2.04 Materials which Showed Evidence of Thermal Damage: N/A

4.2.05 Evidence of Torch or Plume Fire: Vinyl chloride gas vented and burned from domes

4.2.06 Evidence of Rocketing: Thermally-induced explosions of 2 tank cars that had not been punctured caused them to rocket violently.

4.2.07 Evidence of Explosions: First explosion blew in brick front of dwelling 250 ft north. 2 other thermally induced explosions.

4.2.08 No. of Vehicles Affected by Fires, Explosions: 13 train cars

4.2.09 Approximate Area Covered by Flames: 1,000 ft radius of derailment

4.2.10 Evidence of Burial/Duration: N/A

4.3 LEAK OR SPILL DATA

4.3.01 Substance(s) Leaked or Spilled: Phosphoric acid 148,552 gallons, hydrofluosilicic acid 19,780 gallons, sodium hydroxide 15,363 gallons, perchloroethylene 14,028 gallons, ethylene glycol 20,840 gallons, plastic pellets

4.3.02 Hazards/Damage Generated by Leakage/Spill: Acrid smoke and toxic gases as well as danger of fire and explosions

4.3.03 Amount Leaked or Spilled: More than 200,000 gallons of toxic chemical products

4.3.04 Area Contaminated by Spill: Several acres containing more than 60,000 cubic yards of soil to be expected

5.0 MISCELLANEOUS OTHER DATA

Photos of accident and information on chemical compounds included in report. 9999 in fields 6.8 and 6.9 indicates time frame longer

than 6 days. See 4.2.02. 3,000 people within 5-mile radius evacuated as long as 2 weeks

6.0 KEYWORD SUMMARY OF REPORT

6.01 Vehicle Class (R = rail, T = truck, C = rail & truck): R
6.02 Speed of Impact: 40 mph
6.03 Falling Distance: 0 feet
6.04 Crushing Events (C1 = locomotive, C2 = box car, C3 = coal car, C4 = flat car, C5 = tank car, C6 = tractor, C7 = trailer, C8 = unit truck, C9 = heavy cargo, C10 = tank truck, C11 = bridge, C12 = heavy support structure, C13 = no evidence of crushing, C14 = caboose, C15 = other): C5
6.05 Impacting Object (I1 = locomotive, I2 = coupler, I3 = sill, I4 = axle, I5 = bar stock, I6 = plate stock, I7 = I-beam, I9 = rail, I10 = forging/casting, I11 = tractor, I12 = trailer, I13 = no evidence of impacted object, I14 = caboose, I15 = other): I2 I15
6.06 Object Impacted (01 = locomotive, 02 = box car, 03 = tank car, 04 = coal car, 05 = tractor, 06 = trailer, 07 = cargo, 08 = cask, 09 = structural concrete, 010 = building, 011 = bridge, 012 = automobile, 013 = no evidence of impacted object, 014 = caboose, 015 = other): 03 02
6.07 Explosion Event (significant damage to: E1 = train or truck vehicles, E2 = surrounding structural members, E3 = cratering of ground, E4 = cargo, E5 = none): E1 E2 E4
6.08 Fire Duration (note: if 9,999 - see section 4.2.02): 9,999 minutes
6.09 Torch Duration (note: if 9,999 - see section 4.2.02): 9,999 minutes
6.10 Rocketing Distance: 425 feet
6.11 Weight of Rocketed Object: 10,000 pounds
6.12 Burial Event (B1 = evidence of burial larger than 24 hours, B2 = evidence of burial shorter than 24 hours, B3 = no evidence of burial): B3
6.13 Ambient Temperature: 57°F
6.14 Vehicle Damage (thousands of dollars): 1,500
6.15 Other Property Damage (thousands of dollars): 13,064
6.16 Number of Fatalities: 0
6.17 Vehicle Type Involved in Accident (V1 = unit train, V2 = passenger train, V3 = mixed train cargo, V4 = tractor trailer, V5 = tandem trailer, V6 = unit truck, V7 = other): V3
6.18 Cargo Type Involved in Accident (Z1 = flammable, Z2 = explosive, Z3 = toxic, Z4 = ordinance, Z5 = radioactive, Z6 = other): Z1 Z2 Z3 Z6
6.19 CAS Registry Numbers for Cargo Involved in Accident: None

Table A.4
Alabama River Derailment Data Summary Sheet

1.0 ACCIDENT IDENTIFICATION

1.01 Date of Accident: January 19, 1979
1.02 Time of Accident: 0740
1.03 Rail, Highway or Both: R
1.04 Location: Hunter, Alabama
1.05 Railroad and/or Trucking Co. Involved: Illinois Central Gulf Freight Train No. AM 118
1.06 Accident Report No.: ATL 78 F R018
1.07 Source: NTSB
1.08 Title: Accident File
1.09 Location of Document: REA
1.10 Location of Additional Information: NTSB
1.11 No. of Drawings/Photos: 2

2.0 ACCIDENT EVENT DATA

2.01 Initiating Event (derail, skid, overturn, explosion, collision, head to tail, head to head, tail to tail, head to side, fall): Collision with bridge
2.02 Cause: Improper lading
2.03 Number of Vehicles Involved: 72
2.04 Speed of Impact: 8 mph
2.05 Distance of Fall: 75 feet
2.06 Weather Conditions: Cloudy, dawn
2.07 Ambient Temperature: 45°F
2.09 Description of Vehicles Involved: 3 locomotive units, 1 caboose, 2 blkd flat cars, 1 tank car, 46 loads, 19 empties
2.10 Adjacent Structures or Natural Formations: RR bridge over the Alabama River
2.11 Description of Cargo Involved in Accident: Two 54 in. O.D.C.I. pipe cars, 1 tank car with fuel oil
2.12 Elevation of Vehicles at Time of Accident: RR bed on bridge deck
2.13 Description of Surface Impacted: Pipe to bridge, car to bridge, cars to river

3.0 SEQUENCE OF EVENTS

3.01 Description of First Event: Eight 54 in. pipes were strapped together in 2 groups of 4 each. The 2 groups laid in tandem
3.02 Description of Second Event: The pipes were then chained and blocked with wood sprags nailed to the car deck.
3.03 Description of Third Event: Sprags were not predrilled and later split loosening the load which was already unstable because of the "4-together" configuration. (Note: 3 pipes fastened in this fashion would have been stable).

3.04 Description of Fourth Event: One of the loose pipe snagged the bridge superstructure bringing down one span

3.06 Summary of Sequence of Events: 5 loaded cars dropped into the Alabama River

4.0 POST ACCIDENT EVENT DATA

4.1 POST ACCIDENT EVENT DATA

4.1.01 Truck or Rail Car No. 1: 5 cars in river were damaged
4.1.02 Truck or Rail Car No. 2: Bridge was seriously damaged
4.1.06 Evidence of Crushing: None
4.1.07 Evidence of Impact: One of the 54 inch pipes impacted against a bridge truss
4.1.08 Evidence of Falling: 5 cars fell into the river as the bridge collapsed
4.1.09 Evidence of Puncture: Not applicable (N/A)
4.1.10 Evidence of Bending/Deformation of Support Members: N/A
4.1.11 Evidence of Tearing Structural Members: N/A
4.1.12 Evidence of Projectiles Distance Traveled, Size/Weight of Projectile: None
4.1.13 Other Evidence of Severe Structural Damage: See above

4.2 THERMAL/EXPLOSION DAMAGE DATA

4.2.01 Type of Fire(s) and Fuel(s) Involved and Amounts: None
4.2.05 Evidence of Torch or Plume Fire: None
4.2.06 Evidence of Rocketing: None
4.2.07 Evidence of Explosions: None
4.2.10 Evidence of Burial/Duration: Cars were in the river and mud

4.3 LEAK OR SPILL DATA

4.3.01 Substance(s) Leaked or Spilled: The tank car filled with fuel oil was reported not to be leaking

6.0 KEYWORD SUMMARY OF REPORT

6.01 Vehicle Class (R = rail, T = truck, C = rail & truck): R
6.02 Speed of Impact: 8 mph
6.03 Falling Distance: 75 feet
6.04 Crushing Events (C1 = locomotive, C2 = box, C3 = coal car, C4 = flat car, C5 = tank car, C6 = tractor, C7 = trailer, C8 = unit truck, C9 = heavy cargo, C10 = tank truck, C11 = bridge, C12 = heavy support structure, C13 = no evidence of crushing, C14 = caboose, C15 = other): C13
6.05 Impacting Object (I1 = locomotive, I2 = coupler, I3 = sill, I4 = axle, I5 = bar stock, I6 = plate stock, I7 = I-beam, I9 = rail, I10 = forging/casting, I11 = tractor, I12 = trailer, I13 = no evidence of impacted object, I14 = caboose, I15 = other): I10

6.06 Object Impacted (01 = locomotive, 02 = box car, 03 = tank car, 04 = coal car, 05 = tractor, 06 = trailer, 07 = cargo, 08 = cask, 09 = structural concrete, 010 = building, 011 = bridge, 012 = automobile, 013 = no evidence of impacted object, 014 = caboose, 015 = other): 011

6.08 Fire Duration: 0 minutes

6.09 Torch Duration: 0 minutes

6.10 Rocketing Distance: 0 feet

6.11 Weight of Rocketed Object: 0 pounds

6.12 Burial Event (B1 = evidence of burial larger than 24 hours, B2 = evidence of burial shorter than 24 hours, B3 = no evidence of burial): B1

6.13 Ambient Temperature: $45^{o}F$

6.14 Vehicle Damage (thousands of dollars): 76

6.15 Other Property Damage (thousands of dollars): 2,000

6.16 Number of Fatalities: 0

6.17 Vehicle Type Involved in Accident (V1 = unit train, V2 = passenger train, V3 = mixed train cargo, V4 = tractor trailer, V5 = tandem trailer, V6 = unit truck, V7 = other): V3

6.18 Cargo Type Involved in Accident (Z1 = flammable, Z2 = explosive, Z3 = toxic, Z4 = ordnance, Z5 = radioactive, Z6 = other): Z1 Z6

Table A.5 Legend
Rail-Highway Grade-Crossing Accidents

Report Source

FRA	Federal Railroad Administration
NATL, year, report #	Department of Transportation, Federal Railroad Administration, Atlanta Office
NCHI, year, report #	Department of Transportation, Federal Railroad Administration, Chicago Office
N/HAB	National Transportation Safety Board, Highway Accident Brief
NOAK, year, report #	Department of Transportation, Federal Railroad Administration, Oakland Office
N/RHR	National Transportation Safety Board, Railroad Highway Report
NS	Not Stated
NTSB	National Transportation Safety Board

Accident Description

HtoS Col.	Head to Side Collision
Vhcl	Vehicle

Table A.5
Rail-Highway Grade-Crossing Accidents

Location	Report Source	Date of Accident	Accident Description	No. of Vhcl	Acc. vel. (mph)	Fall ht. (ft.)	Fire Y/N (dur)	Object Struck Description
Alabama								
Huntsville	NTSB 82-1	9/15/81	HtoS Col.	2	30	NS	Y(60M)	Cargo Tank
California								
Tracy	NTSB 76-1	3/9/75	HtoS Col.	2	50	NS	N	Gondola Car
Florida								
Plant City	N/RHR-78-2	10/2/77	Train-Truck	8	70	NS	Y(17M)	Pickup Truck
Georgia								
Aragon	N/RHR-75-1	10/23/74	Train-Bus	2	6	0	Y(NS)	Bus
Illinois								
Beckemeyer	N/RHR-76-3	2/7/76	Train-Truck	2	NS	0	N	Pickup Truck
Elwood	N/RHR-76-2	11/19/75	Truck-Train	2	82	0	N	Train
Loda	N/RHR-71-1	1/24/70	Train-Truck	2	79	0	Y(NS)	Tanker Truck

Continued on next page

Table A.5
Rail-Highway Grade-Crossing Accidents

Location	Report Source	Date of Accident	Accident Description	No. of Vhcl	Acc. vel. (mph)	Fall ht. (ft.)	Fire Y/N (dur)	Object Struck Description
Iowa								
Des Moines	N/RHR-77-2	7/1/76	Train-Car	2	30	0	N	Auto
Louisiana								
Goldonna	N/RHR-78-1	11/28/77	Train-Truck	2	56	0	Y(NS)	Truck/Trailer
Kenner	Modern Bulk Trans	11/25/80	Train-Truck	3	17	0	Y(NS)	Truck/Trailer
Kenner	NTSB 81-1	11/25/80	HtoS Col.	3	25	NS	Y(122M)	Cargo Tank
Missouri								
Gera	NCHI79FR019	1/11/79	Train-Truck	2	35	0	N	Truck/Trailer
Boutte	N/HAB-80-1	12/15/78	Train-Truck	2+	NS	0	N	Truck/Trailer
Nebraska								
Edgar	NTSB 76-201	8/31/76	Train-Truck	2	NS	0	N	Truck/Trailer
North Platte	NS	NS	Train-Truck	2	NS	0	Y(NS)	Truck/Trailer
Stratton	N/RHR-77-1	8/8/76	Train-Bus	2	57	0	N	Bus
Nevada								
Ocala	NOAK79FR023	12/18/78	Train-Truck	2	45	0	Y(NS)	Truck/Trailer

Continued on next page

Table A.5
Rail-Highway Grade-Crossing Accidents

Location	Report Source	Date of Accident	Accident Description	No. of Vhcl	Acc. vel. (mph)	Fall ht. (ft.)	Fire Y/N (dur)	Object Struck Description
New York								
Congers	N/RHR-73-1	3/24/72	Train-Bus	2	25	0	N	Bus
Mineola	NTSB 82-2	3/14/82	HtoS Col.	2	65	NS	Y(20M)	Van
North Carolina								
Sellers	NATL78FR011	NS	Train-Truck	2	79	0	NS	Truck/Trailer
Oklahoma								
Collinsville	NTSB 72-1	4/5/71	HtoS Col.	2	71	NS	N	Truck
Marland	N/RHR-77-3	12/15/76	Train-Truck	12	90	0	Y(NS)	Tanker Truck
Oregon								
Lafayette	NS	9/8/76	Train-Bus	2	50+	0	N	Bus
Pennsylvania								
Southampton	NTSB 82-3	1/2/82	Train-Truck	3	20	NS	Y(135)	Trailer
Yardley	N/RHR-76-4	6/5/75	Train-Truck	3	63	0	N	Truck/Trailer

Continued on next page

Table A.5
Rail-Highway Grade-Crossing Accidents

Location	Report Source	Date of Accident	Accident Description	No. of Vhcl	Acc. vel. (mph)	Fall ht. (ft.)	Fire Y/N (dur)	Object Struck Description
Virginia								
Tazewell	NTSB 76-135	NS	Train-Truck	2	31	0	Y(NS)	Trailer
West Virgina								
Woodland	FRA C-8-72	NS	Train-Vhcle	2	40	NS	NS	Earthmover

Table A.6 Legend
Truck Accidents

Report Source

BMCS	Bureau of Motor Carrier Safety
CONF	Conference
DOT	Department of Transportation
DOTHS	Department of Transportation
N/HAB	National Transportation Safety Board, Highway Accident Brief
N/HAR	National Transportation Safety Board, Highway Accident Report
NS	Not Stated
NUREG/CR	Nuclear Regulatory Commission Contractor Report
PATRAM	Conference on Packaging and Transportation of Radioactive Materials

Accident Description

Bldg Col.	Building Collision
Brdg Ovtrn	Bridge Overturn
HtoH Col.	Head to Head Collision
HtoS Col.	Head to Side Collision
HtoT Col.	Head to Tail Collision
Mltpl Col.	Multiple Collision
NS Trk. Fire	Not Stated Truck Fire
Ovtrn Col.	Overturn Collision
Trailer Sep.	Trailer Separation

Table A.6
Truck Accidents

Location	Report Source	Date of Accident	Accident Description	No. of Vhcl	Acc. vel. (mph)	Fall ht. (ft.)	Fire Y/N (dur)	Object Struck Description
Arizona								
Buckeye	N/HAB-80-1	11/15/78	HtoH Col.	2	NS	0	N	Tractor Truck
Gila Bend	BMCS 76-4	NS	HtoH Col.	6	80	0	Y(NS)	Car, Motorcycle
Arkansas								
Brisco	NS	4/27/76	Overturn	1	40	30	Y(NS)	Roadbed
Camden	N/HAB-80-2	4/13/78	HtoH Col.	2	NS	0	N	Pickup Truck
Jasper	N/HAR-81-1	6/5/80	Explosion	1	63	38	N	Hillside
Little Rock	N/HAB-80-1	1/27/78	HtoH Col.	3	NS	0	N	Truck/Trailer
California								
Coachella	N/HAR-80-6	4/23/80	HtoH Col.	2	60	NS	N	Bus
Coalinga	N/HAB-80-1	12/15/78	HtoH Col.	12	47	0	N	Mltpl Cars
Corona	N/HAR-75-7	2/28/75	Mltpl Col.	84	50	0	Y(NS)	Mltpl Cars, Trucks
El Centro 35 MI W	N/HAR-75-6	3/8/74	HtoH Col.	2	45	NS	N	Semi Trailer
Lemoore	N/HAR-83-02	10/8/82	HtoH Col.	3	55	NS	N	Van
Los Angeles	NS	NS	Explosion	6	0	0	Y(NS)	None

Continued on next page

Table A.6
Truck Accidents

Location	Report Source	Date of Accident	Accident Description	No. of Vhcl	Acc. vel. (mph)	Fall ht. (ft.)	Fire Y/N (dur)	Object Struck Description
Los Angeles	NS	NS	HtoH Col.	6	55	0	Y(NS)	Truck/Trailer
California (continued)								
Los Angeles	N/HAR-80-5	3/3/80	StoS Col.	3	45	NS	Y(55M)	Tank Truck
Martinez	N/HAR-77-2	5/21/76	Brdg Ovtrn	1	35	22	N	Ground
Oakland (near)	N/HAR-83-01	4/7/82	HtoH Col.	3	55	NS	Y(162M)	Car
Ontario	NS	11/4/74	Collision	1	50	0	Y(NS)	Tree, Sign, Steel, Concrete Wall
Sacramento	NS	NS	Overturn	4	NS	0	Y(4H)	Roadbed, Cars
Sacramento (near)	N/HAR-74-5	11/11/73	Collision	1	67	NS	N	Concrete
San Bernardino	N/HAR-81-2	11/10/80	HtoH Col.	24	55	NS	N	Semi Trailer
San Francisco Bay	San Jose News	3/81	Overpass Run Off	2	55	64	N	Pickup Truck, Ground
Ventura	N/HAR-72-4	8/18/71	HtoH Col.	13	60	0	Y(60M)	Car
Willow Creek	N/HAR-83-05	2/24/83	Skid	2	38	NS	N	Bus
Winterhaven	BMCS 79-2	4/4/79	Collision	2	NS	0	Y(NS)	Parked Car
Colorado								
Canon City	N/HAR-82-3	11/14/81	HtoS Col.	3	56	NS	Y(170M)	Tractor

Continued on next page

Table A.6
Truck Accidents

Location	Report Source	Date of Accident	Accident Description	No. of Vhcl	Acc. vel. (mph)	Fall ht. (ft.)	Fire Y/N (dur)	Object Struck Description
Fleming	NS	9/29/77	HtoH Col.	2	110	0	Y(NS)	Truck/Trailer
Colorado (continued)								
Golden	NS	6/10/74	Collision	1	35	0	Y(5H)	Rock Wall
Golden	BMCS 8-186	NS	Overturn	1	95	30	NS	Roadbed, Guardrail
Kit Carson	BMCS 8-097	NS	HtoH Col.	2	120	NS	Y(NS)	Truck/Trailer
Kit Carson	BMCS 8-089	NS	HtoH Col.	2	110	NS	Y(NS)	Truck/Trailer
Silverthorne	BMCS 8-028	NS	Collision	2	55	15	Y(NS)	Guardrail
District of Columbia								
Washington	BMCS 76-2	NS	Mltpl Col.	2	NS	NS	NS	Car
Florida								
Gretna	N/HAR-72-3	8/8/71	HtoH Col.	2	50	2	N	Car
Homestead	BMCS 7-178	NS	HtoS Col.	2	51	NS	Y(NS)	Truck/Trailer
Ocala	N/HAR-83-04	2/28/83	HtoT/HtoS	22	55+	NS	Y(120M)	Semi
Georgia								
Atlanta	N/HAR-78-5	6/20/77	HtoH Col.	7	45	0	N	Cars, Truck
Atlanta								

Continued on next page

Table A.6
Truck Accidents

Location	Report Source	Date of Accident	Accident Description	No. of Vhcl	Acc. vel. (mph)	Fall ht. (ft.)	Fire Y/N (dur)	Object Struck Description
W I-20	N/HAR-75-4	8/21/73	Skid, HtoS	2	45	NS	N	Car
Georgia (continued)								
Attapulgus	BMCS 4-206	12/15/73	HtoH Col.	2	90	0	Y(NS)	Truck/Trailer
Dalton	N/HAB-80-1	12/14/78	HtoH Col.	2	NS	0	N	Truck/Trailer
Doraville	N/HAB-80-2	7/21/78	Mltpl Col.	3	NS	0	N	Motorcycle, Dump Truck
Hamilton	H/HAR-76-5	6/6/75	HtoH Col.	7	50	0	N	Bus
Leslie	N/HAB-80-2	4/4/77	HtoH Col.	2	NS	0	N	Car
Lithonia	BMCS 80-2	1/8/80	HtoS Col.	2	35	0	N	Car
Loganville	N/HAB-80-1	6/20/78	HtoS Col.	2	NS	0	N	Car
Ludowici	N/HAB-80-1	5/2/78	HtoS Col.	3	NS	0	N	Car
Richmond Hill	N/HAB-80-1	6/19/78	HtoH Col.	3	NS	0	N	Car
Savannah	N/HAB-80-1	7/6/78	Jackknife	2	NS	0	N	Car
Waco	N/HAR-72-5	6/4/71	HtoH Col.	2	40	0	Y(+15M)	Car
Illinois								
Gibson City	5th PATRAM pg 804-806	NS	Jackknife	1	NS	NS	NS	Roadbed
Rosecrans	BMCS 5-030	4/29/76	Collision	1	55	0	Y(NS)	Bridge Barrier

Continued on next page

Table A.6
Truck Accidents

Location	Report Source	Date of Accident	Accident Description	No. of Vhcl	Acc. vel. (mph)	Fall ht. (ft.)	Fire Y/N (dur)	Object Struck Description
Indiana								
Chesterton	NS	NS	Jackknife	1	55	20	N	Guardrail
Indianapolis	BMCS 75-5	6/13/75	Overturn	1	50	18	NS	Roadbed
Iowa								
Winthrop	N/HAB-80-1	5/2/78	Overturn	1	NS	0	N	Roadbed
Kansas								
Kansas City	BMCS 7-064	8/6/76	Cargo Loss	1	NS	0	Y(NS)	Roadbed
Leon	N/HAB-80-2	5/15/78	HtoH Col.	3	NS	0	Y(NS)	Car
Mayetta	BMCS 80-1	1/6/80	HtoH Col.	2	50	0	Y(NS)	Pickup Truck
Wichita	NUREG/CR-0992	NS	Overturn	1	NS	NS	NS	Roadbed
Kentucky								
Beattyville	N/HAR-78-4	9/24/77	Runaway	17	36	0	Y(5H)	Roadbed
Carroll City	DOTHS602826	8/75	HtoH Col.	3	60	0	Y(105M)	Car/Trailer

Continued on next page

Table A.6
Truck Accidents

Location	Report Source	Date of Accident	Accident Description	No. of Vhcl	Acc. vel. (mph)	Fall ht. (ft.)	Fire Y/N (dur)	Object Struck Description
Louisiana								
Baton Rouge	NS	NS	Overturn	1	NS	0	Y(NS)	Roadbed
Lake Charles	N/HAR-82-4	8/27/81	Skid	26	30+	NS	N	Semi Trailer
Ramah	N/HAB-80-2	12/16/78	Mltpl Col.	4	NS	0	Y(NS)	Bridge Column
Maryland								
Bethesda	BMCS 78-2	3/14/78	Mltpl Col.	3	70	40	N	Car
Frostburg	N/HAR-81-3	2/18/81	HtoS Col.	17	50+	NS	N	Truck
Hagerstown	N/HAB-80-1	1/30/79	HtoH Col.	2	NS	0	N	Truck/Trailer
N. Carrollton	N/HAR-71-9	6/19/70	Skid, HtoT	2	NS	NS	N	Truck
Massachusetts								
Belcherstown	NS	NS	Collision	1	60	25	N	Utility Pole
Braintree	N/HAR-74-4	10/18/73	Overturn	1	55	0	Y(NS)	Roadbed
Michigan								
Detroit	NS	2/7/77	Collision	1	45	30	Y(NS)	Bridge Barrier
Flint	BMCS 5-076	8/19/76	Collision	1+	NS	20	Y(NS)	Bridge Rail, Roadbed

Continued on next page

Table A.6
Truck Accidents

Location	Report Source	Date of Accident	Accident Description	No. of Vhcl	Acc. vel. (mph)	Fall ht. (ft.)	Fire Y/N (dur)	Object Struck Description
Minnesota								
Floodwood	BMCS 5-169	NS	HtoH Col.	3	105	0	NS	Truck/Trailer
Mississippi								
Waynesboro	N/HAR-82-2	10/12/81	HtoH Col.	3	35	NS	N	Car/Pole
Missouri								
Fisk	BMCS 7-064	NS	Collision	1	55	45	NS	Bridge, River
Keytesville	NS	4/7/77	Collision	1	55	30	N	Bridge Barrier
Kansas City	N/HAB-80-2	7/13/77	Collision	1	55	0	N	Bridge Column
St. Louis	N/HAR-79-3	9/25/77	HtoH Col.	2	NS	0	N	Car
North Carolina								
Hertford	NS	1/10/78	Explosion	2	NS	0	Y(NS)	NS
Marion	N/HAR-78-6	1/25/78	HtoH Col.	2	70	0	N	Pickup Truck
Morganton	NS	4/27/78	HtoH Col.	2	75	0	N	Truck
North Dakota								
Freeman	BMCS 80-3	3/12/80	HtoH Col.	4	40	0	Y(NS)	Cars

Continued on next page

Table A.6
Truck Accidents

Location	Report Source	Date of Accident	Accident Description	No. of Vhcl	Acc. vel. (mph)	Fall ht. (ft.)	Fire Y/N (dur)	Object Struck Description
New Jersey								
Bordentown	N/HAR-75-3	10/19/73	Side Col.	4	55	50	Y(NS)	Car
Elizabethtown	NS	9/27/77	Explosion	1	0	0	Y(NS)	NS
Turnpike Exit 8	N/HAR-73-4	10/17/73	Side Col.	3	65+	0	Y(30M)	Guardrail
New York								
Alden	N/HAB-80-1	3/15/78	Collision	4	NS	0	N	Car
Brant	DOTHS801925	6/21/75	Collision	1	55	35	NS	Post, Roadbed
Brooklyn	N/HAR-71-6	5/30/70	Explosion	1	0	0	Y(NS)	NS
Buffalo	DOTHS600979	3/19/71	HtoH Col.	2	55	0	NS	Truck/Trailer
Buffalo	DOTHS600974	3/24/71	Overturn	1	60	NS	NS	Roadbed
Hamburg	DOTHS601762	4/10/72	Overturn	1	40	NS	NS	Roadbed
Locke	NS	NS	Jackknife	21	NS	0	Y(NS)	Building
Moreau	N/HAB-80-1	8/13/78	HtoH Col.	2	NS	0	N	Truck/Trailer
Ohio								
Ashtabula	Newscast	4/1/81	Overturn	1	NS	NS	NS	Roadbed
Valley View	N/HAR-77-3	8/20/76	Mltpl Col.	11	50	0	Y(NS)	Mltpl Cars

Continued on next page

Table A.6
Truck Accidents

Location	Report Source	Date of Accident	Accident Description	No. of Vhcl	Acc. vel. (mph)	Fall ht. (ft.)	Fire Y/N (dur)	Object Struck Description
Oklahoma								
El Reno	BMCS 6-606	NS	HtoH Col.	2	50	31	N	Truck/Trailer
Stroud	BMCS 6-046	NS	Collision	1	45	25	Y(NS)	Guardrail
Oregon								
Portland	DOT 72-5	11/18/72	Side Col.	1	NS	0	N	Concrete Wall
Pennsylvania								
Clarion	BMCS 69-5	NS	Collision	1	20	13	N	Bridge
Fulton County	N/HAB-80-1	2/22/79	Overturn	1	NS	0	N	Ground
Indiana	N/HAR-80-3	9/22/79	HtoH Col.	2	70	NS	N	Car
Lamar	N/HAB-80-1	2/7/79	Run Off Rd	2	NS	0	N	Guardrail
Lancaster Cnty	N/HAR-72-1	2/6/72	Collision	1	55	NS	N	Guardrail
Mt. Pleasant	N/HAB-80-1	2/14/79	Trailer Sep.	2	NS	0	N	Car
N. Cumberland	BMCS 3-208	NS	Overturn	2	55	0	N	Roadbed
Washington	NS	NS	Collision	1	50	0	Y(3H)	Guardrail
Washington	NS	NS	Overturn	7	50	0	N	Roadbed
Warfordsburg	N/HAB-80-1	5/5/79	Overturn	1	70	0	N	Roadbed

Continued on next page

Table A.6
Truck Accidents

Location	Report Source	Date of Accident	Accident Description	No. of Vhcl	Acc. vel. (mph)	Fall ht. (ft.)	Fire Y/N (dur)	Object Struck Description
Rhode Island								
West Greenwich	N/HAB-80-1	1/26/79	Bldg Col.	1	NS	0	N	Building
Tennessee								
Adams	BMCS 69-3	NS	HtoH Col.	3	110	0	N	Truck/Trailer
Carthage	BMCS 70-8	NS	Collision	1	55	50	N	Railing
Church Hill	NS	1/14/76	HtoH Col.	3	70	NS	Y(85M)	Truck/Tractor
Knoxville (east of)	Knoxville News	4/29/81	NS Trk. Fire	1	NS	0	Y(NS)	None
Koko	N/HAB-80-1	10/17/78	HtoS Col.	3	NS	0	N	Pickup Truck
Memphis	BMCS 73-8	NS	Mltpl Col.	4	100	0	N	Truck/Trailer
Nashville	N/HAR-74-2	7/27/73	Bridge Fall Off	1	55	65	N	Bridge Barrier, Ground
Oak Ridge	CONF 090174	NS	Overturn	1	55	7	NS	Ditch
Texas								
Cotulla	N/HAR-72-6	9/5/71	Ovtrn Col.	2	60	0	Y(NS)	Microbus
Eagle Pass	N/HAR-76-4	4/29/75	Overturn	51	55	0	N	Concrete Wall
Fairfield	BMCS 6-012	NS	Overturn	1	60	30	Y(NS)	Bridge Barrier
Fischer City	BMCS 78-3	12/8/78	HtoS Col.	2	55	0	NS	Bus

Continued on next page

Table A.6
Truck Accidents

Location	Report Source	Date of Accident	Accident Description	No. of Vhcl	Acc. vel. (mph)	Fall ht. (ft.)	Fire Y/N (dur)	Object Struck Description
Texas (continued)								
Fort Worth	BMCS 6-183	NS	Overturn	1	55	30	N	Roadbed
Fort Worth	NS	NS	Jackknife	1	55	55	N	Bridge Rail
Houston	N/HAR-77-1	5/11/76	Overturn	1+	54	15	N	Freeway Roadbed
Luling	N/HAR-81-4	11/16/80	Skid	1	55	NS	N	Ditch
Mesquite	BMCS 6-012	NS	HtoH Col.	2	105	0	N	Truck/Trailer
San Antonio	DOTHS800650	9/24/71	Overturn	1	60	0	N	Roadbed
Stratford	BMCS 6-026	NS	HtoH Col.	2	110	NS	NS	Truck/Trailer
Utah								
Bountiful	DOTHS801500	10/5/72	Collision	1	65	20	NS	Guardrail,Rdbed
Delta	N/HAR-80-2	9/12/79	HtoS Col.	2	55	NS	N	Van/Bridge
Farmington	DOTHS602309	1/23/73	Overturn	1	70	0	NS	Roadbed
Salt Lake City	DOTHS801499	10/16/72	Overturn	1	70	0	Y(3H)	Roadbed
Salt Lake City	DOTHS820160	NS	Collision	1	55	20	Y(NS)	Roadbed
Scipio	N/HAR-79-1	8/26/77	HtoH Col.	2	NS	0	N	Van

Continued on next page

Table A.6
Truck Accidents

Location	Report Source	Date of Accident	Accident Description	No. of Vhcl	Acc. vel. (mph)	Fall ht. (ft.)	Fire Y/N (dur)	Object Struck Description
Virginia								
Hanover City	N/HAB-80-1	12/17/79	HtoH Col.	2	NS	0	N	Car
Lynchburg	H/HAR-73-3	3/9/72	Overturn	1	25	0	Y(22H)	Rock
Quantico	Columbus, OH News	2/19/81	Bridge Run Off	1	55	80	N	Brdg Under Structure
Triangle	N/HAR-81-6	2/18/81	Collision	1	60	25	N	Guardrail
Washington								
Pasco	BMCS 10-058	NS	HtoH Col.	4	110	NS	NS	Truck/Trailer
Seattle	N/HAR-76-7	12/4/75	Jackknife	35	52	0	N	Support Column
Wyoming								
Baggs	NS	8/2/74	Side Col.	2	NS	0	Y(NS)	NS
Laramie	N/HAR-80-1	8/22/79	HtoH Col.	3	68	0	N	House, Vehicle

Table A.7 Legend
Train Accidents

Report Source

ASME	American Society of Mechanical Engineers
DOT	Department of Transportation
FRA	Federal Railroad Administration
ICC	Interstate Commerce Commission
NATL, year, report #	Department of Transportation, Federal Railroad Administration, Atlanta Office
NCHI, year, report #	Department of Transportation, Federal Railroad Administration, Chicago Office
NDCA, year, report #	Department of Transportation, Federal Railroad Administration, Washington D.C. Office
NDEN, year, report #	Department of Transportation, Federal Railroad Administration, Denver Office
NFTW, year, report #	Department of Transportation, Federal Railroad Administration, Fort Worth Office
N/HZM	National Transportation Safety Board, Hazardous Material Accident Report
NMKC, year, report #	Department of Transportation, Federal Railroad Administration, Kansas City Office
NNYC, year, report #	Department of Transportation, Federal Railroad Administration, New York City Office
NOAK, year, report #	Department of Transportation, Federal Railroad Administration, Oakland Office
N/RAR	National Transportation Safety Board,Railroad Accident Report
NS	Not Stated

Continued on next page

Table A.7 Legend Continued
Train Accidents

Report Number

NSEA, year	Department of Transportation, Federal Railroad Administration, Seattle Office

Accident Description

Brdg Col.	Bridge Collision
Brdg Fail	Bridge Failure
Drl Col.	Derail Collision
HtoH Col.	Head to Head Collision
HtoS Col.	Head to Side Collision
HtoT Col.	Head to Tail Collision
Int. Fire	Internal Fire

Continued on next page

Table A.7
Train Accidents

Location	Report Source	Date of Accident	Accident Description	No. of Vhcl	Acc. vel. (mph)	Fall ht. (ft.)	Fire Y/N (dur)	Object Struck Description
Alabama								
Florence	N/RAR-79-2	9/18/78	HtoH Col.	2 T	15	12	N	Train
Hunter	NATL78FR018	1/19/79	Brdg Col.	72	8	75	N	Bridge
Muscle Shoals	NATL79FR001	10/8/78	HtoH Col.	2 T	NS	0	N	Train
North Castle	N/RAR-77-9	1/16/77	Derail	22	43	21	N	RR Bed, RR Car
Alaska								
Hurricane	N/RAR-76-3	7/5/75	HtoH Col.	2 T	40	0	N	Train
Talkeetna	NSEA77FR005	12/1/76	Derail	71	NS	25	N	RR Bed, RR Car
Arizona								
Benson	N/RAR-75-2	5/24/73	Explosion	12	45	0	Y(8H)	NS
Benton	NFTW79FR018	12/25/78	Derail	137	45	23	Y(3H)	Bridge, RR Cars, River
Dequeen	NFTW79FR020	1/13/79	Derail	105	25	20	N	RR Bed, RR Car
Raso	NOAK79FR017	12/10/78	Derail	NS	40	0	N	RR Bed, RR Car
Rone	NFTW79FR014	12/4/78	Derail	125	15	14	N	RR Bed, RR Car

Continued on next page

Table A.7
Train Accidents

Location	Report Source	Date of Accident	Accident Description	No. of Vhcl	Acc. vel. (mph)	Fall ht. (ft.)	Fire Y/N (dur)	Object Struck Description
Arkansas								
Gilmore	NFTW79FR019	1/8/79	Derail	97	55	0	N	RR Bed, RR Car
Hartman	NFTW79FR008	2/27/77	Derail	109	40	0	Y(200M)	RR Bed, RR Car
Lewisville	N/RAR-78-8	3/29/78	Derail	47	35	0	Y(24H)	RR Bed, RR Car
Poping-Ozark	NFTW79FR012	11/9/78	Derail	131	38	NS	N	RR Bed, RR Car
Possum Grape (near)	N/RAR-83-06	10/3/82	HtoS Col.	2	50	30	Y(120)	Freight Car
California								
Andesite	NOAK79FR012	11/26/78	Derail	70	NS	0	N	RR Bed, RR Car
Bradley	NOAK79FR001	10/4/78	Derail	56	30	0	Y(5D)	RR Bed, RR Car
Hayward	N/RAR-80-10	4/9/80	Derail	1	52	30	Y(60M)	RR Bed, RR Car
Indio	N/RAR-74-1	6/25/73	HtoH Col.	2 T	60	0	Y(NS)	Train
Kelso	N/RAR-81-7	11/17/80	HtoH Col.	2	118	NS	N	Caboose
Oroville	NOAK79FR011	11/20/78	Derail	61	30	10	N	RR Bed, RR Car
Pinole	NOAK79FR013	12/1/78	Derail	73	40	0	N	RR Bed, RR Car
Roseville	DOT 4187	4/28/73	Explosion	289	0	0	Y(32H)	NS
San Francisco	N/RAR-79-5	1/17/79	Int. Fire	2	NS	0	Y(2H)	NS
Santa Margurita	NOAK79FR005	10/18/78	HtoH Col.	2 T	25	0	N	Train

Continued on next page

Table A.7
Train Accidents

Location	Report Source	Date of Accident	Accident Description	No. of Vhcl	Acc. vel. (mph)	Fall ht. (ft.)	Fire Y/N (dur)	Object Struck Description
California (continued)								
Surf	N/RAR-81-1	5/22/81	Derail	3	60	NS	N	RR Bed, RR Car
Therman	N/RAR-83-1	1/7/82	Derail	61	57	0	N	RR Bed, RR Car
Thousand Palms	N/RAR-80-1	7/24/79	HtoT Col.	2 T	20	0	Y(NS)	Train
Vidal	NOAK79FR025	2/5/79	Derail	78	45	15	N	RR Bed, RR Car
Colorado								
Lambert	NDEN76FR137	7/9/76	Derail	38	60	5	N	RR Bed, RR Car
Connecticut								
Darian	N/RAR-70-3	8/20/69	HtoH Col.	2 T	60	0	N	Train
North Canaan	N/RAR-77-4	7/13/76	HtoH Col.	2 T	20	0	N	Train
Sound View	N/RAR-72-1	10/8/70	Drl. Col.	2 T	60	0	Y(2.5H)	Train
Delaware								
Wilmington	N/RAR-76-7	10/17/75	HtoH Col.	3 T	25	0	N	Train

Continued on next page

Table A.7
Train Accidents

Location	Report Source	Date of Accident	Accident Description	No. of Vhcl	Acc. vel. (mph)	Fall ht. (ft.)	Fire Y/N (dur)	Object Struck Description
District of Columbia								
Washington	NDCA76FR151	7/18/76	Derail	84	36	25	Y(NS)	RR Bed, RR Car, Highway
Washington	N/RAR-82-6	1/13/82	Derail	1	10	NS	N	Wall
Florida								
Crestview	N/RAR-79-11	4/8/79	Derail	119	35	NS	Y(60H)	RR Bed, RR Car
Lochloosa	N/RAR-81-9	5/26/81	Derail	1	76	NS	N	RR Bed, RR Car
Pensacola	N/RAR-78-4	11/9/77	Derail	37	35	0	N	RR Bed, RR Car
Westlake Wales	FRA C71-72	NS	Derail	123	50	NS	NS	RR Bed, RR Car
Youngstown	N/RAR-78-8	2/26/78	Derail	145	45	0	N	RR Bed, RR Car
Georgia								
Covington	NATL79FR025	2/19/79	Derail	80	25	0	N	RR Bed, RR Car
Pembroke	NATL79FR021	2/7/79	Derail	134	31	5	N	RR Bed, RR Car
Rupert	NATL76FR219	9/11/76	Derail	108	50	0	N	RR Bed, RR Car
Vinings	NATL79FR016	1/15/79	Derail	60	35	0	N	RR Bed, RR Car

Continued on next page

Table A.7
Train Accidents

Location	Report Source	Date of Accident	Accident Description	No. of Vhcl	Acc. vel. (mph)	Fall ht. (ft.)	Fire Y/N (dur)	Object Struck Description
Illinois								
Bartonville	NCHI77FR016	NS	Derail	97	52	20	NS	RR Bed, RR Car
Chicago	N/RAR-77-10	2/4/77	HtoH Col.	2 T	9.5	NS	N	Train
Chicago	N/RAR-73-5	10/30/72	HtoH Col.	3 T	50	0	N	Train
Chicago	NCHI79FR004	10/29/78	HtoH Col.	2 T	20	0	N	Train
Chicago	N/RAR-76-9	1/9/76	HtoH Col.	2	35	NS	N	Rail Car
Cresent City	N/RAR-72-2	6/21/70	Derail	113	43	0	Y(56H)	RR Bed, RR Car
Decatur	N/RAR-75-4	7/19/74	Yard Col.	595	8.5	0	Y(NS)	RR Cars
Elburn	NCHI77FR025	2/21/77	Derail	105	53	0	N	RR Bed, RR Car
Flagg	NCHIRR76118	6/28/76	Derail	140	60	12	Y(NS)	RR Bed, RR Car, Bridge
Gorham	NCHI78FR030	NS	HtoH Col.	2 T	50	NS	Y(NS)	Train
Harvey	N/RAR-80-3	10/12/79	HtoH Col.	2 T	58	0	N	Train
Maquon	N/RAR-73-4	5/24/72	HtoH Col.	2 T	80	0	Y(NS)	Train
Morrison	NCHIRR76184	8/22/76	Derail	128	35	0	N	RR Bed, RR Car
Northbrook	NCHI77FR012	12/20/76	Derail	103	30	20	N	RR Bed, RR Car, Bridge
Salem	N/RAR-72-5	6/10/71	Derail	18	90	0	Y(NS)	RR Bed, RR Car
Stratford	NCHI79FR018	1/9/79	Derail	83	50	0	Y(10M)	RR Bed, RR Car
Springfield	N/RAR-81-5	10/30/80	Derail	1	63	NS	N	RR Bed, RR Car

Continued on next page

Table A.7
Train Accidents

Location	Report Source	Date of Accident	Accident Description	No. of Vhcl	Acc. vel. (mph)	Fall ht. (ft.)	Fire Y/N (dur)	Object Struck Description
Indiana								
North Haven	N/RAR-77-6	10/19/76	HtoH Col.	2 T	20	0	Y(NS)	Train
Sullivan	N/RAR-84-02	9/14/83	HtoH Col.	2	35	0	N	Caboose
Veedersburg	NCHI76FR112	6/25/76	Derail	47	44	NS	N	RR Bed, RR Car
Wheatfield	FRA B-8-72	NS	Derail	109	40	NS	Y(2H)	RR Bed, RR Car, Storage Tank
Iowa								
Cedar Rapids	NMKC79FR017	12/25/78	Derail	13	NS	22	N	River, Ice
Central Groove	NMKC79FR009	11/28/78	Derail	104	20	10	N	RR Bed, RR Car
Cudley	FRA B272BN1	NS	Derail	93	60	NS	Y(NS)	RR Bed, RR Car
Des Moines	N/RAR-76-8	9/1/75	Derail	63	25	0	Y(4D)	RR Bed, RR Car
Emerson	N/RAR-83-02	6/15/82	Derail	1	74	NS	N	RR Bed, RR Car
Gordons Ferry	NMKC79FR030	1/28/79	Derail	104	26	35	N	Miss. Rvr, RR
Cars								
Northwood	NMKC77FR010	1/23/77	Derail	104+	40	NS	N	RR Bed, RR Car
Pacific Jnctn	N/RAR-83-09	4/13/83	HtoH Col.	2	47	NS	N	Caboose
Woodburn	NMKC79FR023	1/12/79	Derail	106	50	0	N	RR Bed, RR Car

Continued on next page

Table A.7
Train Accidents

Location	Report Source	Date of Accident	Accident Description	No. of Vhcl	Acc. vel. (mph)	Fall ht. (ft.)	Fire Y/N (dur)	Object Struck Description
Kansas								
Atchison	NMKC79FR024	1/17/79	HtoH Col.	2 T	60	0	Y(100M)	Train
Fort Scott	NMKC79FR036	3/11/79	Derail	147	25	6	N	RR Bed, RR Car
Hecla	NMKC79FR001	10/5/78	HtoS Col.	2 T	32	0	N	Train
Lawrence	N/RAR-80-4	10/2/79	Derail	20	80	NS	N	RR Bed, RR Car
Lehigh	DOT B23-70	11/19/69	Derail	36	27	0	Y(NS)	RR Bed, RR Car
Malvern	N/RAR-75-1	7/5/74	Derail	21	77	NS	N	RR Bed, RR Car
Kansas/Missouri								
Fort Scott/ Liberal	NMKC79FR020	1/3/79	Derail	68	50	0	N	RR Bed, RR Car
Kentucky								
Fort Knox	N/RAR-83-07	3/22/83	Derail	1	28	NS	N	RR Bed, RR Car
Hanson	NDCA79FR020	1/7/79	Derail	115	42	0	N	RR Bed, RR Car
Mularaugh	N/RAR-81-1	7/26/80	Derail	1	35	NS	Y(5760M)	RR Bed, RR Car
Stepstone	NATL77FR007	11/8/76	Derail	54	38	20	N	RR Bed, RR Car

Continued on next page

Table A.7
Train Accidents

Location	Report Source	Date of Accident	Accident Description	No. of Vhcl	Acc. vel. (mph)	Fall ht. (ft.)	Fire Y/N (dur)	Object Struck Description
Louisiana								
Livingston	N/RAR-83-05	9/28/82	Derail	1	40	NS	Y (8D)	RR Bed, RR Car
Meeler	N/RAR-75-9	5/30/75	HtoH Col.	2 T	48	0	N	Train
Taft	N/RAR-73-6	2/21/73	HtoH Col.	2 T	43	0	Y(NS)	Train
West Monroe	NFTW79FR008	10/24/78	Derail	105	10	6	N	RR Bed, RR Car
Maryland								
Baltimore	N/RAR-78-1	6/12/77	HtoH Col.	2 T	30	0	Y(NS)	Train
Corsey	FRA C-17-72	NS	Derail	55	55	NS	NS	RR Bed, RR Car
Germantown	N/RAR-81-6	2/9/81	HtoH Col.	2	88	NS	NS	Train
Seabrook	N/RAR-79-3	6/9/78	HtoH Col.	2 T	35	NS	N	Train
Massachusetts								
Beverly	N/RAR-82-1	8/11/81	HtoH Col.	2	19	NS	N	Train
Somerville	N/HZM-81-1	4/3/80	HtoS Col.	2	4	NS	N	Tank Car

Continued on next page

Table A.7
Train Accidents

Location	Report Source	Date of Accident	Accident Description	No. of Vhcl	Acc. vel. (mph)	Fall ht. (ft.)	Fire Y/N (dur)	Object Struck Description
Michigan								
Kopje (Woodlnad)	NCHI78FR024	NS	Derail	38	34	8	NS	RR Bed, RR Car
Lansing	NCHI79FR015	12/28/78	Derail	74	40	0	N	RR Bed, RR Car
Minnesota								
DeGraff	NMKC76FR126	7/4/76	Derail	61	NS	0	Y(3M)	RR Bed, RR Car
Forbes	NMKC76FR059	NS	Derail	119	30	30	Y(2H)	RR Bed, RR Car
Hills	NMKC79FR012	NS	Derail	44	NS	NS	N	RR Bed, RR Car
Nashau	NMKC79FR011	1/30/78	Derail	55	40	9	N	RR Bed, RR Car
Mississippi								
Goodman	N/RAR-77-3	6/30/76	Derail	13	88	0	N	RR Bed, RR Car
Laurel	N/RAR-69-	1/25/69	Derail	144	30	0	Y(60H)	RR Bed, RR Car
Missouri								
Crystal City	N/RAR-84-01	7/18/83	Derail	94	52	25	N	RR Bed, RR Car
Dexter	NMKC79FR003	10/10/78	HtoH Col.	2 T	NS	0	N	Train
Dresden	NMKC79FR025	1/23/79	Derail	38	50	8	N	RR Bed, RR Car

Continued on next page

Table A.7
Train Accidents

Location	Report Source	Date of Accident	Accident Description	No. of Vhcl	Acc. vel. (mph)	Fall ht. (ft.)	Fire Y/N (dur)	Object Struck Description
Missouri (continued)								
Kansas City	NMKC79FR015	12/16/78	Derail	155	20	24	Y(20M)	RR Bridge, RR Bed, RR Car
Randles	NMKC79FR033	2/9/79	Drl. Col.	2 T	25	0	N	RR Bed, RR Car, Train
Springfield	NMKC79FR022	1/10/79	Derail	124	56	16	Y(NS)	RR Bed, RR Car
Montana								
Belt	N/RAR-77-7	11/26/76	Derail	126	38	NS	Y(12H)	RR Bed, RR Car
Browning	NSEA79FR003	10/23/78	Side Col.	2 T	25	30	N	Train
Butte	NSEA79FR013	12/18/78	Derail	81	26	0	NS	RR Bed, RR Car
Curry	FRA C-7-72	NS	Derail	84	50	NS	NS	RR Bed, RR Car
Essex	NSEA79FR001	10/3/78	Derail	35	59	0	N	RR Bed, RR Car
Glacier Park	N/RAR-80-6	3/14/80	Derail	10	37	12	N	RR Bed, RR Car
Greycliff	NSEA79FR006	11/3/78	Derail	74	55	12	Y(NS)	RR Bed, RR Car
Havre	NSEA79FR008	11/14/78	Derail	81	60	18	N	RR Bed, RR Car
Lohman	N/RAR-79-7	3/28/79	Derail	14	74	0	N	RR Bed, RR Car
Zurich	NSEA79FR009	12/8/78	HtoH Col.	2 T	35	0	N	Train

Continued on next page

Table A.7
Train Accidents

Location	Report Source	Date of Accident	Accident Description	No. of Vhcl	Acc. vel. (mph)	Fall ht. (ft.)	Fire Y/N (dur)	Object Struck Description
Nebraska								
Angora	N/RAR-80-7	2/16/80	HtoH Col.	2 T	49	0	N	Train
Arlington	NMKC79FR031	1/31/79	Derail	82	40	0	N	RR Bed, RR Car
Crete	N/RAR-71-2	2/18/69	Derail	169	52	0	N	RR Bed, RR Car
Glenville	NS	5/19/76	Derail	70	68	0	N	RR Bed, RR Car
Gothenburg	NMKC79FR035	3/12/79	Derail	109	60	0	N	RR Bed, RR Car
Hastings	N/RAR-77-1	8/2/76	Derail	119	45	0	N	RR Bed, RR Car
Josselyn	NMKC7FR006	NS	Derail	116	70	NS	NS	RR Bed, RR Car
Marsland	NMKC79FR026	1/25/79	Derail	110	45	40	N	RR Bed, RR Car
Potter	NMKC77FR004	11/13/76	Derail	90	NS	0	Y(1M)	RR Bed, RR Car
Ralston	N/RAR-77-8	12/16/76	Derail	12	53	40	N	RR Bed, RR Car
Nevada								
Elburz	NOAK76FR127	7/4/76	Derail	41	NS	10	N	RR Bed, RR Car
Hoya	NOAK79FR015	12/4/78	HtoH Col.	2 T	22	0	Y(2.5H)	RR Cars
New Jersey								
Edison	N/RAR-79-10	4/20/79	HtoH Col.	2 T	NS	0	Y(5M)	Truck, Machinery
Linden	N/RAR-80-12	7/9/80	Derail	2	30	NS	N	RR Bed, RR Car

Continued on next page

Table A.7
Train Accidents

Location	Report Source	Date of Accident	Accident Description	No. of Vhcl	Acc. vel. (mph)	Fall ht. (ft.)	Fire Y/N (dur)	Object Struck Description
New Mexico								
Des Moines	NDEN79FR001	10/25/78	Derail	62	23	NS	N	RR Bridge, RR Bed, RR Car
New York								
Brooklyn	N/RAR-82-2	7/3/81	HtoH Col.	2	12.7	NS	N	Subway Car
Dobbs Ferry	N/RAR-81-4	11/7/80	HtoH Col.	2	10	NS	Y(15M)	Power Car
New York City	N/RAR-75-8	1/2/75	HtoH Col.	2	35	NS	N	Rail Car
NY City Subway	N/RAR-79-8	12/12/78	Derail	8	NS	0	Y(NS)	RR Bed, RR Car, Concrete Wall
NY City Subway	N/RAR-79-8	1/15/79	Derail	10	NS	0	N	RR Bed, RR Car
NY City Subway	N/RAR-79-8	2/14/79	Derail	10	NS	NS	N	RR Bed
NY City Subway	N/RAR-79-8	3/21/79	Derail	8	NS	0	N	RR Bed
Oneonta	N/RAR-74-4	2/12/74	Derail	125	32	0	Y(7D)	RR Bed, RR Car
North Carolina								
Laleview	N/RAR-80-10	4/2/80	HtoH Col.	2 T	35	0	N	Train
Spencer	N/RAR-78-3	10/8/77	Side Col.	2 T	50	0	N	Train, RR Bed, RR Car

Continued on next page

Table A.7
Train Accidents

Location	Report Source	Date of Accident	Accident Description	No. of Vhcl	Acc. vel. (mph)	Fall ht. (ft.)	Fire Y/N (dur)	Object Struck Description
North Dakota								
Fairmont	NMKC79FR019	12/31/78	Derail	83	40	0	N	RR Bed, RR Car
Walcott	NMKC79FR034	2/17/79	Derail	64	48	15	N	RR Bed, RR Car
White Earth	NMKC79FR021	1/7/79	Derail	77	45	0	N	RR Bed, RR Car
Ohio								
Albany	FRA C-68-72	NS	Derail	93	30	NS	Y(NS)	RR Bed, RR Car, Creek Bed
Circleville	Columbus, OH News	2/17/81	Derail	490	NS	0	N	RR Bed, RR Car
Cleveland	N/RAR-75-3	5/8/74	Brdg Col.	96	33	25	N	Drawbridge
Columbus	ICC 4036	NS	Derail	29	43	0	Y(2H)	RR Bed, RR Car
Huntington	FRA B-3-72	NS	Derail	108	38	NS	Y(3H)	RR Bed, RR Car
Leetonia	N/RAR-76-2	6/6/75	HtoH Col.	2 T	29	0	N	Train
Leetonia	NCHI79FR005	11/1/78	HtoH Col.	5	32	0	N	Train
Lodi	NCHIRR76081	5/30/76	Derail	72	57	15	Y(2H)	RR Bed, RR Car
Pettisville	N/RAR-76-10	2/4/76	HtoH Col.	2 T	70	0	Y(NS)	Train
Pemberville	NCHI79FR012	12/3/78	Derail	185	35	0	N	RR Bed, RR Car
St. Louisville	Utica News	NS	Derail	83+	25	0	N	RR Bed, RR Car

Continued on next page

Table A.7
Train Accidents

Location	Report Source	Date of Accident	Accident Description	No. of Vhcl	Acc. vel. (mph)	Fall ht. (ft.)	Fire Y/N (dur)	Object Struck Description
Ohio (continued)								
Wooster	NCHI79FR008	11/18/78	HtoS Col.	2 T	23	0	N	Train, Tower
Wooster	NCHI77FR013	12/23/76	Derail	131	30	15	Y(10M)	RR Bed, RR Car
Oklahoma								
Alva	NFTW79FR028	3/21/79	Derail	83	42	5	N	RR Bed, RR Car
Leonard	ASME RAIL TRANSPORT PROCEEDINGS	NS	Derail	23	35	NS	NS	RR Bed, RR Car
Mustang	N/RAR-75-6	9/1/74	HtoH Col.	2 T	40	0	Y(NS)	Train
Sallisaw	NFTW79FR011	11/6/78	Derail	52	37	60	N	RR Bed, RR Car
Oregon								
Huntington	NSEA79FR012	12/18/78	Derail	97	60	20	N	RR Bed, RR Car

Continued on next page

Table A.7
Train Accidents

Location	Report Source	Date of Accident	Accident Description	No. of Vhcl	Acc. vel. (mph)	Fall ht. (ft.)	Fire Y/N (dur)	Object Struck Description
Pennsylvania								
Big Run	NNYC79FR031	2/13/79	Derail	74	34	0	N	RR Bed, RR Car
Bristol	N/RAR-82-5	3/29/82	HtoH Col.	2T	22	0	N	Train
Bryant	NNYC79FR021	NS	Derail	98	30	5	N	RR Bed, RR Car
Culmerville	NNYC79FR003	10/10/78	Derail	145	35	0	N	RR Bed, RR Car
Herndon	N/RAR-73-3	3/12/72	HtoH Col.	2 T	60	0	Y(NS)	Train
Munch	N/RAR-79-6	1/31/79	HtoH Col.	2 T	30	0	N	Train
North Wales	N/RAR-80-11	7/17/80	HtoH Col.	2	39	NS	N	Electric Car
Philadelphia	N/RAR-80-5	10/16/79	2HTOT CL.	3 T	28	0	N	Trains
Royersford	N/RAR-80-2	10/1/79	HtoH Col.	2 T	45	0	N	Train
Weatherby	NNYC78FA015	NS	Derail	145	NS	30	NS	RR Bed, RR Car
South Carolina								
Denmark	NATL79FR013	1/7/79	Derail	103	40	0	N	RR Bed, RR Car
Florence	N/RAR-78-6	2/24/78	Derail	20	20	0	Y(NS)	RR Bed, RR Car

Continued on next page

Table A.7
Train Accidents

Location	Report Source	Date of Accident	Accident Description	No. of Vhcl	Acc. vel. (mph)	Fall ht. (ft.)	Fire Y/N (dur)	Object Struck Description
Tennessee								
Brownsville	NATL77FR020	2/17/77	Derail	101	49	20	Y(4H)	RR Bed, RR Car
Fosterville	FRA C-5-72	NS	Derail	123	47	NS	NS	RR Bed, RR Car
N Johnsonville	N/RAR-82-4	12/28/81	HtoH Col.	2	25	45	N	Caboose
Pulaski	R/RAR-76-6	10/1/75	Derail	14	65	40	N	RR Bed, RR Car
Roddy	NATL79FR012	12/24/78	Derail	231	44	6	N	RR Bed, RR Car
Waverly	N/RAR-79-1	2/22/78	Derail	120	35	0	Y(6H)	RR Bed, RR Car
Texas								
Britton	NFTW79FR016	12/10/78	Derail	98	25	7	N	RR Bed, RR Car
Cotulla	N/RAR-74-3	12/1/73	HtoH Col.	2 T	40	0	Y(1.5H)	Train
Dallas	San Jose News	2/21/81	Derail	60	NS	50	Y(4H)	RR Bed, RR Car, Bridge
Garland	NFTW77FR007	3/20/77	Derail	44	NS	0	Y(NS)	RR Bed, RR Car
Houston	N/RAR-75-7	9/21/74	Yard Col.	503	20	0	Y(9H)	RR Cars
Houston	N/RAR-72-6	10/19/71	Derail	88	45	45	Y(5H)	RR Bed, RR Car
Marquez	NFTW79FR005	10/13/78	Derail	94	30	0	N	RR Bed, RR Car, Timber Brd?
Paxton	N/HZM-80-1	9/8/79	Derail	56	30	15	Y(NS)	RR Bed, RR Car

Continued on next page

Table A.7
Train Accidents

Location	Report Source	Date of Accident	Accident Description	No. of Vhcl	Acc. vel. (mph)	Fall ht. (ft.)	Fire Y/N (dur)	Object Struck Description
Texas (continued)								
Temple	N/RAR-83-08	3/17/83	HtoH Col.	8	35	NS	N	Freight Car
Tyler	NFTW79FR007	10/22/78	Derail	79	45	12	N	RR Bed, RR Car
Utah								
Lakeside	NDEN76FR111	6/25/76	Derail	52	NS	10	N	RR Bed, RR Car, Lake
Virginia								
Arlington	N/RAR-73-2	4/27/72	HtoH Col.	2 T	60	0	N	Train
Colonial Hghts	N/RAR-83-04	5/5/82	Derail	1	64	40	Y (8D)	RR Bed, RR Car
Crewe	N/RAR-82-3	11/28/81	HtoS Col.	3	27	NS	N	RR Car
Elma	N/RAR-79-4	12/3/78	Derail	12	79	NS	Y(NS)	RR Bed, RR Car
Franconia	N/RAR-71-1	1/27/70	Derail	1	65	NS	N	Embankment
Jarratt	N/RAR-76-11	5/5/76	Derail	58	72	0	N	RR Bed, RR Car
Rockfish	N/RAR-83-10	4/3/83	Derail	1	48	NS	N	Landslide

Continued on next page

Table A.7
Train Accidents

Location	Report Source	Date of Accident	Accident Description	No. of Vhcl	Acc. vel. (mph)	Fall ht. (ft.)	Fire Y/N (dur)	Object Struck Description
Washington								
Deer Park	NSEA79FR002	10/4/78	Derail	41	23	0	N	RR Bed, RR Car
Ephrata (Naylor)	NSEA79FR021	2/28/79	Derail	65	50	NS	N	RR Bed, RR Car
Kalama	NSEA76FR028	9/7/76	Derail	NS	52	35	N	RR Bed, RR Car, River
Kapowsin	NSEA79FR023	3/6/79	Brdg Fail	45	10	15	N	River, Bridge
Tacoma	NSEA79FR025	3/22/79	Derail	122	23	0	N	RR Bed, RR Car, RR Bridge
Tukailla	NS	10/8/77	HtoH Col.	2 T	50	NS	Y(NS)	Train
Wenatchee	N/RAR-76-1	8/6/74	Explosion	201	10	0	Y(NS)	NS
West Virginia								
Orleans Road	N/RAR-80-9	2/12/80	HtoH Col.	2 T	38	0	N	Train
South Ruffner	NDCA79FR028	2/4/79	Side Col.	2 T	78	5	N	Train
Welch	N/RAR-81-2	9/6/80	HtoS Col.	2	38	NS	NS	Freight Car

Continued on next page

Table A.7
Train Accidents

Location	Report Source	Date of Accident	Accident Description	No. of Vhcl	Acc. vel. (mph)	Fall ht. (ft.)	Fire Y/N (dur)	Object Struck Description
Wisconsin								
Columbus	NCHI79FR009	11/24/78	Derail	70	50	NS	N	RR Bed, RR Car
Cylon	FRA C-15-72	NS	Derail	95	45	NS	NS	RR Bed, RR Car
Franksville	NCHI79FR028	3/15/79	Derail	81	40	0	N	RR Bed, RR Car
Milawukee	NCHI79FR017	1/7/79	Derail	55	38	0	N	RR Bed, RR Car
Sturtevant	NCHI79FR024	2/12/79	Derail	84	40	NS	N	RR Bed, RR Car
Wyoming								
Dale Junction	NDEN79FR007	1/22/79	Derail	121	40	40	Y(56H)	RR Bed, RR Car
Granite	N/RAR-79-12	7/31/79	Derail	85	75	0	N	RR Bed, RR Car
Hermosa	N/RAR-81-3	10/16/80	HtoH Col.	2	40	NS	N	Caboose
Leroy	NDEN79FR002	11/3/78	Derail	92	60	0	N	RR Bed, RR Car
Ramsey	N/RAR-79-9	3/29/79	HtoH Col.	2 T	48	0	N	Train
Red Desert	NDEN77FR001	NS	Derail	66+	NS	NS	NS	RR Bed, RR Car
Sheridan	N/RAR-72-4	3/28/71	Yard COL.	14	15	0	N	RR Cars
Wamsutter	NDEN77FR007	2/23/77	Derail Side Col.	NS-T	67-54	0-0	N	RR Bed, RR Car, Train

APPENDIX B

List of Tables

		Page
B.1	Petroleum Industry Accident Data Summary, 1973-1981	B-3
B.2	Distribution of Velocities for Truck/Semitrailers Involved in Fatal and Injury Accidents in California, 1958-1967	B-5
B.3	Distribution of Estimated Original Vehicle Velocities for All Types of Accidents, North Carolina, 1979-1981	B-7
B.4	Distribution of Estimated Vehicle Impact Velocities for All Types of Accidents, North Carolina, 1979-1981	B-8
B.5	Distribution of Train Velocities at Rail-Highway Grade-Crossing Accident/Incidents Involving Motor Vehicles, 1975-1982	B-10
B.6	Summary of Objects Struck and Type of Accident for Accidents Involving U.S. Private and For-Hire Motor Carriers, 1973-1983	B-11
B.7	Objects Struck During California Accidents, 1975-1983	B-12
B.8	Objects Struck During California Accidents, Reordered According to Type of Accident, 1975-1983	B-15

APPENDIX B
Truck Accident Data

B.1 Introduction

This appendix summarizes both the highway accident data which form the basis for the distribution of accident scenarios and the estimates of the probability distributions used in the probabilistic analysis of future truck accidents involving the transport of spent nuclear fuel. The primary sources of data are the Bureau of Motor Carrier Safety (BMCS), American Petroleum Institute (API), California Highway Patrol (CHP), and the California Department of Transportation (CALTRANS) reports on highway accidents. In addition, a Sandia report on severe accidents was the source of fire duration distributions and estimates of the probability of a fire.

Section B.2 discusses the data used to estimate the truck accident rate. Section B.3 discusses the distributions of truck velocities. Section B.4 covers the distribution of train velocities used to analyze rail-highway grade crossing accidents. Section B.5 discusses the distribution of objects struck, and, finally, Sections B.6 and B.7 cover the fire accident data.

B.2 Truck Accident Rate

Information concerning truck accidents involving motor carriers of property that operate in interstate commerce is available in reports published by the BMCS of the U.S. Department of Transportation (DOT).[B.1-B.13] Truck accidents are defined by the BMCS as occurrences involving a motor vehicle operated by a motor carrier subject to the Federal Motor Carrier Safety Regulations (49 CFR 390-397) resulting in (1) the death of one or more human beings; (2) bodily injury to one or more persons who, as a result, receives medical treatment away from the scene of the accident; and/or (3) total damage to all property aggregating dollar damage at or above the dollar damage threshold limit based on actual cost or reliable estimates.

Prior to 1973, the BMCS tabulated only those truck accidents with damage of $250 or greater involving for-hire carriers, i.e., trucking firms that haul freight owned by another party. Since 1973, the BMCS has also tabulated

accidents involving private, i.e., firms using their own, or leased, vehicles as part of their commercial operation to transport their own goods, as well as accidents of for-hire carriers. However, since 1973, the total vehicle miles have not been included in the BMCS reports. The accident rate for the period 1960-1972, 2.48×10^{-6} accidents/vehicle-mile, is an estimate; however, (1) it is based on the experience some years ago, and (2) it is not clear what is defined as a truck. This definition is important because pickup trucks and vans, i.e., non tractor/semitrailer trucks, tend to have an accident rate closer to that of automobiles. Therefore, it was decided not to base the accident rate for this study on the BMCS data.

Another source of truck accident data is the database maintained by the API consisting of information supplied by petroleum industry companies. Accident data is available for the API for the period 1968 through 1981 for large trucks.[B.14-B.18] Although a precise definition of an accident is not included in the reports, an accident rate based on the API data was used in this study. The API accident rate data was judged to be more reliable because shipments involving hazardous materials are usually more tightly controlled than shipments involving non-hazardous materials. In addition, the API data was judged to be most applicable to spent fuel shipment because trucks that transport gasoline type products are of similar size and weight to trucks that transport spent fuel. The API data is expected to be conservative because the average trip length of a gasoline truck is less than 28 miles and involves all types of roads. This will result in a higher accident rate than an accident rate based on cross-country trips that involve primarily interstates.

To allow for the imposition of the national speed limit in 1973, only the data from 1973 through 1981 was used to estimate a truck accident rate. Table B.1 summarizes the API accident data for the years 1973 to 1981. The estimated accident rate, $5.94 \text{Ex} 10^{-6}$ accidents/truck-mile, is higher than the rate based on the BMCS data.

Table B.1
Petroleum Industry Accident Data Summary, 1973-1981[a/]

Year	No. of Compy.	No. of Trucks	No. of Accidents	Truck Miles x 1000	Accident Rate/ Truck-Mile
1973	73	20,046	3,804	508,783	$7.48\ 10^{-6}$
1974	73	20,147	3,151	469,804	$6.71\ 10^{-6}$
1975	69	29,071	4,089	779,260	$5.25\ 10^{-6}$
1976	70	22,748	3,528	585,609	$6.02\ 10^{-6}$
1977	69	21,508	2,784	519,446	$5.36\ 10^{-6}$
1978	68	19,113	2,562	404,748	$6.33\ 10^{-6}$
1979	63	21,414	2,889	467,939	$6.17\ 10^{-6}$
1980	62	21,970	2,391	455,324	$5.25\ 10^{-6}$
1981	81	21,158	2,445	465,571	$5.25\ 10^{-6}$
Total		197,175	27,643	4,656,484	$5.94\ 10^{-6}$
Avg/year		21,908	3,071	517,387	

a/ American Petroleum Institute.[B.14-B.18]

B.3 Distributions of Velocity for Truck Accidents

The velocity of the truck at the time of an accident is an important parameter in determining impact forces on cargos involved in highway accidents. This parameter, in combination with the angle of impact, is an estimate of the impact velocity of the cask at the time of the accident. The impact velocity, in combination with the cask orientation and the object struck or subsequent interaction of the truck with its environment after the accident begins, determines the forces and damage experienced by the cask. Thus, the distribution of truck velocities at the time of an accident is one of the necessary inputs into the probabilistic analysis of accidents involving spent fuel casks.

Considerable effort went into attempting to accumulate a database of accident data from past events which reasonably reflects what might be experienced by trucks transporting spent fuel casks in the future. To this end, annual reports on motor vehicle accidents, as accumulated by the CHP formed the basis for developing an appropriate collection of accident statistics.[B.19-B.29] Although data from several classifications of accidents have been reported, e.g., all injury accidents, injury truck accidents, and all fatal accidents, we chose to estimate the desired distribution of velocities on fatal and injury accidents involving truck/semitrailers.

The distribution of velocities covering the years 1958-1967 is given in Table B.2. An important question with regard to the use of the data in Table B.2 as a basis for estimating velocities for future truck accidents is whether the traffic conditions in the 1958-1967 time period is comparable to traffic conditions which can be expected to be experienced in the future. Prior to 1959 California highway speed limits were 55 mph for automobiles and 45 mph for trucks (defined as trucks with three or more axles and any truck or truck tractor pulling one or more trailers) and cars with trailers. In 1959 the motor vehicle code was changed to limit cars to 65 mph; however, trucks and cars with trailers were still limited to 45 mph except on highways with four or more lanes (at least two lanes in each direction), where the speed limit was 50 mph. In 1963, the motor vehicle code was changed to limit cars on

Table B.2
Distribution of Velocities for Truck/Semitrailers Involved in Fatal and Injury Accidents in California, 1958-1967[a/]

Velocity (mph)	Number of Accidents	Fractional Percent (%)	Cumulative Percent (%)
0	1,774	6.41	6.41
1-10	4,143	14.96	21.37
11-20	4,122	14.89	36.25
21-30	4,248	15.34	51.59
31-40	4,733	17.09	68.69
41-50	7,264	26.23	94.92
51-60	1,173	4.24	99.15
61-70	171	0.62	99.77
>70	63	0.23	100.00
Total	27,691	100.00	

a/ California Highway Patrol.[B.19-B.29]

freeways to 70 mph while trucks and cars with trailers were restricted to 50 mph on all highways.

The speed limits were again changed in 1967 to allow trucks and cars with trailers to travel up to 55 mph over all highways. These regulations remained in effect until superseded by the national speed limit in 1973. Because the speed limits during the 1958-1967 time period were lower than the present 55 mph limit for all vehicles, the velocities in Table B.2 may be biased towards lower velocities. However, by choosing fatal and injury accidents, rather than all accidents (including non injury accidents), this bias has been somewhat compensated for because injury and fatal accidents generally involve higher velocities.

Accident data from North Carolina[B.30] was used to estimate the effects of braking on impact velocity. Tables B.3 and B.4 summarize the distribution of velocities for accidents involving all types of vehicles resulting in fatalities, injuries, or property damage for the years 1979-1981. In Table B.3, the velocities are based on estimates of the original vehicle velocity while in Table B.4 the velocities are estimates of the velocity at impact. As discussed in Section 5.0, a comparison of these two distributions was used as a basis for adjusting the distribution of truck velocities for the effects of braking during the evolution of an accident prior to vehicle impact.

B.4 Distribution of Train Speeds at Rail-Highway Grade-Crossing Accidents

The U.S. DOT Federal Railroad Administration (FRA) defines rail-highway grade-crossing accidents as any impact between railroad on-track equipment and an automobile, bus, truck, motorcycle, bicycle, farm vehicle, or pedestrian at a highway-rail grade crossing in which the amount of damage done to railroad equipment is at least a specified damage threshold limit. If the impact causes damage to railroad equipment less than the dollar damage threshold limit, it is classified as an incident. Prior to 1975, the damage threshold limit was $750 and only rail-highway grade-crossing accidents were tabulated by the FRA.[B.34] In 1975, the threshold was increased to $1750 to account for

Table B.3
Distribution of Estimated Original Vehicle Velocities for All Types of Accidents, North Carolina, 1979-1981[a/]

Velocity (mph)	Year 1979	1980	1981	Total	Avg.	Fra. Pct. (%)	Cum. Pct. (%)
0	512	214	188	914	305	0.14	0.14
1-5	22,191	19,976	19,205	61,372	20,457	9.25	9.39
6-10	20,335	18,655	17,865	56,855	18,952	8.57	17.96
11-15	13,846	12,697	12,051	38,594	12,865	5.82	23.77
16-20	20,417	18,965	18,042	57,424	19,141	8.65	32.43
21-25	17,336	16,388	16,100	49,824	16,608	7.51	39.94
26-30	23,336	21,472	21,582	66,390	22,130	10.01	49.94
31-35	33,147	33,147	34,030	100,324	33,441	15.12	65.06
36-40	17,245	16,317	16,075	49,637	16,546	7.48	72.54
41-45	22,028	21,049	21,156	64,233	21,411	9.68	82.22
46-50	16,144	14,889	14,315	45,348	15,116	6.83	89.06
51-55	15,336	14,301	14,784	44,421	14,807	6.69	95.75
56-60	3,559	3,492	3,261	10,312	3,437	1.55	97.31
61-65	2,071	1,907	1,991	5,969	1,990	0.90	98.21
66-70	1,621	1,604	1,476	4,701	1,567	0.71	98.92
71-75	751	685	719	2,155	718	0.32	99.24
76-80	603	584	539	1,726	575	0.26	99.50
81-85	134	127	143	404	135	0.06	99.56
>85	1243	855	807	2,905	968	0.44	100.00
Not Stated[b/]	45,590	43,290	42,526	131,406	43,802	N/A	N/A

a/ University of North Carolina Highway Safety Research Center.[B.30]

b/ Excluded from percentage calculations.

Table B.4
Distribution of Estimated Vehicle Impact Velocities for All Types of Accidents, North Carolina, 1979-1981[a/]

Velocity (mph)	Year 1979	1980	1981	Total	Avg.	Fra. Pct. (%)	Cum. Pct. (%)
0	818	413	412	1643	548	0.26	0.26
1-5	30,831	29,125	29,181	89,137	29,712	14.08	14.34
6-10	29,236	28,273	28,026	85,535	28,512	13.51	27.85
11-15	20,279	19,905	19,811	59,995	19,998	9.48	37.33
16-20	26,955	26,958	26,423	80,336	26,779	12.69	50.02
21-25	18,904	18,386	18,619	55,909	18,636	8.83	58.85
26-30	23,914	23,301	23,023	70,238	23,413	11.09	69.94
31-35	19,368	19,123	18,706	57,197	19,066	9.03	78.98
36-40	15,991	15,091	14,589	45,671	15,224	7.21	86.19
41-45	11,589	10,866	10,554	33,009	11,003	5.21	91.41
46-50	9,754	9,249	8,726	27,729	9,243	4.38	95.79
51-55	4,936	4,945	4,730	14,611	4,870	2.31	98.10
56-60	2,056	2,028	1,861	5,945	1,982	0.94	99.03
61-65	818	678	691	2,187	729	0.35	99.38
66-70	697	687	673	2,057	686	0.32	99.71
71-75	250	241	239	730	243	0.12	99.82
76-80	262	251	205	718	239	0.11	99.93
81-85	58	55	52	165	55	0.03	99.96
>85	94	87	73	254	85	0.04	100.00
Not Stated[b/]	60,635	50,952	50,261	161,848	53,949	N/A	N/A

a/ University of North Carolina Highway Safety Research Center.[B.30]

b/ Excluded from percentage calculations.

the effects of inflation. Also, at this time, the FRA started to include rail-highway grade-crossing incidents in their grade crossing accident data.[B.31-B.38] This resulted in a substantial increase in the reported number of impacts between trains and other mobile objects in the grade-crossing accident data after 1975. Because of the difference in types of events recorded, only the rail-highway grade-crossing accident data after 1974 was used.

Table B.5 presents the distribution of train velocities at grade-crossing accidents/incidents involving motor vehicles. The reliability of the train accident/incident velocity at rail-highway grade-crossings can be considered good because railroad locomotives are equipped with accident recorders to record the train's velocity prior to, during, and after the accident, although on a very crude scale. The recorded train velocity while probably no more accurate than 5 to 10 mph, is certainly more reliable than after-the-fact velocity estimates made by investigating officers at highway accident sites.

B.5 Highway Accident Object Frequency

Data were collected from several sources to estimate the frequency of impact with particular objects. Two of the primary data sources were the CALTRANS for all vehicles and the BMCS for trucks.

Table B.6 presents the truck highway accident data obtained from the BMCS for the years 1973 through 1983.[B.4-B.13] The object struck (for collision accidents) or accident type (for noncollision accidents) are categories as given by the BMCS. These categories are divided into nonfixed-object collisions, fixed-object collisions (for collision accidents), ran-off-road accidents, impact-with-roadbed accidents, or other noncollision accidents (for noncollision accidents). The BMCS data were divided this way in order to provide subcategories that would correspond with those defined by the CALTRANS in their reports on objects struck during highway accidents.

Table B.7 presents the primary objects struck during highway accidents, as reported by the CALTRANS for all vehicles for 1975 through 1983.[B.39-B.47] All object struck subcategories are as defined by the CALTRANS and the object numbering system follows the CALTRANS convention.

Table B.5
Distribution of Train Velocities at Rail-Highway Grade-Crossing Accident/Incidents Involving Motor Vehicles, 1975-1982[a/]

Velocity (mph)	Year 1975	1976	1977	1978	1979	1980	1981	1982	Total	Fra. Pct (%)	Cum. Pct. (%)
0-9	3,887	3,793	3,923	4,098	3,788	3,224	2,715	2,125	27,553	33.79	33.79
10-19	2,221	2,428	2,339	2,431	2,303	1,950	1,724	1,364	16,765	20.56	54.35
20-29	1,919	2,098	2,152	2,097	2,042	1,589	1,459	1,257	14,611	17.92	72.27
30-39	1,365	1,511	1,600	1,582	1,457	1,277	1,061	935	10,788	13.23	85.50
40-49	960	1,026	1,086	1,106	985	887	825	742	7,617	9.34	94.84
50-59	391	433	419	382	351	330	279	294	2,879	3.53	98.37
60-69	109	127	119	95	87	96	94	97	824	1.01	99.38
70-79	61	59	68	62	51	49	55	56	461	0.56	99.94
80-89	4	6	8	2	2	2	4	1	29	0.04	99.98
>90	8	1	2	2	1	0	1	2	17	0.02	100.00
Total[b/]	10,925	11,482	11,716	11,857	11,067	9,402	8,222	6,873	81,544	100.00	

a/ U.S. Department of Transportation, Federal Railroad Administration, Office of Safety, Rail-Highway Grade-Crossing Accident/Incidents Bulletins.[B.34-B.41]

b/ Excludes accidents of unknown velocities.

Table B.6
Summary of Objects Struck and Type of Accident for Accidents Involving U.S. Private and For-Hire Motor Carriers, 1973-1983[a/]

Type of Accident	Total	Avg.[b/]	Fra. Pct. (%)	Remarks
I. Nonfixed Object Collision				
w/ Commercial Truck	42,848	3,895	12.88	
w/ Automobile	143,573	13,052	43.15	
w/ Pedestrian	4,493	408	1.35	
w/ Bus	1,477	134	0.44	
w/ Train	2,575	234	0.77	
w/ Bicyclist	1,259	114	0.38	
w/ Animal	2,111	192	0.63	
w/ Motorcycle	2,680	244	0.81	
w/ Other or Not Specified	16,157	1,469	4.86	Note 1
Subtotal	217,173	19,743	65.26	
II. Fixed Object Collision	29,476	2,680	8.86	Note 1
Collision Accidents Subtotal	246,649	22,423	74.12	
III. Ran Off Road	30,104	2,737	9.05	Note 1
IV. Impact with Roadbed				
Jackknife	18,184	1,653	5.46	
Overturn	27,792	2,527	8.35	
Subtotal	45,976	4,180	13.82	
V. Other Noncollision Accidents				
Separation of Units	1,033	93.9	0.31	
Fire	3,219	293	0.97	
Cargo Loss/Spillage	1,433	130	0.43	
Cargo Shift	1,139	104	0.34	
Other or Not Specified	3,213	292	0.97	
Subtotal	10,037	912	3.02	
Noncol. Accidents Subtotal	86,117	7,829	25.88	
Total Accidents	332,766	30,251	100.00	

a/ U.S. Department of Transportation, Bureau of Motor Carrier Safety. B.4-B.13

b/ Based on 11 year period.

Note 1: Object distribution from California TASAS accident survey, see Table B.8.

Table B.7
Objects Struck During California Accidents, 1975-1983[a/]

Object Struck		Total	Avg.[b/]	Fra. Pct. (%)
1.	Side of Bridge Railing	9,473	1,053	0.82
2.	End of Bridge Railing	1,689	188	0.15
3.	Pier, Column, Abutment	810	90	0.07
4.	Bottom of Structure (Overhead Bridge Structure)	639	71	0.06
5.	Bridge End Post in Gore (Older Bridge w/Protective Island)	275	30.6	0.02
10.	Light or Signal Pole	8,384	932	0.72
11.	Utility Pole	8,140	904	0.70
12.	Pole (Type Note Stated)	454	50	0.04
13.	Traffic Sign/Sign Post	9,687	1,076	0.83
14.	Other Signs Not Traffic	333	37	0.03
15.	Guardrail	25,354	2,817	2.18
16.	Barrier	41,432	4,604	3.57
17.	& 30. Wall (Concrete/Wood/Sound)	3,751	417	0.32
18.	Dike or Curb	69,134	7,682	5.96
19.	Traffic Island	2,590	288	0.22
20.	Raised Bars (Delineation Bars, as Traffic Islands w/o Curb)	67	7.4	0.01
21.	Concrete Object (Headwall, Drop Inlet)	921	102	0.08
22.	Guidepost, Culvert, Postmile Marker	9,020	1,002	0.78
23.	Cut Slope or Embankment	22,403	2,489	1.93
24.	Over Embankment	12,758	1,418	1.10
25.	In Water	45	5.0	0.004
26.	Drainage Ditch	7,850	872	0.68
27.	Fence	13,701	1,522	1.18
28.	Trees	8,392	932	0.72
29.	Plants	5,111	568	0.44
40.	Natural Material on Road	1,785	198	0.15
41.	Temporary Barricades, Cones	1,337	149	0.12
42.	Other Object on Road	10,517	1,169	0.91
43.	Other Object off Road	10,153	1,128	0.87
44.	Overturned	61,848	6,872	5.33
45.	Crash Cushion	1,199	133	0.10
98.	Unknown Object Struck	975	108	0.08
99.	No Object Involved	9,386	1,043	0.81
00.	Other Vehicle	801,256	89,028	69.02

Table B.7 Continued

Object Struck	Total	Avg.[b/]	Fra. Pct. (%)
Total Primary Object Struck	1,160,869	128,985	100.00
XX. Not Stated	180	20	N/A
YY. Not Applicable	239,655	26,628	N/A
ZZ. Invalid Code	164	18	N/A
Total Accidents	1,165,097	129,455	N/A

a/ TASAS Selective Record Retrieval.[B.39-B.47]

b/ Based on 9 year period.

N/A Not applicable.

The CALTRANS accident data were reordered according to the accident categories defined in Table B.6. The result is Table B.8. Certain objects in Table B.8 were combined because of the similarity of these objects when considered in structural analysis calculations. The BMCS and the CALTRANS data on the object frequencies were combined to derive the probability of occurrences of the different accident scenarios.

B.6 Truck Fire Duration Distributions

The thermal response of the cask during a truck fire depends on the temperature of the fire, location of the fire relative to the cask and the duration of the fire. The type and amount of combustible materials will significantly affect the duration of a fire. Thus, the fire duration distribution will vary for different accident scenarios. For example, a fire involving a collision with a tanker truck can be expected to last longer than a fire involving a collision with an automobile or a collision with a noncombustible fixed object. To assess the probabilities of a truck cask's experiencing different thermal response levels, five fire duration distributions were developed. These distributions were associated with automobile collisions, truck collisions, collisions with fixed objects, other collisions including overturns and jackknifing, and noncollision fires. The basis for these distributions was the fire duration program developed by Sandia.[B.48] These distributions are summarized in Table 5.5.

B.7 Probability of Fire

Not all truck accidents will involve a fire; thus it is necessary to estimate the probability of a fire given an accident. The likelihood of a fire can be expected to vary between accident scenarios. Several sources provided statistical information for several types of accidents.[B.1-B.13,B.48] The probabilities of a fire given each of the different accident scenarios used in this study and listed in Table 5.9, are based on the statistics presented in the Sandia report on severe accidents.[B.48]

Table B.8
Objects Struck During California Accidents
Reordered According to Type of Accident, 1975-1983[a/]

Type of Accident	Total	Avg.[b/]	Fra. Pct. (%)	Remarks
I. Nonfixed Object Collision				
40. Natural Material on Road	1,785	198	0.15	
41. Temporary Barricades, Cones	1,337	149	0.12	
42. Other Object on Road	10,517	1169	0.91	
98. Unknown Object Struck	975	108	0.08	
00. Other vehicle	801,256	8,9028	69.02	
Subtotal	815,870	9,0652	70.28	
II. Fixed Object Collision				
1-2. Side or End of Bridge Railing	11,162	1,240	0.96	Note 1
3. Pier, Column, Abutment	810	90	0.07	Note 2
4. Bottom of Structure	639	71	0.06	
5. Bridge End Post in Gore	275	30.6	0.02	
10-12. Light, Signal, Utility or Other Type Pole	16,978	1,886	1.46	
13-14. Traffic Sign/Sign Post or Other Signs	10,020	1,113	0.86	
15. Guardrail	25,354	2,817	2.18	
16. Barrier	41,432	4,604	3.57	
17&30. Wall (Concrete/Wood/Sound)	3,751	417	0.32	
18-20. Dike, Curb, Traffic Island or Raised Bars	71,791	7,977	6.18	
21. Concrete Object (Headwall, Drop Inlet)	921	102	0.08	
22. Guidepost, Culvert, Postmile Marker	9,020	1,002	0.78	
45. Crash Cushion	1,199	133	0.10	
Subtotal	193,352	21,484	16.66	
Collision Accidents Subtotal	1,009,222	112,136	86.94	
III. Ran Off Road				
23. Cut Slope or Embankment	22,403	2,489	1.93	Note 3
24. Over Embankment	12,758	1,418	1.10	Note 3
25. In Water	45	5.0	0.004	
26. Drainage Ditch	7,850	872	0.68	
27. Fence	13,701	1,522	1.18	
28. Trees	8,392	932	0.72	
29. Plants	5,111	568	0.44	
43. Other Object off Road	10,153	1,128	0.87	
Subtotal	80,413	8,935	6.93	

Table B.8 Continued

Type of Accident	Total	Avg.[b/]	Fra. Pct. (%)	Remarks
IV. Impact with Roadbed				
44. Overturned	61,848	6,872	5.33	
V. Other Noncollision Accidents				
99. No Object Involved	9,386	1,043	0.81	
Noncollision Accidents Subtotal	151, 647	16,850	13.06	
Total Accidents	1,160,869	128,985	100.00	

All LLNL calculations are based on static analysis. Static force is defined as ultimate static force at which complete collapse of object occurs.

a/ TASAS Selective Record Retrieval.[B.39-B.47]

b/ Based on 9 year period.

Note 1 Assume worst case that truck goes off bridge. Distributions of bridge heights and surfaces below bridges determined from Engineering Computer Corporation (ECC) survey in Appendix D.

Note 2 Distribution of bridge column size determined from ECC survey in Appendix D.

Note 3 Distribution of soil types and surfaces determined from ECC survey in Appendix D.

B.8 References

B.1 1969 Accidents of Large Motor Carriers of Property, Bureau of Motor Carrier Safety, Federal Highway Administration, U.S. Department of Transportation, Washington, DC, December 1970.

B.2 1970 Accidents of Large Motor Carriers of Property, Bureau of Motor Carrier Safety, Federal Highway Administration, U.S. Department of Transportation, Washington, DC, March 1972.

B.3 1971-1972 Accidents of Large Motor Carriers of Property, Bureau of Motor Carrier Safety, Federal Highway Administration, U.S. Department of Transportation, Washington, DC, May 1974

B.4 1973 Accidents of Motor Carriers of Property, Bureau of Motor Carrier Safety, Federal Highway Administration, U.S. Department of Transportation, Washington, DC, July 1975.

B.5 1974 Accidents of Motor Carriers of Property, Bureau of Motor Carrier Safety, Federal Highway Administration, U.S. Department of Transportation, Washington, DC, 1975.

B.6 1975 Accidents of Motor Carriers of Property, Bureau of Motor Carrier Safety, Federal Highway Administration, U.S. Department of Transportation, Washington, DC, 1976.

B.7 1976 Accidents of Motor Carriers of Property, Bureau of Motor Carrier Safety, Federal Highway Administration, U.S. Department of Transportation, Washington, DC, October 1977.

B.8 1977 Accidents of Motor Carriers of Property, Bureau of Motor Carrier Safety, Federal Highway Administration, U.S. Department of Transportation, Washington, DC, May 1980.

B.9 1978 Accidents of Motor Carriers of Property, Bureau of Motor Carrier Safety, Federal Highway Administration, U.S. Department of Transportation, Washington, DC, May 1980.

B.10 1979 Accidents of Motor Carriers of Property, Bureau of Motor Carrier Safety, Federal Highway Administration, U.S. Department of Transportation, Washington, DC, 1980.

B.11 1980-1981 Accidents of Motor Carriers of Property, Bureau of Motor Carrier Safety, Federal Highway Administration, U.S. Department of Transportation, Washington, DC, August 1982.

B.12 1982 Accidents of Motor Carriers of Property, Bureau of Motor Carrier Safety, Federal Highway Administration, U.S. Department of Transportation, Washington, DC, May 1983.

B.13 1983 Accidents of Motor Carriers of Property, Bureau of Motor Carrier Safety, Federal Highway Administration, U.S. Department of Transportation, Washington, DC, October 1984.

B.14 Summary of Motor Vehicle Accidents in the Petroleum Industry for 1977, American Petroleum Institute, Washington, DC, May 1978.

B.15 Summary of Motor Vehicle Accidents in the Petroleum Industry for 1978, American Petroleum Institute, Washington, DC, August 1979.

B.16 Summary of Motor Vehicle Accidents in the Petroleum Industry for 1979, American Petroleum Institute, Washington, DC, June 1980.

B.17 Summary of Motor Vehicle Accidents in the Petroleum Industry for 1980, American Petroleum Institute, Washington, DC, September 1981.

B.18 Summary of Motor Vehicle Accidents in the Petroleum Industry for 1981, American Petroleum Institute, Washington, DC, August 1982.

B.19 1957 Annual Statistical Report, Department of California Highway Patrol, Sacramento, CA, May 1958.

B.20 1958 Annual Statistical Report, Department of California Highway Patrol, Sacramento, CA, May 1959.

B.21 1959 Annual Statistical Report, Department of California Highway Patrol, Sacramento, CA, May 1960.

B.22 1960 Annual Statistical Report, Department of California Highway Patrol, Sacramento, CA, May 1961.

B.23 1961 Annual Statistical Report, Department of California Highway Patrol, Sacramento, CA, May 1962.

B.24 1962 Traffic Accident Statistics, Department of California Highway Patrol, Sacramento, CA, May 1963.

B.25 1963 Traffic Accident Statistics, Department of California Highway Patrol, Sacramento, CA, May 1964.

B.26 1964 Traffic Accident Statistics, Department of California Highway Patrol, Sacramento, CA, May 1965

B.27 1965 Traffic Accident Statistics, Department of California Highway Patrol, Sacramento, CA, April 1966.

B.28 1966 Report of Fatal and Injury Motor Vehicle Traffic Accidents, Department of California Highway Patrol, Sacramento, CA, July 1967.

B.29 1967 Report of Fatal and Injury Motor Vehicle Traffic Accidents, Department of California Highway Patrol, Sacramento, CA, July 1968.

B.30 E. G. Hamilton, Single, Variable Tabulations for 1979-1981 North Carolina Accidents, University of North Carolina Highway Safety Research Center, Chapel Hill, NC, September 1977.

B.31 Rail-Highway Grade-Crossing Accidents/Incidents Bulletin for the Year Ended December 31, 1975, Office of Safety, Federal Railroad Administration, U.S. Department of Transportation, Washington, DC.

B.32 Rail-Highway Grade-Crossing Accidents/Incidents Bulletin for the Year Ended December 31, 1976, Office of Safety, Federal Railroad Administration, U.S. Department of Transportation, Washington, DC, December 1977.

B.33 Rail-Highway Grade Crossing Accident/Incident Bulletin No. 43, Calendar Year 1977, Office of Safety, Federal Railroad Administration, U.S. Department of Transportation, Washington, DC, July 1978.

B.34 Rail-Highway Crossing Accident/Incident and Inventory Bulletin No. 1, Calendar Year 1978, Office of Safety, Federal Railroad Administration, U.S. Department of Transportation, Washington, DC, October 1979.

B.35 Rail-Highway Crossing Accident/Incident and Inventory Bulletin No. 2, Calendar Year 1979, Office of Safety, Federal Railroad Administration, U.S. Department of Transportation, Washington, DC, September 1980.

B.36 Rail-Highway Crossing Accident/Incident and Inventory Bulletin No. 3, Calendar Year 1980, Office of Safety, Federal Railroad Administration, U.S. Department of Transportation, Washington, DC, June 1981.

B.37 Rail-Highway Crossing Accident/Incident and Inventory Bulletin No. 4, Calendar Year 1981, Office of Safety, Federal Railroad Administration, U.S. Department of Transportation, Washington, DC, June 1982.

B.38 Rail-Highway Crossing Accident/Incident and Inventory Bulletin No. 5, Calendar Year 1982, Office of Safety, Federal Railroad Administration, U.S. Department of Transportation, Washington, DC, June 1983.

B.39 TASAS Selective Record Retrieval Statewide Accident Summary for Year 1975, State of California Department of Transportation, Sacramento, CA, October 1979.

B.40 TASAS Selective Record Retrieval Statewide Accident Summary for Year 1976, State of California Department of Transportation, Sacramento, CA, October 1979.

B.41 TASAS Selective Record Retrieval Total Statewide Accidents for Year 1977, State of California Department of Transportation, Sacramento, CA, May 1978.

B.42 TASAS Selective Record Retrieval Statewide Accident Summary for Year 1978, State of California Department of Transportation, Sacramento, CA, April 1979.

B.43 TASAS Selective Record Retrieval, Summary Only, All Accidents for the Year 1978, State of California Department of Transportation, Sacramento, CA, August 1984.

B.44 TASAS Selective Record Retrieval, Summary Only, All Accidents for the Year 1979, State of California Department of Transportation, Sacramento, CA, August 1984.

B.45 TASAS Selective Record Retrieval Statewide Accidents for Year 1981, State of California Department of Transportation, Sacramento, CA, April 1982.

B.46 TASAS Selective Record Retrieval Statewide Summary 1982, State of California Department of Transportation, Sacramento, CA, May 1983.

B.47 TASAS Selective Record Retrieval Statewide Summary 1983, State of California Department of Transportation, Sacramento, CA, April 1984.

B.48 R. K. Clarke, et al., Severities of Transportation Accidents, Sandia National Laboratory, Albuquerque, NM, SAND77-0001, 1977.

APPENDIX C

List of Tables

		Page
C.1	Railroad Accident Rate, 1975-1982	C-2
C.2	Distribution of Types of Railroad Accidents, 1975-1982	C-5
C.3	Distribution of Train Velocities, Collisions, Main Line, 1979-1982	C-6
C.4	Distribution of Train Velocities, Derailments, Main Line, 1979-1982	C-7
C.5	Distribution of Train Velocities for Rail-Highway Grade-Crossing Accidents/Incidents Involving Motor Vehicles, 1975-1982	C-8
C.6	Distribution of Train Velocities, Other Accidents, Main Line, 1979-1982	C-9
C.7	Railroad Fires Survey Results	C-11

APPENDIX C
Railroad Accident Data

C.1 Introduction

This appendix summarizes both the railroad accident data which form the basis for the estimates of accident scenarios and the probability distributions used in the probabilistic analysis of future train accidents involving the transport of spent nuclear fuel. The primary sources of data were the statistical reports of railroad accidents produced by the Office of Safety, Federal Railroad Administration (FRA) of the U. S. Department of Transportation (DOT).[C.1-C.7] A Sandia report on severe accidents was the source of estimates of the probability of fire duration distributions.[C.8] Section C.2 discusses the data used to estimate the railroad accident rate and distribution of types of accidents. Section C.3 discusses the distributions of train velocity at the time of an accident; Section C.4 discusses the fire duration distribution.

C.2 Railroad Accident Rate

Federal law (49 CFR 225) requires all railroads to file monthly accident/incident reports with the Office of Safety, FRA of the U. S. DOT. A railroad is defined, by regulation, as any system of surface transportation of persons or property over rails. It includes line-haul freight and passenger railroads; switching and terminal railroads; and passenger-carrying railroads including rapid transit, commuter, scenic, street, subway, elevated cable, and cog railways.

Train accidents are defined by the FRA Office of Safety as any event involving on-track railroad equipment that results in damage to railroad on-track equipment, signals, track or track structure, and roadbed at or exceeding the dollar damage threshold. Prior to 1975, the threshold was $750. Since 1975 this limit has been adjusted, to account for inflation, from $1750 in 1975 to $4100 in 1982, the last year available for use in this study. Although initially adjusted biennially (i.e., every two years), since 1977 the adjustment has been annual. The yearly threshold limits are included in Table C.1.

Table C.1
Railroad Accident Rate, 1975-1982[a/]

Year	Train Miles X 1000	Number of Accidents	Accident Rate	Damage Threshold
1975	755,033	8,041	$1.06E\ 10^{-5}$	$1,750.00
1976	774,764	10,248	$1.32E\ 10^{-5}$	$1,750.00
1977	750,042	10,362	$1.38E\ 10^{-5}$	$2,300.00
1978	751,964	11,277	$1.50E\ 10^{-5}$	$2,600.00
1979	763,429	9,740	$1.28E\ 10^{-5}$	$2,900.00
1980	717,662	8,451	$1.18E\ 10^{-5}$	$3,200.00
1981	676,216	5,781	$8.55E\ 10^{-6}$	$3,700.00
1982	573,369	4,589	$8.00E\ 10^{-6}$	$4,100.00
Total	5,762,479	68,489	$1.19E\ 10^{-5}$	

a/ U.S. Department of Transportation, Federal Railroad Administration, Accident/Incident Bulletins[C.1-C.7]

In addition to train accidents, the FRA Office of Safety compiles and reports statistics on two related events: train incidents, and non-train incidents. Train incidents are defined as events involving on-track railroad equipment that result in the reportable death and/or injury or illness of one or more persons, but do not result in damage at or beyond the damage threshold, as defined in the previous paragraph. Non-train incidents are defined as events which result in a reportable death, injury, or illness arising from the operation of a railroad but not from the movement of railroad on-track equipment.

Damage to casks containing spent nuclear fuel will necessarily involve severe accidents (hence significant damage); thus, for this project, train accidents formed the basis for estimating railroad accident rates. Because of the effect of the damage threshold levels on the reported accidents, data from the period 1975 to 1982 were used to estimate the accident rate used in this study. The estimated railroad accident rate, 1.19×10^{-5} accidents/train-mile/year, is the ratio of the number of reported accidents to the total miles for the 1975 to 1982 period.

Table C.1 presents the train mileage and number of accidents, as well as rate and damage threshold for each year during 1975 to 1982. Train-miles, for this report, is defined as the sum of the locomotive miles, yard switching miles, and motor train miles as tabulated for each year by the FRA. The FRA defines a locomotive mile as the movement under its own power of a locomotive the distance of one mile whether coupled or without cars. This item covers miles run by locomotives in road services and in train and yard switching service. Switching miles are computed at the rate of 6 miles/hour for the time actually engaged in such service. A motor train-mile is a movement under its own power of a motor train a distance of one mile.

Accident severity varies between accidents, thus the level of damage that a cask might experience during an accident depends on the type of accident. Therefore, train accidents were subdivided into four types--collisions, derailments, rail-highway grade-crossing accidents, and other types of accidents. Data relevant to this distribution, derived from the FRA reports,

is given in Table C.2. Again, the distribution of accident types is based on the accidents during the 1975-1982 period. The important statistics are the percentages, for each type of accident, of all accidents presented in the bottom row of the table. For example, 13.41% of the train accidents were collisions.

Approximately 36% of the collisions involved derailment of at least one car.[C.8] These were grouped with the original derailment accidents. Derailment accidents were further partitioned into accident scenarios based on the events following the derailment. Accident scenarios considered included the car(s) falling over a bridge or embankment, hitting a slope or a structure, or rolling over. Categorization of derailment accidents into scenarios was not found in the literature. Thus, a distribution was developed based on similar statistics for truck accidents. This distribution is included in Fig. 2-5. To distinguish between the severity of accident scenarios, some of the accident scenarios were further subdivided, e.g., derailments involving a car's hitting a structure were subdivided into hitting small and large columns, abutments, and other accidents. Categorization of accidents into these types of scenarios was based on the Eggers study.[C.9]

C.3 Impact Velocity Distribution

The forces imposed on the cask at the moment of impact during an accident depend on the impact velocity of the cask or impacting object. Since impact velocity is a function of velocity and angle of impact, it is necessary to estimate the distributions of train velocities. Information on the train velocity at the time of an accident was derived, again, from the FRA data. Reliability of these statistics can be considered good since railroad locomotives are equipped with recorders to record the train's velocity prior to, during, and after the accident. The scale, although crude, is more reliable than the velocity estimates made by investigating officers at highway accident sites.

Distributions of train velocities based on accidents occurring on main lines during 1979 to 1982 are summarized in Tables C.3 through C.6 for

Table C.2
Distribution of Types of Railroad Accidents, 1975-1982[a/]

Year	Train Collisions	Train Derailments	Rail-Highway Grade-Xing Accidents	Other Accidents	Total Accidents	Accident Damage Threshold
1975	1,002	6,328	248	463	8,041	$1,750.00
1976	1,370	7,934	352	592	10,248	$1,750.00
1977	1,362	8,073	323	604	10,362	$2,300.00
1978	1,476	8,763	286	752	11,277	$2,600.00
1979	1,425	7,482	248	585	9,740	$2,900.00
1980	1,201	6,442	246	562	8,451	$3,200.00
1981	776	4,366	199	440	5,781	$3,700.00
1982	572	3,383	178	456	4,589	$4,100.00
Total	9,184	52,771	2,080	4,454	68,489	
Fra. Pct.(%)	13.41	77.05	3.04	6.50		

a/ U.S. Department of Transportation, Federal Railroad Administration, Accident/Incident Bulletins[C.1-C.7]

Table C.3
Distribution of Train Velocities, Collisions, Main Line, 1979-1982[a/]

Velocity (mph)	Year 1979	1980	1981	1982	Total	Fra. Pct. (%)	Cum. Pct. (%)
1-10	136	112	85	59	392	46.12	46.12
11-20	70	46	32	34	182	21.41	67.53
21-30	44	31	17	25	117	13.76	81.29
31-40	23	26	24	19	92	10.82	92.12
41-50	9	19	10	9	47	5.53	96.65
51-60	4	6	4	0	14	1.65	99.29
61-70	2	1	0	0	3	0.35	99.65
71-80	1	1	0	0	2	0.24	99.88
81-90	0	0	0	0	0	0.00	99.88
91	0	1	0	0	1	0.12	100.00
Total[b/]	289	243	172	146	850	100.00	

a/ U.S. Department of Transportation, Federal Railroad Administration, Accident/Incident Bulletins[C.1-C.7]

b/ Excludes accidents of unknown velocities

Table C.4
Distribution of Train Velocities, Derailments, Main Line, 1979-1982[a/]

Velocity (mph)	Year 1979	1980	1981	1982	Total	Fra. Pct. (%)	Cum. Pct. (%)
1-10	1,736	1,278	793	587	4,394	40.42	40.42
11-20	841	634	416	359	2,250	20.70	61.12
21-30	783	616	444	340	2,183	20.08	81.20
31-40	325	333	238	195	1,091	10.04	91.24
41-50	202	191	137	129	659	6.06	97.30
51-60	64	60	54	61	239	2.20	99.50
61-70	19	6	10	6	41	0.38	99.88
71-80	6	1	2	1	10	0.09	99.97
81-90	1	1	0	1	3	0.03	100.00
91	0	0	0	0	0	0.00	100.00
Total[b/]	3,977	3,120	2,094	1,679	10,870	100.00	

a/ U.S. Department of Transportation, Federal Railroad Administration, Accident/Incident Bulletins[C.1-C.7]

b/ Excludes accidents of unknown velocities

Table C.5
Distribution of Train Velocities for Rail-Highway Grade-Crossing Accidents/Incidents Involving Motor Vehicles, 1975-1982[a/]

Velocity (mph)	Year 1975	1976	1977	1978	1979	1980	1981	1982	Total	Fra. Pct. (%)	Cum. Pct. (%)
0-9	3,887	3,793	3,923	4,098	3,788	3,224	2,715	2,125	27,553	33.79	33.79
10-19	2,221	2,428	2,339	2,431	2,303	1,950	1,729	1,364	16,765	20.56	54.35
20-29	1,919	2,098	2,152	2,097	2,042	1,587	1,459	1,257	14,611	17.92	72.27
30-39	1,365	1,511	1,600	1,582	1,457	1,277	1,061	935	10,788	13.23	85.50
40-49	960	1,026	1,086	1,106	985	887	825	742	7,617	9.34	94.84
50-59	391	433	419	382	351	330	279	294	2,879	3.53	98.37
60-69	109	127	119	95	87	96	94	97	824	1.01	99.38
70-79	61	59	68	62	51	49	55	56	461	0.56	99.94
80-89	4	6	8	2	2	2	4	1	29	0.04	99.98
>90	8	1	2	2	1	0	1	2	17	0.02	100.00
Total[b/]	10,925	11,482	11,716	11,857	11,067	9,402	8,222	6,873	81,544	100.00	

a/ U.S. Department of Transportation, Federal Railroad Administration, Office of Safety, Rail-Highway Grade-Crossing Accident/Incidents Bulletins[B.34-B.41]

b/ Excludes accidents of unknown velocities

Table C.6
Distribution of Train Velocities, Other Accidents, Main Line, 1979-1982[a/]

Velocity (mph)	Year 1979	1980	1981	1982	Total	Fra. Pct. (%)	Cum. Pct. (%)
1-10	83	83	60	59	285	17.59	17.59
11-20	73	46	53	56	228	14.07	31.67
21-30	104	93	59	59	315	19.44	51.11
31-40	89	104	58	63	314	19.38	70.49
41-50	72	65	64	61	262	16.17	86.67
51-60	35	38	26	23	122	7.53	94.20
61-70	13	16	7	13	49	3.02	97.27
71-80	7	9	14	7	37	2.28	99.51
81-90	0	1	3	2	6	0.37	99.88
91	0	0	0	2	2	0.12	100.00
Total[b/]	476	455	344	345	1,620	100.00	

a/ U.S. Department of Transportation, Federal Railroad Administration, Accident/Incident Bulletins[C.1-C.7]

b/ Excludes accidents of unknown velocities

collisions, derailments, highway grade-crossing accidents, and other accidents respectively. The percentages and cumulative percentages shown in the bottom two rows of each table were used to estimate probability distributions for train velocities. The estimation procedure is discussed in Appendix G.

C.4 Probabilities of Fire and Fire Duration Distributions for Train Accidents

There is very little useful data regarding the occurrence of fires and the properties of the fire, such as duration, given a train accident. Table C.7 presents the results of surveys of train fires, compiled by the National Fire Protection Association for the years 1976-78 and 1982-83.[C.10,C.11] Over this time, for the railroads surveyed, approximately 1.24% of all railroad fires occur as a result of a collision or derailment. This is interpreted probabilistically as the (conditional) probability, given a fire, that the cause of the fire is either a collision or derailment. On the other hand, the probability of interest for this study is the (conditional) probability, given a collision (or a derailment), that a fire also occurs. To derive the latter probability from the former, it is necessary to have some estimate of the probability of a fire given an accident. The necessary data to estimate this probability was not found. Therefore, the Sandia study estimate of the probabilities of a fire's occurring, given an accident scenario was used.[C.8]

No information was found regarding the duration of fires resulting from train accidents. Therefore, the simulated estimates for fire duration as developed in the Sandia study were used.[C.8]

Table C.7
Railroad Fires Survey Results[a/]

Category	Year 1976	1977	1978	1982	1983	Total	Avg.	Pct.of Total(%)
Class I Railroads Surveyed:	22	16	16	NA	22	76	19.0	N/A
Trackage Surveyed (miles):	129,382	116,405	94,509	NA	NA	340,296	113,432	N/A
Total Class I Trackage (miles):	240,250	236,351	233,956	NA	NA	710,557	236,852	N/A
Percentage of Total (%):	53.85	49.25	40.40	N/A	N/A	N/A	47.89	N/A
Number of Fires due to Operations and Transportation								
Collisions and Derailments	18	24	14	19	12	87	17.4	1.24
Brake Shoe Sparks	198	157	115	188	63	721	144.2	10.30
Electrical Components	34	35	136	53	42	300	60.0	4.28
Engine Exhaust Sparks	354	23	17	120	195	709	141.8	10.12
Car and Van Heaters	34	10	12	3	17	76	15.2	1.09
Fuses	13	10	7	7	5	42	8.4	0.60
Hot Journal Boxes	20	33	19	11	11	94	18.8	1.34
Materials in Transit	19	64	22	5	8	118	23.6	1.68
I. C. Engines	23	10	14	25	8	80	16.0	1.14
Other	63	22	58	82	78	303	60.6	4.33
Subtotal	776	388	414	513	439	2,530	506.0	36.13
Number of Fires due to Maintenances and Services								
Smoking	23	20	13	11	19	86	17.2	1.23
Electrical	28	26	26	22	22	124	24.8	1.77
Flammable Liquids	3	10	3	6	7	29	5.8	0.41
Heaters and Appliances	72	69	78	69	29	317	63.4	4.55
Burning on Right-of-Way	11	12	1	117	8	149	29.8	2.13
Spontaneous Ignition	18	27	9	20	15	89	17.8	1.27
Welding, Cutting, Brazing	74	55	64	59	63	315	63.0	4.50
Other	41	43	26	29	24	163	32.6	2.33
Subtotal	270	262	220	333	187	1,272	254.4	18.16
Number of Fires due to Outside or Undetermined Causes								
Exposure Fires	56	50	25	27	16	174	34.8	2.48
Lightning and Storms	7	9	33	6	8	63	12.6	0.90
Trespassing (including Arson)	272	170	193	269	202	1,106	221.2	15.79
Other	29	51	16	27	13	136	27.2	1.94
Undetermined Causes	346	318	92	359	607	1,722	344.4	24.59
Subtotal	710	598	359	688	846	3,201	640.2	45.71
Grand Total	1,756	1,248	993	1,534	1,472	7,003	1,400.6	100.00

a/ National Fire Protection Association[C.8,C.9]
NA Information not available at time of table preparation
N/A Not applicable

C.5 References

C.1 Accident/Incident Bulletin No. 145, Calendar Year 1976, Office of Safety, Federal Railroad Administration, U.S. Department of Transportation, Washington, DC, December 1977.

C.2 Accident/Incident Bulletin No. 146, Calendar Year 1977, Office of Safety, Federal Railroad Administration, U.S. Department of Transportation, Washington, DC, August 1978.

C.3 Accident/Incident Bulletin No. 147, Calendar Year 1978, Office of Safety, Federal Railroad Administration, U.S. Department of Transportation, Washington, DC, October 1979.

C.4 Accident/Incident Bulletin No. 148, Calendar Year 1979, Office of Safety, Federal Railroad Administration, U.S. Department of Transportation, Washington, DC, July 1980.

C.5 Accident/Incident Bulletin No. 149, Calendar Year 1980, Office of Safety, Federal Railroad Administration, U.S. Department of Transportation, Washington, DC, June 1981.

C.6 Accident/Incident Bulletin No. 150, Calendar Year 1981, Office of Safety, Federal Railroad Administration, U.S. Department of Transportation, Washington, DC, June 1982.

C.7 Accident/Incident Bulletin No. 151, Calendar Year 1982, Office of Safety, Federal Railroad Administration, U.S. Department of Transportation, Washington, DC, June 1983.

C.8 R. K. Clarke, et al., Severities of Transportation Accidents, Sandia National Laboratory, Albuquerque, NM, SAND77-0001, 1977.

C.9 P. Eggers, Severe Rail and Truck Accidents: Toward a Definition of Brounding Environments for Transportation Packages, U.S. Nuclear Regulatory Commission, Washington, DC, NUREG/CR-3499, 1983.

C.10 Fire Protection Handbook, 15th Edition, G. P. McKinnon, Ed., National Fire Protection Association, Quincy, MA, 1981.

C.11 R. L. Best, National Fire Protection Association, Railroad Section, Quincy, MA, private communication, 1985.

APPENDIX D

List of Figures

Page

D-1 Single column bent bridge structure configuration D-8
D-2 Multi-column bent bridge structure configuration D-9
D-3 Column stiffness for four bridge types D-13
D-4 Force-displacement curves for single, square bridge columns D-16
D-5 Force-displacement curves for single, rectangular bridge columns D-17
D-6 Force-displacement curves for multi, square bridge columns D-18
D-7 Force displacement curves for multi, rectangular bridge columns D-19

List of Tables

Page

D.1 Type of Soil Adjacent to Interstate 5 from San Diego County/Orange County Line to Los Angeles County/Kern County Line D-3
D.2 Type of Soil Adjacent to Interstate 80 from Davis, California to Nevada Border D-4
D.3 Type of Surface below Bridges on Interstate 80 from Davis, California to Nevada Border D-5
D.4 Bridges Along Interstate 5 from San Diego County/Orange County Line to Los Angeles County/Kern County Line Classified by Height..... D-7
D.5 Twenty-Four Representative Column Configurations for Calculating Force-Displacement Curves D-11

APPENDIX D

Highway Survey Data and Bridge Column Properties[a/]

D.1 Introduction

One important element in calculating shipping cask responses to accident loads is object hardness. When a shipping cask strikes a soft surface such as sand, the response of the cask is much less than when striking a hard object such as a concrete column. This appendix presents the data and evaluation results on two major subjects related to hard objects:

1) Statistical data on the total number of bridges, bridge heights, and surface conditions adjacent to highways, and below bridges,

2) The characteristics of bridge columns.

D.2 Survey

D.2.1 Surface Conditions Adjacent to Highways and below Bridges

The hardness of earth surfaces adjacent to highways can vary over a wide range. This variability can have a significant effect on the loadings that could be imposed on a cask or any other impacting object. The water and land (hard rock, soft rock/hard soil, and tillable soil) distribution along proposed spent fuel shipment routes between the east coast and west coast was initially estimated using agricultural soil survey data and geological highway maps for the United States.[D.3,D.4] The initial distributions estimated from these sources were considered to be indicative of the types of surfaces which could be impacted along highways in the various regions of the United States. However, since highway construction and landscaping can greatly affect the adjacent surroundings, the initial distributions were used to select representative portions of Interstates 5 and 80 in California to

---

a/ The Engineering Computer Corporation (ECC) was the subcontractor that performed the highway surveys and bridge column analyses.[D.1,D.2]

perform detailed highway surveys and to establish final distributions along highways.

A 133-mile portion of Interstate 5 was selected for the study. This portion of highway starts from the borderline between San Diego County and Orange County and ends at the borderline between Kern County and Los Angeles County. This portion of highway contains 20 miles of suburban, 50 miles of city, and 63 miles of rural area. The terrain which this portion of the highway crosses is essentially flat for 70 miles, rolling hills for 41 miles, and mountains for 22 miles. The types of earth adjacent to the highway were classified into three groups: tillable soil, non-tillable soil, and hard rock. The survey was performed by viewing the California Department of Transportation (CALTRANS) photo log. The result of the survey is summarized in Table D.1. Although the highway crossed the Santa Susana Mountains, no hard rock, such as granite, was identified in the survey.

A similar highway survey of earth types adjacent to 122 miles of the roadway along a section of Interstate 80 from Davis, California, to the Nevada border was then performed. This section of Interstate 80 crosses the Sierra where numerous outcroppings of granite rock occur. The result of the soil survey is summarized in Table D.2. The survey also included the types and frequencies of surfaces that could be impacted below a bridge. These surfaces were classified into four categories: roadbeds, railbeds, water, and earth. The result of the survey is summarized in Table D.3.

D.2.2 Highway Bridges

The same portion of Interstate 5 was used to compile statistical data on the number of bridges, bridge heights, and the size of columns. A two-step procedure was used in compiling data.

Step 1: View the California Department of Transportation (CALTRANS) photo log (a motion picture of the roadway as viewed by a motorist). Estimate the bridge column sizes and the number of bridges.

Table D.1
Type of Soil Adjacent to Interstate 5 from San Diego County/Orange County Line to Los Angeles County/Kern County Line

County	Adjacent Soil Type (miles)			
	Tillable	Nontillable	Hard Rock	Total
Orange	44.27	0.12	0	44.39
Los Angeles	62.65	5.80	0	68.45
	16.39	3.60	0	19.99
Total	123.31	9.52	0	132.83

Table D.2
Type of Soil Adjacent to Interstate 80 from Davis, California to Nevada Border[a]

County	Adjacent Soil Type (miles)			
	Tillable	Nontillable	Hard Rock	Total
Yolo	2	0	0	2
Sacramento	18	0	0	18
Placer	60	2	3	65
Nevada	29	6	0	35
Sierra	1	1	0	2
Total	110	9	3	122

[a] 122-mile highway through mountainous terrain from Davis, California, to the California-Nevada borderline.

Table D.3
Type of Surface below Bridges on Interstate 80 from Davis, California to Nevada Border[a/]

County	Surface below Each Bridge (bridge totals)				
	Road	River	Earth	Railroad	Total
Yolo	1	1	0	1	3
Sacramento	7	0	0	1	8
Placer	22	5	1	1	29
Nevada	12	6	0	1	19
Sierra	0	0	0	0	0
Total	42	12	1	4	59

a/ 122-mile highway through mountainous terrain from Davis, California, to the California-Nevada border line.

Step 2: Review the general plans for several of the bridges to confirm the column sizes identified by visual inspection through the photo log and to obtain bridge heights.

Table D.4 presents the result of the survey for the total number of bridges tabulated according to the bridge heights. Along the 133-mile roadway, 121 bridges were counted. Only 3 bridges exceed 50 feet in height. The rate is approximately 0.91 bridges/mile.

While collecting data about the bridge rate, information was also collected on all of California state and interstate highways. The total number of bridges in California is 12,574 and the miles of state and interstate highways is 15,183. This is very close to the detailed survey results of Interstate Highway 5.

D.3 Bridge Column Structural Characteristics

In order to estimate the response of a cask when impacting a bridge column, it is necessary to determine the level of hardness for that particular column. The level of hardness is normally represented by the force-displacement curve.

This subsection describes the approach used to develop the force-displacement curves for various column designs and the results of the detailed sensitivity study.

From the survey of Interstate 5, two typical bridge constructions are commonly seen along interstate highways: single-column bent bridge and multi-column bent bridge, as shown in Figs. D-1 and D-2 respectively. Most of the bridge columns are either square or rectangular. Bridge span lengths and column bent widths vary from bridge to bridge. Since more than 12,000 bridges exist on state and interstate highways in California, estimating the column force-displacement curve for each bridge is a very complex task. In order to control the task, 13 different sizes of column cross-sections from 1 ft x 1 ft to 4 ft x 64 ft were selected. In combination with the number of bents, a total of 24 column configurations were selected for sensitivity study in

Table D.4
Bridges Along Interstate 5 from San Diego County/Orange County Line to Los Angeles County/Kern County Line Classified by Height[a/]

	Bridge Height (ft)								
County	0-10	11-20	21-30	31-40	41-50	51-60	61-70	71-80	81-90
Orange	3	4	16	4					
	1	3	7						
Los Angeles	1	3	17	6			1		
		7	16	2	2				
		5	18	1	1	1			1
Total	5	22	74	14	3	1	1		1

Total Mileage = 133 miles[a/]
Total Bridges = 121

a/ Each set (left/right pair, on/off ramps, etc.) counts only once. Special truck lanes in northern Los Angeles County are not counted.

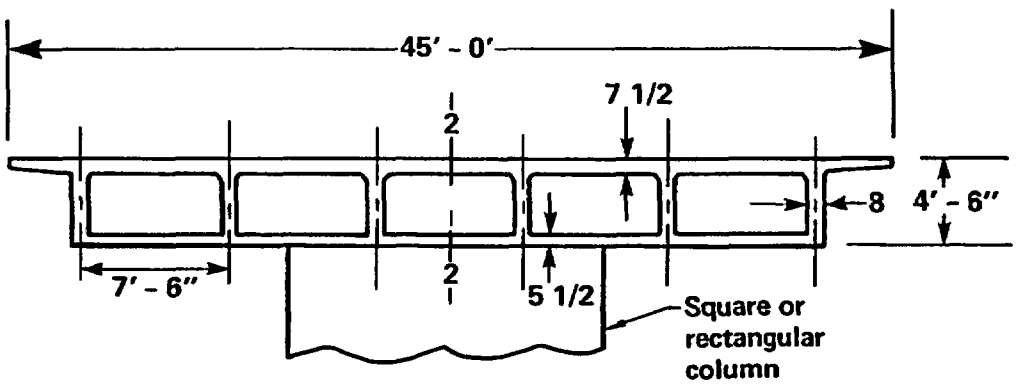

Section

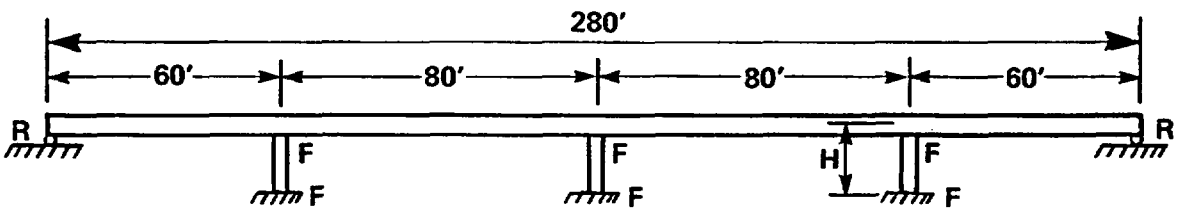

Elevation

Figure D-1 Single column bent bridge structure configuration.

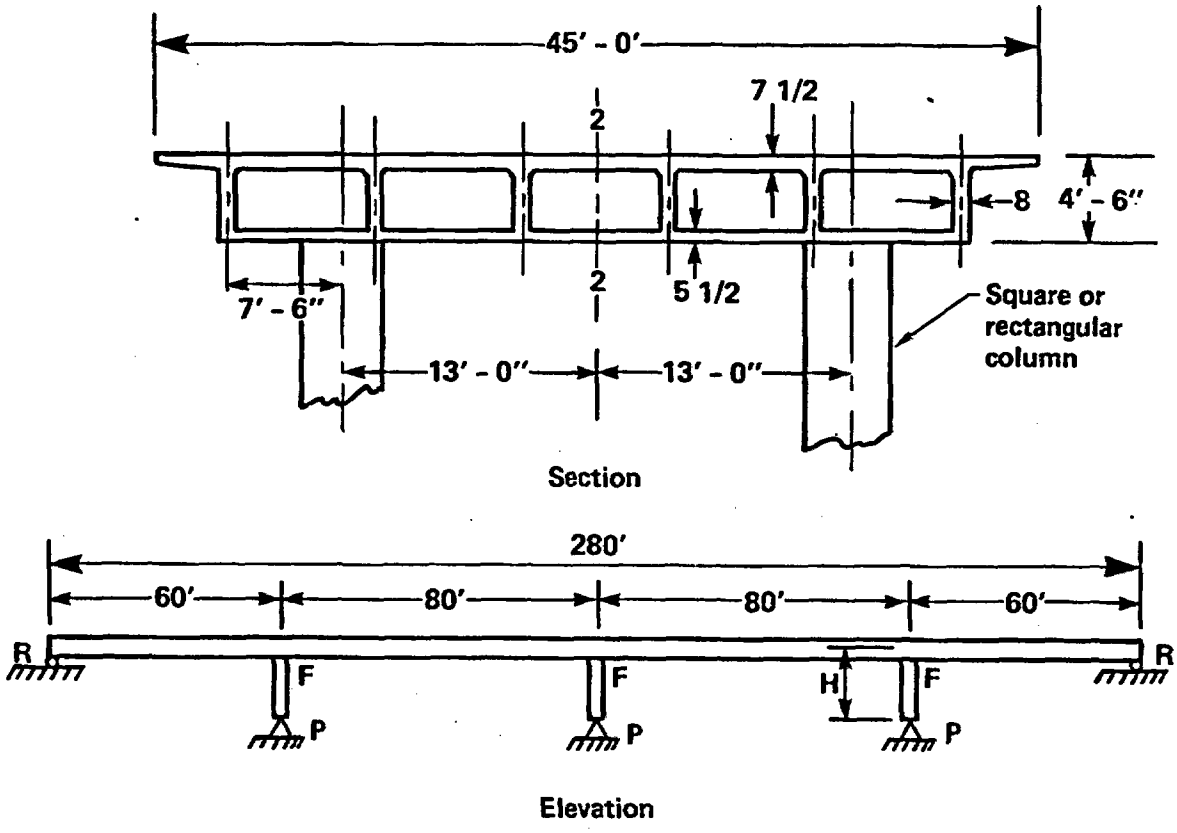

Figure D-2 Multi-column bent bridge structure configuration.

developing force-displacement curves. Table D.5 lists all column configurations selected for the sensitivity study. Some of the column dimensions, such as 32 ft x 32 ft, 16 ft x 16 ft, are not real structures. The inclusion of these dimensions in the analytical study is to help develop a set of continuous curves.

All 24 different configurations were categorized into four groups according to the shape of columns, i.e., square or rectangular, and number of bents, i.e., single-bent or multi-bent. These four groups formed the four basic cases for the sensitivity study as listed below and indicated in Table D.5.

Case A: Bridges with square columns and single-column bents.

Case B: Bridges with rectangular columns and single-column bents.

Case C: Bridges with square columns and multi-column bents.

Case D: Bridges with rectangular columns and multi-column bents.

D.4 Column Stiffness Sensitivity Study

The sensitivity study assumed that a shipping cask would strike the bridge column 4 feet above the rough surface, or 6 feet above the bottom of the column (bottom of pier). The study includes column heights of 20 feet and 30 feet.

For a single-bent column, the assumption is that the bottom of the column is pinned and the top of the column is fixed. A normalized static force of 1,000 kips is applied at 6 feet above the bottom of the column to represent the impact force of the shipping cask. Deformation at the point of impact is calculated for all column sizes of both cases A and B. The stiffness of the column is determined from the applied force and calculated deformation.

For the multi-bent configuration, the bridge is assumed to be a four-span bridge, which is most commonly seen along interstate highways. A beam-element

Table D.5
Twenty-Four Representative Column Configurations for Calculating Force-Displacement Curves

Class	Number of Bents	Shape of Column	Column Size (cross-section)
A	Single	Square	1 ft x 1 ft 2 ft x 2 ft 4 ft x 4 ft 8 ft x 8 ft 16 ft x 16 ft 32 ft x 32 ft
B	Single	Rectangular	4 ft x 1 ft 4 ft x 2 ft 4 ft x 8 ft 4 ft x 16 ft 4 ft x 32 ft
C	Multi	Square	1 ft x 1 ft 2 ft x 2 ft 4 ft x 4 ft 8 ft x 8 ft 16 ft x 16 ft 32 ft x 32 ft
D	Multi	Rectangular	4 ft x 1 ft 4 ft x 2 ft 4 ft x 8 ft 4 ft x 16 ft 4 ft x 32 ft 4 ft x 64 ft

model along the bridge roadway was developed to represent the bridge superstructure. The bridge is assumed to be pinned at both ends. At each pier location, the multiple-bent column configuration is modeled by a space frame pinned at the bottom of the frame structure. The combined bridge superstructure and column space frames formed the total bridge design. A normalized static force of 1,000 kips is applied 6 feet above the bottom of the column. The deformation at the point of impact is calculated by the Structural Analysis Program 6 (SAP6) program. The force-deformation relationship is used to determine the stiffness of the columns for each pier. This process is performed on all the column sizes for cases C and D.

Figure D-3 presents the results of this sensitivity study.

D.5 Force-Displacement Curve

The force-displacement curve was developed by following similar procedures to those described in the stiffness calculation. The same four groups (Cases A through D) were used. All the column sizes given in Table D.5 were included in the sensitivity study. During this exercise, column capacity was considered in resisting axial force, shear force, and bending moment. The angle of impact to the column was also considered. The impact was analyzed for every 15^{o} angle. The smallest column capacity for resisting impact at the various impact angles is selected to represent the column capacity. In estimating column capacity, the following assumptions were made to simplify the problem:

1. Vertical reinforcement is 2%

2. $fc' = 3,250$ psi

3. Tensile stress capacity of concrete $= 0.1\ fc' = 325$ psi

4. Ties are determined by the following formula

$$A_{sh} = 0.30\ S_t\ h_c\ \frac{fc'}{f_y}\ \left(\frac{Ag}{Ac} - 1\right) \qquad (D.1)$$

Case A : Square column, single-bent, column size D' x D'

Case B: Rectangular column, single-bent, column size 4' x D'

Case C: Square column, multi-bent, column size D' x D'

Case D: Rectangular column, multi-bent, column size 4' x D'

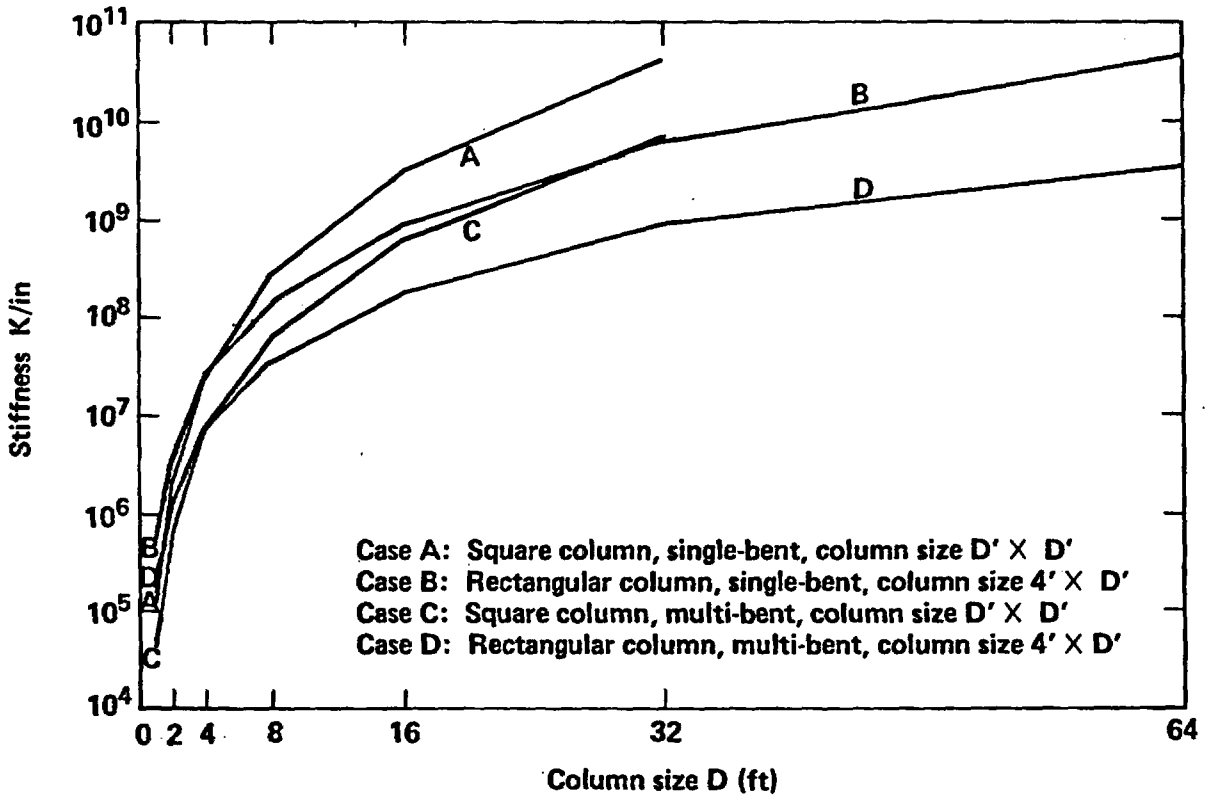

Figure D-3 Column stiffness for four bridge types.

or

$$A_{sh} = 0.12\ S_t\ h_c\ \frac{fc'}{f_y}\ (0.5 + 1.25\ \frac{Pe}{fc'Ag}) \qquad (D.2)$$

where

A_{sh} = area of transverse hoop bar, ft^2
fc' = specified compressive strength of concrete, psi
h_c = total depth of shear head cross-section, ft
S_t = vertical spacing of ties, ft
Pe = maximum design axial load, lbs
Ag = gross area of section, ft^2
Ac = area of concrete enclosed by tie, ft^2
f_y = specified yield strength of re-bar, psi

5. Height of column is 20 feet.

6. Distance from the face of concrete to the center of vertical re-bars is 3 inches.

7. Moment magnification due to slenderness is ignored.

8. P - Δ effect is ignored.

From assumption number 3, an axial force capacity was calculated for each different column size (cross section). For the flexural capacity, the Reinforced Column (RECOL) computer code was used to estimate column strength at yield point. These axial and flexural capacities of a column are combined with the results from the stiffness calculation as generated in the bridge model by using the SAP6 computer code to correlate the force-displacement relationship for each different column size.

These force-displacement relation curves used to relate the column yield force and displacement at the location of impact are listed in

Figs. D-4 through D-7 for all the column sizes listed in Table D.5. The possible dominant failure modes are identified in each curve. For example, for each column size, we identify whether a plastic hinge or a sudden shear failure occurs first. The shear capacity for a column is based on the equation

$$V_u = 2 (fc')^{1/2} bd + \frac{A_{sh} f_y d}{s} \qquad (D.3)$$

where

b = width of compression face, ft
d = distance from extreme compression fiber to centroid of tension reinforcement, ft
s = tie spacing, ft.

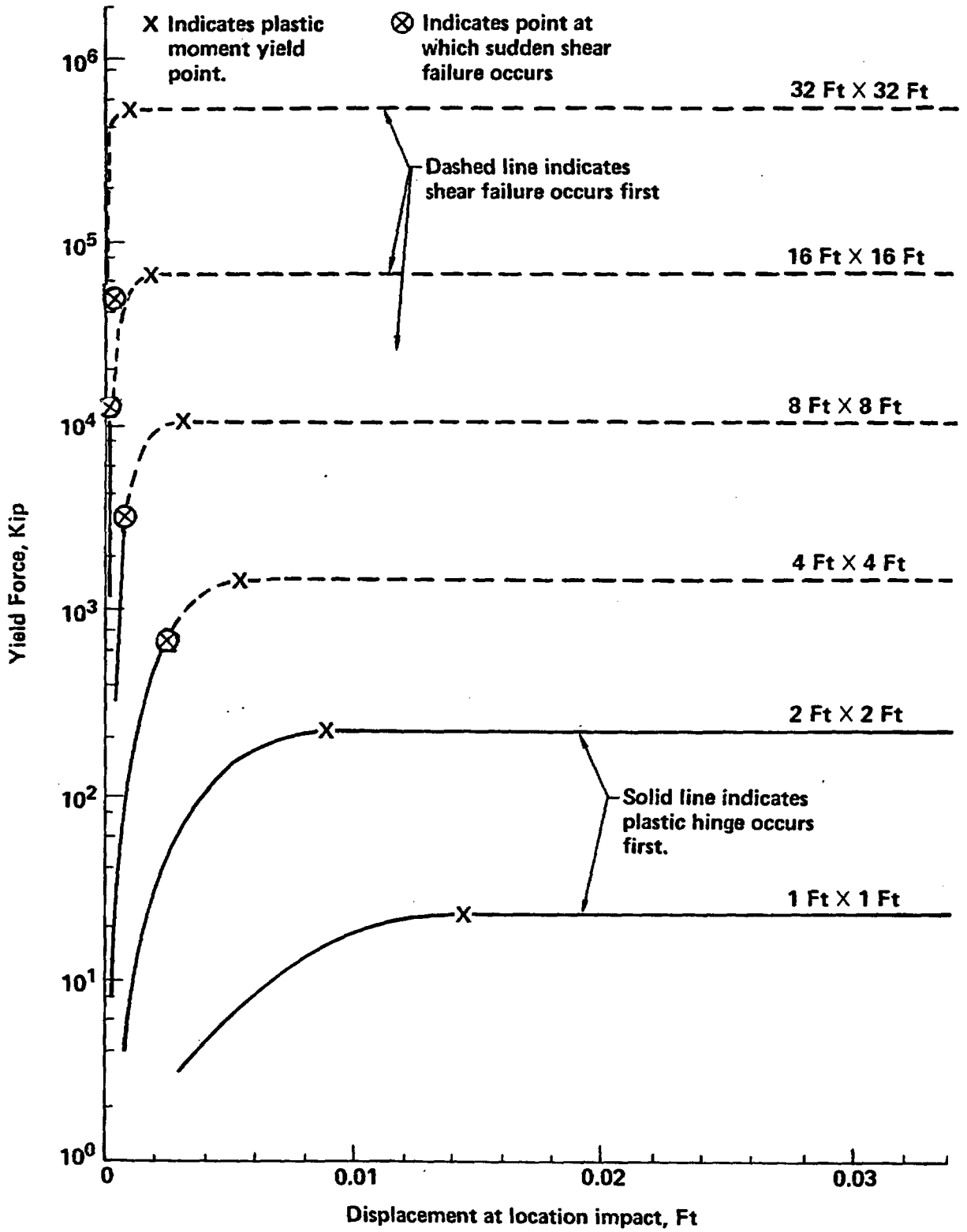

Figure D-4 Force-displacement curves for single, square bridge columns.

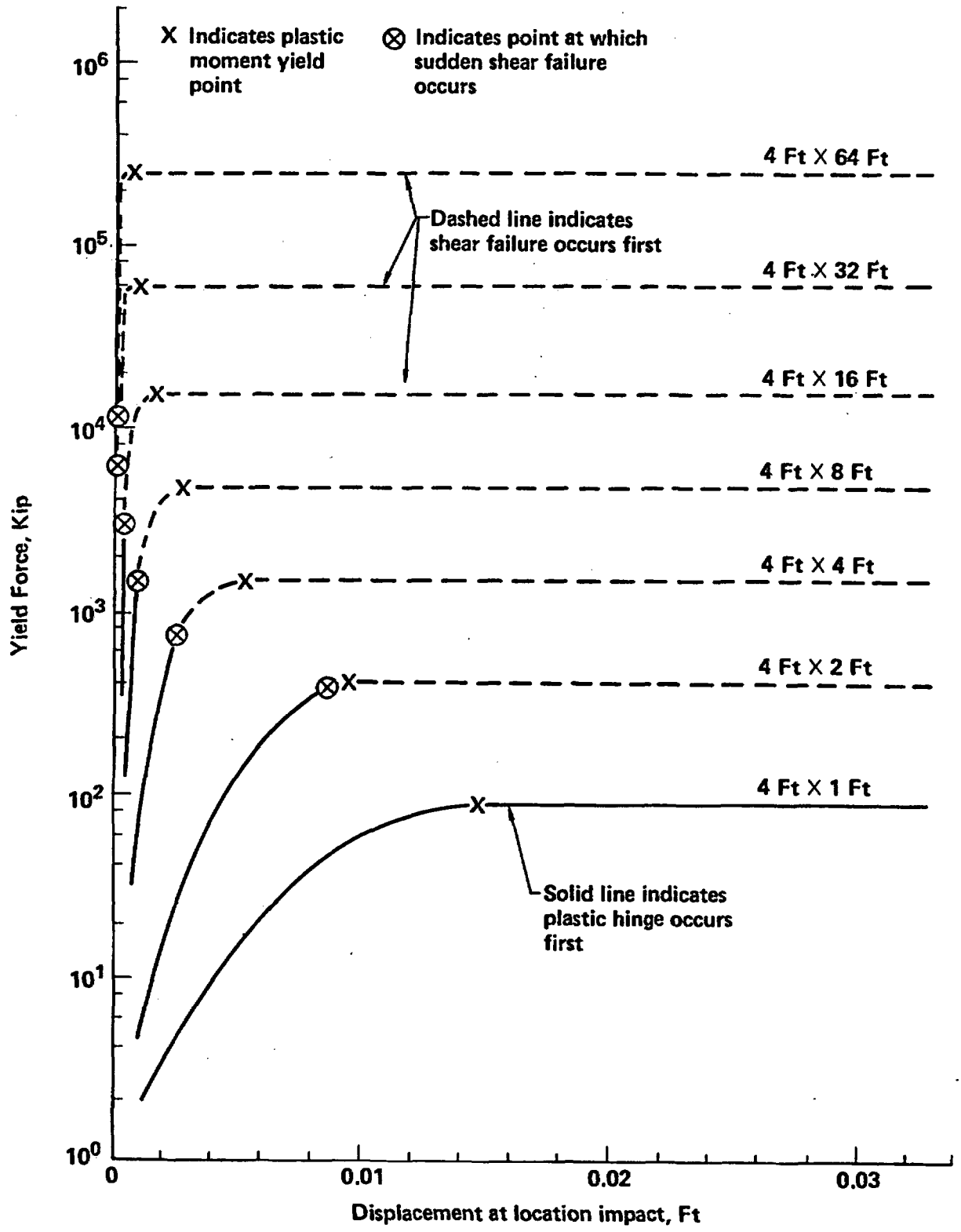

Figure D-5 Force-displacement curves for single, rectangular bridge columns.

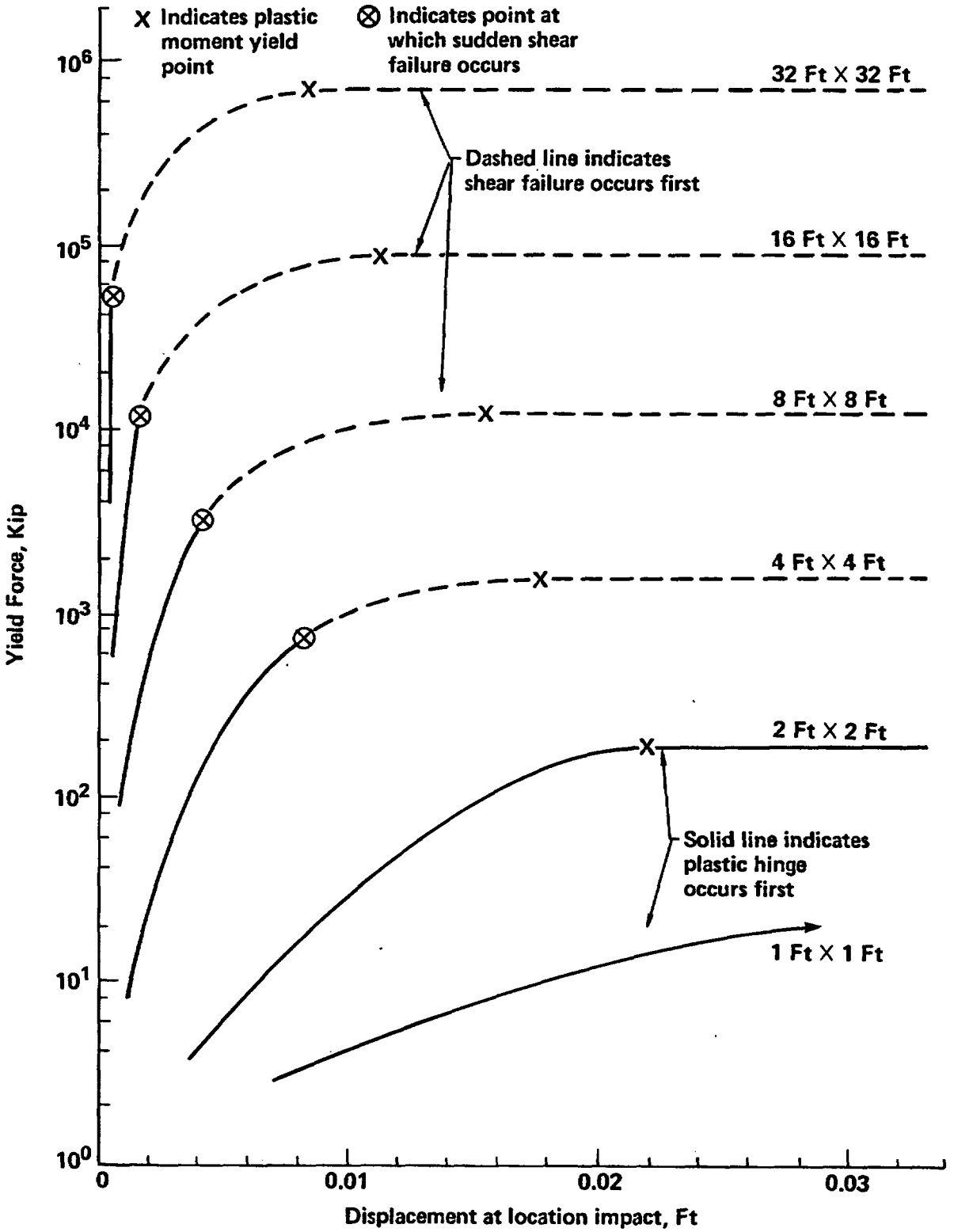

Figure D-6 Force-displacement curves for multi, square bridge columns.

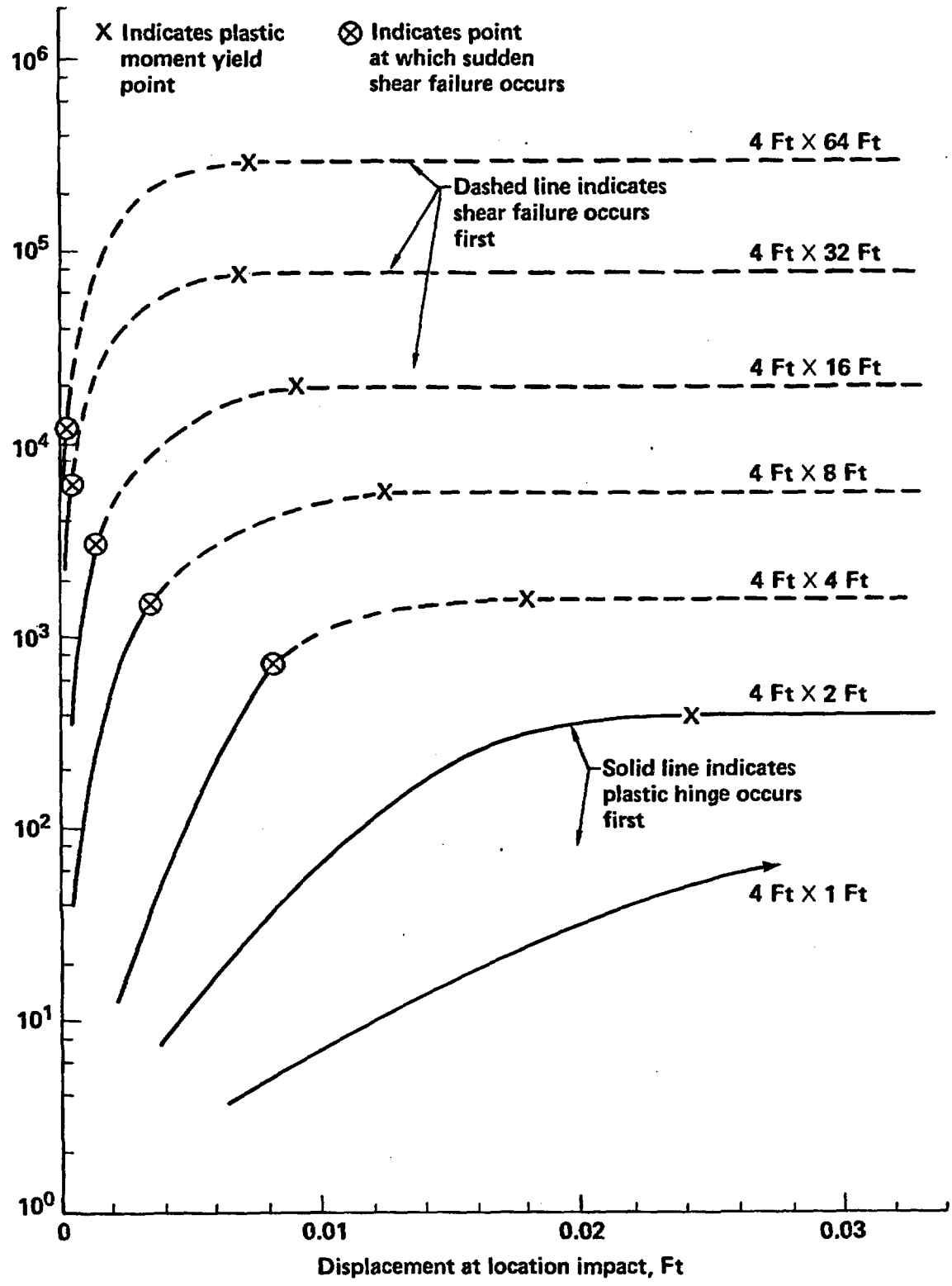

Figure D-7 Force-displacement curves for multi, rectangular bridge columns.

D.6 References

D.1 Assessment of the Stiffness Characteristics of Bridge Substructure Components Encountered along a Section of Interstate 5, Engineering Computer Corporation, Sacramento, CA, February 1985. A contractor report to the Lawrence Livermore National Laboratory.

D.2 R. Imbsen, et al., Soil and Terrain Surveys, Engineering Computer Corporation, Sacramento, CA, January 1985. A contractor report to the Lawrence Livermore National Laboratory.

D.3 Soil Survey, United States Department of Agriculture, Bureau of Chemistry and Soils, Superintendent of Documents, Washington, DC.

D.4 Geological Highway Map, American Association of Petroleum Geologist, Tulsa, OK.

D.5 University of Southern California, Structural Analysis Program 6 (SAP6), University of Southern California, Los Angeles, CA, 1980.

D.6 Engineering Computer Corporation, Reinforced Column (RECOL), Engineering Computer Corporation, Sacramento, CA, 1983.

APPENDIX E

List of Figures

		Page
E-1	Preliminary truck casks with three types of shielding, used for static load analysis	E-10
E-2	Preliminary rail casks with three types of shielding, used for static load analysis	E-11
E-3	Representative cask models used for truck and rail cask analysis	E-13
E-4	Deformation of truck cask during 60 mph impact by a 21-inch I-beam	E-15
E-5	Distribution of plastic strain in outer shell due to I-beam impact	E-16
E-6	Static force versus deflection for endwise loading of truck cask	E-18
E-7	Static force versus deflection for sidewise loading of truck cask	E-19
E-8	Static force versus deflection for endwise loading of rail cask	E-20
E-9	Static force versus deflection for sidewise loading of rail cask	E-21
E-10	Loading conditions on trees and poles	E-24
E-11	Finite element mesh for two-element inner-wall model by truck cask	E-37
E-12	Lead slump in truck cask at 60 mph impact	E-39
E-13	Strain in lower steel structure for truck cask impact at 60 mph	E-40
E-14	Velocity versus time for truck cask impact at 60 mph	E-41
E-15	Finite element mesh for rail cask	E-43
E-16	Lead slump in rail cask at 90 mph impact	E-45
E-17	Strain in lower steel structure for rail cask impact at 90 mph	E-46
E-18	Velocity versus time for rail cask impact at 90 mph	E-47
E-19	Model of a truck cask impacting an unyielding surface	E-48
E-20	Truck cask impact on unyielding surface at 60 mph	E-50
E-21	Impact on unyielding surface at 60 mph - maximum plastic strain location	E-52
E-22	Rail cask impact on unyielding surface at 60 mph	E-53
E-23	Rail cask impact on unyielding surface at 60 mph - maximum plastic strain location	E-55
E-24	Full side drop geometry including impact limiters	E-56

E-25 Deformations of truck cask during 60 mph side drop (side view) E-58
E-26 Distribution of plastic strain at end of impact (outer shell) E-59
E-27 Comparison of 2-D deformations with 3-D deformations at the center of the cask E-60
E-28 Equivalent damage technique E-62
E-29 Soil model comparison with penetration test data E-75
E-30 Finite element mesh for drops on soils E-76
E-31 Maximum plastic strain location on truck cask for impact at 60 mph on soft rock E-79
E-32 Maximum plastic strain location on rail cask for impact at 60 mph soft rock E-81
E-33 Locomotive sill cross section E-86
E-34 Sidewise off-center locomotive sill impact E-87
E-35 Thirty mph sidewise off-center sill impact E-88
E-36 Thirty mph sidewise off-center sill impact-maximum plastic strain location E-91
E-37 Model configurations for sidewise head-on sill impact E-92
E-38 Sidewise head-on sill impact at 30 mph E-93
E-39 Thirty mph sidewise head-on sill impact-maximum plastic strain location E-95

APPENDIX E

List of Tables

		Page
E.1	304 Stainless Steel Structural Properties	E-4
E.2	Lead Structural Properties	E-6
E.3	Uranium Structural Properties	E-7
E.4	Balsa Wood Structural Properties	E-9
E.5	Summary of Static Loading Calculations for Six Preliminary Cask Designs	E-12
E.6	Bounding Crush Loads Comparison with Crush Loading Capabilities of the Truck and Rail Casks	E-22
E.7	Quasi-Static Force Evaluation for Objects Potentially Impacted	E-26
E.8	Impact Velocities Required to Include Cab and Rail Car Crush Energy Absorption	E-30
E.9	Truck Cask Strain Response to Impact on Unyielding Surface at Various Cask Orientations	E-32
E.10	Rail Cask Strain Response to Impact on Unyielding Surface at Various Cask Orientations	E-33
E.11	IMPASC Endwise Impact Benchmark Calculation Against NIKE 2-D	E-34
E.12	Summary of Truck Cask Endwise Impact Results	E-38
E.13	Summary of Rail Cask Endwise Impact Results	E-44
E.14	Results of Truck Cask Sidewise Impact on an Unyielding Surface	E-51
E.15	Results of Rail Cask Sidewise Impact on an Unyielding Surface	E-54
E.16	Comparison of Equivalent Damage Technique Result with Real Surface Impact Results	E-66
E.17	Soil Parameters	E-69
E.18	Plate Bearing Test Simulation with NIKE 2-D	E-71
E.19	Summary of Soil Types and Range of Soil Parameters	E-72
E.20	Selected Soil Parameters for this Study	E-74
E.21	Summary of Cask Responses to Endwise Impacts on Real Surfaces	E-77

E.22 Results of Truck Cask Sidewise Impacts on Real Surfaces (without Impact Limiters) E-80
E.23 Results of Rail Cask Sidewise Impacts on Real Surfaces (without Impact Limiters) E-82
E.24 Interface Force for Water Impact (All Results Listed in Multiples of Cask Weight, No Impact Limiters or Cab Crush Included) E-85
E.25 Results of Sidewise Off-Center Sill Impact Against Truck Cask E-90
E.26 Results of Sidewise Head-on Sill Impact Against Truck Cask E-94
E.27 Estimated Response of Rail Cask to Impact by Train Sill E-97

APPENDIX E
Structural Analysis

E.1 Introduction

This appendix provides the structural models developed and the analyses performed to determine the responses of the representative truck and rail casks to a wide range of impact loads. The family of DYNA and NIKE computer codes were used extensively to calculate the responses of the casks.[E.1,E.2]

In Section E.2, the material properties used in the process for selecting the representative casks and evaluating the responses of the representative casks are presented. In Section E.3, the static analyses evaluations of different cask designs used to select the representative cask are presented.

In Section E.4, the types of mechanical loading conditions that can affect the strain response of a cask in an accident are discussed. In Section E.5, the quasi-static load evaluation performed for minor accidents are presented. In Section E.6, the structural model and strain response of the two representative casks to impacts on an unyielding surface are discussed. In Section E.7, the response of the two representative casks to impacts on real objects is estimated.

E.2 Materials Properties

Spent fuel casks must be designed and fabricated to national codes and standards or equivalent requirements. Although there is no specific section in the American Society of Mechanical Engineers (ASME) pressure vessel code applicable to spent fuel casks, the industry has used the ASME code extensively for designing and fabricating spent fuel casks. In this study, to the extent possible, properties of materials were taken from the ASME code.[E.3]

Although it is preferred to use probability distributions for material properties that are based on actual fabrication data, discrete bounding values from the ASME code were used in this study. This approach was taken to simplify the modeling and analysis. If distribution had been used, the modeling and analysis would have been unnecessarily complex and unwarranted for the scope of this study. Consequently, conservative material properties

based on the ASME code were used with loading calculations to estimate seal and weld damage to the representative casks.

Using ASME code properties, limiting plastic strain criteria were used in estimating the response and damage to the representative casks. In this case, the maximum strains would be associated with end-on impact caused by lead slump. Large local strains would be generated at the junctions of the inner containment shell and outer shell with the end closure. Ideally, weld joints would not be present in these areas where high local strains could occur. However, even if welds were present in these areas, most strains would be highly concentrated and could cause only local cracking. Since the extent of lead slump deformation would be limited, it would not be likely that the inner containment would completely rupture. Furthermore, the primary membrane strain on the inner containment cylinder would be compressive and a small fraction of the selected strain levels. The large strains developed at the discontinuities would be highly localized and oriented axially. On the outer shell, the primary membrane strains would be tensile. Even if complete separation from the end plate is postulated, the deformation of the lead would also limit the primary membrane strain to a small fraction of 30% strain. Consequently, the outer shell would remain intact and continue to maintain the integrity of the lead shielding. In conclusion, the postulated local strains on the order of 30% would not result in breaching of the cask but may result in local cracking.

Instead of evaluating specific closure and penetration designs, it was assumed for comparative purposes that closure and penetration seals fail when the strain level in the inner shell exceeds 0.2% (S_1). This approach was based on a review of current cask designs and their ability to withstand impact forces with large strains. Temperature effects on the material properties were included in the analysis performed. Strain-rate effects were not included for most material properties for the following reasons:

(1) There is no standard set of strain-rate properties in the ASME code or adopted by industry.

(2) Strain-rate effects generally improve material yield and ultimate strength by 0-30%, but reduce ductility. When strain-rate effects are included for the cask structural materials, then they should be included for surface materials such as rock and concrete. In general, the improvement of material strength properties is greater for ductile type metallic materials than for ceramic type materials. For the purpose of evaluating representative casks impacting representative surfaces, the inclusion of strain-rate effects is not warranted and their exclusion is reasonably conservative.

(3) The strain effect in reducing the structural material ductility was accounted for by using conservative static ultimate strain values for the structural materials.

E.2.1 304 Stainless Steel

Material properties were obtained for 304 stainless steel from the ASME code.[E.3] The properties are tabulated in Table E.1. The elastic-plastic material model used a bilinear fit representation with isotropic hardening. No strain-rate effects were included. The material model used was Material Type 3 in the NIKE 2-D/DYNA 2-D family of finite element codes; the 2-D designation indicating that two-dimensional modeling was performed.[E.1,E.2] These codes use an updated geometry to calculate strains. Therefore, it was necessary to use true stress and true strain data, rather than the engineering stress and strain data provided in the ASME code. In order to approximate a value for ultimate true stress, based on ultimate engineering stress, data from Conway, et al., was used.[E.4] The stress/strain data of Conway, et al., was not for SA-240, but for another 304 stainless. This, however, provided a means to interpolate a value of true stress for a given engineering stress from the ASME code.

$$\frac{75{,}000 - 71{,}300}{76{,}390 - 71{,}300} = \frac{\sigma_{u_{true}} - 85{,}730}{97{,}760 - 85{,}730} \qquad \text{(E.1)}$$

$$\sigma_{u_{true}} = 94{,}475 \text{ psi} .$$

Table E.1
304 Stainless Steel Structural Properties

Elastic modulus	E	=	27.6×10^6 psi
Hardening modulus	E_n	=	2×10^5 psi
Poisson's ratio	ν	=	0.29
Engineering ultimate stress	$\sigma_{u_{eng}}$	=	75×10^3 psi
True ultimate stress	$\sigma_{u_{true}}$	=	94.5×10^3 psi
Engineering ultimate strain	$\epsilon_{u_{eng}}$	=	0.40
True ultimate strain	$\epsilon_{u_{true}}$	=	0.34
Yield stress	σ_y	=	25×10^3 psi
Density	ρ	=	7.44×10^{-4} lb-sec^2/in^4

The ultimate engineering strain value provided by the ASME code of 40% is equivalent to a true strain value:

$$\varepsilon_{u_{true}} = \ln (1 + \varepsilon_{u_{eng}}) \qquad (E.2)$$

$$= \ln (1 + 0.4)$$

$$= 0.34.$$

The ultimate strain percentage used in this study is 30% (S_3) to accommodate for the effects of strain rate on the reduction of ductility. The hardening modulus was calculated as follows:

$$E_n = \frac{94,475 - 25,000}{0.34 - .00091} = 2 \times 10^5 \text{psi}. \qquad (E.3)$$

E.2.2 Lead

The material properties used for lead in this study are presented in Table E.2.[E.5] A bilinear fit was used to represent the elastic-plastic material. Strain hardening was used, with isotropic hardening in all calculations. It is considered to be unnecessarily conservative to exclude the strain-rate effect for the lead. The hardening modulus is more significant than the elastic modulus for lead because the lead shield yields relatively easily on impact. The hardening modulus used in this study compares well with the test results reported by Counts and Payne.[E.6] Additional benchmarking testing is required to define the lead properties and bonding effects at the cask inner shell with high confidence.

E.2.3 Uranium

The material properties used for uranium are summarized in Table E.3.[E.7] A bilinear fit was used to model its elastic-plastic characteristics for stress/strain.

Table E.2
Lead Structural Properties

Elastic modulus	E =	2.22×10^6 psi
Hardening modulus	E_n =	4.5×10^4 psi
Poisson's ratio	ν =	0.43
Yield stress	σ_y =	500 psi
Density	ρ =	1.06×10^{-3} lb sec^2/in^4

Table E.3
Uranium Structural Properties

Elastic modulus	E =	26×10^6 psi
Hardening modulus	E_n =	1×10^6 psi
Poisson's ratio	ν =	0.21
Yield stress	σ_y =	4.6×10^4 psi
Density	ρ =	1.74×10^{-3} lb-sec^2/in^4

E.2.4 Balsa Wood

An elastic-plastic model was selected for modeling the balsa wood.[E.8] The material properties used are tabulated in Table E.4.[E.8] Material Type 10, from DYNA 2-D, was used for the wood material model.

E.3 Preliminary Cask Designs and Cask Selection

Six preliminary cask designs were developed to perform screening analyses to assess their responses to high-loading conditions. The designs included the use of three types of gamma shielding materials: lead, depleted uranium, and steel. Three truck and three rail casks were developed using each type of shielding. The pertinent materials and dimensions for the six preliminary cask designs are provided in Figs. E-1 and E-2 for the truck and rail casks, respectively.

Static force evaluations were performed using the NIKE 2-D finite element computer code for the six casks. The loading conditions applied on each of the casks are illustrated in Table E.5. In case (a), a pressure load was applied on one end over the entire closure region of the cask in increments of 200 psi with the other end of the cask resting on an unyielding surface. In case (b), a circular cross-section of the cask was loaded in increments of 200 psi over the top area of the cask with the bottom resting on an unyielding surface. In case (b), the model had a unit or one inch thickness. The yield force results of the two loading calculations for each of the six casks are summarized in Table E.5. The lead cask yielded at significantly lower loading conditions in all cases. Based on these results, the lead shielded cask was selected for developing a representative cask design for impact analysis.

E.4 Mechanical Loading Conditions Caused by Accidents

Mechanical loading conditions on a cask caused by an accident can result in damage to the inner shell of the cask. Mechanical loading conditions include impact, puncture (including missiles), and crush. Two representative cask designs were developed as shown in Fig. E-3: one for truck shipments and one for rail shipments of spent fuel. The representative truck cask

Table E.4
Balsa Wood Structural Properties

Elastic modulus	E =	5.9×10^5 psi
Poisson's ratio	ν =	0.0
Yield stress	σ_y =	1.7×10^3 psi
Sheer modulus	G =	2.95×10^5 psi
Density	ρ =	1.35×10^{-5} lb-sec^2/in^4

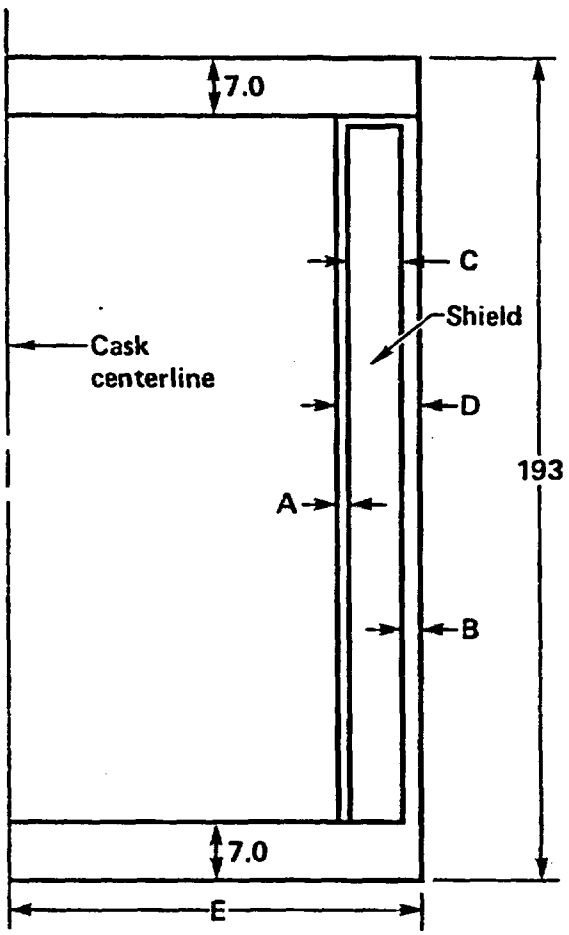

Dim	Thickness (in.)	Material
	Truck Cask 1	
A	0.5	304SS
B	1.25	304SS
C	5.25	Lead
E	13.75	304SS
	Truck Cask 2	
A	0.5	304SS
B	1.25	304SS
C	4.25	Depleted uranium
E	12.75	304SS
	Truck Cask 3	
D	12.25	Steel
E	19.00	Steel

Figure E-1 Preliminary truck casks with three types of shielding, used for static load analysis.

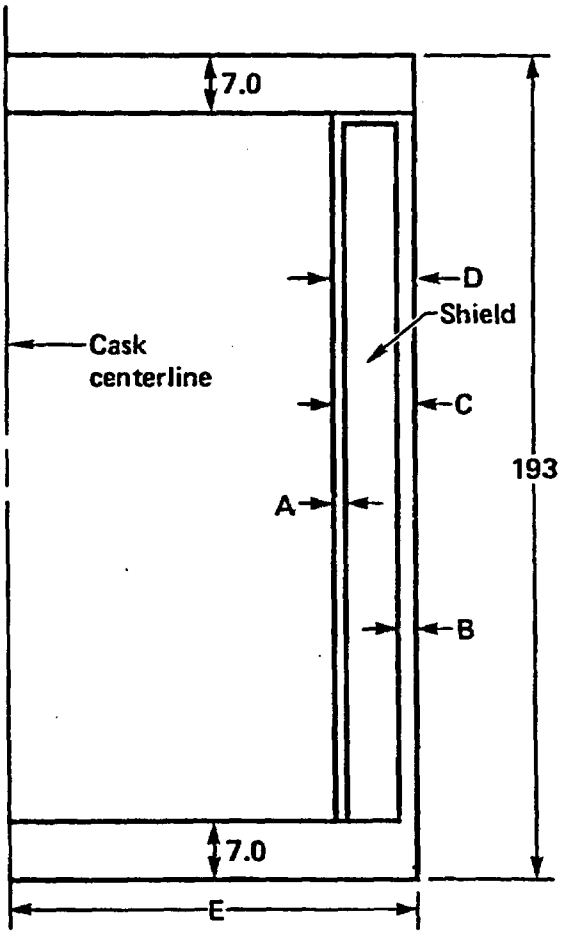

Dim	Thickness (in.)	Material
	Rail Cask 1	
A	0.5	304SS
B	1.5	304SS
C	5.25	Lead
E	26.0	304SS
	Rail Cask 2	
A	0.5	304SS
B	1.5	304SS
C	4.0	Depleted uranium
E	24.8	304SS
	Rail Cask 3	
D	12.25	Steel
E	30.75	Steel

Figure E-2 Preliminary rail casks with three types of shielding, used for static load analysis.

Table E.5
Summary of Static Loading Calculations for Six Preliminary Cask Designs

Loading Configuration	Cask Type	Yield Force (lbs)
	ENDWISE LOADING	
Case (a), endwise 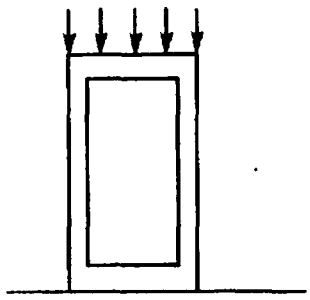	Truck	
	Lead	3,300,000
	Depleted uranium	8,000,000
	Steel	11,000,000
	Rail	
	Lead	8,000,000
	Depleted uranium	17,000,000
	Steel	40,000,000
	SIDEWISE LOADING	
Case (b), sidewise 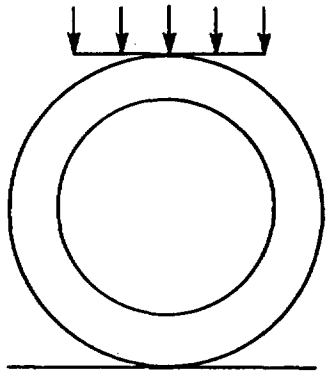	Truck	
	Lead	1,600,000
	Depleted uranium	11,000,000
	Steel	26,000,000
	Rail	
	Lead	260,000
	Depleted uranium	3,700,000
	Steel	11,500,000

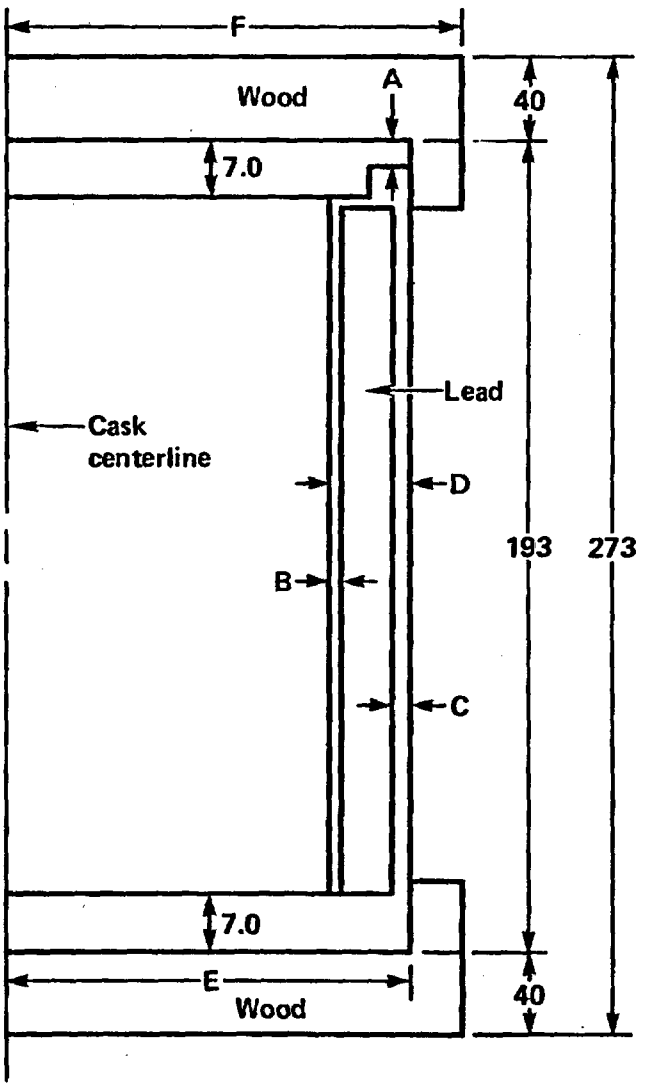

Dim	Truck inches	Rail inches
A	1.5	3.0
B	0.5	1.5
C	1.25	2.5
D	7.0	8.0
E	13.75	38.0
F	38.25	58.0

All material is 304SS except that noted otherwise

Figure E-3 Representative cask models used for truck and rail cask analysis.

(Fig. E-3) design uses the same dimensions as the preliminary lead truck cask design (Fig. E-1). The truck cask design allows transport of a single PWR fuel assembly. The representative rail cask design (Fig. E-3) dimensions differ from the preliminary lead rail cask design (Fig. E-2). The capacity of the rail cask is 21 PWR fuel assemblies which reflects the greater capacities of anticipated cask designs. Each design uses helium in the cask cavity.

Typically, as discussed in Sections E.6 and E.7, the dynamic force caused by impact on a hard surface can be in the range of 1-10 million pounds on the representative truck cask depending on the impact velocity (velocity component perpendicular to the surface impacted), the cask orientation, and the hardness of the surface. The strain at the inner wall of the cask can exceed 30% (S_3) at impact velocities greater than 75 mph. The dynamic forces generated by impacts on a hard surface are even higher for the rail cask compared to the truck cask because of the larger size and weight of the rail cask.

The possibility of puncture of the cask by a high energy-density object was evaluated. It was concluded that a high velocity I-beam would have the highest energy density of probable missiles generated in an accident and that the I-beam represented the bounding case for the puncture of a cask wall.[E.9] Assuming that the I-beam is the bounding case, the representative truck cask was analyzed with DYNA 3-D (the 3-D designation indicating that three-dimensional modeling was performed) for impact by a high energy I-beam.

The representative truck cask and I-beam were modeled using two planes of symmetry. The truck cask model included the inner and outer steel walls and the lead shielding but did not have end closures or impact limiters. The back side of the cask was supported by an unyielding surface. The 40 foot WF-21/96 I-beam was modeled as 1/4 of the length unit with an equivalent weight.

The impact velocity was 60 mph, resulting in an impact force of 40,000 pounds by the I-beam. The deformations due to the impact are shown in Fig. E-4. The impact caused the cask wall to flatten locally and the I-beam to yield significantly at the point of impact. A maximum plastic strain of 5% developed in the outer wall of the cask as shown in Fig. E-5. The maximum

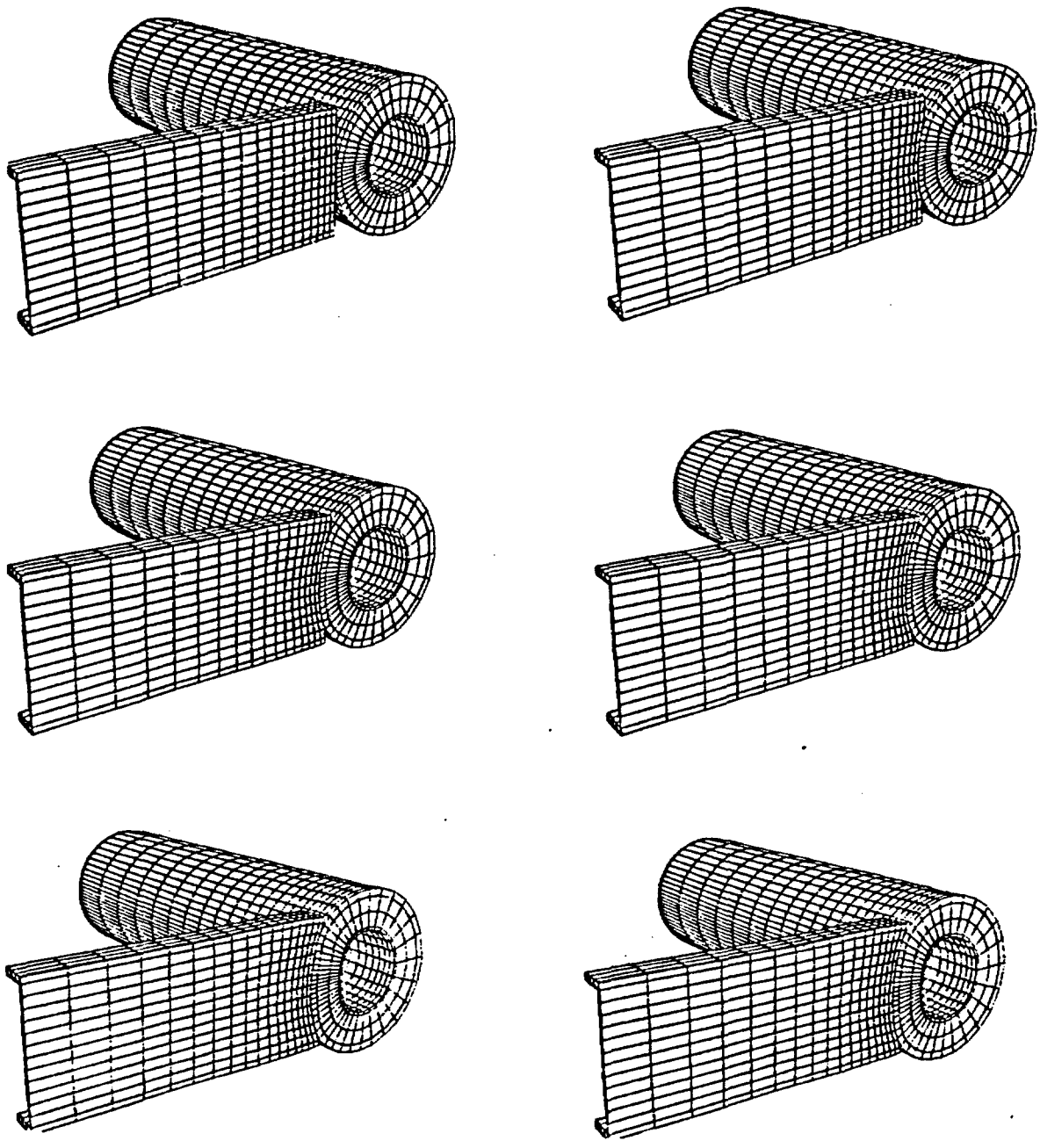

Figure E-4 Deformations of truck cask during 60 mph impact by a 21-inch I-beam.

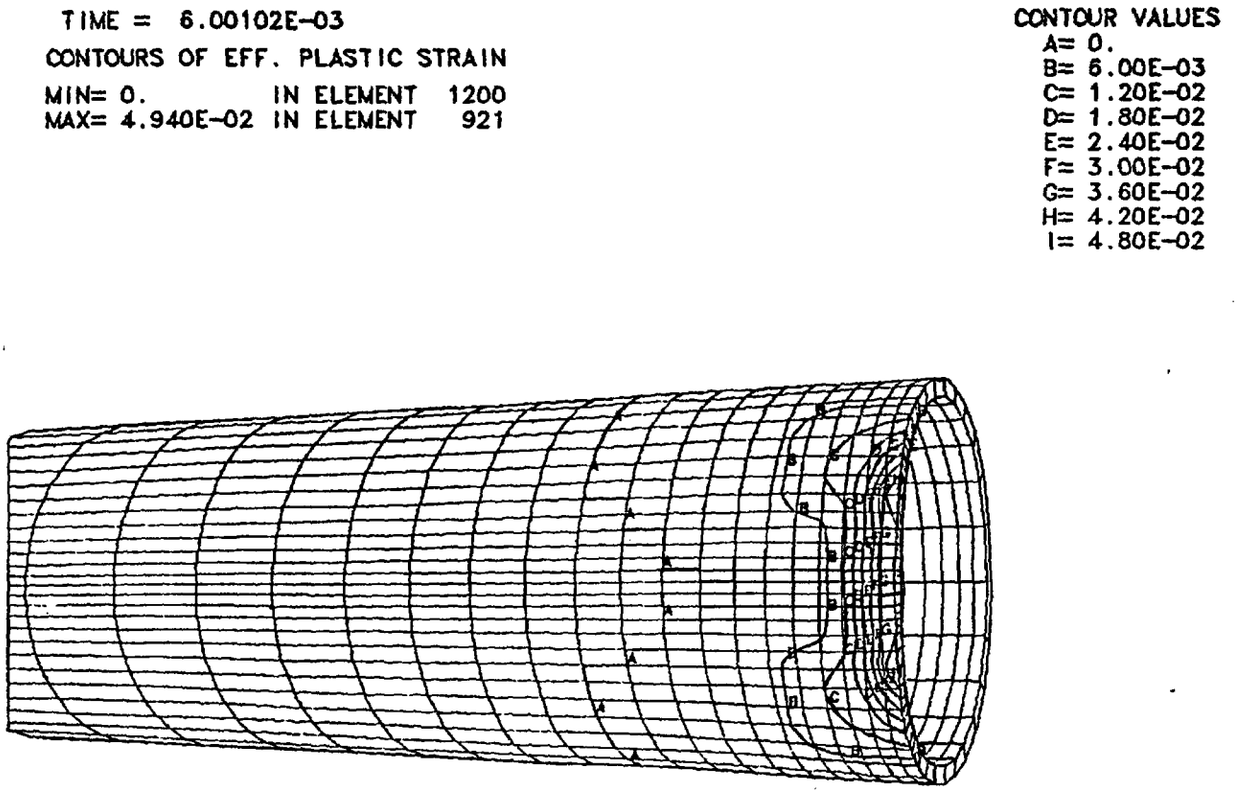

Figure E-5 Distribution of plastic strain in outer shell due to I-beam impact.

stress and shear in the outer wall were 34,950 psi and 19,500 psi, respectively. The I-beam did not penetrate the cask wall.

In comparison with the I-beam impact, the train sill impact discussed in Section 7.4 on the truck cask is more severe. The impact force exceeded 9 million pounds and the strain was 20% for a 60 mph impact. Therefore, it was concluded that the impact by a train sill is a more severe accident that may cause high local strains and stress to the cask walls. Due to the larger size and weight of the rail cask, it was also concluded that the impact of a train sill on the rail cask is more severe than the impact by an I-beam.

The possibility of crush of the representative casks by a heavy object was evaluated. Static force evaluations of the representative casks shown in Fig. E-3 were performed using the NIKE 2-D finite element computer code. As discussed in Section E.3, the loading conditions applied on each of the representative casks are the same as those used for the preliminary cask designs in Table E.5. The force deflection characteristics for each of the representative casks are shown in Figs. E-6 through E-9. The force where general yielding of the cask body occurs was selected for comparing their loading capabilities with the bounding crush loads from NUREG/CR-3498.[E.9]

In Table E.6, typical crush loads that could occur in real accidents are compared with the crush loading capabilities of the representative casks. The bounding crush load is a 200-ton locomotive that would rest on the rail cask by its sill. Both the truck and rail cask can support the weight of the locomotive without yielding.

Based on severe accident data, the frequency of occurrence of impact loads is at least a factor of 10 times higher than for puncture or crush loads. Therefore, since impact can generate higher loads and can occur more frequently, it is concluded that impact loads dominate the potential mechanical loading environment and only impact loads will be considered further.

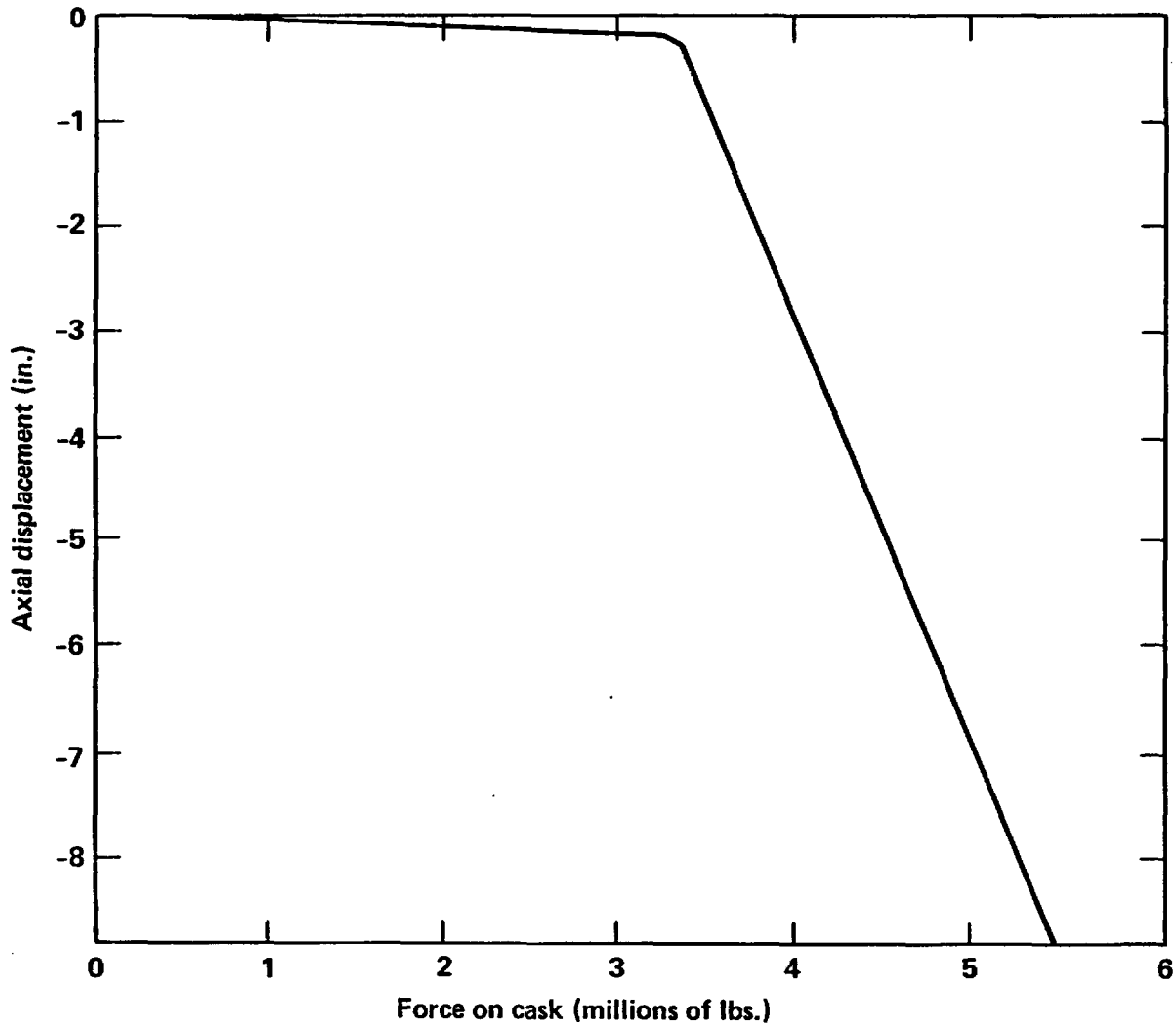

Figure E-6 Static force versus deflection for endwise loading of truck cask.

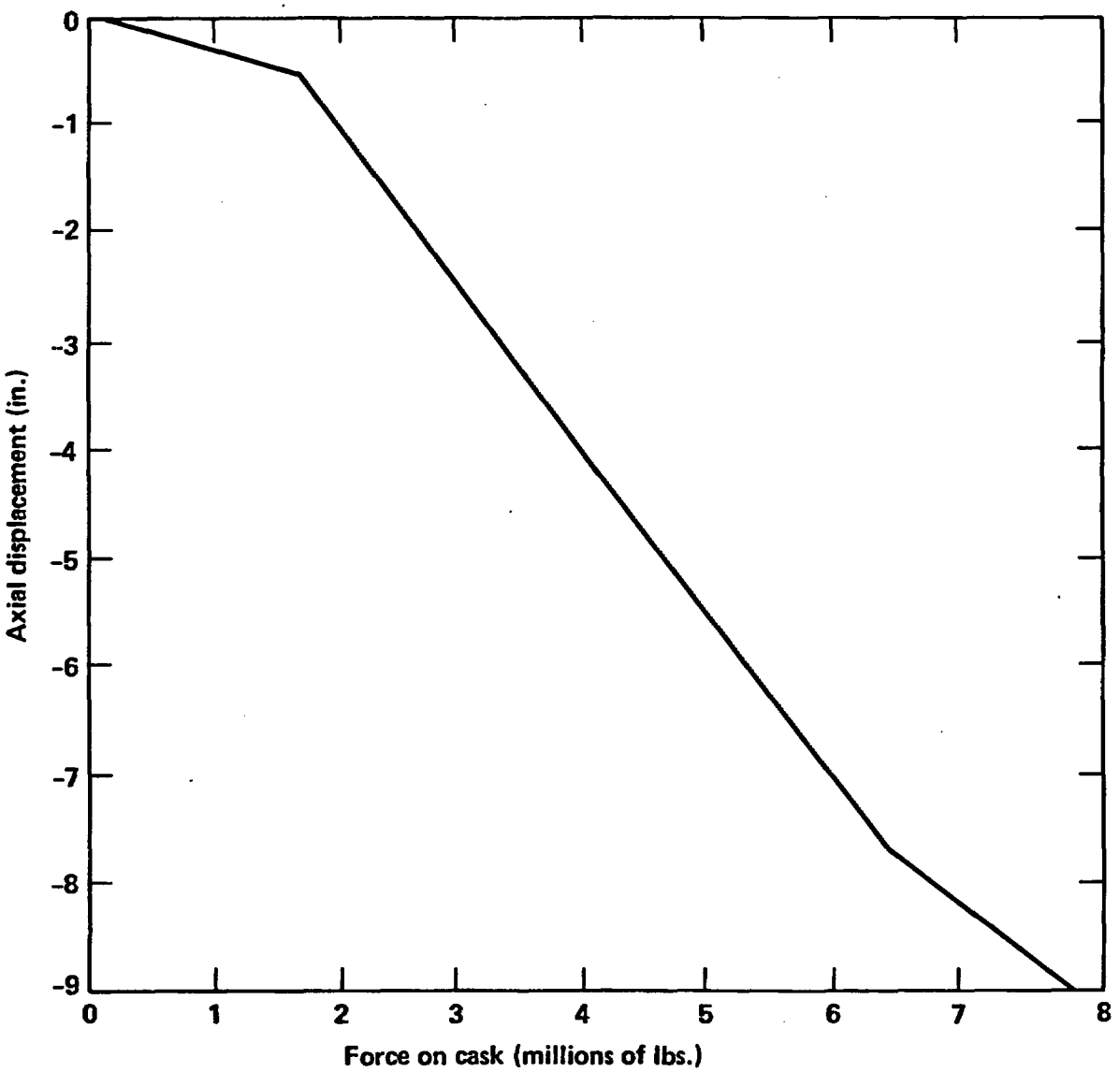

Figure E-7 Static force versus deflection for sidewise loading of truck cask.

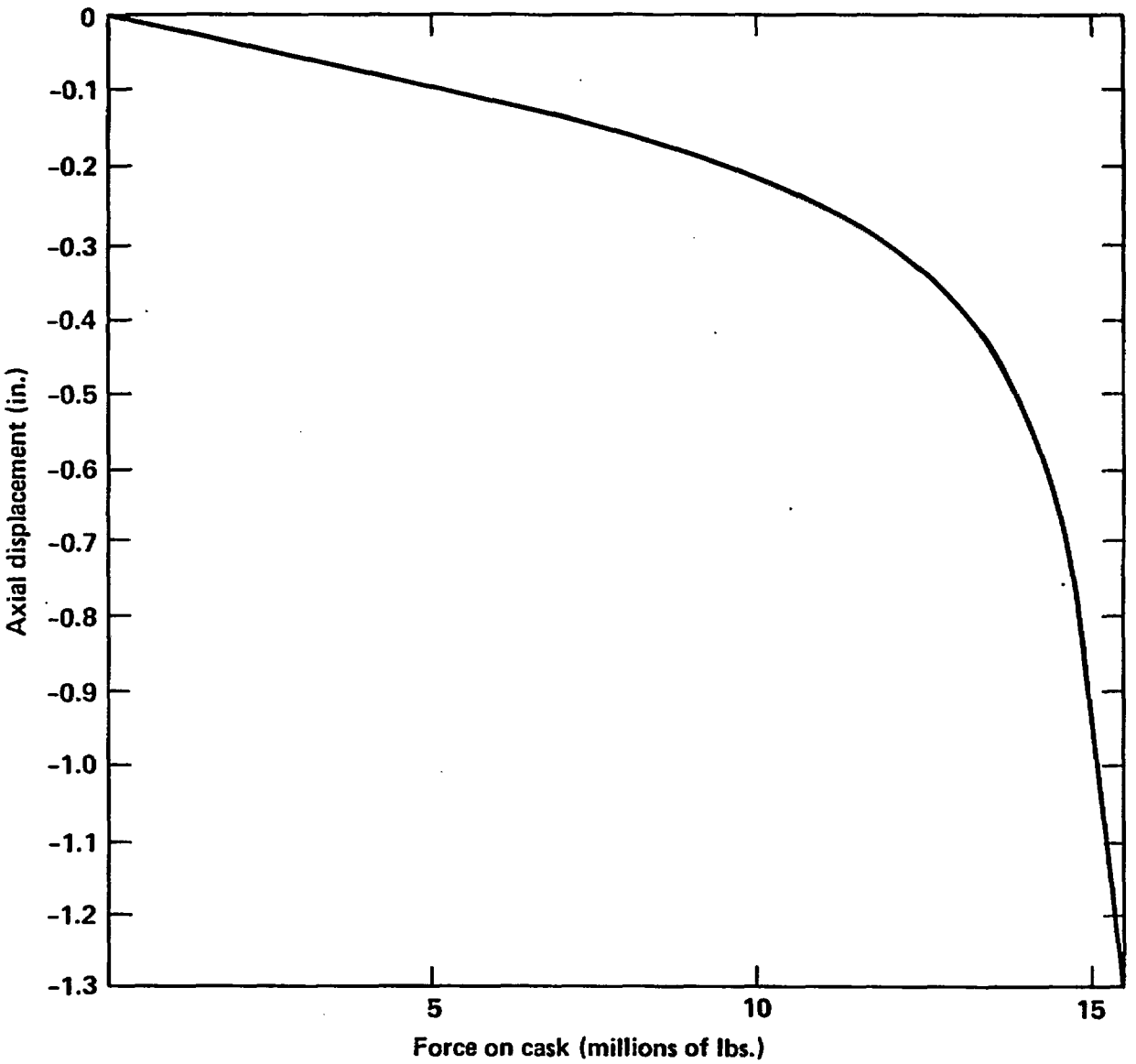

Figure E-8 Static force versus deflection for endwise loading of rail cask.

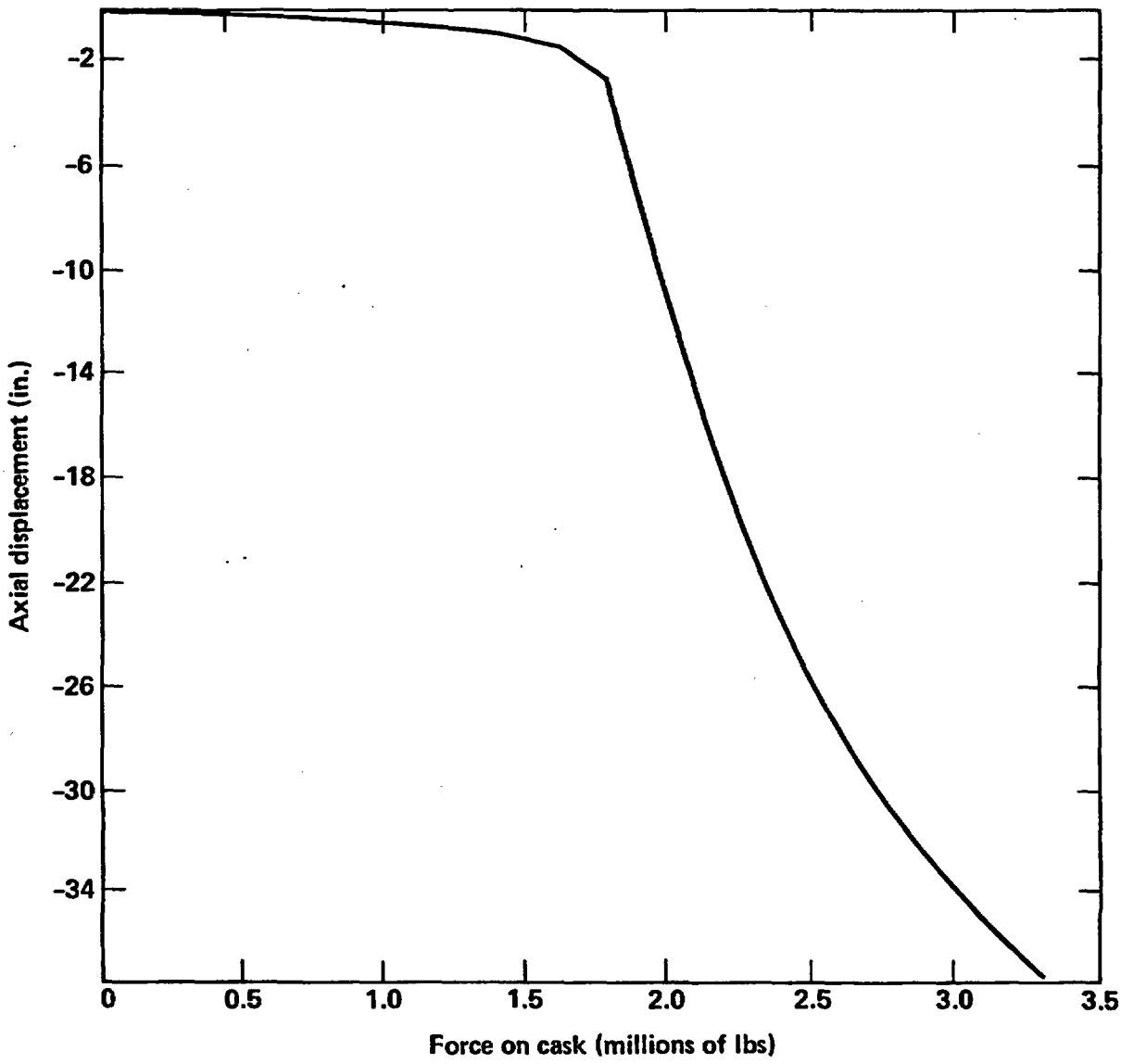

Figure E-9 Static force versus deflection for sidewise loading of rail cask.

Table E.6
Bounding Crush Loads Comparison with Crush Loading Capabilities of the Truck and Rail Casks

Bounding Crush Force Description	Resultant Force (lbs)	Truck Cask Capability (lbs)	Rail Cask Capability (lbs)
For highway accidents the weight of a 60,000 pound truck with its contents. Weight is carried across truck frame width.	60 thousand	1.6 million	1.6 million
For railway accidents the weight of a 200 ton locomotive. Weight is distributed across the train sill.	400 thousand	1.6 million	1.6 million

E.5 Quasi-Static Loads Due to Minor Accidents

In Section E.4, the minimum static force required to yield either the representative truck or rail cask was determined to be 1.6 million pounds. The static force required to yield the impacted object completely is in most cases significantly less than 1.6 million pounds. The static force required to yield either the representative truck or rail cask was compared with the force required to collapse potential objects to screen out low resistance objects from further analysis.

The maximum force that an object can generate during a high velocity impact was estimated using quasi-static methods. D'Alembert's principle was used to establish static force equivalent to the inertial force caused by deceleration. It was concluded that objects such as automobiles or truck trailers cannot generate forces greater than 400,000 pounds even at high velocities.

The static force required to collapse an automobile is less than 50,000 pounds.[E.10] The maximum impact forces for rail cars and truck tractor-trailers are estimated from the static forces reported for the crash tests of spent fuel casks.[E.11,E.12] The quasi-static forces for concrete structures such as walls, columns, and abutments were estimated from the mechanical loading analyses of the roadside structures given in Appendix D.

The method used to determine the maximum impact force trees and posts could resist was a one-dimensional (1-D) beam hand calculation to determine the limit moment. The loading condition we assumed is shown on Fig. E-10a. A plastic hinge forms when the entire tree/pole cross section yields at the location of maximum moment as shown in Fig. E-10b. A yield stress of 8,400 psi is assumed, based on three times the allowable for Douglas fir.[E.13] The bounding force (force to produce plastic hinge) for a solid circular Douglas fir cross section is $P = 233.38R^3$ lbs, where R is the radius of the tree in inches.

The bounding force for a pole, assuming a yield strength of 36 ksi, is

$$P = 1000\, R_o(R_o^2 - R_i^2)\left(\frac{1}{2 - \frac{t}{R_o}} + 1 - \frac{t}{R_o}\right) \qquad \text{(E.4)}$$

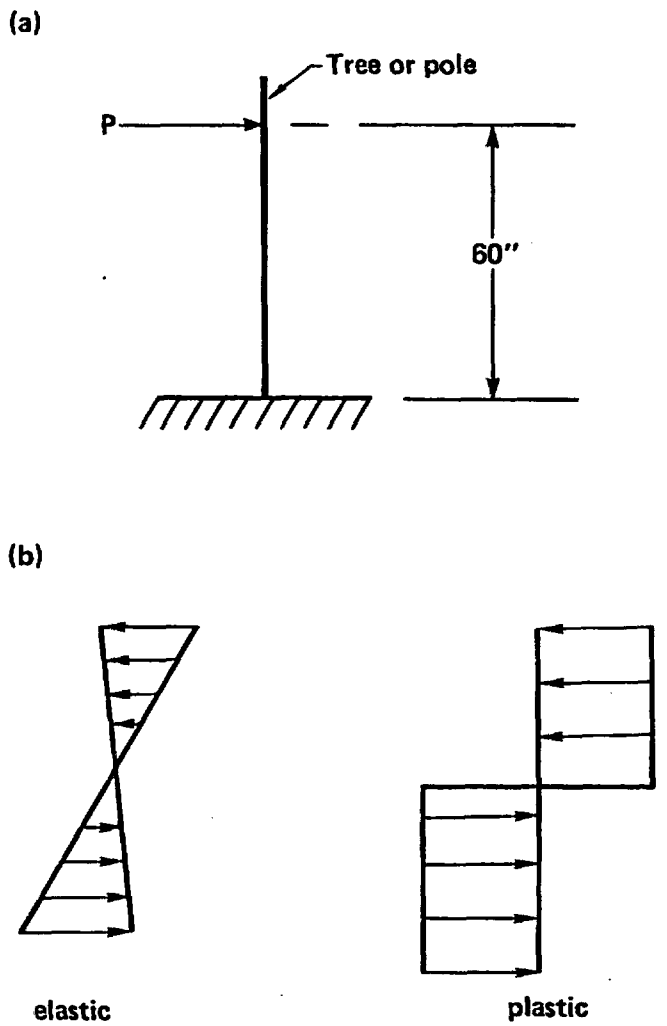

Plastic hinge forms when the entire cross section yields

Figure E-10 Loading conditions on trees and poles.

where

R_o = the pole outside diameter, inches,

R_i = the pole inside diameter, inches,

t = the pole wall thickness, inches.

Two examples of minor target bounding forces follow: a 1.5-foot-diameter Douglas fir tree has a bounding force of 1.7×10^5 lbs, and a 10-inch-diameter standard schedule pole has a bounding force of 2.95×10^4 lbs.

Low-resistance objects such as trees, road signs, electricity poles, motorcycles, passenger cars, trailers, and trucks can be screened out based on static analysis. Assuming that the impact force is linearly applied, the force/unit length that could cause local deformation can be estimated. The representative cask can resist a linear force of 100,000 pounds/foot to generate a strain of less than 0.2% (S_1) at the inner shell. The linear force to crush objects in many accidents is much less than 100,000 pounds/foot. Table E.7 lists objects that are typically impacted in an accident, many of which do not generate a maximum total force greater than 400,000 pounds or a linear force greater than 100,000 pounds/foot.

Stronger and more massive objects, such as trains, bridge columns, abutments, and real surfaces such as roadbeds are analyzed in Section E.7.

E.6 Impacts on Unyielding Surfaces

Impact calculation for the representative casks onto unyielding surfaces were divided into two categories: those where the cask structural response is essentially elastic and those where the cask structural response is elastic-plastic. The elastic response evaluations discussed in Subsection E.6.1 were performed primarily using the 1-D beam element code IMPASC.[E.14] The elastic-plastic response evaluations discussed in Subsection E.6.2 were performed using the DYNA and NIKE family of computer codes.

Table E.7
Quasi-Static Force Evaluation for Objects Potentially Impacted

Object	Total Force (lbs)	Linear Force (lbs/ft)
Truck Cask		
Endwise	3,300,000	
Sidewise	1,600,000	100,000
Rail Cask		
Endwise	13,000,000	
Sidewise	1,600,000	100,000
Auto	50,000	<10,000
Truck Tractor	100,000	<17,000
Truck Trailer	450,000	<70,000
Train	2,000,000	>250,000
Motorcycle	20,000	<10,000
Bus	300,000	<50,000
Sound Wall	50,000	<50,000
4 x 4 Column	900,000	>225,000

E.6.1 Elastic Response of the Cask

In order to perform the response calculation, it is essential that a proper computer code be selected. This computer code(s) must have the following special capacities or features:

1. Can provide dynamic impact analysis

2. Can analyze oblique impact

3. Can analyze impact limiter nonlinear behavior

4. Can analyze lead slump effect

5. Can be run inexpensively.

Three computer codes were selected, NIKE 2-D/3-D,[E.1] DYNA 2-D/3-D,[E.2] and IMPASC.[E.13] Each code has its special features, but also has weaknesses in meeting all the requirements. NIKE 2-D/3-D and DYNA 2-D/3-D are two of the most powerful finite element codes for dynamic impact analysis. They meet all the requirements listed above except that they are expensive to run. Especially when dealing with oblique impact and nonlinear impact limiters, the required 3-D modeling can result in costly calculations.

In order to manage the large amount of analysis required for this study, a code had to be found that could do analysis less expensively. The IMPASC code was selected. IMPASC was developed specifically for dynamic impact analysis of shipping casks to assess whether they meet the 10 CFR 71 design requirements. It has a special feature for handling oblique impact. This code can also analyze nonlinear behavior of the impact limiter, and is inexpensive to run. The deficiency is that IMPASC cannot assess the lead-slump effect.

The approach benchmarked the IMPASC results with DYNA/NIKE results to assess the lead slump, and then used the IMPASC code to run production calculations for impacts on an unyielding surface. From the sensitivity study

performed with the DYNA/NIKE codes in Subsection E.6.1.3, it was found that lead slump will not occur under any conditions as long as the axial force on the cask is smaller than 40 g. This is also the level at which it could be assured that the strain on the inner shell is less than 0.2% (S_1) and the closure seal is functional, since the impact limiter is designed to completely absorb the energy of this impact force level.

Sensitivity studies were performed to show that the inclusion of the cask contents does not significantly change the strain levels in the cask. The sensitivity studies included the following: lumping the weight of the contents at the bottom end of the cask, modeling the contents as elements with mass but no stiffness in the cask cavity, and modeling the contents with mass and an estimated stiffness to simulate fuel bundles and the fuel basket. Liquids such as water are not contained in the cask, because helium is the coolant. The resulting changes in stress-strains and g loads for the various models were not significant for the purposes of this study.

E.6.1.1 Truck Cask Impact

The IMPASC code was used to perform impact analysis on an unyielding surface for the truck cask. The analysis was done by varying the other two parameters: cask orientation angle and impact velocity. The cask response was calculated for the cask orientation angles of 0^{o}, 10^{o}, 30^{o}, 50^{o}, 70^{o}, and 90^{o} and impact velocities of 30 mph, 38 mph, and 45 mph. The impact velocity is defined as the velocity component in the direction perpendicular to the impact surface. The 0^{o} cask orientation angle represents impact to the side of the cask, whereas the 90^{o} cask orientation angle represents impact to the end of the cask.

For the 90^{o} angle case, the effects due to the truck cab crushing and lead slump pressure were included. The effects of lead pressure were calculated using NIKE and are discussed in Subsection E.6.1.3. The effects of the cab crush for front-wise impacts, which can be taken into account by increasing the impact velocity required to give equivalent strain, was estimated using an energy balance. The energy absorbed by the cab is estimated as

$$E_a = F_I \times d \tag{E.5}$$

where F_I is the impact or crush force of the truck cab in inches and d is the total distance the cab can be crushed in inches.[E.11] The kinetic energy required to cause the same response for the cask when the cab crush is included is estimated as

$$\left(\tfrac{1}{2} MV_2^2\right)_C = E_a + \left(\tfrac{1}{2} MV_1^2\right)_{WC} \tag{E.6}$$

where M is the mass of the truck and cask in lbs; V_2 is the impact velocity in ft/sec used to find the strain, taking into account cab crush energy absorption; and V_1 is the impact velocity in ft/sec without cab crush energy absorption as used in IMPASC code calculations. The mass of the truck was taken from SAND77-0270.[E.11] The velocity required to cause the same cask response when cab crush is considered is

$$V_2^2 = \frac{2E_a + MV_1^2}{M} \quad . \tag{E.7}$$

The effects of cab crush are included only for impact velocities up to 60 mph; at higher velocities the cask will break from its tie-downs and leave the truck without any velocity reduction caused by truck cab crush.[E.11] Table E.8 summarizes the velocities required to cause the same cask response when cab crush is included as compared to the velocities without cab crush. The effective impact velocity to take into account cab crush, V_2, is used to determine the strain for a given impact velocity as calculated by the IMPASC code. For instance, the strain at 30 mph as calculated by IMPASC for a truck cask is assumed to occur at 34.6 mph when cab crush is taken into account.

Table E.8
Impact Velocities Required to Include Cab and
Rail Car Crush Energy Absorption

Velocity without Crush (mph)	Velocity with Cab Crush (mph)	Velocity with Rail Car Crush (mph)
30	34.6	35
45	48.2	48.5
60	62.4	62.8

The strain variation with cask orientation angle for various impact velocities are given in Table E.9. From these results it was concluded that for the representative truck cask the endwise and sidewise strain responses bound the strain responses for all cask orientations. For cask orientations from $0\text{-}90^{0}$ the structural strain responses can be linearly interpolated between the sidewise and endwise strain responses. The strain is 0.2% (S_1) at the impact velocity of 32 mph for sidewise impacts and 38 mph for endwise impacts.

E.6.1.2 Rail Cask Impact

The IMPASC code was used to perform these analyses. The analysis was done by varying the other two parameters, i.e., cask orientation angle and impact velocity. The cask response was calculated for the cask orientation angles of 0^{0}, 10^{0}, 30^{0}, 50^{0}, 70^{0}, and 90^{0} and impact velocities of 30 mph, 45 mph, and 60 mph. The impact velocity is defined as the velocity component in the direction perpendicular to the object surface. The 0^{0} cask orientation angle represents the impact to the side of the cask, whereas the 90^{0} cask orientation angle is the impact to the end of the cask. The results of this sensitivity study are given in Table E.10. As done for the truck cask, for the 90^{0} angle case we included the effects of lead slump pressure and crushing the front end of the rail car transporting the cask. Table E.8 summarizes the velocities required to include the rail car crush effects. From the results it is concluded that for the representative rail cask, the endwise and sidewise strain responses bound the strain responses for all cask orientations. For cask orientations from $0\text{-}90^{0}$, the structural strain responses can be linearly interpolated between the sidewise and endwise strain responses. The strain at the inner wall is 0.2% (S_1) at the impact velocity of 55 mph for sidewise impacts and 38 mph for endwise impacts.

E.6.1.3 IMPASC and NIKE Comparison

The IMPASC code was benchmarked for endwise impacts at 30 mph on an unyielding surface against the NIKE computer code. Table E.11 summarizes the pertinent results for the representative truck and rail casks. For the truck

Table E.9
Truck Cask Strain Response to Impact on Unyielding Surface at Various Cask Orientations

Cask Orientation Angle (°)	Strain (%) Impact Velocity (mph) 30	38	45
0	0.175	0.270	0.650
10	0.133	0.210	0.260
30	0.115	0.180	0.255
50	0.107	0.180	0.244
70	0.064	0.081	0.115
90[a/]	0.060	0.200	2.00

[a/] Includes effects of cab crush and lead slump for 90° impact

Table E.10
Rail Cask Strain Response to Impact on Unyielding Surface at Various Cask Orientations

Cask Orientation Angle (°)	Strain (%) Impact Velocity (mph) 30	45	60
0	0.046	0.135	0.235
10	0.027	0.057	0.091
30	0.027	0.059	0.096
50	0.026	0.059	0.088
70	0.015	0.031	0.060
90[a/]	0.05	1.00	7.00

[a/] Includes effects of cab crush and lead slump for 90° impact

Table E.11
IMPASC Endwise Impact Benchmark Calculation
Against NIKE 2-D

	Truck at 30 mph		Rail at 30 mph		
	NIKE 2-D	IMPASC	Bonded Elastic NIKE 2-D	Unbonded Elastic-Plastic NIKE 2-D	IMPASC
Force (g)	37.5	45.0	36	36	28.6
σ axial (psi)	-9543.	-12200	-6732	-12035	-7100
Maximum deflection of limiter (inches)	25.8	26.5	25.3	25.8	26.5
Maximum plastic strain or effective strain if elastic (°)	0.00077	N/A	0.00038	0.0012	N/A

cask calculations, the material properties of Section E.2 and cask configuration of Fig. E-15 were used. In the NIKE calculation the lead was assumed to be unbonded from the stainless steel shells, whereas in the IMPASC calculation the lead was assumed to be bonded. The calculated impact force was approximately 38 g at 30 mph and the impact limiter deflection was approximately 26 inches in both calculations. Rail cask calculations were made with NIKE for bonded and unbonded lead. The results for the bonded lead are in good agreement with the IMPASC results which are also based on the assumption of bonded lead. The effect of assuming the lead unbonded is primarily an increase of the stress and strain on the inner shell of the cask caused by the lead pressure. From this benchmark comparison it was concluded that significant lead slump would not occur and the plastic strain is less than 0.2% (S_1) when the axial impact force on the cask is less than 40 g.

E.6.2 Elastic-Plastic Response by Cask

Elastic-plastic calculations were necessary when cask impact forces exceeded 40 g. Several of the capabilities of the DYNA and NIKE finite element codes that are critical to such calculations are (1) elastic-plastic material models, (2) sliding interfaces, (3) dynamic solutions, and (4) the ability to solve large deformation problems. The cask models include a 304 stainless steel inner wall, lead shielding and a 304 stainless steel outer wall. Each of the materials was modeled as a bilinear elastic-plastic material. The material properties used are summarized in Section E.2. The calculations were performed for endwise and sidewise impacts. The cask responses to impacts at other cask orientations are assumed to be bounded by the endwise and sidewise response results.

E.6.2.1 Endwise Impacts

Endwise impact calculations were performed for the representative truck and rail casks striking an unyielding surface. The casks were dropped from several heights onto an unyielding surface to obtain their responses over a range of impact conditions. The casks were modeled as 2-D axisymmetric composite cylinders with closures as shown in Fig. E-5. MAZE was used to

generate the finite element meshes. DYNA 2-D/NIKE 2-D were used to perform the impact calculations.[E.15]

E.6.2.1.1 Truck Cask Impact

The truck cask was modeled using two elements for the inner shell as shown in Fig. E-11. The results of the endwise impact calculations are summarized in Table E.12. The sudden deceleration of impact caused the lead shielding to slump and the cask length to decrease as shown in Fig. E-12 for the 60 mph impact. The maximum strain conditions occur at the inner wall at the flange joint as shown in Fig. E-13 for the 60 mph impact. The velocity changes with time, or decelerations, of the steel structure and the lead shielding were significantly different as shown in Fig. E-14 for the 60 mph impact. All impact calculations were terminated after rebound occurred. The lead slump is determined by finding the void between the cask steel body and lead shield. For example, consider a truck cask impacting at 60 mph. The time for the lead and the steel to reach zero velocity is extrapolated from Fig. E-14 as 19 msecs. Then the curves on Fig. E-12 are extrapolated to 19 msecs. This gives 16.5 inches of axial displacement at the top of the lead, and 4.2 inches in the steel at the top of the lead cavity. The relative displacement is the lead slump, and is (16.5 - 4.2) 12.3 inches.

An average interface deceleration force was calculated for the cask at each impact velocity by averaging the interface force over the time it took the steel structure to come essentially to a stop as shown in Fig. E-14. For example, consider the truck cask impacting at 60 mph. The time for the total steel mass to come nearly to a stop is 6 msecs as determined from Fig. E-14. The steel interface force acting for the first 6 msec of impact ranges from a high of 373 g to a low of 143 g, therefore the average interface force is the sum of the forces divided by 2 or 258 g. The average interface deceleration force was used to estimate the cask response to impacts on real surfaces as discussed in Section E.7.

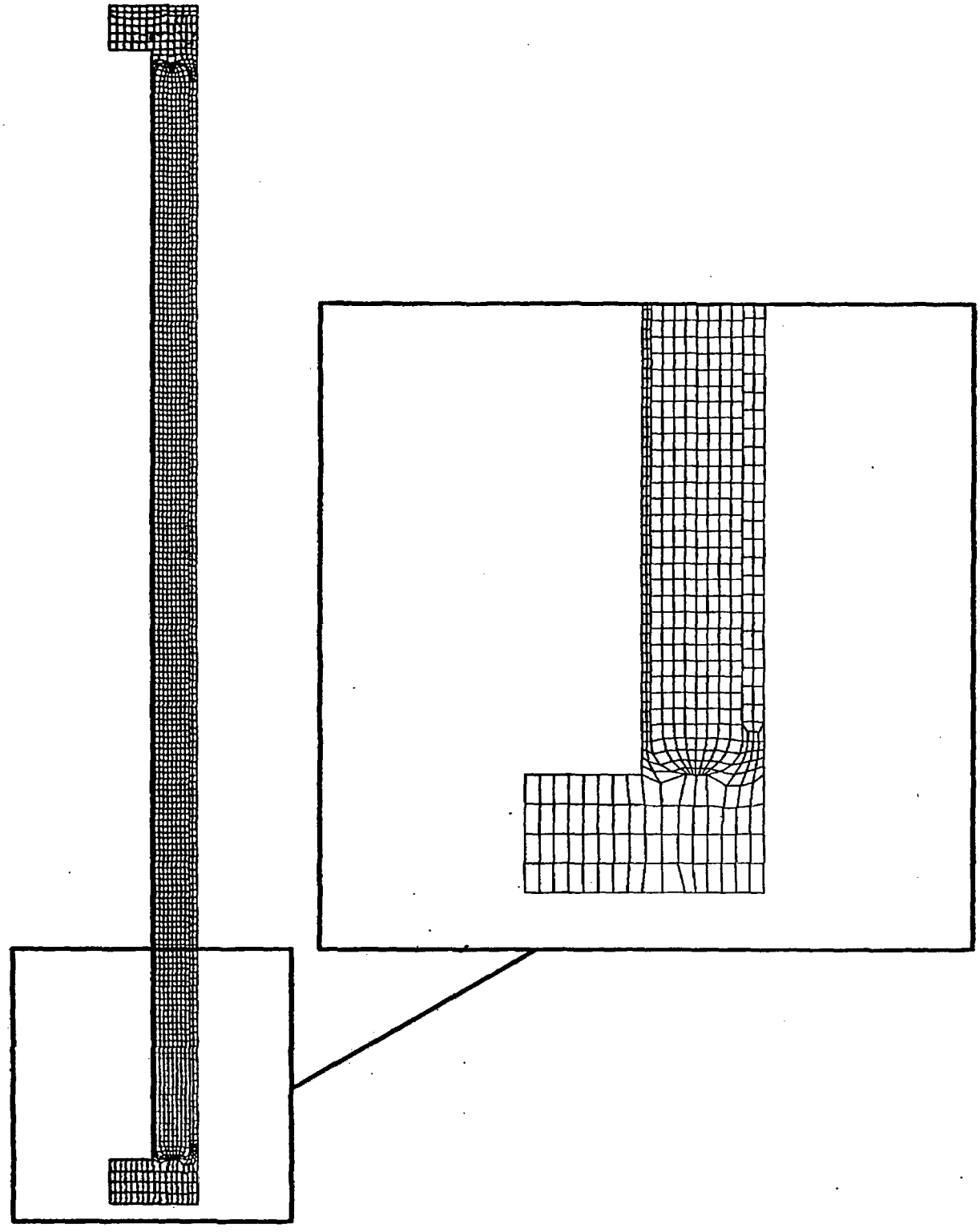

Figure E-11 Finite element mesh for two-element inner-wall model by truck cask.

Table E.12
Summary of Truck Cask Endwise Impact Results[a/]

Velocity (mph)	Interface Deceleration Force (g)	Strain Inner Shell (%)	Lead Slump (in)
30	38	0.077	0
45	90	3.60	4
60[b/]	258	23.3	12.3
90[b/]	353	36.2	24

[a/] Cab crush not included in analysis.

[b/] Impact limiter not included in analysis.

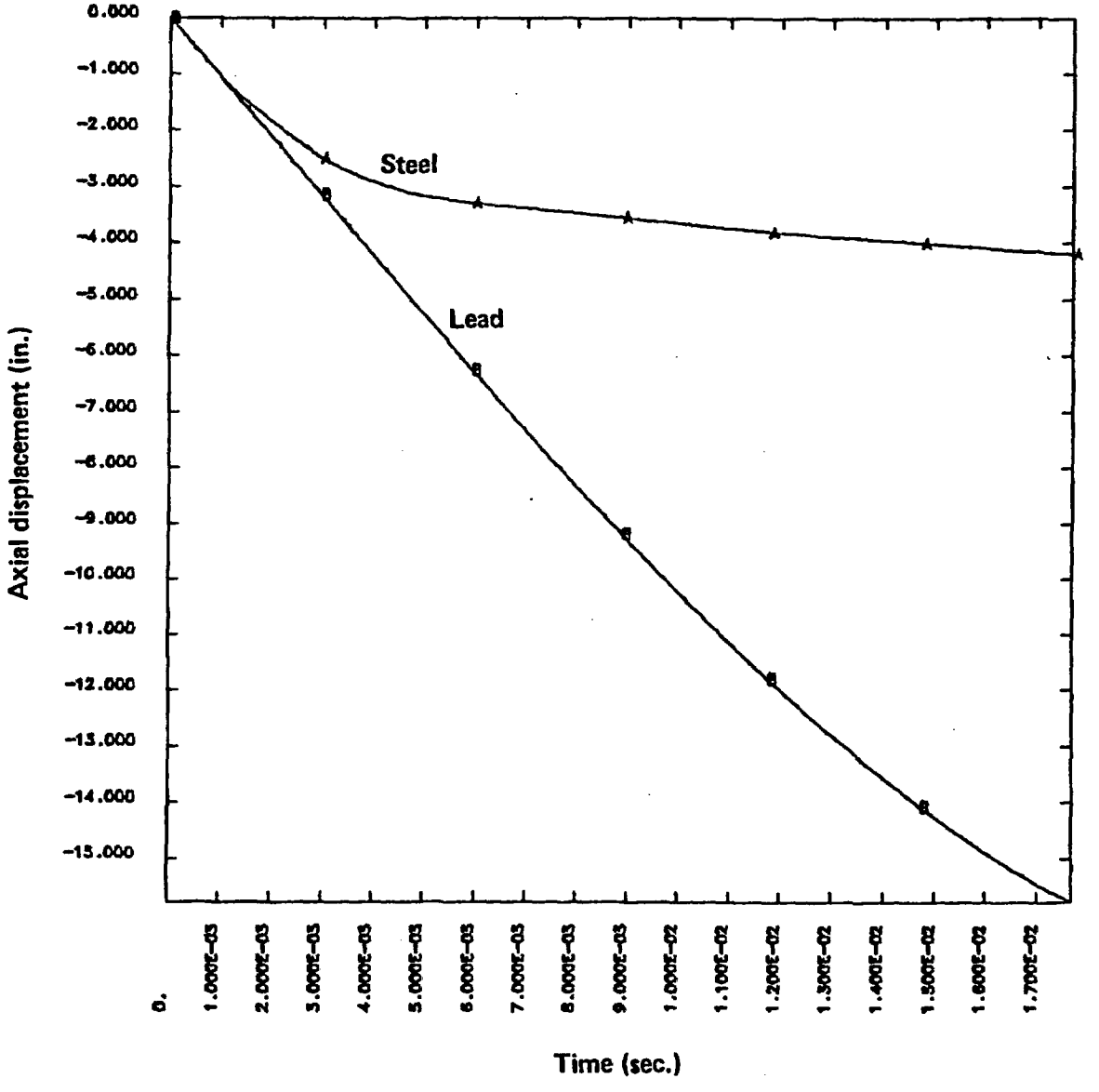

Figure E-12 Lead slump in truck cask at 60 mph impact.

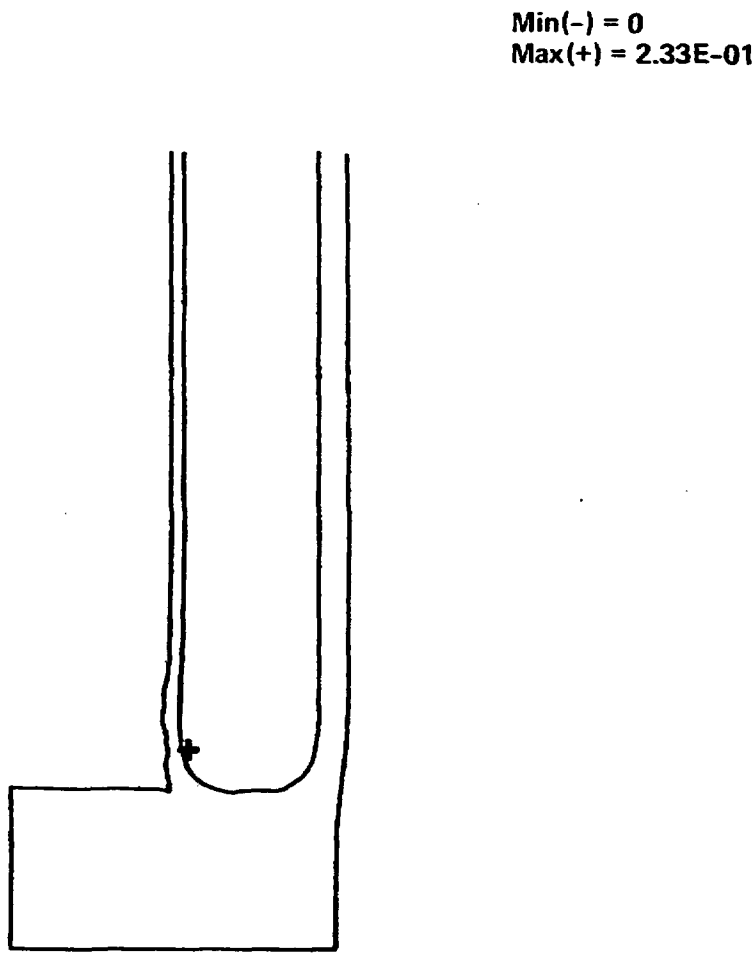

Figure E-13 Strain in lower steel structure for truck cask impact at 60 mph.

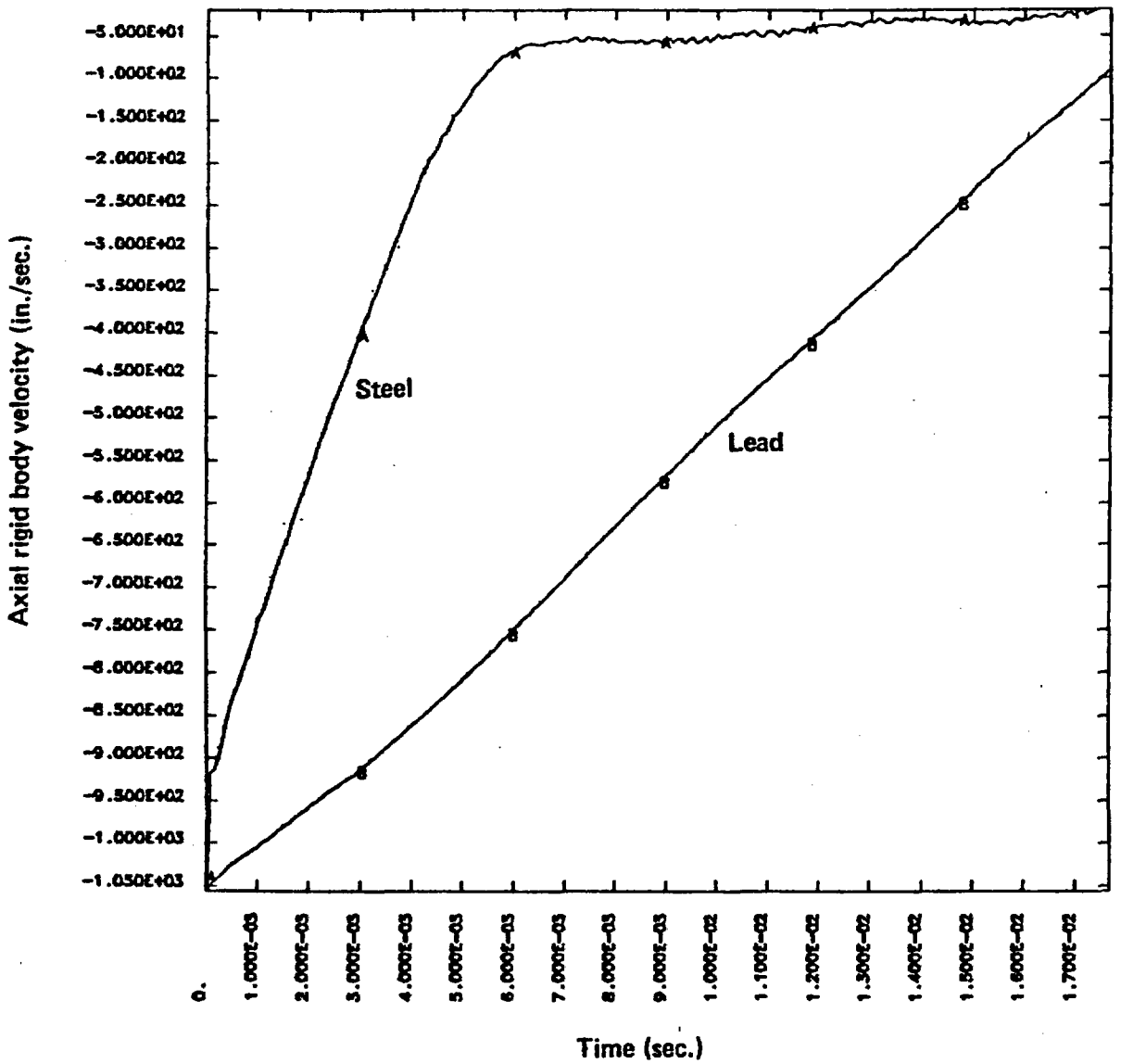

Figure E-14 Velocity versus time for truck cask impact at 60 mph.

E.6.2.1.2 Rail Cask Impact

The rail cask was modeled using two elements for the inner shell as shown in Fig. E-15. The results of the endwise impact calculations are summarized in Table E.13. The lead slump that occurred in the rail cask is shown in Fig. E-16 for the 90 mph impact. The strain condition in the steel structure at the end of impact is shown Fig. E-17 for the 90 mph impact. The velocity change for the steel structure and lead shielding is shown in Fig. E-18. The average interface deceleration force was calculated from Fig. E-18 for the 90 mph impact with the method discussed in Subsection E.6.2.1.1 for the truck cask.

E.6.2.2 Sidewise Impacts

Two-dimensional plane strain analyses without impact limiters or end enclosures were performed for sidewise impacts on an unyielding surface to estimate the 3-D responses for the casks. This approximate 2-D method overestimates strain responses of the representative casks, particularly for impact velocities less than 60 mph and for impacts on soft surfaces such as soil. The 2-D method was benchmarked in Subsection E.6.2.2.3 with a 3-D impact analysis that modeled the representative truck cask with impact limiters and end closures. This approximate method eliminates the need to perform a series of 3-D sidewise impact analyses.

The 2-D truck cask models were developed using the SLIC interactive mesh generator.[E.16] The dimensions in the SLIC command file were modified to generate the rail cask models. The cask models do not include contents. DYNA 2-D (2), an explicit 2-D hydrodynamic finite element program, was used to do the plane strain analysis.

E.6.2.2.1 Truck Cask Impact

For unyielding surface impacts, a vertical symmetry plane was used in the modeling as shown in Fig. E-19 to reduce the solution cost. The calculations were performed for three different truck cask initial velocities: 30 mph, 60 mph, and 90 mph. The calculations were terminated when the cask started to

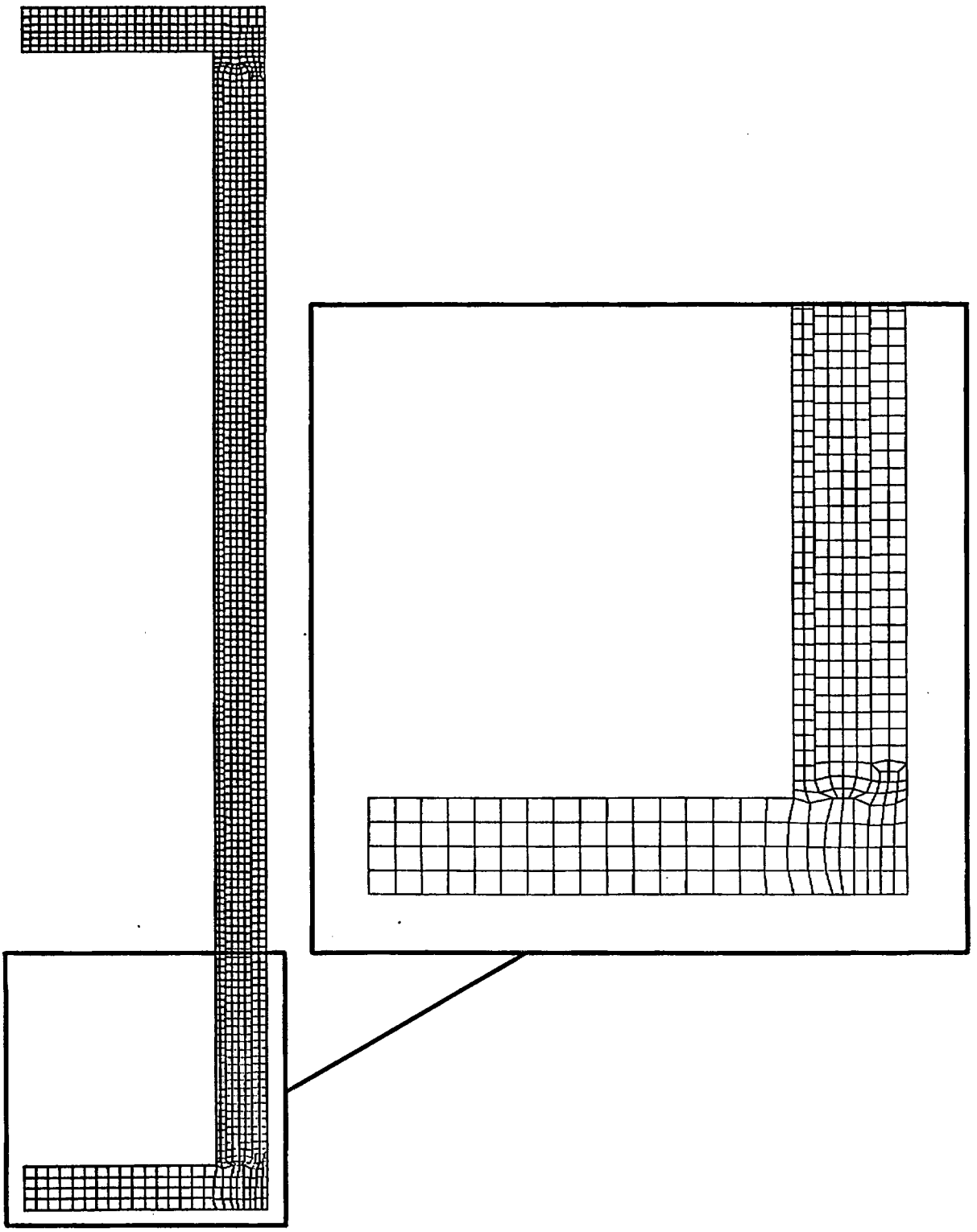

Figure E-15 Finite element mesh for rail cask.

Table E.13
Summary of Rail Cask Endwise Impact Results[a/]

Velocity (mph)	Interface Deceleration Force (g)	Strain Inner Wall (%)	Lead Slump (in)
30	36	0.12	0.5
45	103	1.9	6.0
90[b/]	425	24.3	24.8

[a/] Cab crush not included in analysis.

[b/] Impact limiter not included in analysis.

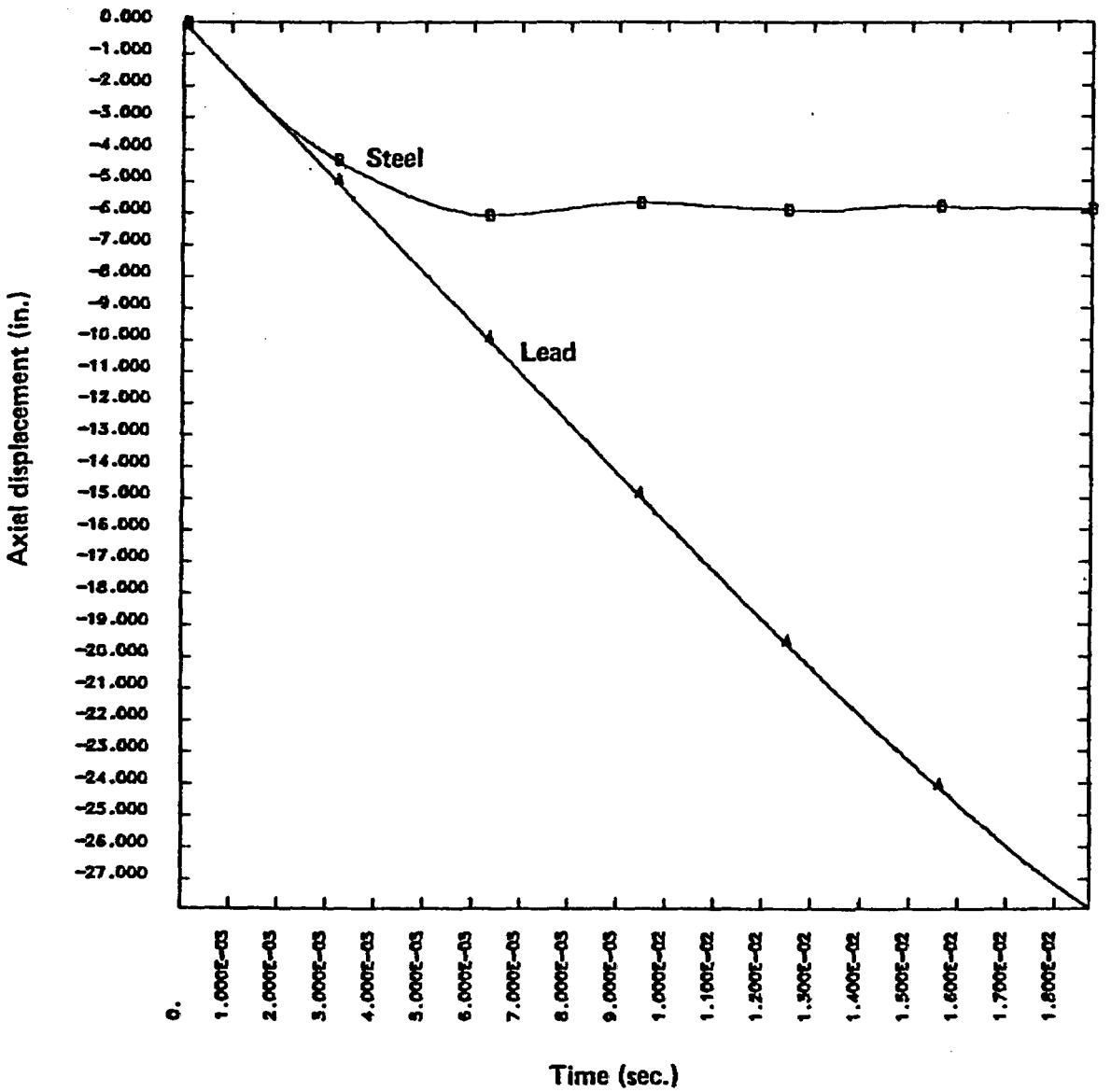

Figure E-16 Lead slump in rail cask at 90 mph impact.

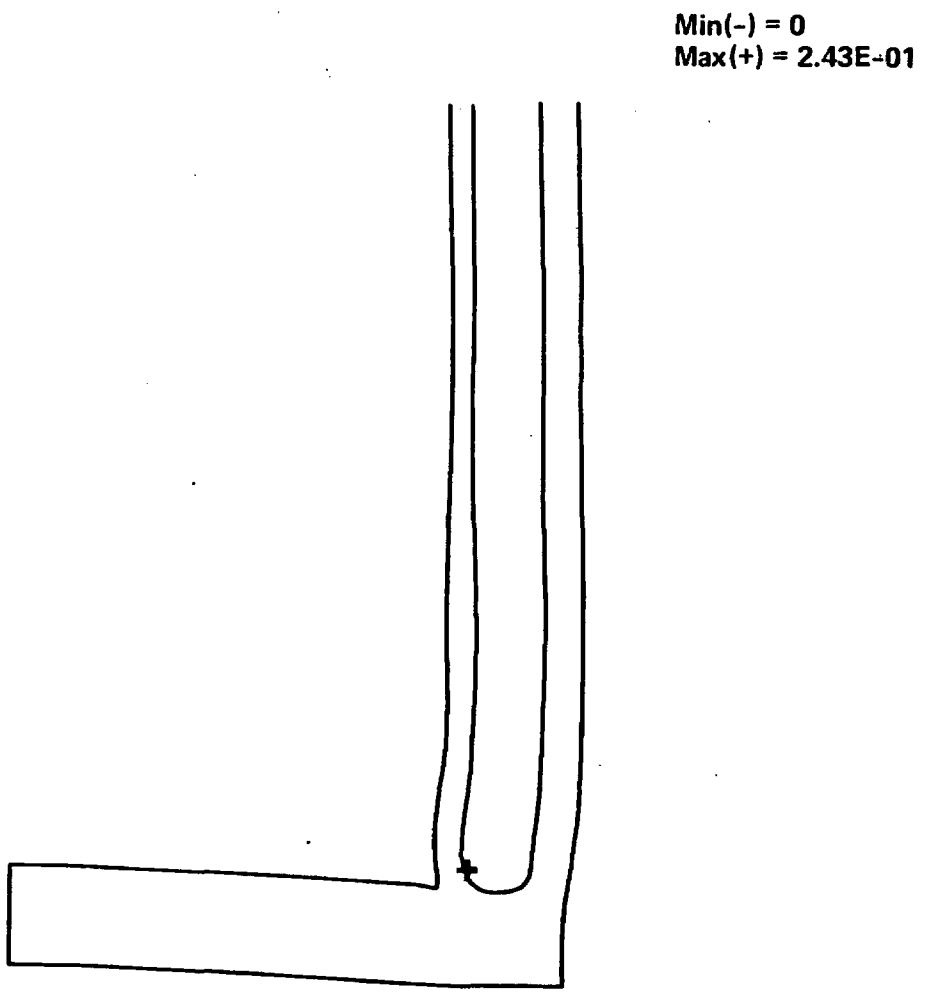

Figure E-17 Strain in lower steel structure for rail cask impact at 90 mph.

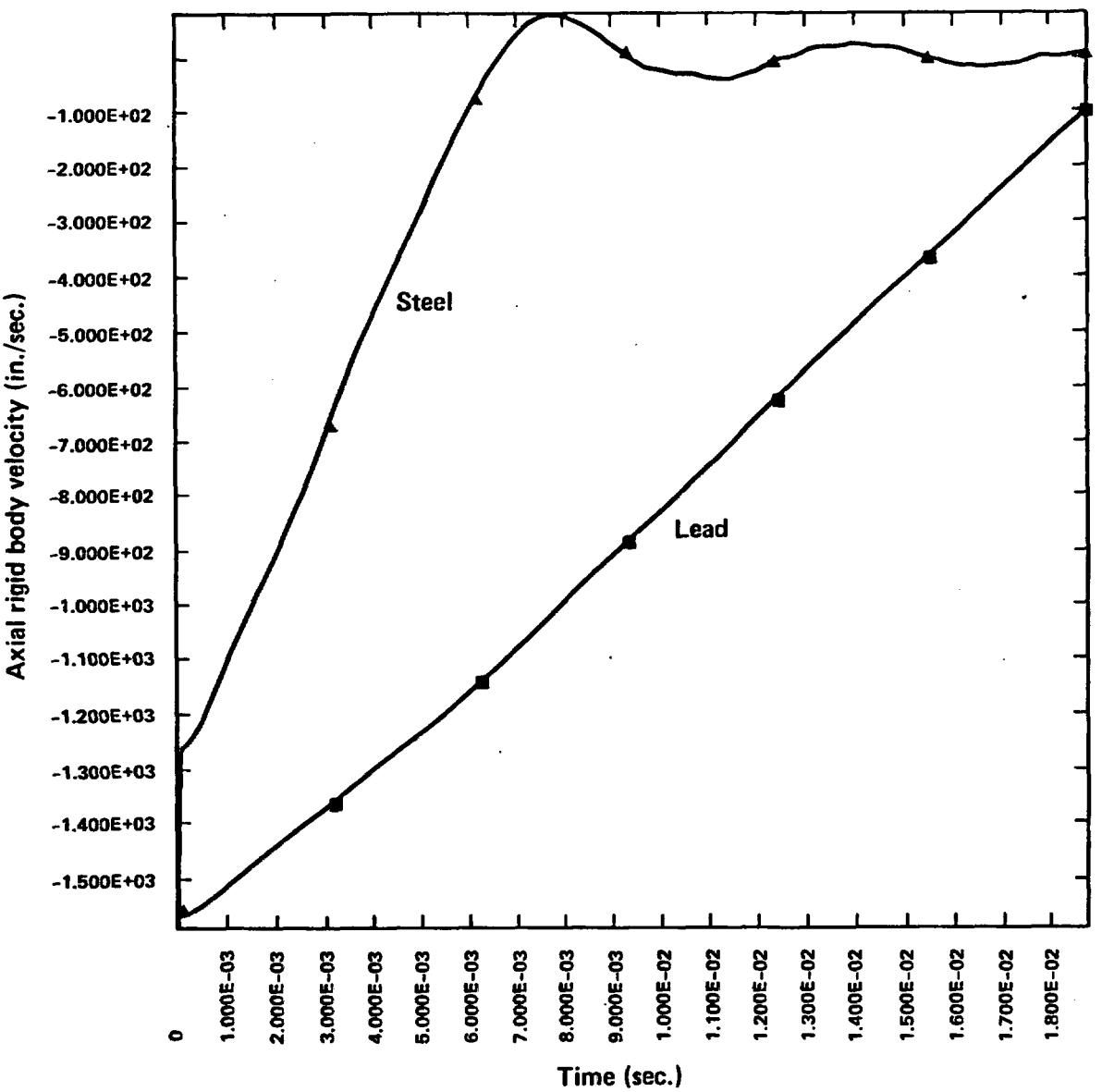

Figure E-18 Velocity versus time for rail cask impact at 90 mph.

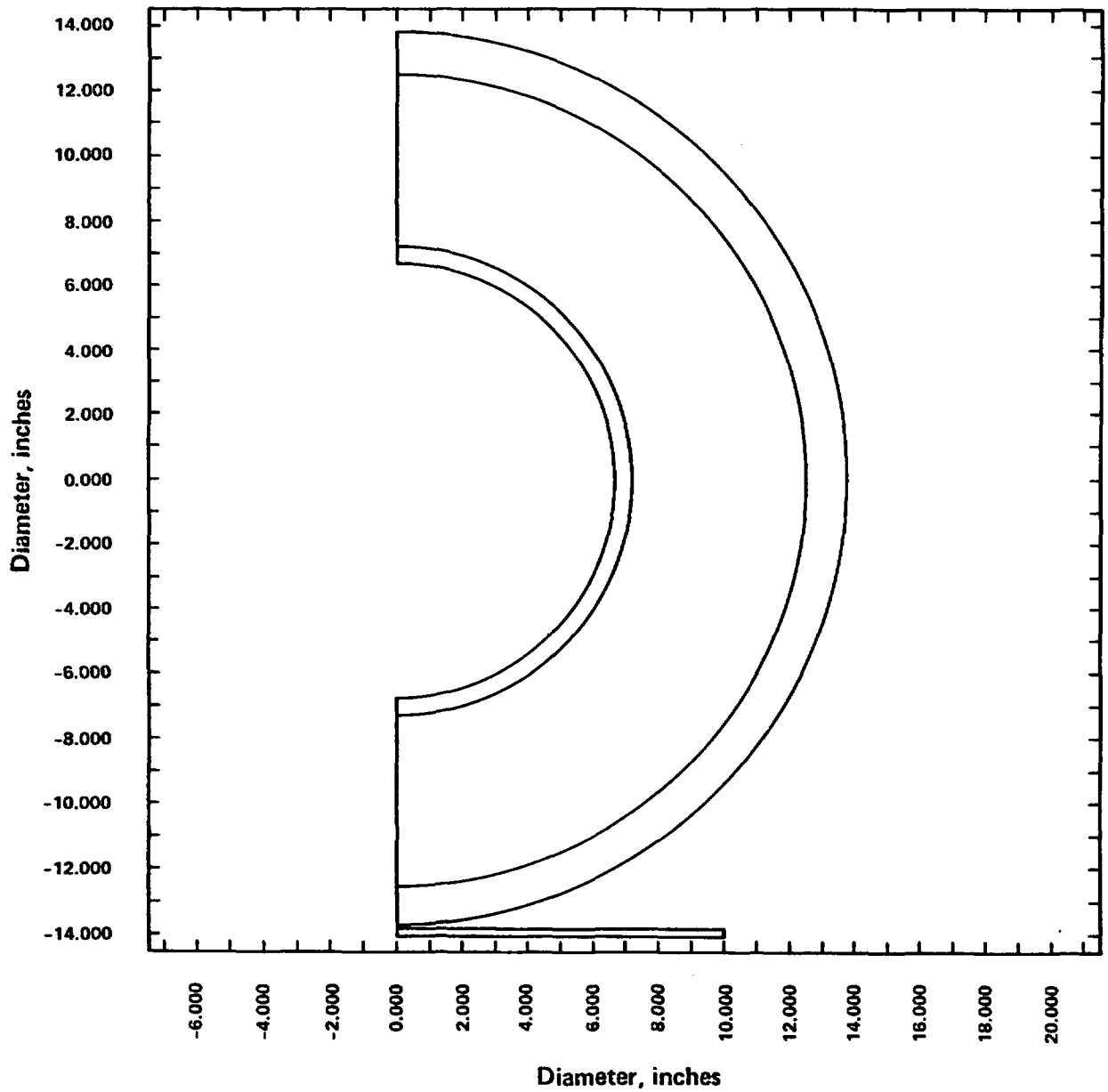

Figure E-19 Model of a truck cask impacting an unyielding surface.

rebound. The sudden deceleration caused the cask to flatten as shown in Fig. E-20.

For the 30 mph impact, the cask experienced 160 g's and sustained a maximum effective stress of 36,000 psi and maximum plastic strain of 5.9% in the steel shells. For 60 mph, the g's increased to 342, the maximum effective stress increased to 45,300 psi and the maximum plastic strain increased to 14%. These results are summarized in Table E.14. The location of the maximum plastic strain is shown in Fig. E-21 for the 60 mph impact.

E.6.2.2.2 Rail Cask Impact

Calculations were performed for the rail cask with initial velocities of 30 mph and 60 mph. The 30 mph calculation was terminated when the cask started to rebound. The 60 mph calculation was terminated when the cask started to fold on itself. The sudden deceleration caused the cask to flatten considerably and, in the 60 mph case, to develop a plastic hinge as shown in Fig. E-22. The cask contents would to some degree resist the formation of the plastic hinge. However, the cask contents were not modeled.

For the 30 mph impact, the cask experienced a force of 29 g's and sustained a maximum effective stress of 32,400 psi and maximum plastic strain of 4.1% in the steel shells. For 60 mph, the g's increased to 47, the maximum effective stress increased to 37,400 psi and the maximum plastic strain increased to 7.2%. These results are summarized in Table E.15. The location of the maximum plastic strain is shown in Fig. E-23 for the 60 mph impact.

E.6.2.2.3 Three-Dimensional Sidewise Impact

A 3-D truck shipping cask was modeled for the side-drop analysis with impact limiters. As shown in Fig. E-24, the model includes the inner and outer steel shells, the lead shielding, the steel end caps, and the balsa wood impact limiters. The finite element model was generated using SLIC, an interactive mesh generator. The impact limiters were not tied to the cask, conservatively allowing them to slide relative to the cask because any bolt retaining forces that could be present are unknown. Two planes of symmetry

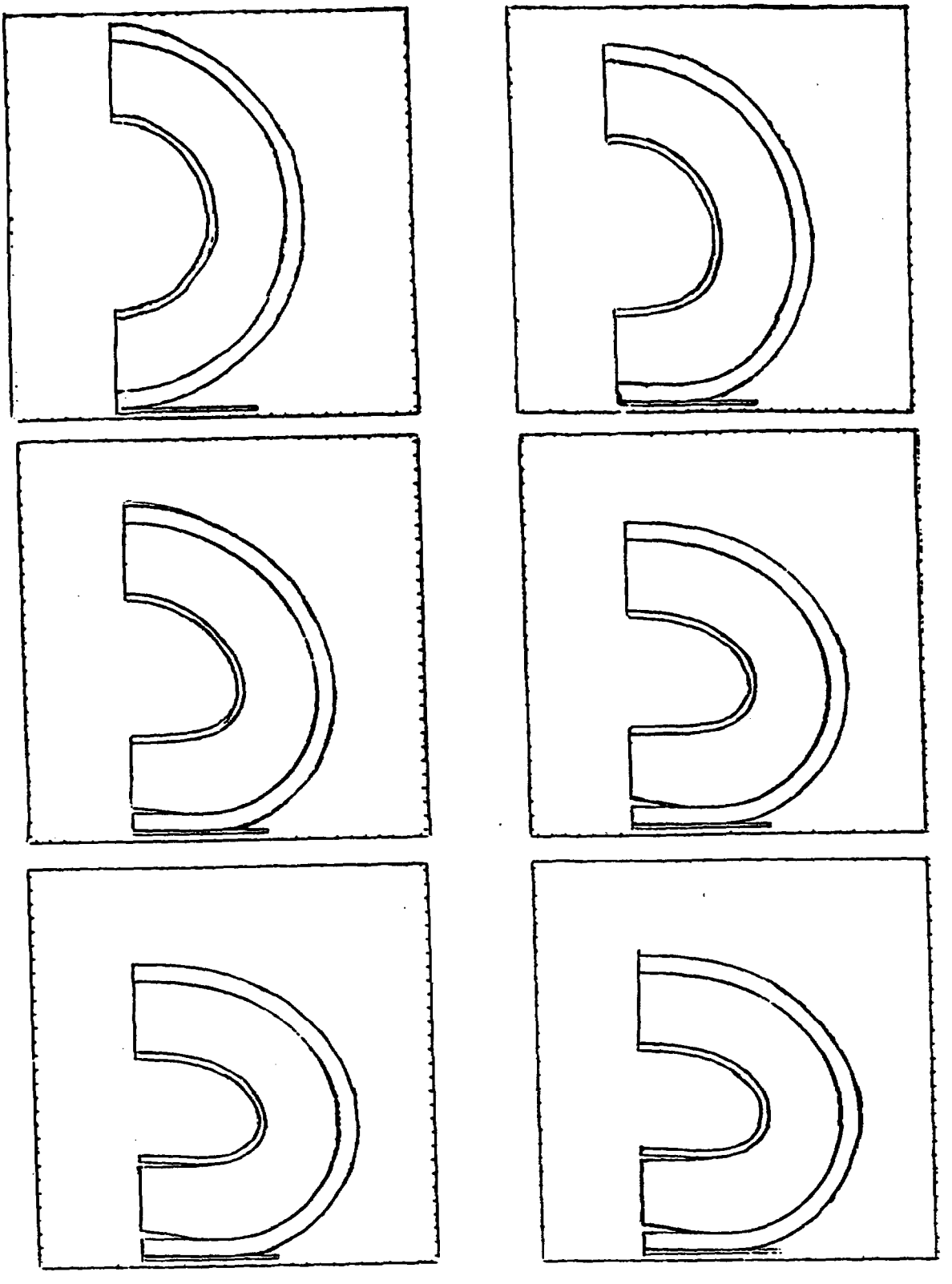

Figure E-20 Truck cask impact on unyielding surface at 60 mph.

Table E.14
Results of Truck Cask Sidewise Impact on an Unyielding Surface

Cask impact velocity (mph)	30	60	90
Time at which rebound starts (sec)	0.0085	0.008	0.0075
g load on cask (g)	160	342	547
Maximum effective stress (psi)	36,000	45,300	63,100
Maximum plastic strain (%)	5.9	14.	23.1

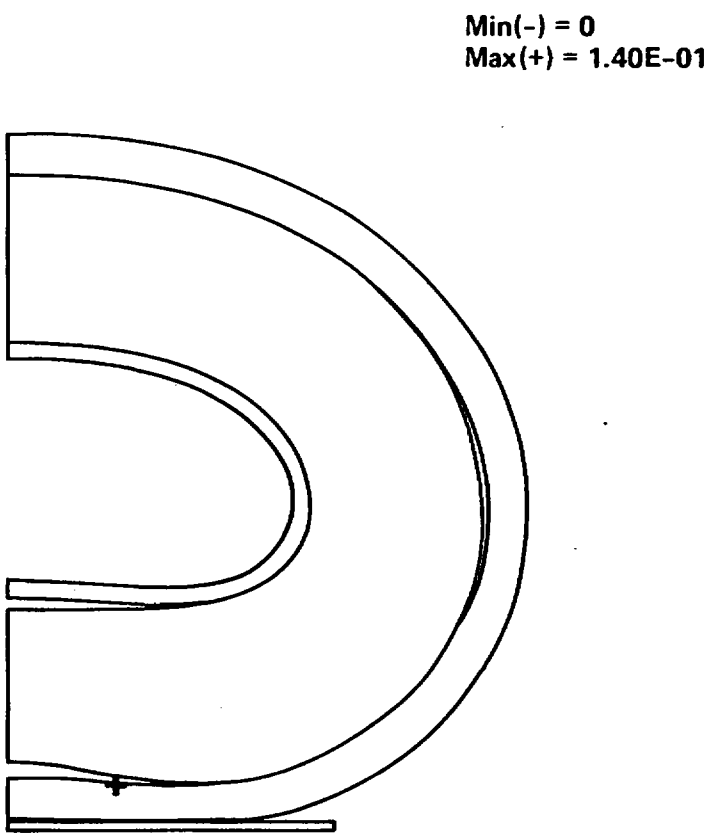

Figure E-21 Impact on unyielding surface at 60 mph - maximum plastic strain location.

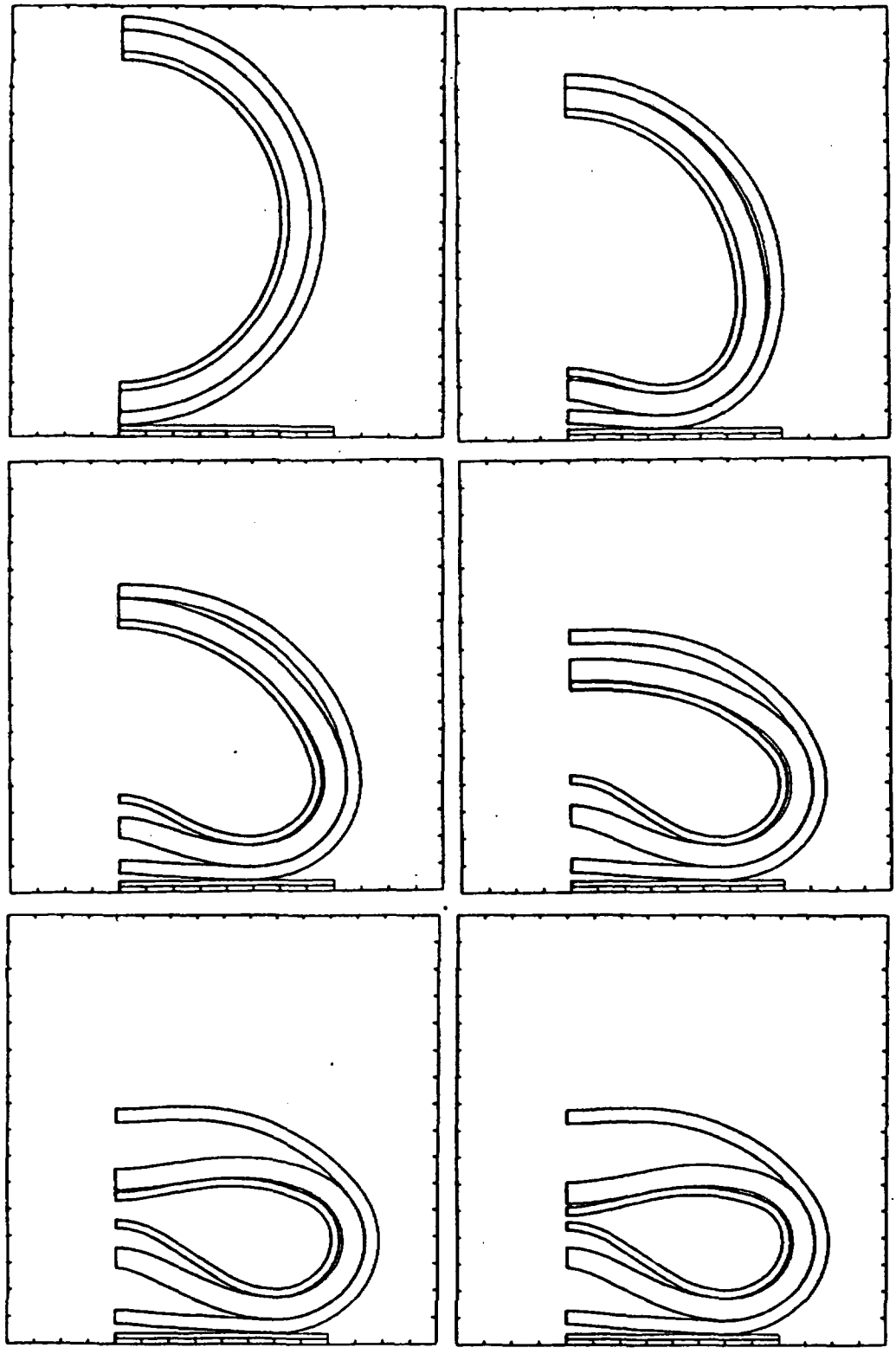

Figure E-22 Rail cask impact on unyielding surface at 60 mph.

Table E.15
Results of Rail Cask Sidewise Impact on an Unyielding Surface

Cask impact velocity (mph)	30	60
Time at which rebound starts (sec)	0.048	N/A
g load on cask (g)	29	47
Maximum effective stress (psi)	32,400	37,400
Maximum plastic strain (%)	4.1	7.2

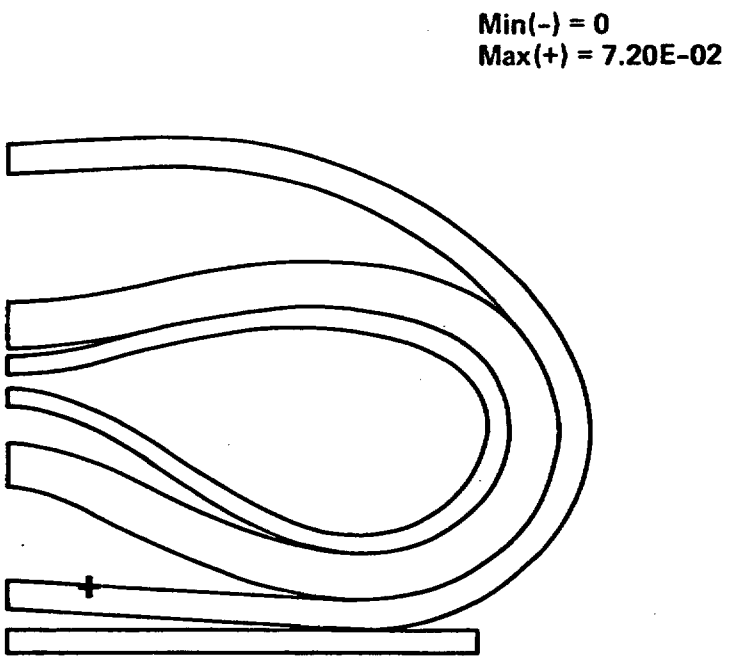

Figure E-23 Rail cask impact on unyielding surface at 60 mph - maximum plastic strain location.

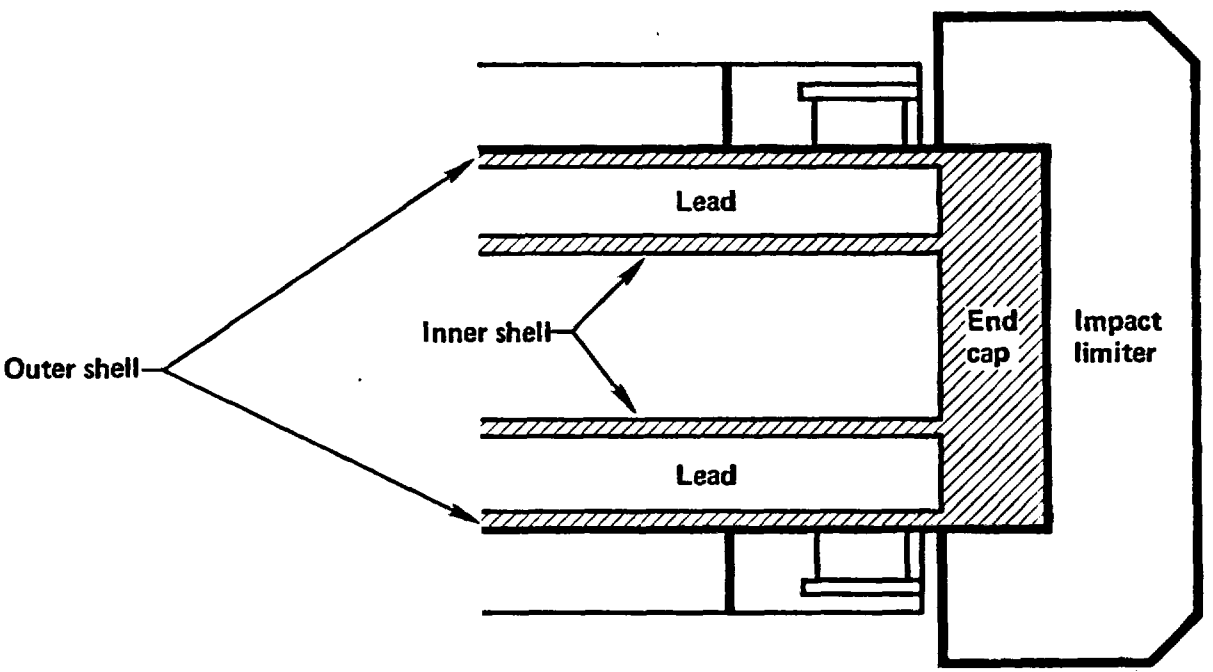

Figure E-24 Full side drop geometry including impact limiters.

were incorporated to reduce the model's complexity. The inner and outer steel shells were modeled using the thick shell option in DYNA 2-D.

The impact velocity was 60 mph, resulting in deceleration of 108 g's and the deformation shown in Fig. E-25. The cask bowed because it was supported by the impact limiters around the end caps. The center of the cask impacted the unyielding surface at almost 60 mph. The contact area increased to approximately half the length of the cask when impact was complete and rebound started to occur. The strain distribution shown in Fig. E-26 indicates that the maximums occur at the center of the cask. The maximum effective stress was 42,500 psi; the maximum plastic strain was 8.7%; and the maximum shear stress was 24,400 psi.

The calculation of the full side-drop with impact limiters showed several things. First, the cask bows when the ends impact first because of the impact limiters. Second, as the cask bows and the center of the cask impacts the unyielding surface, the center of the cask is still traveling at almost full speed. The bowing does not slow down the center of the cask.

A thin slice of the cask was isolated at the center and compared with a 2-D plane strain calculation with the same impact velocity of 60 mph. The deformations are virtually the same as shown in Fig. E-27. The stresses and strains also compared favorably. Since the deformed slopes compared so closely, it was concluded that 2-D calculations can be used to represent 3-D impacts on surfaces at 60 mph and greater.

E.7 Impacts on Real Objects

Ideally, it would be desirable to perform the response calculations assuming both representative casks and real impact surfaces. This can be done using either DYNA 2-D/3-D or NIKE 2-D/3-D computer codes. However, given that computer runs have to be performed to cover many variations in cask orientation angle, surface hardness, and impact velocities, expense precludes the use of DYNA or NIKE codes for each case.

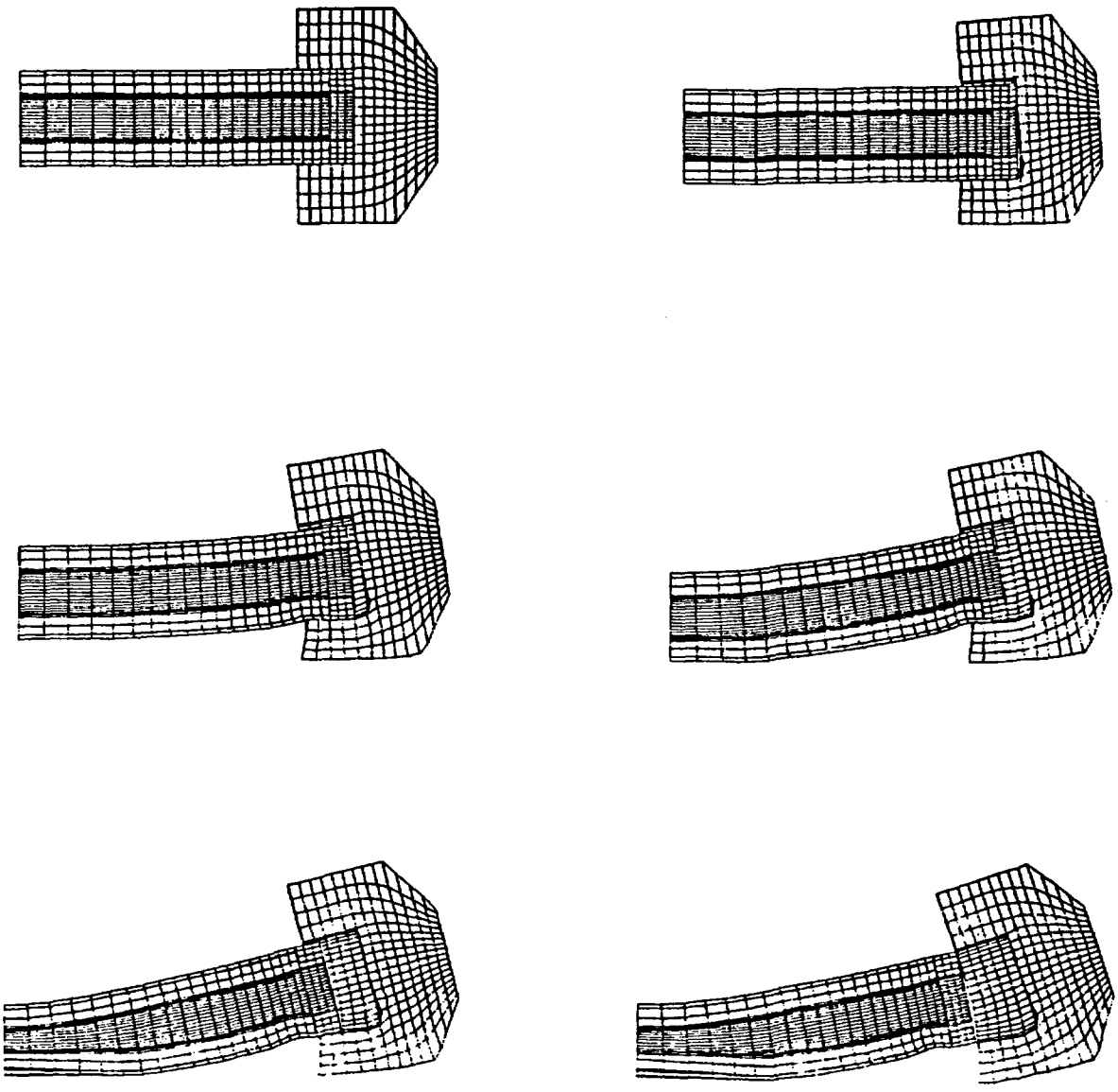

Figure E-25 Deformations of truck cask during 60 mph side drop (side view)

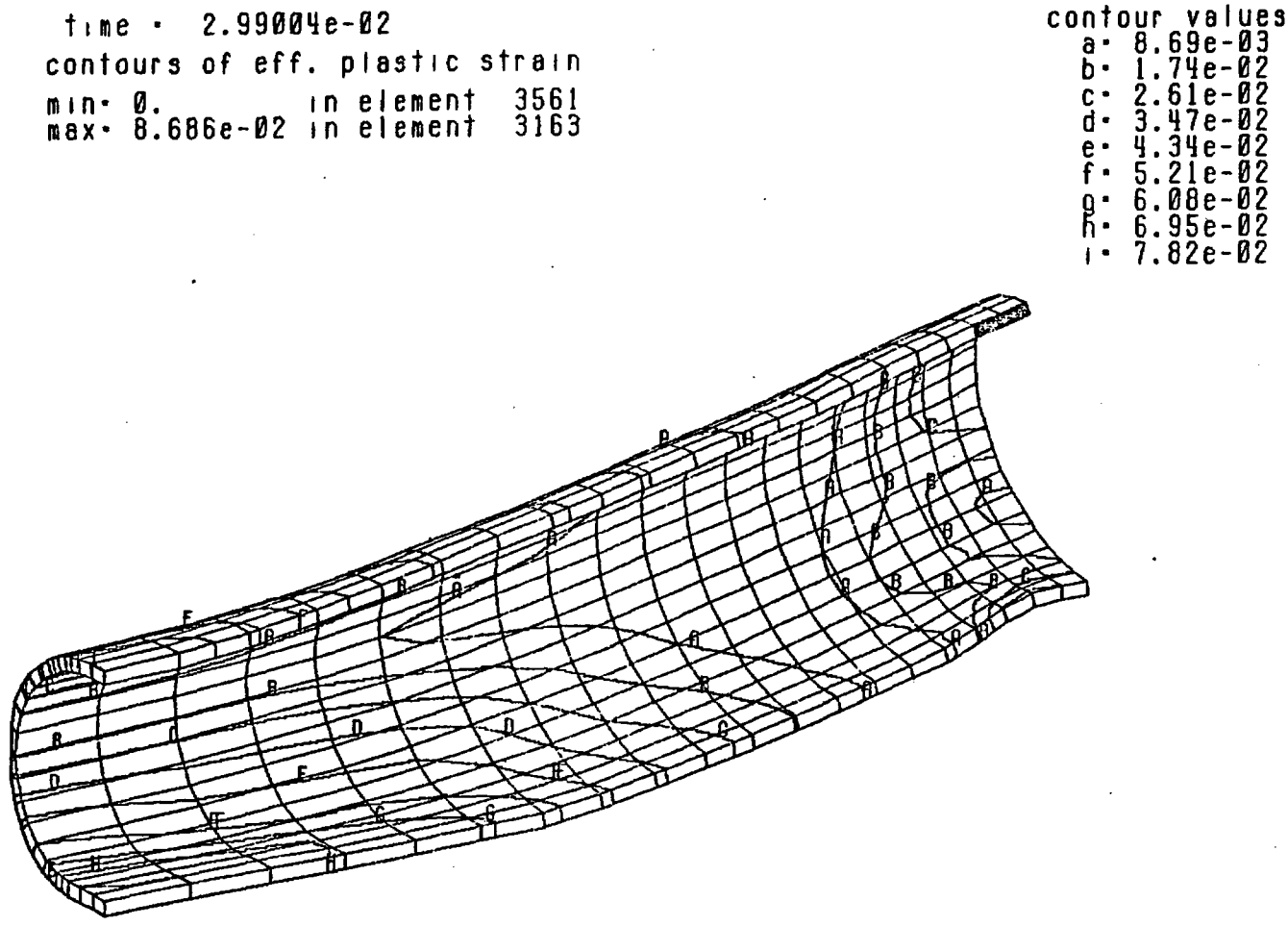

Figure E-26 Distribution of plastic strain at end of impact (outer shell).

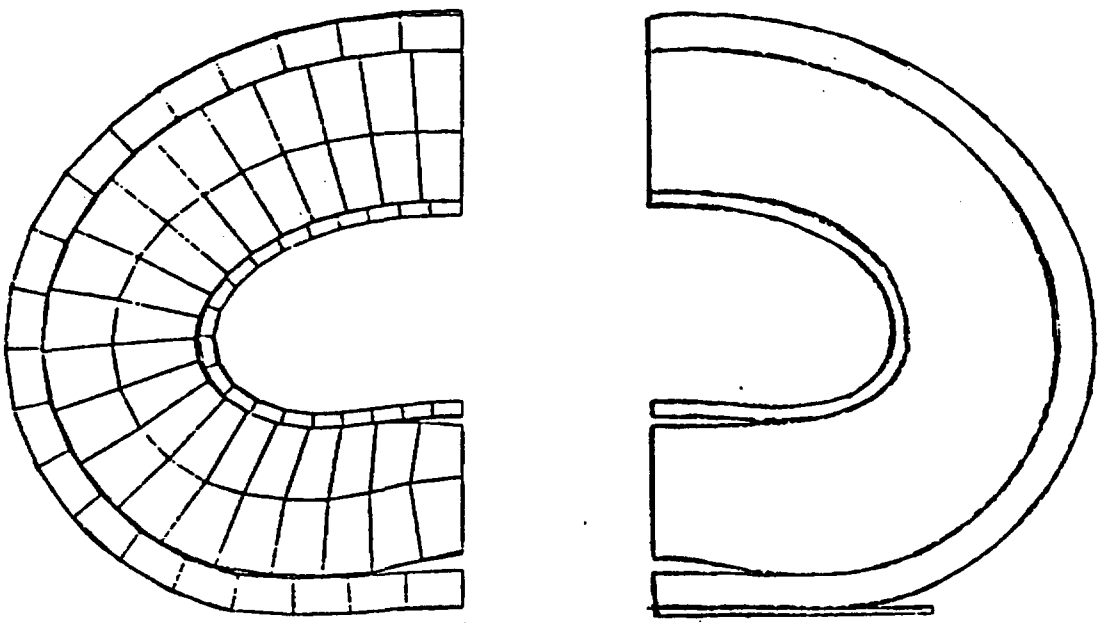

3-D Calculations

2-D Calculations

Figure E-27 Comparison of 2-D deformations with 3-D deformations at the center of the cask.

To simplify the otherwise massive finite element analyses necessary to analyze a representative, i.e., a deformable cask impacting a deformable surface, an equivalent damage technique was devised. Using the equivalent damage technique described in Subsection E.7.1, the cask response was estimated for impacts on real surfaces.

E.7.1 Equivalent Damage Technique

In the equivalent damage technique, the total deformation, and thus the total energy absorption caused by impact, is divided into two parts. The basic assumption is that the total energy of the falling cask is absorbed by deformation of the cask itself and the surface that it hits. In order to estimate how much of the energy is absorbed by the surface, the cask is modeled as a rigid body, and the surface is modeled as an energy-absorbing medium. Using this model, the impact force on the rigid cask can be determined for several velocities. In order to accomplish the necessary analyses, the characteristics of several real target surfaces must be determined.

The energy absorbed by the cask itself is estimated by modeling a deformable cask impacting an unyielding surface. Impact forces and corresponding cask deformations are determined for different impact velocities using this model. In a real situation both the cask and surface would deform. Taking the deformations from the two separate calculations and summing them gives a conservative estimate of the total deformation when a real cask hits a real surface. Since the force required to cause a 0.2% strain (S_1) in the cask is known, the product of this force and the sum of the separately calculated deformations, calculated for the same force, conservatively gives the total deformation energy. By equating this total deformation energy to the kinetic energy, an equivalent velocity can be calculated. This equivalent velocity is then used to modify the curves generated by use of the IMPASC code (in which only an unyielding surface can be modeled) to take into account the effect of the real surface. Figure E-28 shows the analysis for the case of vertical end-drop without limiters.

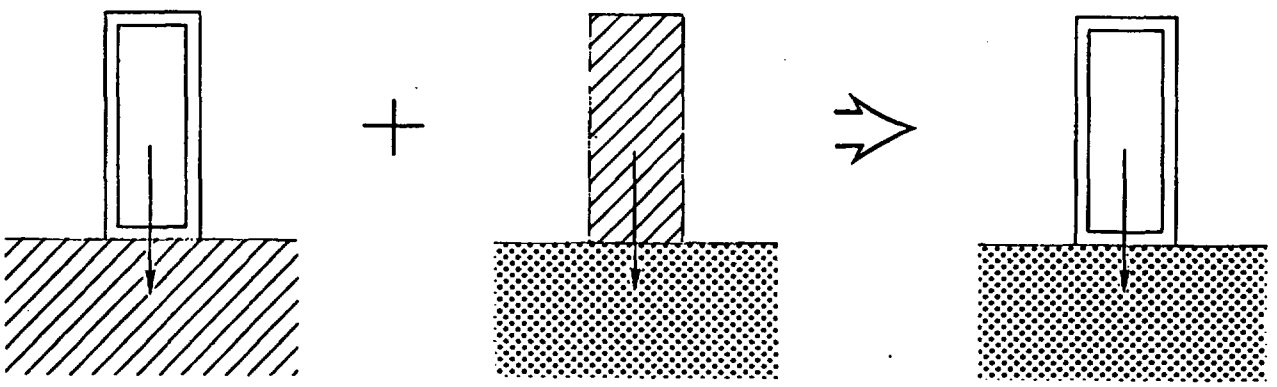

(a) Rigid cask impacts real surface

$$\left(\frac{F}{W}\right) g = \frac{V_1^2}{2d_{c1}}$$

(b) Representative cask impacts unyielding surface

$$\left(\frac{F}{W}\right) g = \frac{V_2^2}{2d_{s1}}$$

(c) Representative cask impacts real surface

$$\left(\frac{F}{W}\right) g = \frac{V_3^2}{2(d_{s1} + d_{c1})}$$

Figure E-28 Equivalent damage technique.

To illustrate the application of the equivalent damage technique, this discussion is restricted to the case of cask end-drop without limiters and a strain of 0.2% (S_1) even though this technique was used to calculate cask responses for other orientations, for casks with limiters, and higher strain levels.

In case (a), the representative truck or rail cask is impacted onto an unyielding surface so that all the kinetic energy is absorbed by the cask. The strain response of the cask is calculated as a function of impact velocity. Assuming constant deceleration during impact, the deceleration force can be estimated from an energy balance:

$$\left(\frac{F}{W}\right) g = \frac{V_1^2}{2d_{c1}} = \text{deceleration force in g for unyielding surface} \quad \text{(E.8)}$$

where F is the force of impact in pounds, W is the cask weight in pounds, g is the gravitational constant in ft/sec^2, V_1 is the impact velocity in ft/sec, and d_{c1} is the cask deformation in inches.

The cask deformation, d_{c1}, is related to the maximum strain on the inner wall where the 0.2% strain (S_1) level is defined. The deceleration force, cask deformation, and the maximum strain at the inner wall are calculated over a range of impact velocities. The deceleration force, (F/W)g, is identified where the 0.2% strain (S_1) level occurs.

In case (b), a rigid body with the same outer dimensions as the cask is impacted onto real surfaces such as hard rock, soft rock, and tillable soil. All the kinetic energy is then absorbed by the surface. The deceleration force can be estimated by

$$\left(\frac{F}{W}\right) g = \frac{V_2^2}{2d_{s1}} = \text{deceleration force in g of a rigid cask on a real surface} \quad \text{(E.9)}$$

where V_2 is the impact velocity in ft/sec and d_{s1} is the penetration into the surface in inches Again the deceleration force is calculated over a range of impact velocities. The impact velocity V_2 is determined for the same impact force identified in case (a) at the 0.2% strain (S_1) level.

In case (c), the representative cask is impacted onto real surfaces. The impact velocity and kinetic energy are absorbed by both the cask and the surface. The deceleration force can be estimated by

$$\left(\frac{F}{W}\right) g = \frac{V_3^2}{2(d_{s1} + d_{c1})} = \text{deceleration force in g of a representative cask on a real surface} \qquad (E.10)$$

where V_3 is the impact velocity corresponding to the 0.2% strain (S_1) level, and d_{s1} and d_{c1} are the penetration into the surface and cask deformation, respectively, as calculated separately for the same force. By equating Equations E.9 and E.10, the velocity V_3 is calculated:

$$V_3^2 = \frac{V_2^2(d_{s1} + d_{c1})}{(d_{s1})} \geq V_2^2 \quad . \qquad (E.11)$$

A higher impact velocity is required to give equivalent damage for the case where energy is absorbed by both the cask and the surface. The equivalent damage technique was conservatively applied by assuming that either the cask or the impacted surface absorb all of the impact energy. The resulting average force on the cask was then used to estimate the strain on the inner shell. Consequently, the strain is significantly overestimated in those cases when significant energy is absorbed by both the cask and the surface. As shown by the benchmark calculation, this approach over compensates for the simplifying assumptions made to develop the equivalent damage technique.

This equivalent damage technique was benchmarked by impacting the representative truck cask on soft rock and then comparing the calculated strain with the estimated strain from the equivalent damage technique for the same impact conditions.

To simplify the comparison, the impact limiter was not included in the benchmark analysis. The representative cask was impacted at 30 mph on the soft rock surface. The cask response to the impact is summarized in Table E.16. The cask response using the equivalent damage technique is also summarized. The percentage strain response for the actual case is 5.4% compared to 14.3% estimated using the equivalent damage technique. In this benchmark case, it was assumed that all of the energy is absorbed by the soft rock, because the resultant force is lower than that resulting from an equivalent drop onto an unyielding surface. From this benchmark calculation it was concluded that the equivalent damage technique as used in this study overestimates the cask response, yet provides reasonable results for estimating purposes.

E.7.2 Soil Impacts

A simple soil model was developed and benchmarked for evaluating impacts on soil with the representative casks as discussed in Subsections E.7.2.1 and E.7.2.2. The responses of the representative casks for endwise impacts on soil were estimated in Subsection E.7.2.3 using the equivalent damage technique. The responses of the casks were calculated with 2-D cask models in Subsection E.7.2.4 for sidewise impacts.

E.7.2.1 Soil Model

Three surfaces are considered to represent a range of credible impact scenarios. The surfaces considered simulate a hard rock, a soft rock including concrete, and tillable soil. Real surfaces exhibit complex characteristics but can be considered to deform elastically during the early part of the impact, followed by an energy dissipation phase. The exact nature of the energy dissipation mechanisms is not well known; therefore, a reasonable and simple elastic-perfectly plastic formulation was used. The two

Table E.16
Comparison of Equivalent Damage Technique Result
with Real Surface Impact Results

	Real Cask on Soft Rock Surface	Rigid Cask on Soft Rock Surface	Real Cask on Unyielding Surface	Equivalent Damage Technique
Cask Velocity (mph)	30	30	28.4	30.0
Duration of Impact (msecs)	17	7.5	17.0	17.0
Interface Force at Impact (g)	203	222	222.0	222.0
Maximum Plastic Strain (%)	5.4	N/A	14.3	14.3
Lead Slump (in)	6	N/A	6.12	6.12

parameters used in this formulation, namely the initial elastic modulus and the yield stress, can be calibrated to approximate an equivalent energy-absorbing medium. To provide the calibration, penetration data[E.19] were used as discussed in Subsection E.7.2.2. Reasonable predictions of penetration were possible using the equivalent elastic-plastic formulation.

The material parameters required by the bilinear computer model, an elastic-plastic model referred to as Material Type 3 in the NIKE/DYNA input manuals, are

E = Young's modulus, psi,

ν = Poisson's ratio, unitless,

σ_y = yield strength, psi,

ρ = density, lb-sec^2/in^4,

β = hardening parameter, unitless,

E_n = hardening modulus, psi,

σ_{1ult} and σ_{3ult} = principle stresses at ultimate stress state, psi.

A suitable range of yield stresses had to be determined for use within the elastic-perfectly plastic model. The standard method for predicting soil failure is the Mohr-Coulomb failure criterion, which states that soil will fail in shear at a value proportional to the applied confining pressure, which varies with soil depth. Even if it is assumed that yielding begins at a stress level equal to the failure stress (corresponding to the elastic-perfectly plastic response assumption), it is necessary to consider a range of failure stress levels.[E.17]

To calculate the failure stress, σ_{ult}, the data of J.M. Duncan, et al., were used to provide an extensive list of soil parameters.[E.18] Also, a

relationship between the deviatoric failure stress, $(\sigma_1 - \sigma_3)_f$, the friction angle, θ, and the cohesion intercept is given by Duncan with the formula

$$(\sigma_1 - \sigma_3)_f = \frac{2c \cos \theta + 2\sigma_3 \sin \theta}{1 - \sin \theta} \quad . \tag{E.12}$$

The deviatoric failure stress is related to the ultimate deviatoric stress as follows:[E.17]

$$(\sigma_1 - \sigma_3)_f = R_f(\sigma_1 - \sigma_3)_{ult} . \tag{E.13}$$

where R_f is the failure ratio. Because $(\sigma_1 - \sigma_3)_f$ is always less than $(\sigma_1 - \sigma_3)_{ult}$, the value of R_f is always less than 1, usually 0.5-0.9. Duncan lists soil parameters for about 150 soils. If, for a particular type of soil, e.g. sandy clay, the largest θ, c, and σ_3, and the lowest value for R_f are selected, a conservative value for the deviatoric failure stress can be calculated. Rearranging equation (E.13) gives:

$$\sigma_{ult} = \sigma_{1ult} = \frac{(\sigma_1 - \sigma_3)_f}{R_f} + \sigma_{3ult} \quad . \tag{E.14}$$

For an elastic-plastic model it is conservative to use the ultimate stress as the yield stress to estimate the maximum force on the cask.

From Duncan's data a summary of the conservative parameters found for 12 general categories of soils is given in Table E.17.

Table E.17
Soil Parameters

Soils	Max θ (°)	Max c (tons/ft^2)	Max σ_3 (psi)	Min R_f (unitless)	σ_y (psi)
Rockfill	53	0	728	0.51	12051
Sandy Gravel	58	10.01	728	0.57	15107
Clayey Gravel/Clayey Sand	34	2.6	504	0.55	2847
Silty Sand/Sandy Silt	53	0.54	219	0.57	3277
Sand	49	0	1104	0.63	11892
Silty Clay	33	3.3	222	0.58	1161
Lean Clay	3	1.10	93.33	0.52	118
Fat Clay	4	1.5	156	0.65	196
Silt	45	0	115	0.57	1090

E.7.2.2 Soil Model Benchmark Calculations

The soil model was benchmarked by comparing with test data. This was accomplished in two phases. The first was an analytical plate bearing test. This test is often used to evaluate soils, subgrades, and pavements, especially in road design, and uses the modulus of subgrade reaction, k, which is measured in situ with a plate bearing test. The test involves loading a circular disk, or stack of disks, usually 30 inches in diameter, at a specified deflection rate, and measuring the deflection at a predetermined load, usually 10 psi. The modulus k is calculated as follows:

$$k = \frac{p}{\Delta} \text{ , psi/in,} \qquad \text{(E.15)}$$

where

p = unit load on plate, psi

Δ = deflection of plate, inches.

The results obtained for the modulus of subgrade reaction, k, were compared with predicted values[E.18] and are summarized in Table E.18. The purpose of this check was to verify that the selected elastic plastic material model produced results that were not completely out of line. The results indicate that for elastic loads, the model significantly over-predicts the soil stiffness. The over-prediction is conservative for this study.

The second phase of the benchmark process was a review of work presented by C.W. Young,[E.20] and a comparison of his results with the soil model results. Young's method was developed to predict depth of earth-penetrating projectiles. Young uses a material parameter, which he calls S, in his formulation and has tabulated values of S for a large variety of soils. Typical values of S from Young[E.20] are listed in Table E.19 with the bilinear soil parameters.[E.17,E.19,E.21]

From Table E.18 it is concluded that the parameters used to model soils can vary over a wide range for different types of soil and rocks. Also the types of soils and rocks can vary significantly within a specific land region. To make the work manageable in analyzing impact with surfaces, the

Table E.18
Plate Bearing Test Simulation with NIKE 2-D

Soil	Calculated k (psi/in)	Predicted k[E.19] (psi/in)
Dense Sand $E = 10^4$ psi $\nu = 0.3$	1100	300 or more
Sandy Clay $E = 5 \times 10^3$ psi $\nu = 0.3$	750	200-300
Hard Sand $E = 5 \times 10^3$ psi $\nu = 0.48$	840	300-800

Table E.19
Summary of Soil Types and Range of Soil Parameters[E.17,E.19,E.21]

Soils	Range of Soil Parameters			
	Bilinear Model Parameter			Soil Constant,
	E (psi)	ν	σ_y (psi)	S ($sec^2/\sqrt{lb}$)
Clay	50-38,000	0.1-0.5	100-3,000	4-50
Silt	300-500	0.3-0.35	1,000-3,500	8-50
Sand	1,000-28,000	0.15-0.4	2,800-15,000	4-12
Soft Rock	20,000-2,000,000	0.1-0.4	10,000-16,000	0.8-5
Hard Rock	5,000,000-26,000,000	0.12-0.4	12,000-25,000	0.3-0.8
Concrete	3,000,000-5,000,000	0.1-0.2	3,000-8,000	0.8-3

surfaces were classified into three groups: hard rock, soft rock including concrete, and tillable soil. The material properties selected to represent each of these groups are tabulated in Table E.20. The range of values for the parameters and Young's[E.20] soil constant S are tabulated for each group.

In Fig. E-29, the impact forces calculated using the elastic plastic model are plotted for impact on each of the three surfaces by a rigid truck cask as a function of impact velocity. Impact force ranges calculated using experimental formulas[E.20] and a rigid truck cask are also plotted for general S soil constants for comparison. For each of the groups there is good agreement between the DYNA 2-D results and the experimental ones.

E.7.2.3 Endwise Impacts on Soil

In order to use the equivalent damage technique to estimate the response of the representative casks for endwise impacts on real surfaces, the impact forces had to be calculated. These analyses were 2-D axisymmetric dynamic finite element analyses, using the code DYNA 2-D. A typical mesh is shown in Fig. E-30. The model includes an unyielding cylindrical falling body which has the same weight and radius as the representative truck and rail casks. A slideline was included between the unyielding cask and the surface. Slideline type three, sliding with voids, was selected from the DYNA 2-D Users Manual. The other possibility, slideline type four, was rejected because the penalty formulation required some adjustment depending upon the stiffness of the soil and the impact velocity, which was not suitable for a parametric study. The impact forces were calculated at four velocities, 30, 60, 90, and 120 mph. The impact forces are summarized in Table E.21 for the representative truck and rail casks.

E.7.2.4 Sidewise Impacts on Soil

Two-dimensional plane strain analysis without impact limiters or end closures were performed for sidewise impacts on the three surfaces to estimate the 3-D responses of the two representative casks. The 2-D truck and rail cask models were developed using the MAZE interactive mesh generators. The cask models do not include contents. DYNA 2-D was used to calculate the responses.

Table E.20
Selected Soil Parameters for this Study

Represented Surface	Bilinear Model Parameter			Soil Constant, S Range
	E (psi)	ν	σ_y (psi)	($sec^2/in/lb$)
Soil	6,000	0.4	1,000	5-50
Soft Rock, Concrete	3,640,000	0.2	4,000	1-5
Hard Rock	7,000,000	0.28	25,000	0.3

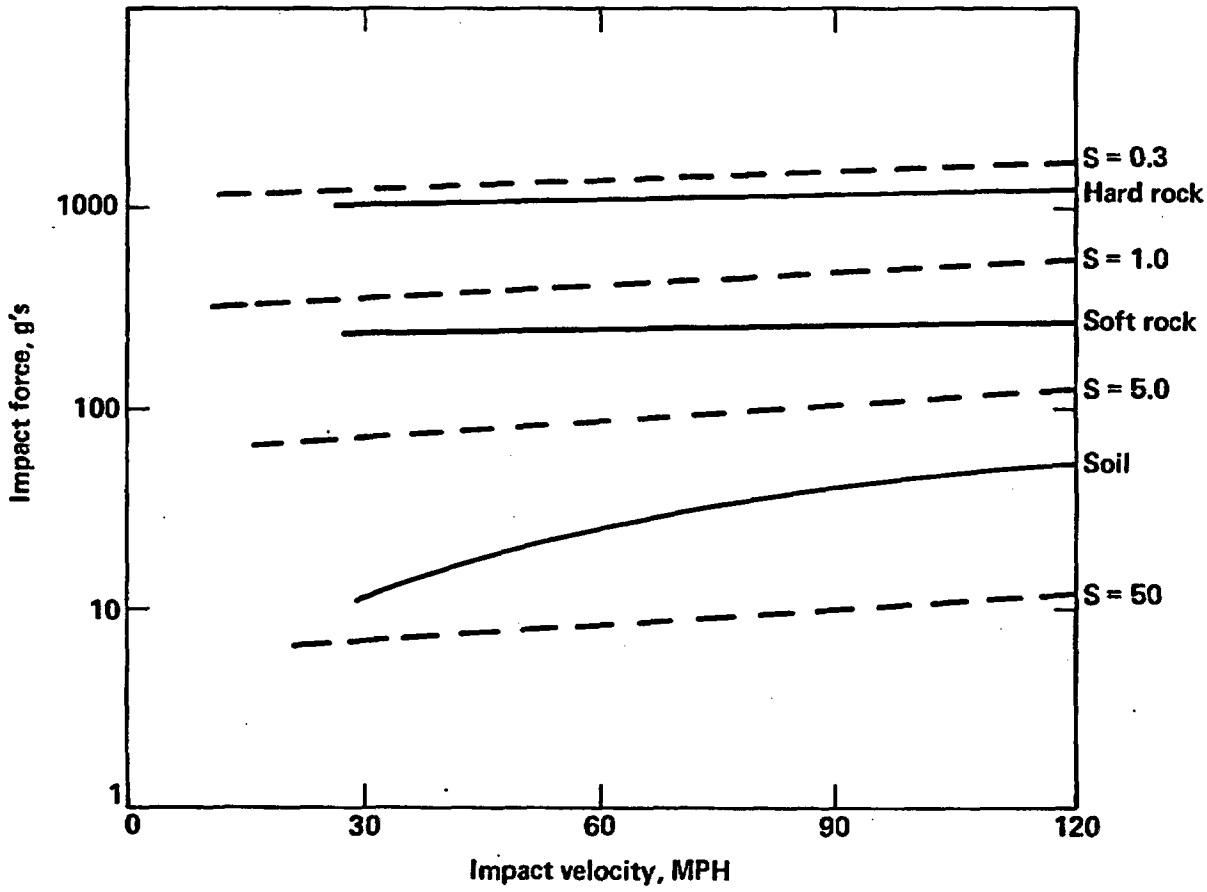

S = Soil constant

Figure E-29 Soil model comparison with penetration test data.

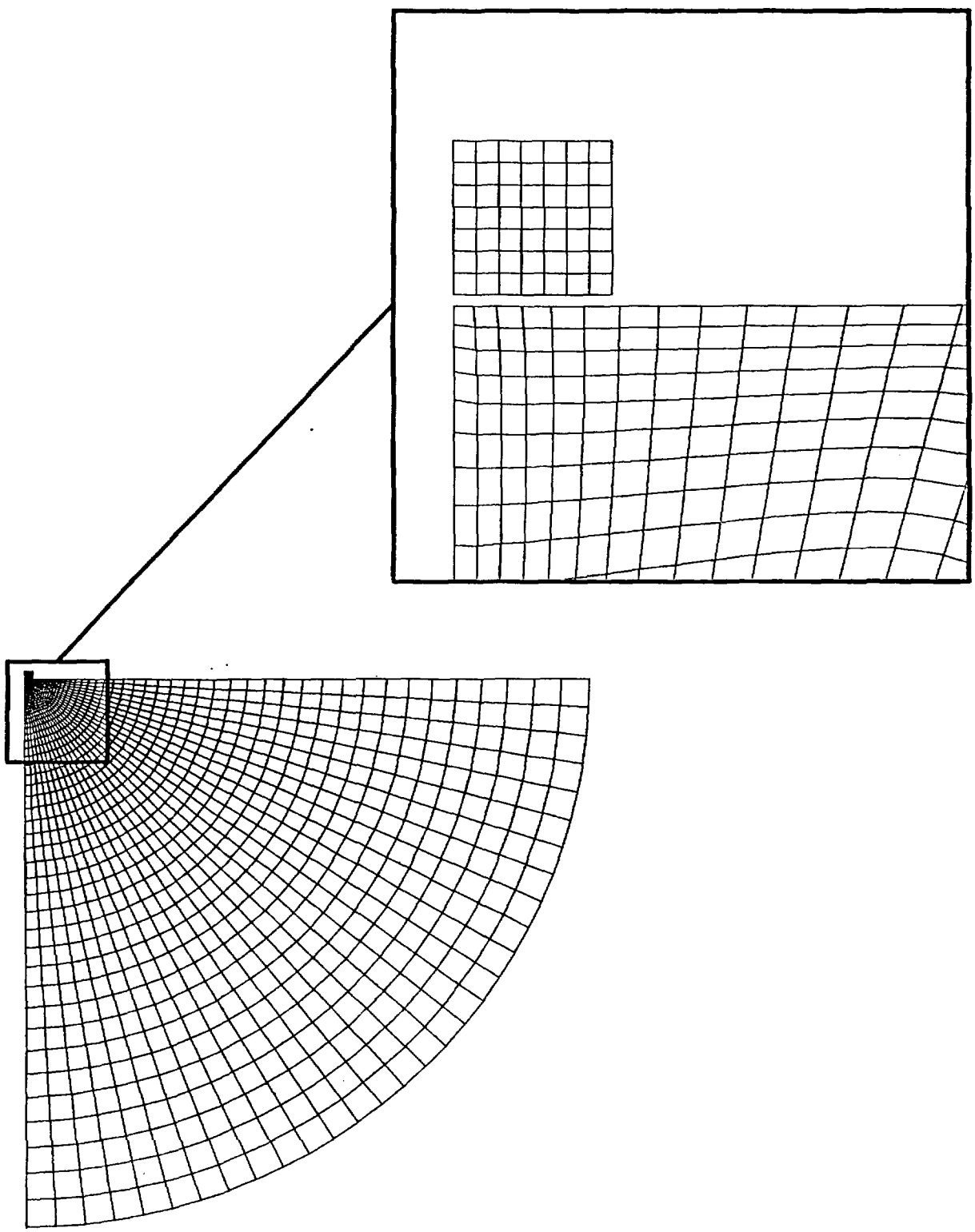

Figure E-30 Finite element mesh for drops on soils.

Table E.21
Summary of Cask Responses to Endwise Impacts on Real Surfaces

Velocity (mph)	Impact Force (g)					
	Truck Cask			Rail Cask		
	Surface Type			Surface Type		
	Hard Rock	Soft Rock	Soil	Hard Rock	Soft Rock	Soil
30	1050	250	12	--	420	16
60	1310	270	26	--	--	110
90	1340	--	40	--	600	200
120	1360	290	54	--	--	--

E.7.2.4.1 Truck Cask Impacts

The truck cask response to endwise impacts on hard rock surfaces was essentially the same as the response to impact on an unyielding surface. Since the cask stiffness is less for sidewise impacts, sidewise impact analyses were performed only for impacts on soil and soft rock. The calculations were performed for 30 mph and 60 mph impacts on soil and 30 mph and 90 mph impacts on soft rock. The effective plastic strain distribution at the time the maximum occurs is shown in Fig. E-31 for the 60 mph impact on soil. The results of the impact calculations are summarized in Table E.22. The maximum strain response of the cask was 2.45% and 7.62% at the inner shell for the 30 mph and 60 mph impacts on the soil. The strain response at the inner shell was 5.03% and 13.6% for the impacts on the concrete surface at 30 mph and 90 mph, respectively.

E.7.2.4.2 Rail Cask Impacts

As was done for the truck cask, sidewise impact analyses were performed for the rail cask for impacts on soil and soft rock. The calculations were performed for 30 mph and 60 mph impacts on soil and 30 mph and 90 mph impacts on soft rock. The effective plastic strain distribution at the time the maximum occurs is shown in Fig. E-32 for one of the cases studied. The results of the impact calculations are summarized in Table E.23. The maximum strain responses at the inner shell for impacts on soil were 2.17% and 3.37% at 30 mph and 60 mph, respectively. The maximum strain responses of the rail cask was lower than those of the truck cask because of its greater flexibility.

E.7.3 Water Impact

An analysis of water impact for wedge shaped bodies is provided in the literature for use in ship hull design.[E.22,E.23] A phenomenon, substantiated during an experimental investigation of flat bottom slamming at the Naval Ship Research and Development Center, is described wherein, during flat bottom slamming, air is trapped between the impact surface of the falling body and the water surface, thereby cushioning the impact.[E.23] Thus the impact angle

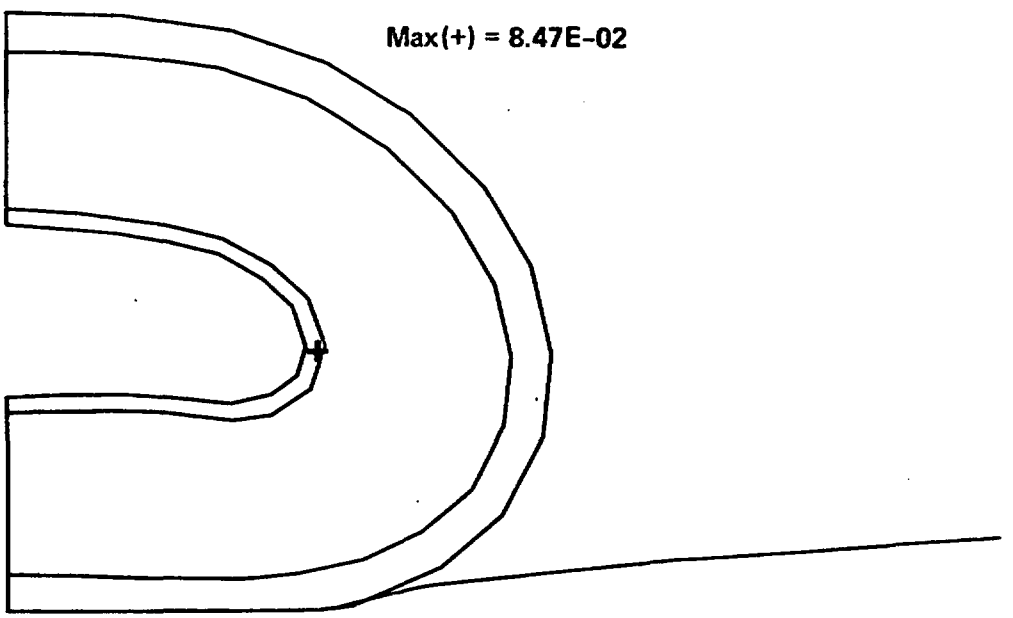

Figure E-31 Maximum plastic strain location on truck cask for impact at 60 mph on soft rock.

Table E.22
Results of Truck Cask Sidewise Impacts on Real Surfaces
(without Impact Limiter)

Velocity (mph)	Strain at Inner Wall (%)	
	Surface Type	
	Soil	Soft Rock
30	2.45	5.03
60	7.62	--
90	--	13.6

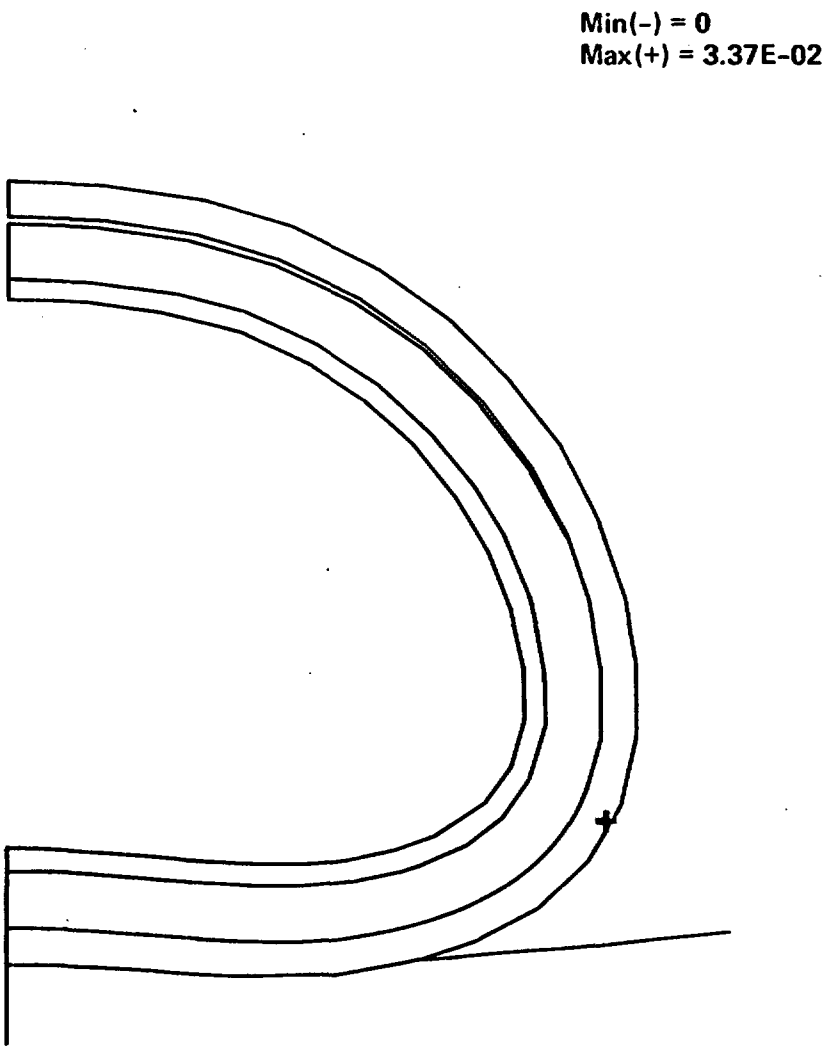

Figure E-32 Maximum plastic strain location on rail cask for impact at 60 mph on soft rock.

Table E.23
Results of Rail Cask Sidewise Impacts on Real Surfaces
(without Impact Limiter)

Velocity (mph)	Strain at Inner Wall (%)	
	Surface Type	
	Soil	Soft Rock
30	2.17	3.78
60	3.37	--
90	--	10.10

producing the highest impact force is not 90^{o}, but 87^{o}. An approximation of the impact force on a cask falling into a body of water is made by integrating the pressure, over an area equal to the cask end cross sectional area:[E.23]

$$p(x) = \frac{1}{2}\rho V^2\left[\frac{\pi}{(90-\beta)\left(1-\frac{x^2}{L^2}\right)^{1/2}} - \frac{\frac{x^2}{L^2}}{1-\frac{x^2}{L^2}} + \frac{2\bar{z}}{V^2}\left(L^2-x^2\right)^{1/2}\right] \qquad (E.16)$$

and

$$\text{Force} = \int_0^L q\, p(y)\,dy \qquad (E.17)$$

where

$y = Lx$, ft,

$q = 2L\left(x - x^2\right)^{1/2}$, ft,

β = compliment of deadrise angle, ^{o},

ρ = mass density of water, lb/ft^3,

L = cask diameter, ft,

V = cask impact velocity, ft/sec,

$\bar{z} = 0$ (i.e., assume that impact acceleration, = 1 g, is negligible).

Using Simpson's Rule for integration, the interface forces were calculated for the two unyielding casks with the same external dimensions as the representative casks for four impact velocities and three cask orientations. For the large diameter rail cask, the loads due to impact on water can be quite high for the 87^{o} impact angle. However these loads drop off rapidly for other impact angles. The results of the calculations are summarized in Table E.24. The equivalent damage technique is used to estimate the strain response of the casks to the calculated impact forces.

E.7.4 Train Sill Impacts

E.7.4.1 Impact on Truck Cask

Two scenarios were evaluated for a locomotive sill impacting a truck cask: the sill impacting the cask sidewise head-on; and the sill impacting the cask sidewise off-center. The cross-section of the model used to simulate a locomotive sill is shown in Fig. E-33 and consists of two plates connected with two large I-beams.[E.9] The sill was modeled as a solid object with modified properties. For the sidewise head-on impacts the sill was modeled as a plate 3.5 inches thick to approximate its axial strength. For the sidewise off-center impacts the sill was modeled as a plate 11.5 inches thick to approximate its bending strength. In both cases, the density of the sill was calculated for a locomotive weight of 200 tons.

The sill was first modeled as shown in Fig. E-34 to impact at a point at 45^{o} on the truck cask from the sidewise head-on position. Calculations were made with the locomotive sill impacting the cask at velocities of 30 mph and 60 mph. In both cases, the cask moved away from the sill at an angle and achieved a velocity lower than the initial sill velocity. Also, the sill underwent a slight rotation and remained undamaged. However, the cask sustained large deformations where the sill scraped across it. Also as illustrated in Fig. E-35, the sudden acceleration caused the cask to flatten.

For the 30 mph impact, the cask experienced a force of 110 g's and sustained a maximum effective stress of 40,100 psi and maximum plastic strain of 7.5% in the steel shells. For 60 mph, the force increased to 206 g's, the

Table E.24
Interface Force for Water Impact
(All Results Listed in Multiples of Cask Weight,
No Impact Limiters or Cab Crush Included)

Velocity (mph)	Unyielding Truck Cask Impact Orientation			Unyielding Rail Cask Impact Orientation		
	87^0	45^0	0^0	87^0	45^0	0^0
30	17.7	0.9	12.6	37.8	1.9	10
60	70.8	3.6	50.4	151.3	7.6	39
90	159.3	8.5	119	340.5	17.1	88
120	283.2	14.5	203	605.3	30.4	155

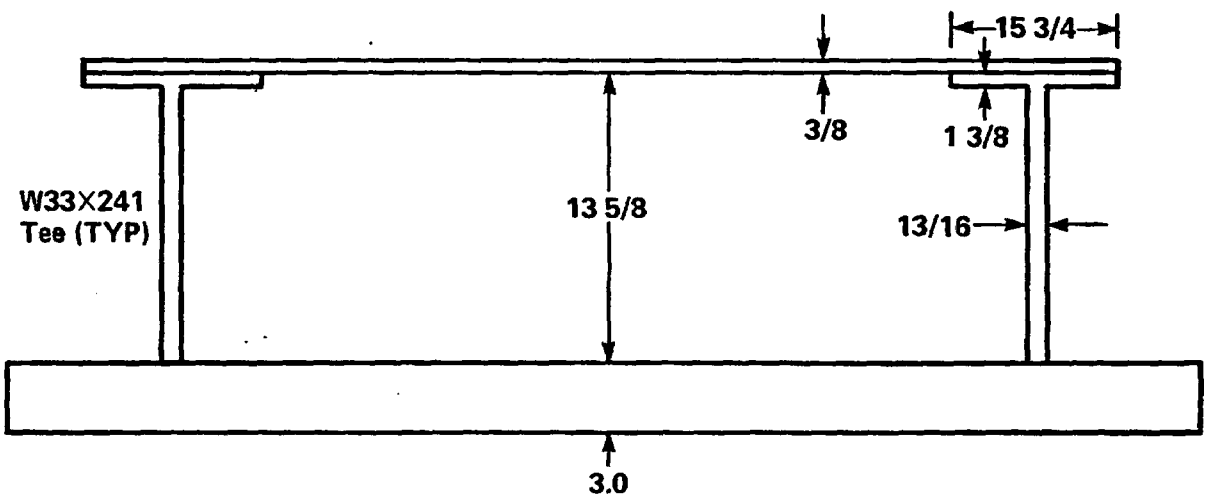

Figure E-33 Locomotive sill cross section.

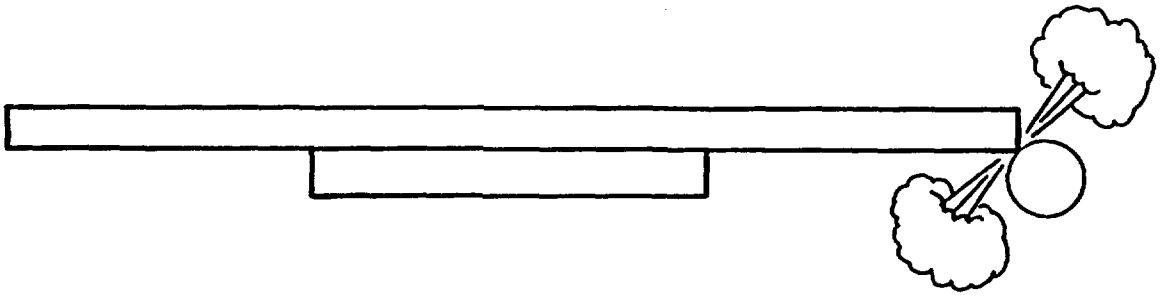

Figure E-34 Sidewise off-center locomotive sill impact.

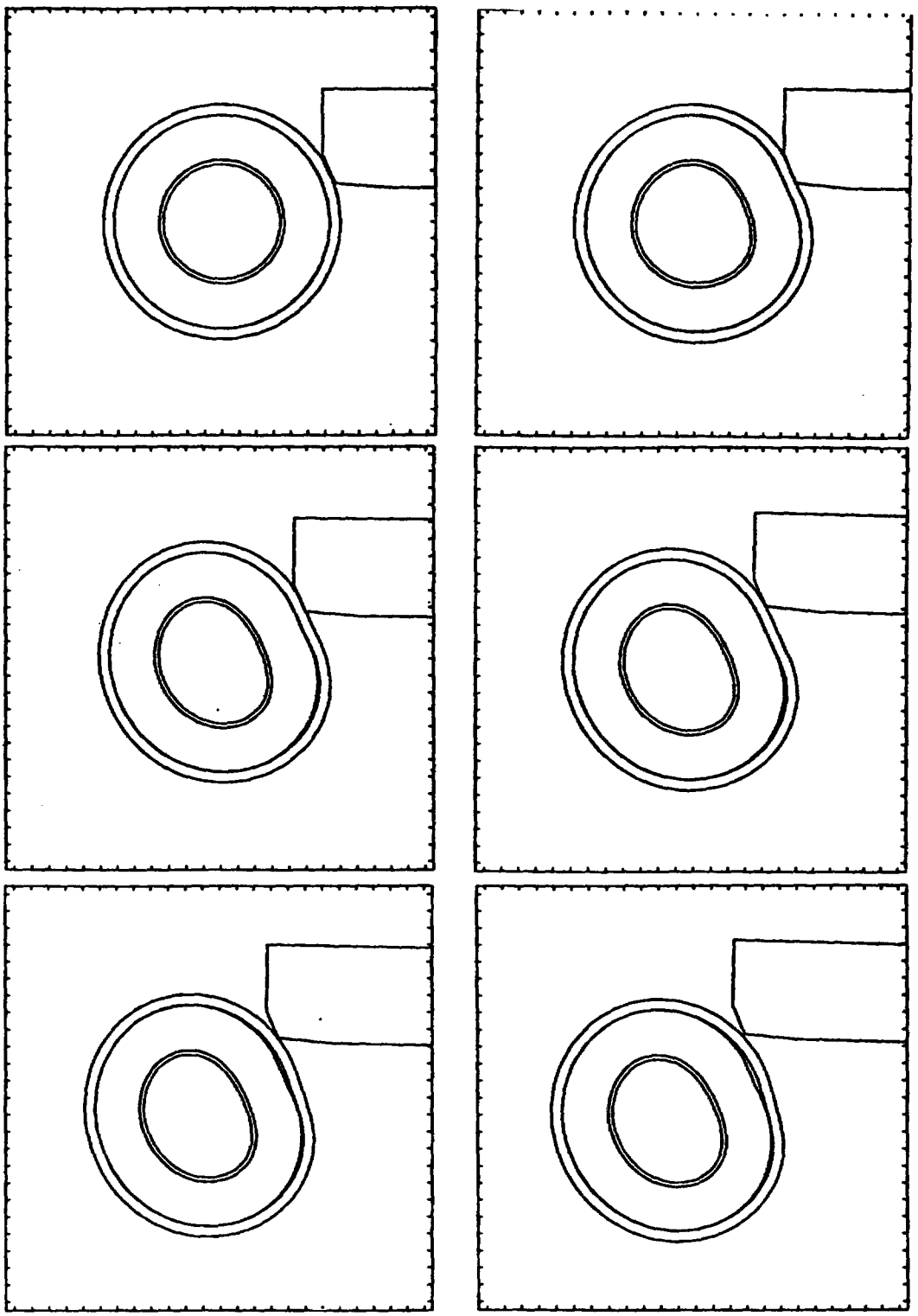

Figure E-35 Thirty mph sidewise off-center sill impact.

maximum effective stress increased to 50,000 psi, and the maximum plastic strain increased to 12.8%. These results are summarized in Table E.25. The location of the maximum plastic strain is shown in Fig. E-36.

For the sidewise head-on impact, the complete 2-D strain truck cask model was analyzed for impact with the locomotive sill. This model was used only for the impact at 30 mph; based on these results, symmetry was used for the 60 mph impact to reduce the solution cost. The modeling is shown in Fig. E-37. In both cases, the cask achieved a velocity higher than the sill velocity and the sill was undamaged. However, the cask sustained large deformations in the impact zone. Also, the sudden acceleration caused the cask to flatten as shown in Fig. E-38.

For the 30 mph impact, the cask experienced a force of 138 g's, a maximum effective stress of 50,000 psi, and a maximum plastic strain of 12.4% in the steel shells. For 60 mph, the force increased to 265 g's, the maximum effective stress increased to 65,000 psi, and the maximum plastic strain increased to 20%. These results are summarized in Table E.26. The location of the maximum plastic strain is shown in Fig. E-39.

None of our cask models included contents. For the truck cask, the mass of the contents is not large compared to the mass of the cask. The truck cask is very much like a thick-walled cylinder and under the severe impact conditions, it is able to support itself. For the rail cask, the mass of the contents is very large compared to the mass of the cask. Also, the rail cask is like a thin-walled cylinder. Under the severe impact conditions, it is unable to support itself. Thus, contents are very important to the rail cask calculations and should be modeled to provide more accurate impact forces and g loads and to support the cask as it collapses.

Our comparison of the maximum effective stresses and plastic strains sustained by the two casks for the different impact conditions shows that the sidewise sill head-on impact into the truck cask is the most severe. The off-center impact is less severe because the sill transfers less energy as it strikes a glancing blow to the cask. The truck cask impacting on the unyielding surface is less severe than the sidewise head-on impact. However, the maximum g loads occur in the impacts on an unyielding surface. The

Table E.25
Results Sidewise of Off-Center Sill Impact Against Truck Cask

Locomotive sill velocity (mph)	30	60
Locomotive sill velocity (in/sec)	528	1056
Duration of impact (sec)	0.012	0.011
Velocity at end of impact (in/sec)	425	637
Angle of departure of cask (°)	52	42
g load on cask (g)	110	206
Maximum effective stress (psi)	40,100	50,800
Maximum plastic strain (%)	7.5	12.8
Maximum plastic strain at inner shell(%)	2.3	3.8

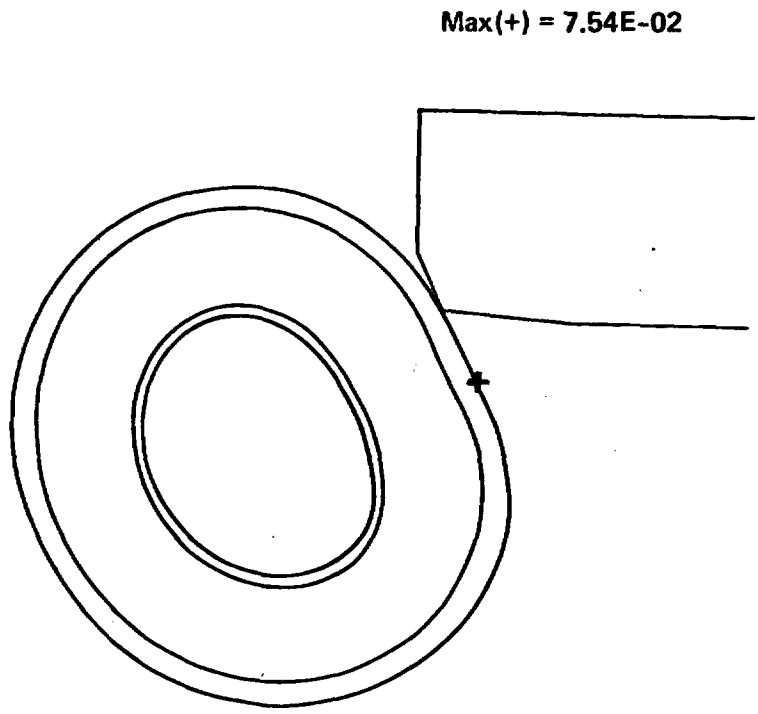

Figure E-36 Thirty mph sidewise off-center sill impact-maximum plastic strain location.

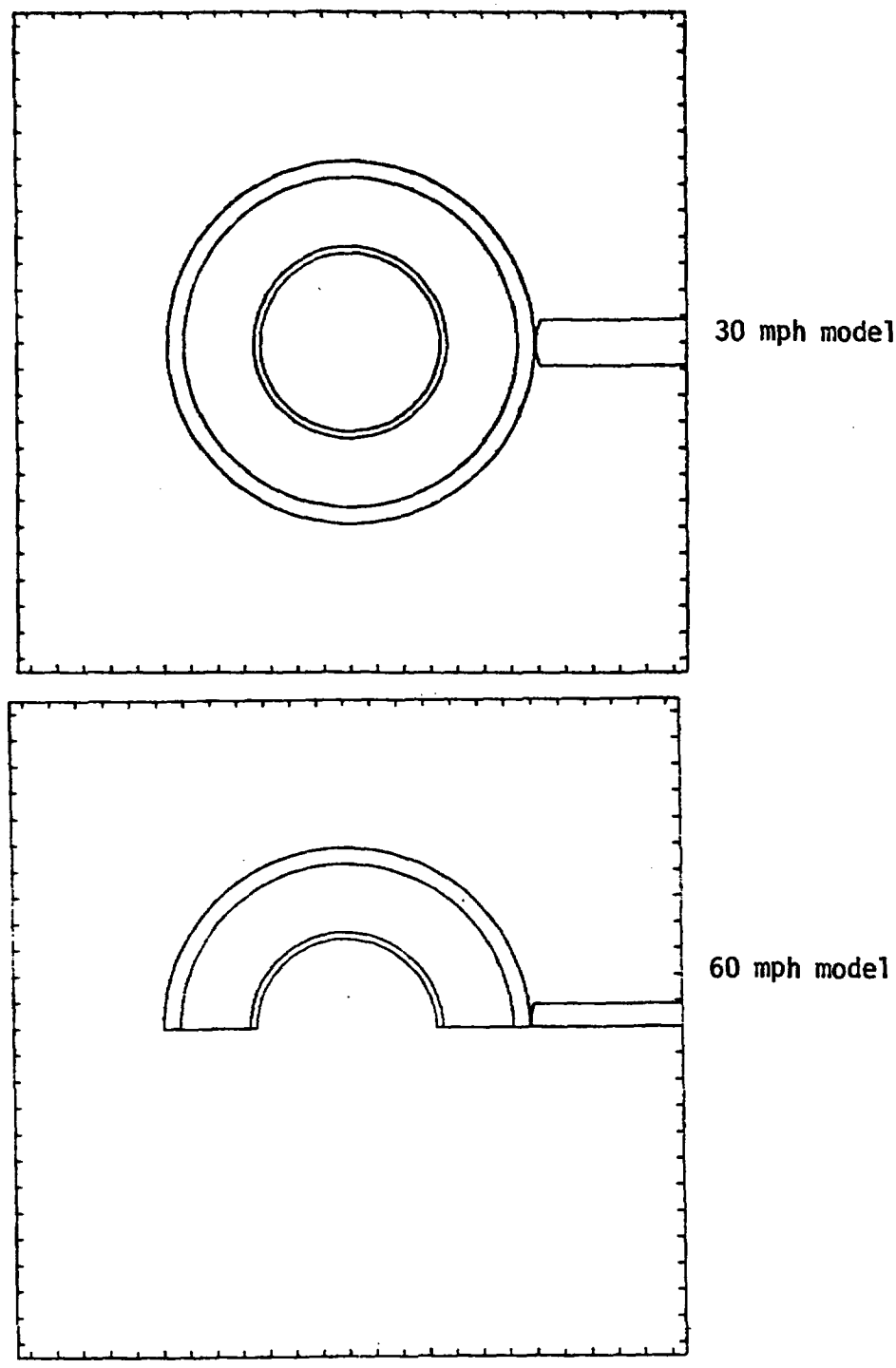

Figure E-37 Model configurations for sidewise head-on sill impact. Note use of symmetry for 60 mph case.

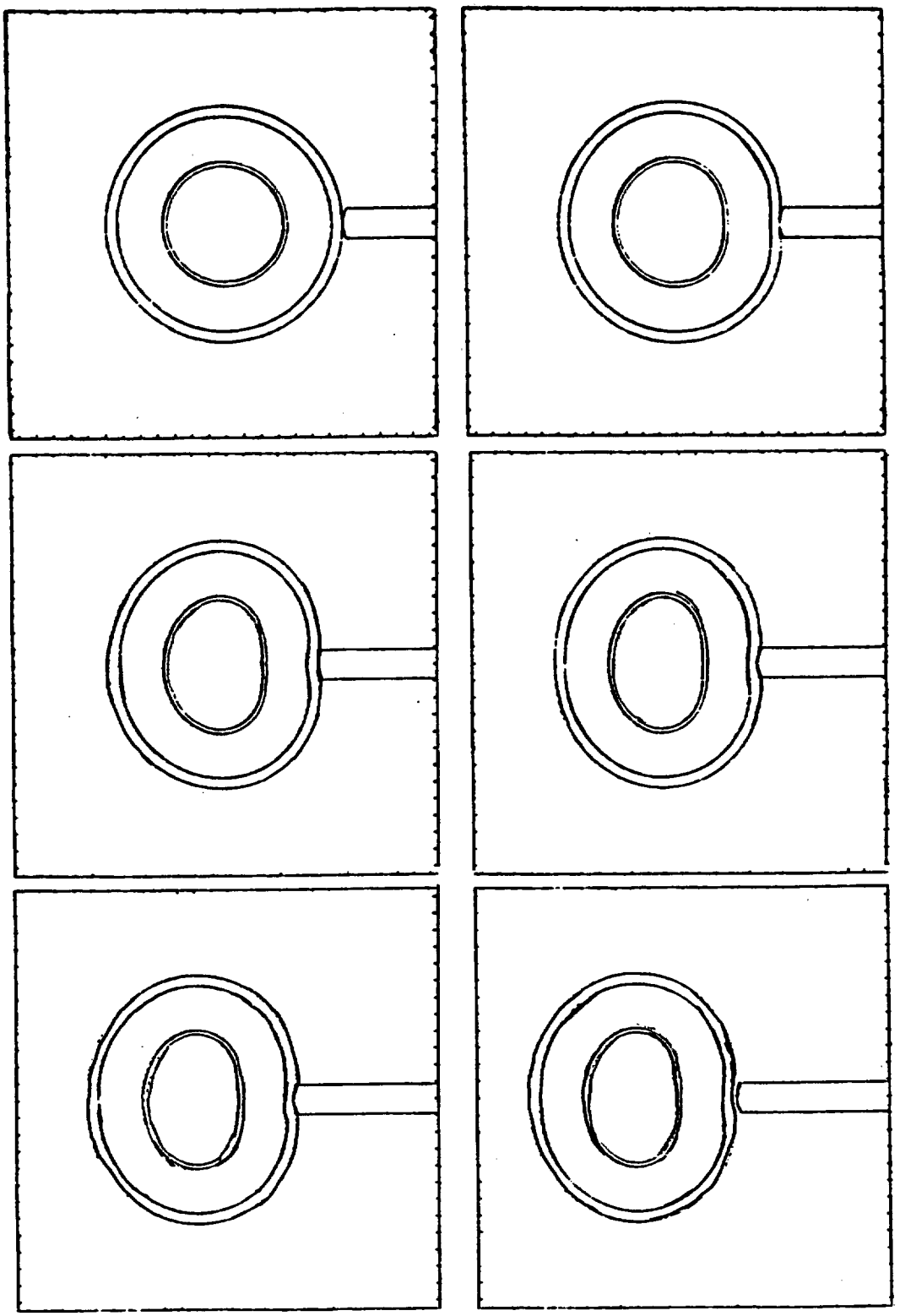

Figure E-38 Sidewise head-on sill impact at 30 mph.

Table E.26
Results of Sidewise Head-on Sill Impact Against Truck Cask

Locomotive sill velocity (mph)	30	60
Locomotive sill velocity (in/sec)	528	1056
Duration of impact (sec)	0.0125	0.0135
Velocity at end of impact (in/sec)	575	1130
g load on cask (g)	138	265
Maximum effective stress (psi)	50,000	65,000
Maximum plastic strain (%)	12.4	20
Maximum plastic strain at inner shell (%)	3.7	6.0

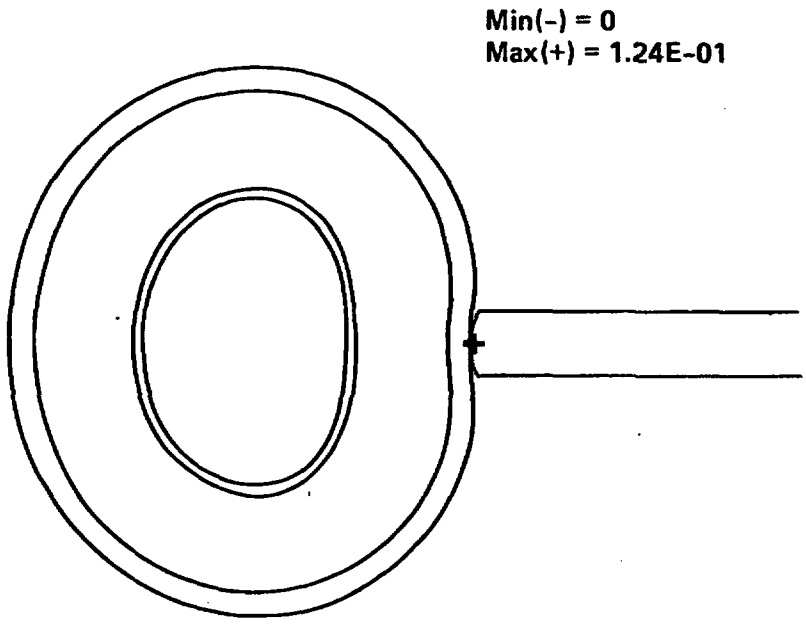

Figure E-39 Thirty mph sidewise head-on sill impact-maximum plastic strain location.

sidewise head-on impact causes severe local deformations before the cask is accelerated to its final speed. Also, the locomotive sill has some give to it. These combined effects soften the impact. The rail cask endures the least severe stresses, strains, and g loads, yet it sustains the most severe deformations. This is because the rail cask is more ductile than the truck cask, causing a very soft impact.

E.7.4.2 Impact on Rail Cask

The response of the representative rail cask was estimated for impacts with a train sill by using the truck cask results. The response was estimated by multiplying the truck cask results for the train sill impact times the rail cask results for the unyielding surface impact and dividing by the truck cask results for the unyielding surface impact. The estimated responses of the representative rail cask to impacts by a train sill are summarized in Table E.27. The estimated strains are conservatively high because of the greater size and weight of the rail cask compared to the truck cask.

Table E.27
Estimated Response of Rail Cask to Impact by Train Sill

Velocity (mph)	Strain Response (%) Impact Orientation	
	0^{o}	45^{o}
30	2.3	1.4
60	3.6	2.3

E.8 References

E.1 J. O. Hallquist, NIKE 2-D: An Implicit, Finite-Deformation, Finite Element Code for Analyzing the Static and Dynamic Response of Two-Dimensional Solids, Lawrence Livermore National Laboratory, Livermore, CA, UCRL-52678, 1979, and Revision 1, NIKE 2-D: An Implicit, Finite-Deformation, Finite Element Code for Analyzing the Static and Dynamic Response of Two-Dimensional Solids, Lawrence Livermore National Laboratory, Livermore, CA, UCID-18822, 1981.

E.2 J. O. Hallquist, User's Manual for Dyna 2-D--An Explicit Two-Dimensional Hydrodynamic Finite Element Code with Interactive Rezoning, Lawrence Livermore National Laboratory, Livermore, CA, UCID-18756, Rev. 2, 1984.

E.3 American Society of Mechanical Engineers, ASME Boiler and Pressure Vessel Code, Section III, Division 1, The American Society of Mechanical Engineers, United Engineering Center, 345 East 47th Street, New York, NY 10017, July 1983.

E.4 J. B. Conway, R. h. Stentz, and J. T. Berling, Fatigue, Tensile, and Relaxation Behavior of Stainless Steels, Technical Information Center, Office of Information Services, United States Atomic Energy Commission, Oak Ridge, TN, 1975.

E.5 Safety Analysis Report for the NLI-10-24 Shipping Cask, Docket No. 70-9023, National Lead Industries, Inc., Wilmington, DE, February 1976.

E.6 J. Counts and J. B. Payne, Evaluation of Analysis Methods for Type B Shipping Container Impact Problems, Los Alamos Scientific Laboratory, Los Alamos, NM, LA-6640-MS, 1979.

E.7 Consolidated Safety Analysis Report IF-300 Shipping Cask "Appendix I", Docket No. 70-1220, General Electric Company, San Jose, CA, January 1971.

E.8 C. R. Adams, et al, A Comparison of Analytical Techniques for Analyzing a Nuclear-Spent-Fuel Shipping Cask Subjected to an End-on Impact, U.S. Nuclear Regulatory Commission, Washington, DC, NUREG/CR-2018, 1981.

E.9 P. Eggers, Severe Rail and Truck Accidents: Toward a Definition of Bounding Environments for Transportation Packages, U.S. Nuclear Regulatory Commission, Washington, DC, NUREG/CR-3498, 1984.

E.10 N. E. Shoemaker, et al., Consumer Information Crash Test Program, U.S. Department of Transportation, Washington, DC, DOT HS-802011, September 1976.

E.11 M. Huerta, Analysis, Scale Modeling, and Full-Scale Tests of a Truck Spent-Nuclear-Fuel Shipping System in High Velocity Impacts Against a Rigid Barrier, Sandia National Laboratory, Albuquerque, NM, SAND77-0270, 1978.

E.12 M. Huerta, Analysis, Scale Modeling, and Full-Scale Tests of a Railcar and Spent-Nuclear-Fuel Shipping Cask in a High Velocity Impact Against a Rigid Barrier, Sandia National Laboratory, Albuquerque, NM, SAND78-0458, Febuary 1980.

E.13 Uniform Building Code, International Conference of Building Officials, Whittier, California, 1979.

E.14 T. A. Nelson, et. al., SCANS - Shipping Cask Analysis System, Vol. 1, Impact Analysis Code User's Manual, Lawrence Livermore National Laboratory, Livermore, CA, UCID-20674/Vol. 1, Draft Report to be published, U.S. Nuclear Regulatory Commission, Washington, DC, NUREG/CR-4554, 1986.

E.15 J. O. Hallquist, MAZE, An Input Generator for DYNA 2-D and NIKE 2-D, Lawrence Livermore National Laboratory, Livermore, CA, UCID-19029, June 1983.

E.16 M. A. Gerhard, SLIC, Interactive Graphic Mesh Generator, Lawrence Livermore National Laboratory, Livermore, CA, UCRL-52823, September 1979.

E.17 G. F. Sowers, Introductory Soil Mechanics and Foundations: Geotechnical Engineering, Fourth Edition, MacMillan Publishing Company, New York, NY, 1979.

E.18 J. M. Duncan, P. Byrne, K. S. Wong, and P. Mabry, Strength, Stress-Strain and Bulk Modulus Parameters for Finite Element Analyses of Stresses and Movements in Soil Masses, University of California at Berkeley, Berkeley, CA, UCB/GT/80-01, 1980.

E.19 W. Yoder, Principles of Pavement Design, Second Edition, J. Wiley and Sons, New York, NY, 1975.

E.20 C. W. Young, "Depth Prediction for Earth-Penetrating Projectiles", Journal of the Soil Mechanics and Foundations Division, Proceedings of the American Society of Civil Engineers Vol. 95, No. SM3, Proceedings Paper 6558, American Society of Civil Engineers, New York, NY, May 1969.

E.21 J. E. Bowles, Foundation Analysis and Design, Second Edition, McGraw-Hill, New York, NY, 1977

E.22 H. Wagner, Über Stoss und Gleitvorgänge an der Oberfläche von Flussigkeiten," Zeitschrift Für Angewandte Mathematik und Mechanik, August 1932.

E.23 S. L. Chuang, "Experiments on Slamming of Wedge-Shaped Bodies," Journal of Ship Research, September 1967.

APPENDIX F

List of Figures

Page

F-1 Fire modeling of casks F-3
F-2 Modeled cask dimensions for TACO input F-8
F-3 Lead mid-thickness temperatures for truck cask versus duration of regulatory fire F-14
F-4 Lead mid-thickness temperatures for rail cask versus duration of regulatory fire F-16
F-5 Initial heat flux on truck cask for various fire conditions (1-D model) F-19
F-6 Heat flux on truck cask versus duration of 1475°F and 1825°F fires F-21
F-7 Integrated heat flux on truck cask versus duration of 1475°F and 1825°F fires F-22
F-8 Lead mid-thickness temperature for truck cask versus duration of 1825°F fire F-23
F-9 Heat flux on rail cask versus duration of 1475°F and 1825°F fires F-25
F-10 Lead mid-thickness temperature for rail cask versus duration of 1825°F fire F-26
F-11 Initial and average heat flux on truck and rail cask versus flame temperature F-27
F-12 Cask on ground with tangent flame front F-29
F-13 Cask on ground--distant from flame front F-30
F-14 Fraction of heat load from nonengulfing fires F-32

List of Tables

Page

F.1 Material Thermal Properties F-11
F.2 Internal Heating from Fuel Assemblies F-12

APPENDIX F
Thermal Analysis

F.1 Introduction

This appendix provides the thermal models developed and the analyses performed to determine the responses of the representative truck and rail casks to a wide range of fire conditions. The computer code TACO-2D was used to perform the calculations.[F.1]

In Section F.2, the types of thermal loading conditions that can effect the temperature response of a cask in an accident are discussed. The highest loading condition is caused by large, long-duration fires and is selected for further evaluation. In Section F.3, the thermal loading conditions on a cask caused by real fire conditions are discussed. Referenced fire conditions and modeling are defined for evaluating real fire effects on casks.

In Section F.4, the thermal model and transient temperature response of the two representative casks to regulatory fire conditions are discussed. In Section F.5, the transient temperature response of the two representative casks is estimated for different heat loading conditions and a wide spectrum of real fire conditions defined by fire duration, temperature, and location.

F.2 Thermal Loading Conditions Caused by Accidents

Thermal loading conditions on a cask caused by an accident can result in cask temperature increases. The thermal loading conditions include fires, torch fires, and cask burial. Typically, as discussed in Section F.5, a fire can heat a cask at an average heat flux of 5,000 Btu/hr-ft^2 from several minutes to several hours. The total heat absorbed in a fire can be 1,000 to 50,000 BTU/ft^2 depending on the fire temperature, location, and duration.

Torch fires can heat a localized area of a cask at rates 1.5 to 2.5 times higher than a fire, but in comparison to fires, do not deposit large quantities of heat into the cask. As demonstrated in torch fire tests at Sandia,[F.2] no significant localized damage occurs to the cask even at the high heating fluxes because the heat is quickly dissipated to other portions of the cask thus limiting the rise in the local temperature.

Burial of the cask can cause the temperature of the cask and contents to rise because of the decay heat from the fuel. Burial of the cask can cause thermal isolation, where the decay heat from the fuel may have to be transferred through the surrounding material causing the burial. The decay heat flux from the fuel in a cask is typically 50-350 Btu/hr-ft^2 depending primarily on the number of fuel assemblies, their burnup, and their time out of a reactor. The decay heat flux from the fuel assemblies is 15-50 times lower than that which can be typically absorbed from a fire. The cask, which is relatively large and not easily buried, would have to be buried for several days before any significant damage to the cask could occur that could result in radioactive releases.

Based on severe accident data, the frequency of occurrence of fires is at least 10 times higher than for torch fires or complete burial of a cask. Therefore, since fires can generate higher heat loads and can occur more frequently, it is concluded that fires dominate the potential thermal environment and only fires require further evaluation.

F.3 Reference Fire Conditions and Modeling

In Fig. F-1(a), a three-dimensional (3-D) model of a cask engulfed in a real fire is given. The heat transfer from the fire to the cask can vary with time and position along the length and around the diameter of the cask. The effects of the fire can be significantly different on the various components located on the cask. To simplify the heating analysis of the cask and its components, currently licensed cask designs were reviewed to relate the temperatures at the middle portion of the cask to the temperatures of the other positions of the cask, particularly the closure seals. The location of valve boxes was also considered because they could be exposed to heat loads and temperatures approaching this middle portion of the cask. From this review, it was concluded that the temperature response and damage to the cask and its components could be conservatively bounded by analyzing the middle portion of the cask and using the four temperature response levels defined in Section 4.0 for the centerline of the lead shielding. Using this approach, the 3-D model in Fig. F-1(a) is reduced to the two-dimensional (2-D) model in Fig. F-1(b) for analysis.

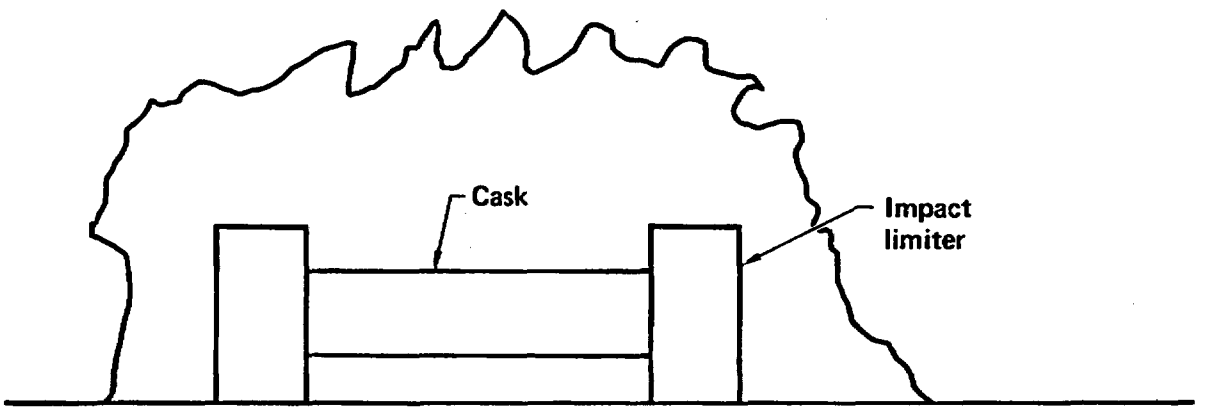

a) Three-dimensional cask fire model

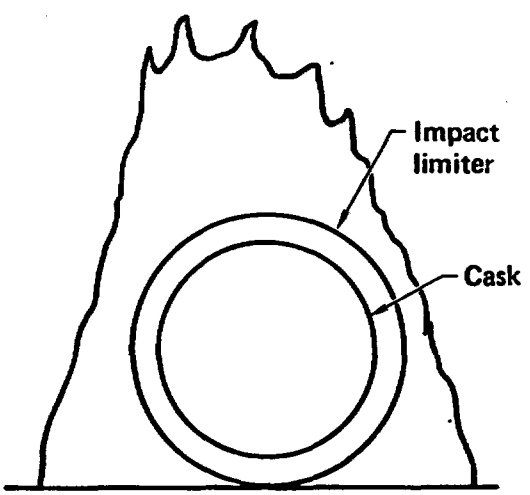

b) Two-dimensional cask fire model

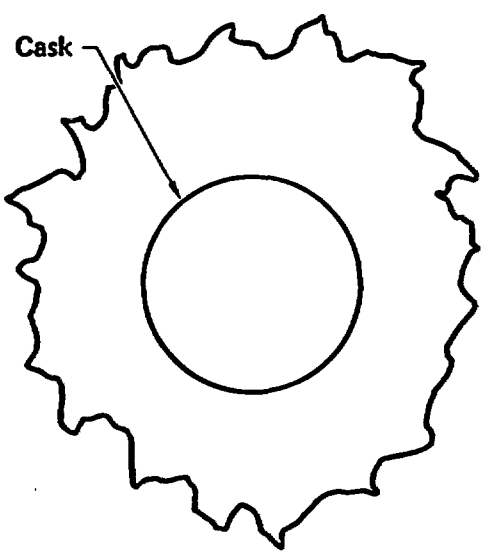

c) One-dimensional cask fire model

Figure F-1 Fire modeling of casks.

In a real engulfing fire, the spent fuel cask is partially shielded from the heat by either the transport vehicle or the ground. In real fires the amount of heat transferred to the cask differs significantly from that from a hypothetical totally engulfing fire, represented by the one-dimensional (1-D) model in Fig. F-1(c).

The role of convection from the flame may be significant for cases in which the cask is enclosed within or very near the flame while on either the ground or the vehicle. There does not appear to be sufficient experimental evidence to formulate any general rule to evaluate convection coefficients in this geometry. Also the flame temperature can vary significantly along the diameter of the cask. A common analytical approach is to consider the flame to be isothermal, with a single value for emissivity and a conservatively high temperature to attempt to account for the convective effects, since these are the most highly variable and difficult effects to measure and to model.

In the case of engulfing fires, the radiative heat load from an isothermal fire to the cask can be calculated as follows:[F.3]

$$\dot{Q}_r = \sigma A_s \, C_{s-f}(T_f^4 - T_{s,o}^4) \qquad \text{(F.1)}$$

where

$\dot{Q}_r$ = radiant heat load per unit length and time, Btu/ft-hr

σ = Stefan-Boltzman constant , Btu/hr-ft^2-°K^4

C_{s-f} = configuration factor, unitless

A_s = area of cask exposed to flame, ft^2/ft

T_f = flame temperature, absolute, °R

$T_{s,o}$ = initial cask surface temperature, absolute, °R

For a real fire the configuration factor for two gray, diffuse bodies exchanging heat is given by:

$$A_s C_{s-f} = \frac{1}{\frac{1-\varepsilon_f}{\varepsilon_f A_f} + \frac{1}{A_s F_{s-f}} + \frac{1-\varepsilon_s}{\varepsilon_s A_s}} , \text{ ft}^2/\text{ft} \qquad \text{(F.2)}$$

where

A_f = area of flame involved, ft^2/ft

F_{s-f} = geometric view factor from cask to fire, unitless

ε_f = flame emissivity = 0.9, unitless

ε_s = cask surface emissivity = 0.8, unitless

and all other terms are as previously defined.

If it is assumed as shown in Fig. F-1(b) that no significant fire exists below the horizontal centerline and within the diametral dimension of the cask, the geometric view factor from the cask to the fire below the centerline for one side of the lower portion of the cask is given by:

$$(A_s F_{s-f})_B = \frac{\pi r}{4} , \text{ ft}^2/\text{ft} \qquad \text{(F.3)}$$

where

r = radius of cask, ft

for a 2-D infinitely long cylinder. The area-configuration factor calculated using Equation F.2 is:

$$(A_s C_{s-f})_B = \frac{2\pi}{\frac{1-\varepsilon_f}{\varepsilon_f} + \frac{2}{\pi}\left(\frac{1+\varepsilon_s}{\varepsilon_s}\right)} \text{ , } ft^2/ft \qquad (F.4)$$

Assuming that the cask is completely engulfed by the fire above the centerline, the area-configuration factor above the centerline is given by:

$$(A_s C_{s-f})_A = \pi r \bar{\varepsilon} \text{ , } ft^2/ft \qquad (F.5)$$

where

$$\bar{\varepsilon} = \text{effective emissivity} = \frac{1}{1/\varepsilon_f + 1/\varepsilon_s - 1} \text{ .}$$

Adding the results of Equations F.4 and F.5 together, the total area-configuration factor for a real fire is:

$$(A_s C_{s-f})_T = \frac{2\pi}{\frac{1-\varepsilon_f}{\varepsilon_f} + \frac{2}{\pi}\left(\frac{1+\varepsilon_s}{\varepsilon_s}\right)} + \pi r \bar{\varepsilon} \text{ , } ft^2/ft \qquad (F.6)$$

A hypothetical regulatory engulfing fire is shown as a 1-D fire in Fig. F-1(c). The regulatory fire is defined as having a fire temperature of 1475°F, a flame emissivity of 0.9, and a fire duration of 0.5 hour. The area-configuration factor for the regulatory fire is:

$$(A_s C_{s-f})_T = 2\pi r\bar{\varepsilon} \quad , \ ft^2/ft \tag{F.7}$$

Then the ratio of the heat load of real fires to a hypothetical uniform fire is the ratio of Equations F.6 and F.7:

$$\frac{\dot{Q}_r}{\dot{Q}_h} = \frac{\left[\frac{1-\varepsilon_f}{\varepsilon_f} + \frac{2}{\pi}\left(\frac{1+\varepsilon_s}{\varepsilon_s}\right)\right]^{-1}}{r\bar{\varepsilon}} + 1/2 = 0.78 \tag{F.8}$$

for the same flame emissivity of 0.9, cask surface emissivity of 0.8, fire temperature, and cask surface temperature.

Based on Equation F.8, a higher flame temperature is required for the cask to absorb the same amount of heat for a real fire compared to a hypothetical fire. As derived in Section F.5, the hypothetical regulatory fire with a fire temperature of 1475°F generates the same heat load on a cask as a 1700°F real fire. The reference fire conditions are defined to be the 1700°F real fire that generates the same heat load as the regulatory fire. The 1-D model (Fig. F-1(c)) can be used to approximate the 2-D model (Fig. F-1(b)) provided that the heat loading conditions are appropriately accounted for.

F.4 Cask Temperature Response to Regulatory and Reference Fire Conditions

The transient thermal response of a representative truck and rail cask to an engulfing reference fire was analyzed using TAC0.[F.1] A 1-D model of the casks engulfed by the regulatory fire simplifies the calculation and predicts reasonably well the thermal response of the major volume of the casks. This model is used to estimate the cask response to the reference 1700°F real fire engulfing a cask. Figure F-2 shows the geometry of the modeled casks.

The initial temperature distribution within each cask from heat generated by the spent fuel was established before subjecting the cask to the modeled

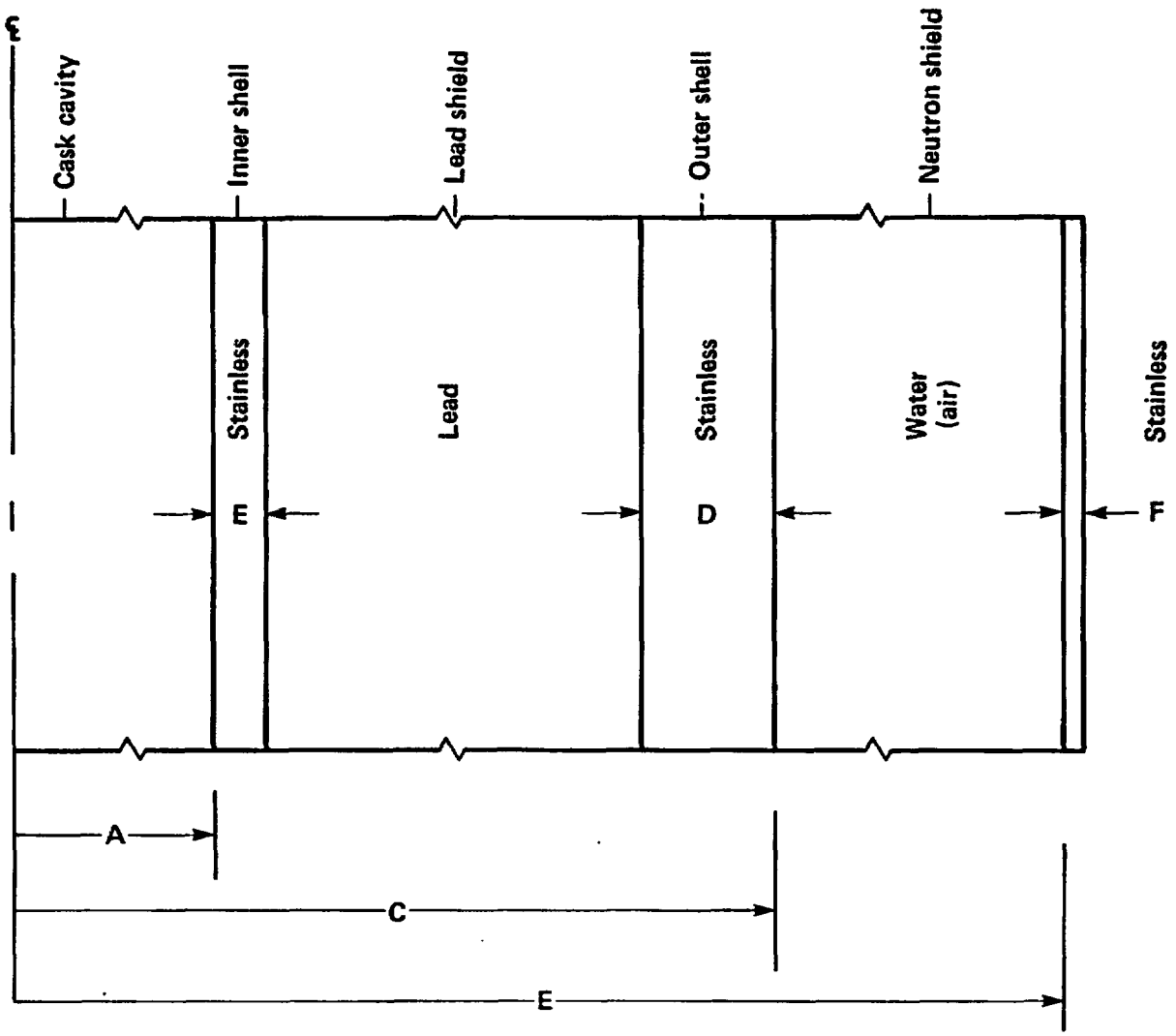

Dimension	Truck cask (in.)	Rail cask (in.)
A	6.75	30.00
B	0.50	1.50
C	13.75	38.00
D	1.25	2.50
E	18.25	42.50
F	0.25	0.25

Figure F-2 Modeled cask dimensions for TACO input.

fire environment. The steady-state evaluation was performed using TACO, with the assumption that the neutron shield tank is filled with water. The heat transfer through the water is by conduction and natural convection. A convenient way to model the natural convection is through the use of an effective conductivity for the water. Holman gives a relationship for effective conductivity of a fluid in a horizontal cylindrical annulus as:[F.4]

$$\frac{k_e}{k} = C(Gr_\delta \, Pr)^r, \text{ unitless} \qquad (F.9)$$

where

k_e = effective thermal conductivity, Btu/hr-ft-°F,

k = thermal conductivity, Btu/hr-ft-°F,

Gr_δ = Grashof Number = $\frac{g\rho^2\beta\delta^3\Delta T}{\mu^2}$, unitless

Pr = Prandtl Number, unitless

g = gravitational constant, ft/sec^2

β = volume coefficient of expansion, 1/°F

δ = annulus width, ft

ρ = density, lb/ft^3

μ = dynamic viscosity, lb/sec-ft

ΔT = temperature difference across annulus, °F

$$r = 0.29 \text{ for } 6 \times 10^3 \leq GrPr < 10^6$$

$$0.20 \qquad 10^6 \leq GrPr < 10^8$$

$$C = 0.11 \text{ for } 6 \times 10^3 \leq GrPr < 10^6$$

$$0.40 \qquad 10^6 \leq GrPr < 10^8.$$

This expression was evaluated over the expected temperature range, and an average value of effective conductivity of water as a function of bulk temperature was used.

Table F.1 tabulates the material thermal properties used in the analysis. Table F.2 lists the internal heat assumed for the fuel assemblies within the two casks. A uniform value of 1.0 Btu/hr-ft^2-°F was used to represent natural convective heat removal from the cask surface.

The results of the steady-state analysis for the casks show a surface temperature of 147°F for the truck and 242°F for the rail cask.

For the regulatory fire, only radiation heat transfer occurs. The heat flux from a hypothetical engulfing fire on the surface of the cask due to radiation heat transfer is given by:

$$q = \sigma\tilde{\varepsilon}(T_f^4 - T_s^4) \text{ , Btu/hr-ft}^2 \qquad \text{(F.10)}$$

where

T_s = cask (neutron shield) surface temperature, absolute, °R

and all other terms are as previously defined.

It is next assumed that before being engulfed by fire, the water leaks out of the neutron shield tank. Heat transfer in the annulus is now through the combined modes of radiation across the gap and convection and conduction

Table F.1
Material Thermal Properties

Stainless Steel
Density 494.2 lb/ft^3

Temperature (°F)	Thermal Conductivity (Btu/hr-ft-°F)	Specific Heat (Btu/lb)
50	7.92	0.107
250	8.64	0.11
500	9.72	0.120
750	10.86	0.133
1000	12.06	0.138
1250	13.5	0.144
1500	14.46	0.150
2372	16.92	0.170

Lead
Density 708.5 lb/ft^3
Melt Point 621.5°F
Latent Heat 10.25 Btu/lb

Temperature (°F)	Thermal Conductivity (Btu/hr-ft-°F)	Specific Heat (Btu/lb)
50	19.97	0.031
250	19.2	0.032
619	10.4	0.0332
1500	8.64	0.034
1832	8.64	0.0328

Water
Density 62.43 lb/ft^3
Specific Heat 1.0 Btu/lb°F

Temperature (°F)	Eff. Thermal Conductivity (Btu/hr-ft-°F)
104	2.76
140	3.01
176	3.25
212	3.46
284	4.34

Table F.2
Internal Heating from Fuel Assemblies

	Heat Load (KBtu/hr)
Truck Cask	6.82
Rail Cask	71.4

through the air. As in the case for water, the same relationship holds, but a single value of effective thermal conductivity of the air as a function of bulk temperature can lead to serious errors. The equation for total heat transfer in the annulus is:

$$q_{an} = \frac{\sigma(T_s^4 - T_i^4)}{\frac{1}{\varepsilon_i} + \frac{d_i}{d_o}\left(\frac{1}{\varepsilon_o} - 1\right)} + \frac{2K_e(T_s - T_i)}{d_i \ln(d_o/d_i)}, \text{ Btu/hr-ft}^2 \qquad \text{(F.11)}$$

where

d_i = neutron shield inner diameter, ft

d_o = neutron shield outer diameter, ft

K_e = effective air thermal conductivity, Btu/hr-ft-°F

T_i = neutron shield inner diameter temperature, absolute, °R

and all other terms are as previously defined.

Solving this equation over the entire expected temperature range for both surfaces of the annulus and then using an interval halving technique results in a constant value for the effective air thermal conductivity, with a maximum root-mean-square error in the total heat transferred of less than 2.5%, for equal surface emissivities between 0.3 and 0.5.

The temperature response of the representative truck cask was calculated for the regulatory fire with a flame temperature of 1475°F, a flame emissivity of 0.9, and a cask surface emissivity of 0.8. The temperature at the middle of the lead shield thickness is plotted in Fig. F-3. The cask temperature reaches 500°F (T_1) in 1.08 hours and 600°F (T_2) in 1.35 hours. As the lead mid-thickness temperature increases beyond the 600°F (T_2) level, the lead at

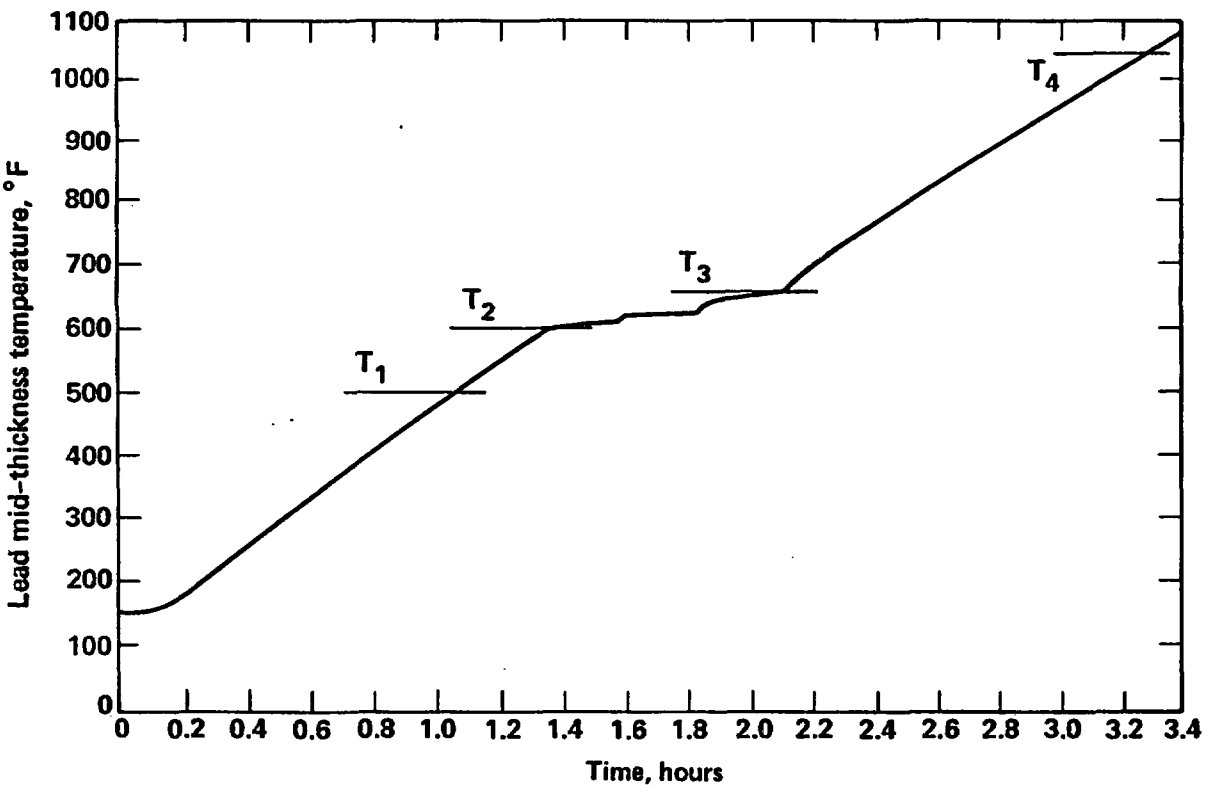

Figure F-3 Lead mid-thickness temperatures for truck cask versus duration of regulatory fire.

the outer shell starts to melt. The lead melts at the inner shell in 2.1 hours as the mid-thickness temperature reaches 650°F (T_3). The 1050° temperature (T_4) level is reached in 3.3 hours.

The temperature response of the representative rail cask was also calculated for the hypothetical engulfing fire. The temperature at the middle of the lead shield thickness is plotted in Fig. F-4. The cask temperature reaches 500°F (T_1) in 1.35 hours, and 600°F (T_2) in 1.8 hours. As the lead mid-thickness temperature of the lead increases beyond the 600°F (T_2) level, the lead at the outer shell starts to melt. The lead melts at the inner shell in 2.6 hours as the mid-thickness temperature reaches 650°F (T_3). The 1050°F temperature (T_4) level is reached in 5.1 hours.

These temperature response and heat flux results for the regulatory fire were used to evaluate real fires.

F.5 Cask Response to a Spectrum of Real Fire Conditions

In order to calculate the thermal response of a cask to a real engulfing fire, certain fire parameters are required. The principal parameters required are fire temperature, flame emissivity, convection velocities, and fire duration. These fire parameters depend upon variables that include type of fuel, amount of fuel, the fuel-air mixture, fire geometry, local temperatures, humidity, and wind conditions. Based on the information provided, the fire temperatures range from 1400 to 2400°F, flame emissivities range from 0.4 to 1.0, and convection velocities range from nearly 0 to 20 feet/second.[F.5-F.10]

The initial heat flux from a hypothetical engulfing fire on the surface of the cask is given by:

$$\dot{q} = \sigma\tilde{\varepsilon}(T_f^4 - T_{s,o}^4) + h\,(T_f - T_{s,o})\ ,\ \text{Btu/hr-ft}^2 \qquad \text{(F.12)}$$

where

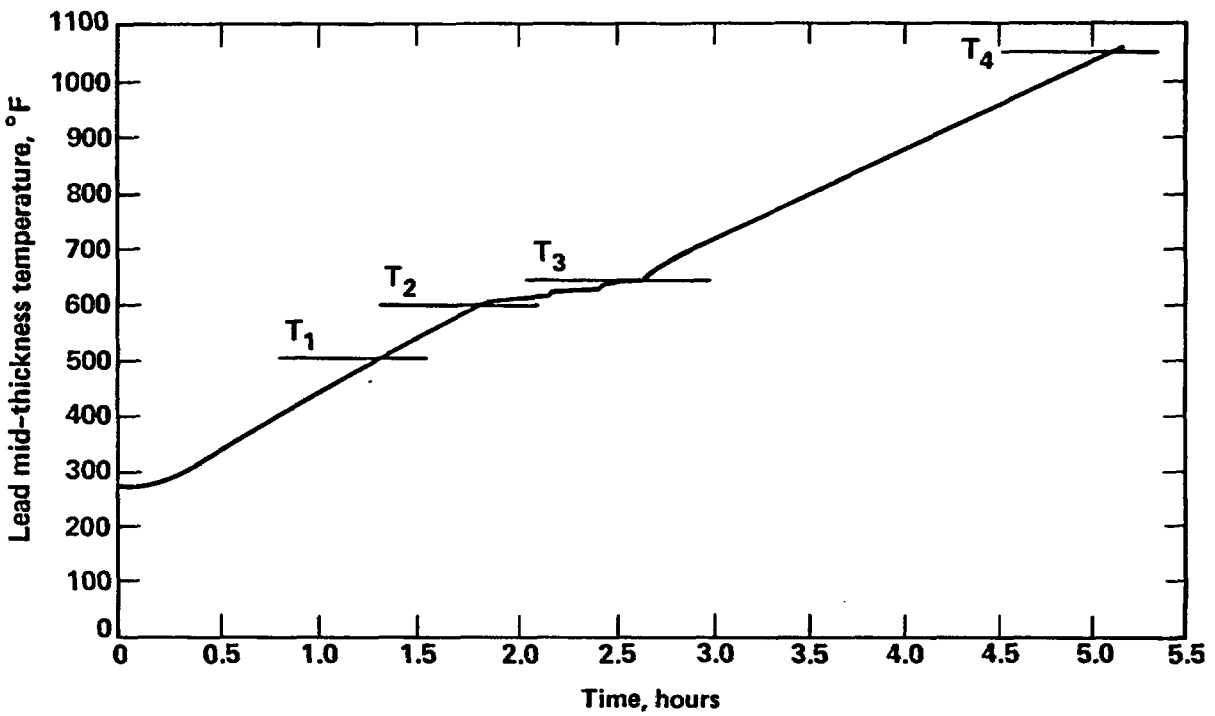

Figure F-4 Lead mid-thickness temperatures for rail cask versus duration of regulatory fire.

h = convective heat transfer coefficient, Btu/hr-ft^2-^{o}F

and all other terms are as previously defined.

Experimentally determined values for the convection heat transfer coefficient in an engulfing fire have been determined.[F.7] The values given for an 8.53 inch diameter cylinder range from 5.2 to 15.8 Btu/hr-ft^2-^{o}F as a perimeter mean. These values can be scaled within the scaled Reynolds Number by the following relationship:

$$h = h_{ref}\left(\frac{d_{ref}}{d}\right)^{0.195} \text{, BTU/hr-ft}^2\text{-}^o\text{F} \qquad \text{(F.13)}$$

where

h_{ref} = reference convection heat transfer coefficient, Btu/hr-ft^2-^{o}F

d_{ref} = reference diameter = 8.53 inches,

d = diameter, inches

as long as the scaled Reynolds Number is within the range of applicability. The scaled Reynolds Number is given by:

$$R_e = Re_{ref}\left(\frac{d}{d_{ref}}\right)^{0.805} \text{, unitless} \qquad \text{(F.14)}$$

where

R_e = scaled Reynolds Number, unitless

Re_{ref} = reference Reynolds Number = 73,725.

The scaled values of the convection heat transfer coefficient are found to be:

3.9 to 11.9 Btu/hr-ft^2-°F for the truck cask,

and

3.3 to 10.1 Btu/hr-ft^2-°F for the rail cask.

Figure F-5 gives the initial heat flux on the surface of the truck cask as a function of flame temperature, flame emissivity, cask emissivity, and convection heat transfer coefficient. This figure provides a wide spectrum of fire conditions which can be related to the regulatory fire conditions in terms of initial heat fluxes. For example, from Fig. F-5, it is determined that an engulfing fire with a flame temperature of 1300°F, a flame emissivity of 0.9, a cask emissivity of 0.8, and a convection heat transfer coefficient of 5 Btu/hr-ft^2-°F generates the same initial heat flux to a cask surface as a regulatory fire. For these specific conditions, the initial response of the cask would be essentially the same as its initial response to a regulatory fire. The initial heat fluxes for a rail cask are similar.

A sensitivity study was performed to compare the response of the representative cask for different fire conditions and initial heat fluxes to the responses calculated for the regulatory fire. The initial heat flux to the cask when engulfed by a regulatory fire is:

q = 17,646 Btu/hr-ft^2 for the truck cask and

q = 17,510 Btu/hr-ft^2 for the rail cask.

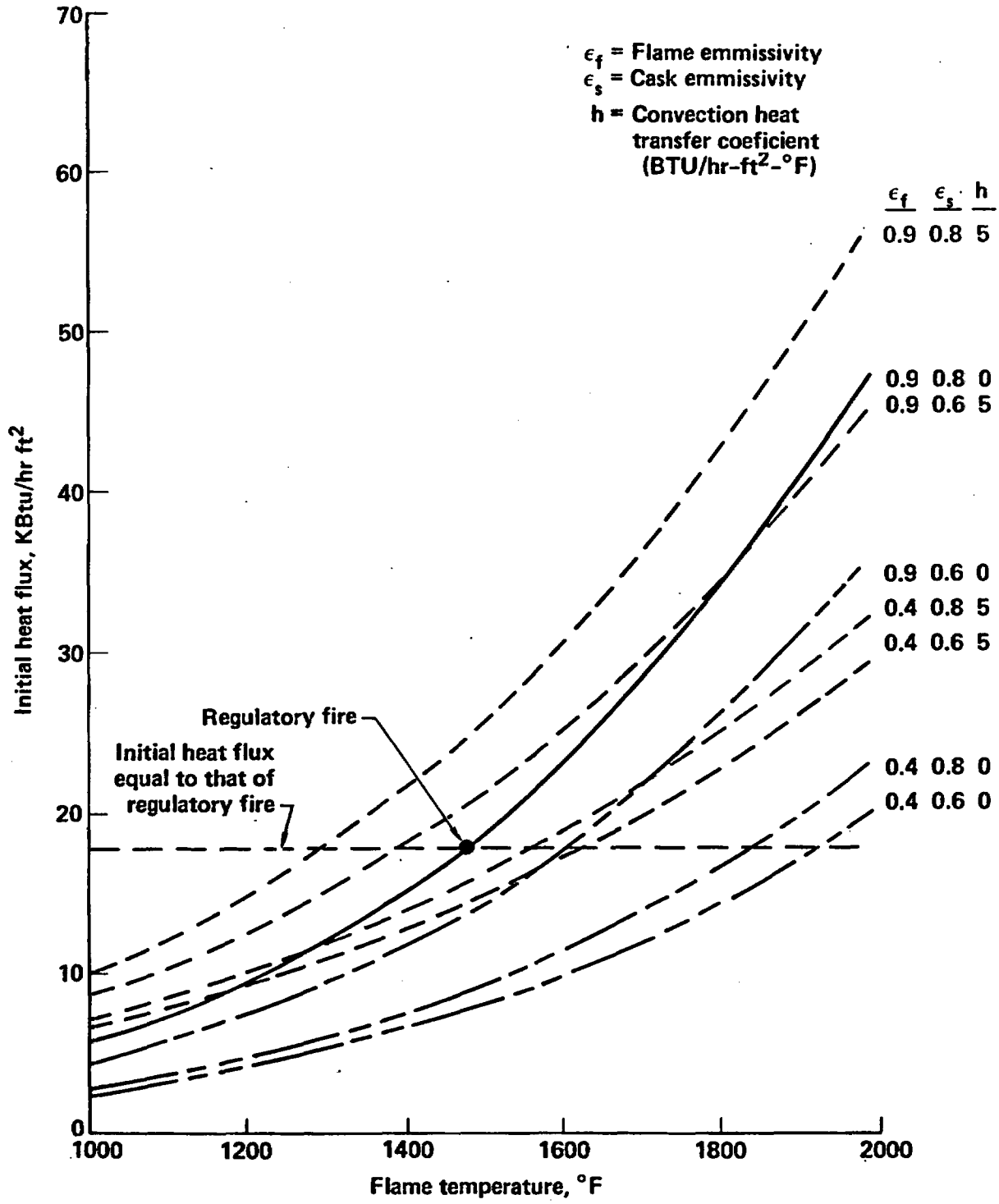

Figure F-5 Initial heat flux on truck cask for various fire conditions (1-D model).

The second fire for comparison was chosen arbitrarily, but within the limits of real fires. The flame temperature was chosen to be 1825°F, flame emissivity of 0.9, and a surface emissivity of 0.8. The initial heat flux to the cask is:

$q = 35{,}260$ Btu/hr-ft^2 for the truck cask and

$q = 34{,}650$ Btu/hr-ft^2 for the rail cask.

Thus the initial heat flux is about double that caused by the regulatory fire for each of the casks.

The variations of the heat flux for the regulatory and 1825°F fires are plotted in Fig. F-6 as a function of time for the truck cask. The heat flux drops rapidly and then decreases slowly because the water jacket acts as a thermal barrier. The heat fluxes after about 1 hour are reduced to 4,500 Btu/hr-ft^2 for the regulatory fire and 6,750 BTU/hr-ft^2 for the 1825°F fire. The integrated heat flux absorbed into the cask is plotted in Fig. F-7 for the regulatory and 1825°F fires. The integrated flux rises rapidly at first until the thermal barrier heats up and then limits the heat flux to the cask. The centerline temperatures for the lead shield are plotted in Figs. F-3 and F-8 for the regulatory and 1825°F fires, respectively. For the regulatory fire, lead melt starts after 1.35 hours and takes 0.75 hours to complete all the melting. As would be expected for the 1825°F fire with a heat flux 1.5 times higher than lead, melt starts at 0.9 hours and is completed after 0.5 hours or times which are 1.5 times shorter than the regulatory fire. The times to reach the melting temperatures and to melt the lead are actually determined when the total integrated heat flux values of approximately 6,000 Btu/ft^2 and 9,000 Btu/ft^2, respectively, are reached.

The cask heat-up rate and temperature are primarily determined by the heat flux from the fire because the heat from the fuel bundle is about 41 Btu/hr-ft^2. Therefore, it is concluded that the time it takes a specific fire to heat the cask to a specific temperature is approximately proportional to the average heat flux or heat load to the cask.

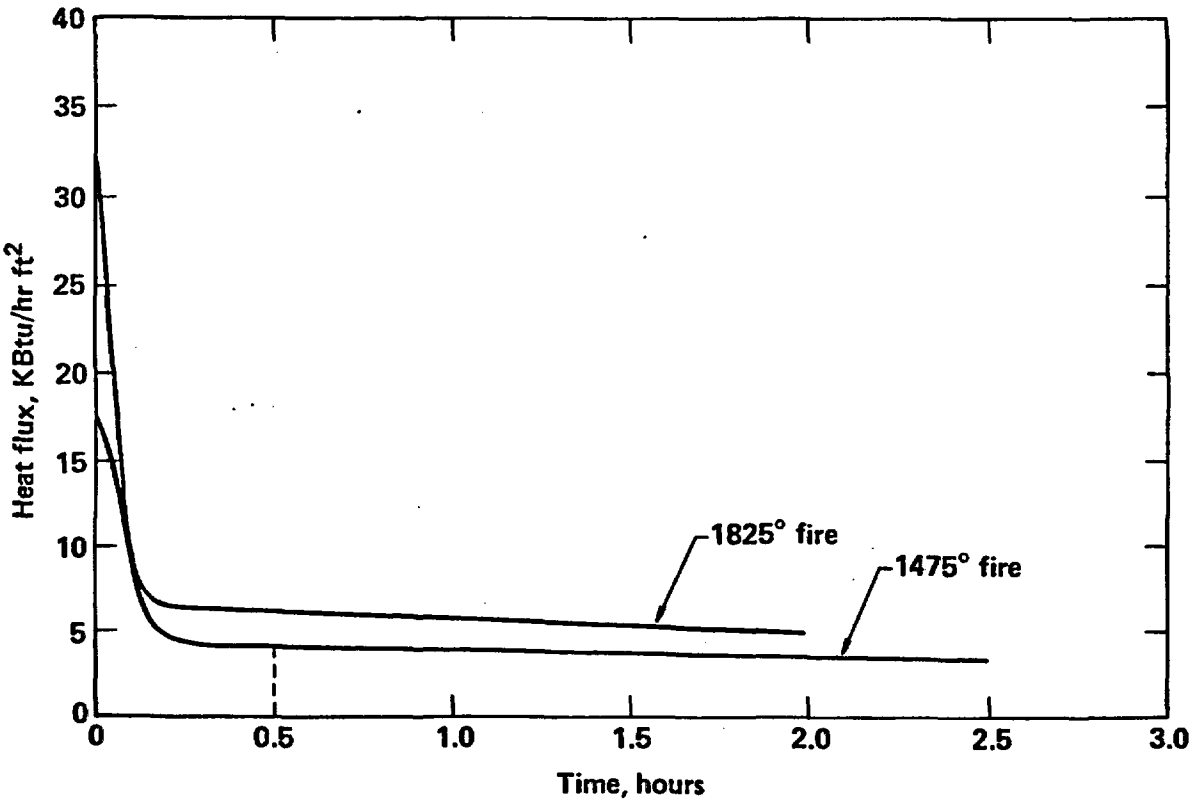

Figure F-6 Heat flux on truck cask versus duration of 1475°F and 1825°F fires.

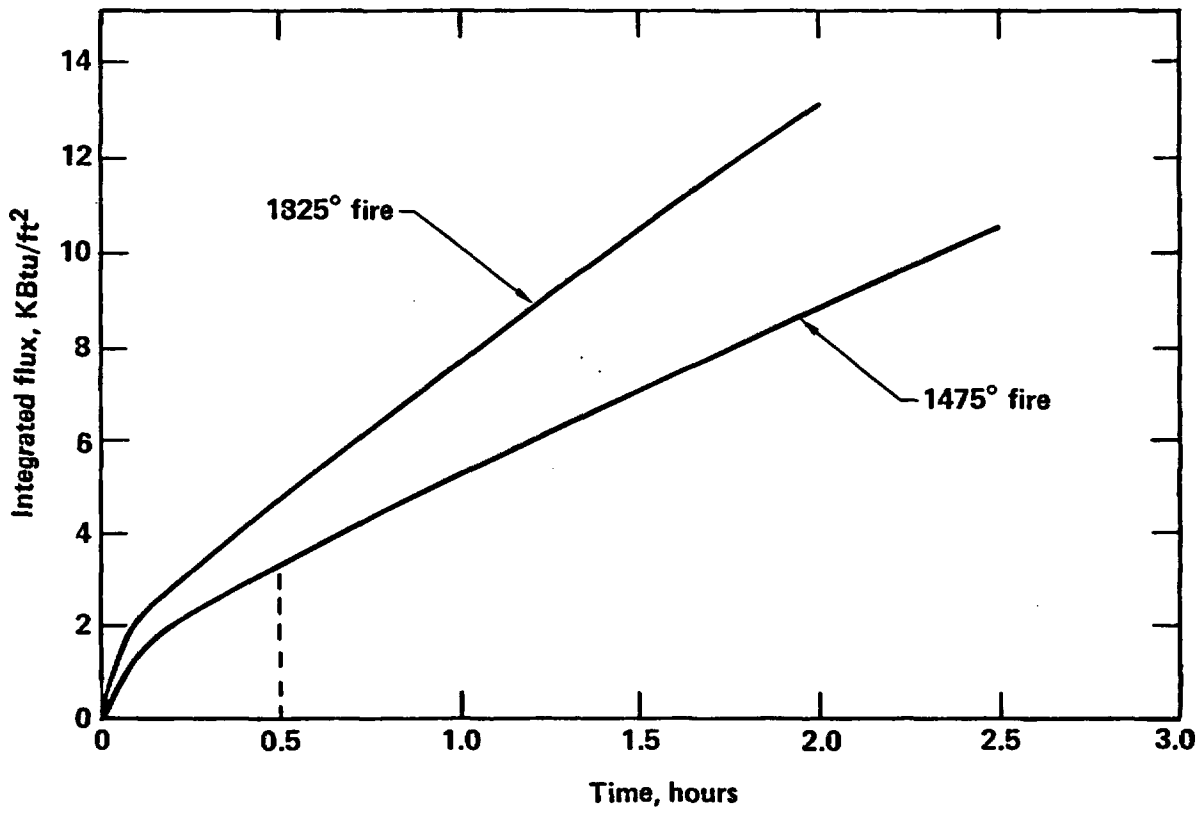

Figure F-7 Integrated heat flux on truck cask versus duration of 1475°F and 1825°F fires.

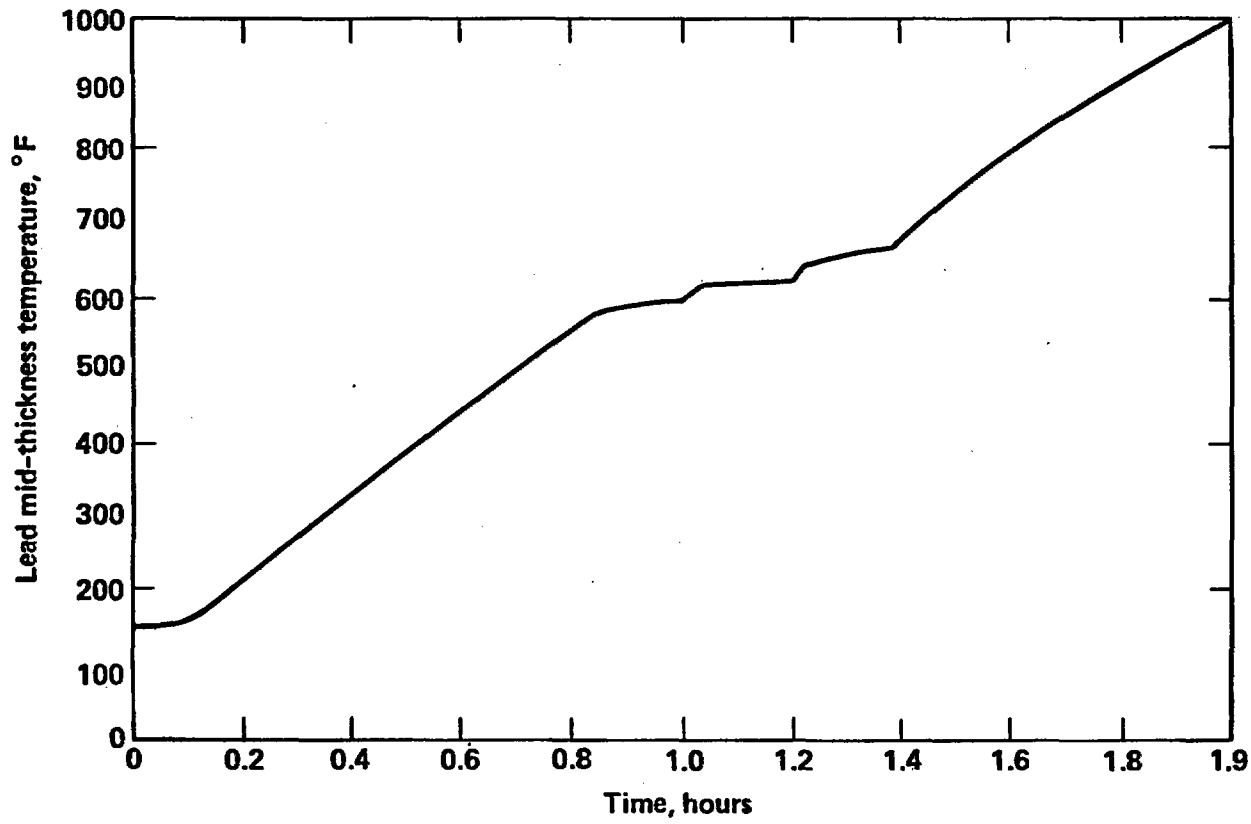

Figure F-8 Lead mid-thickness temperature for truck cask versus duration of 1825°F fire.

The transient thermal analysis for the rail cask was performed in a manner similar to that used for the truck cask. The variations of the heat fluxes for the regulatory and 1825°F fires are plotted in Fig. F-9 as functions of time. As with the truck cask case, the heat flux drops rapidly and levels off because the water jacket acts as a thermal barrier. The heat fluxes after about 1 hour are reduced to 4,500 Btu/hr-ft^2 for the regulatory fire and 7,000 BTU/hr-ft^2 for the 1825°F fire. These results are similar to those calculated for the truck and indicate that these heat flux values apply to a wide range of cask sizes. The cask will heat up at a rate determined by the heat flux from the fire. The time to reach a particular temperature for the cask is determined by the heat flux. The centerline temperatures for the lead shielding are plotted in Figs. F-4 and F-10 for the regulatory and 1825°F fires, respectively. For the regulatory fire, the lead melting begins about 1.8 hours after the fire initiation and is complete at about 2.6 hours. For the 1825°F fire, the lead melt begins at 1.2 hours and is complete within 1.8 hours. These melting times are nearly proportional to the fire heat fluxes or heat loads.

In Fig. F-11, the heat flux on the surfaces of the truck and rail cask is plotted as a function of flame temperature, flame emissivity of 0.9, and cask emissivity of 0.8. The initial heat flux is given. Also, the average heat flux values are given at 1 hour durations for the 1475°F and 1825°F fires.

As derived in Section F.3, the heat load ratio of a real fire to a hypothetical fire is 0.78 for the same flame temperature. To absorb the same heat load per unit time from a real engulfing fire compared to a hypothetical engulfing fire, the average heat flux on the cask has to be increased. The required heat flux is 1.28 times higher for a real fire. From Fig. F-11 it is determined that a flame temperature of 1700°F is required to provide an average flux of 6,400 Btu/hr-ft^2 which is 1.28 times higher than the heat flux derived from regulatory conditions. Therefore, it is concluded that a 1700°F real fire provides a heat load to the cask and results in temperature responses similar to those for a 1475°F regulatory fire.

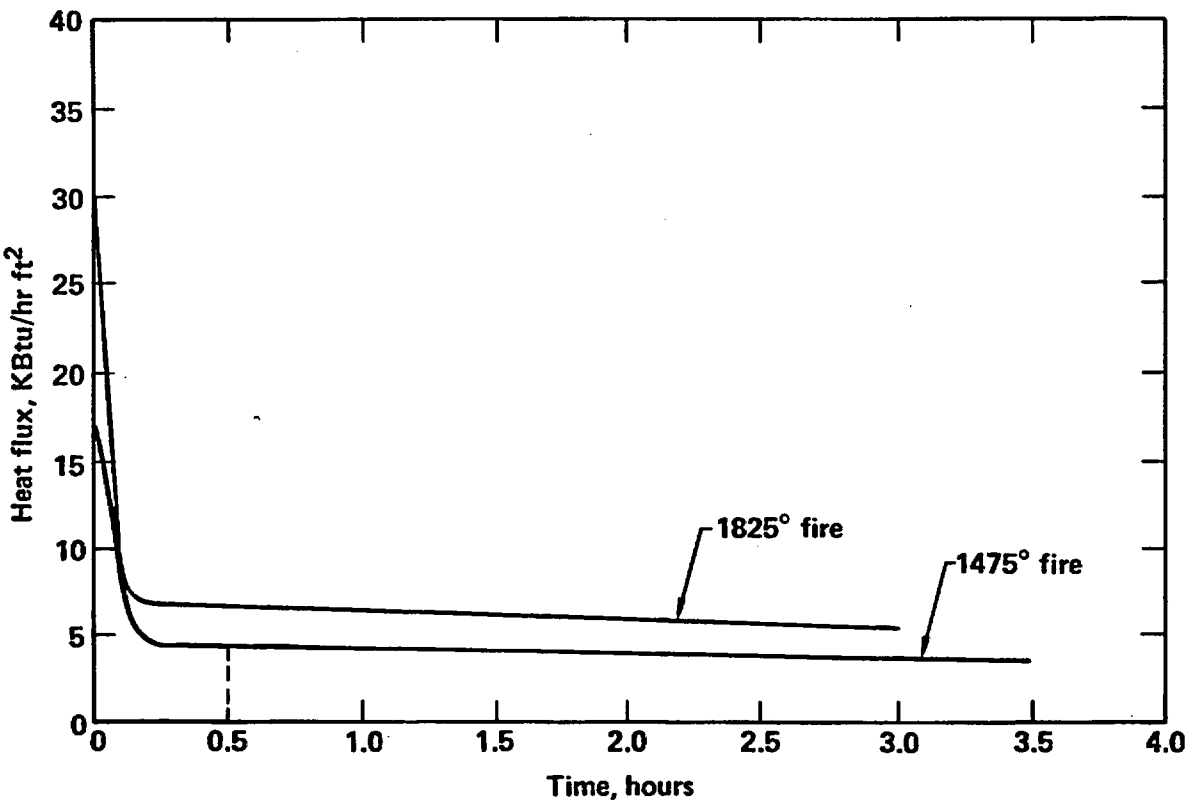

Figure F-9 Heat flux on rail cask versus duration of 1475°F and 1825°F fires.

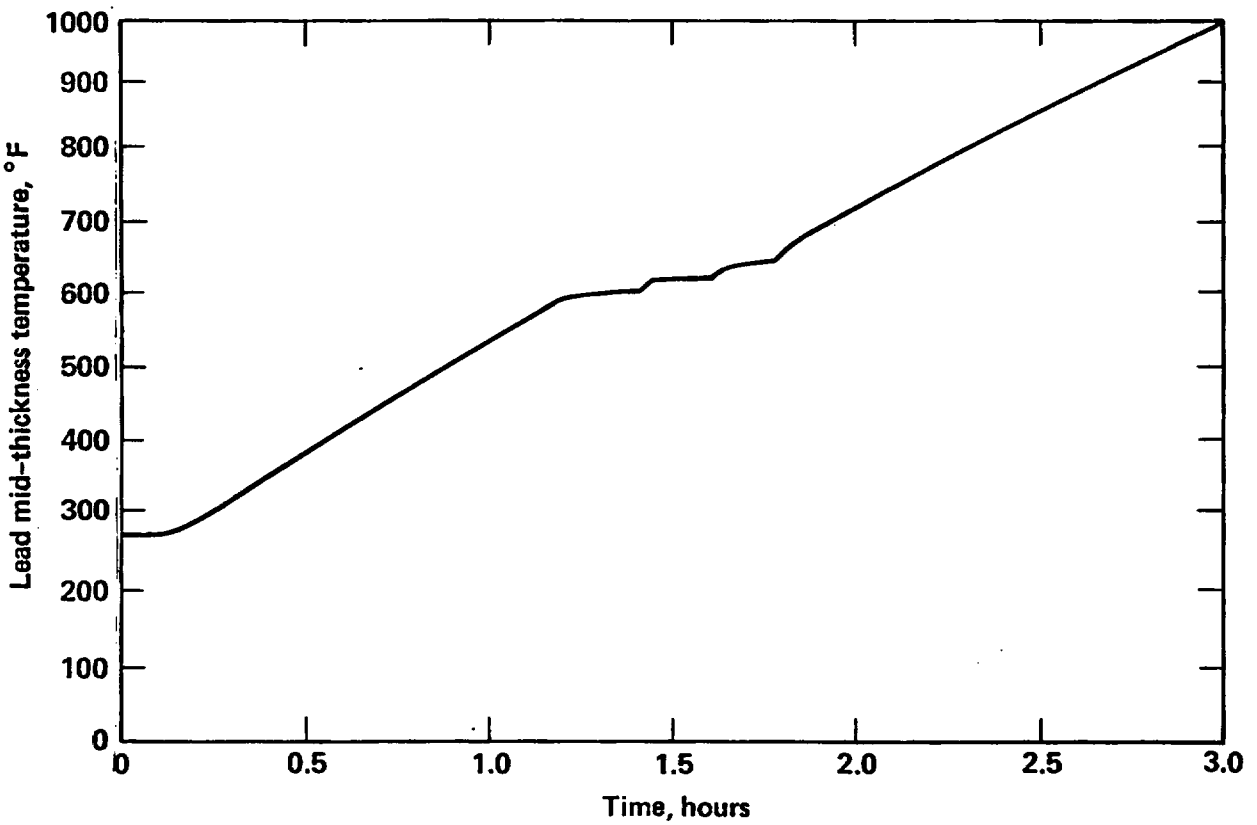

Figure F-10 Lead mid-thickness temperature for rail cask versus duration of 1825°F fire.

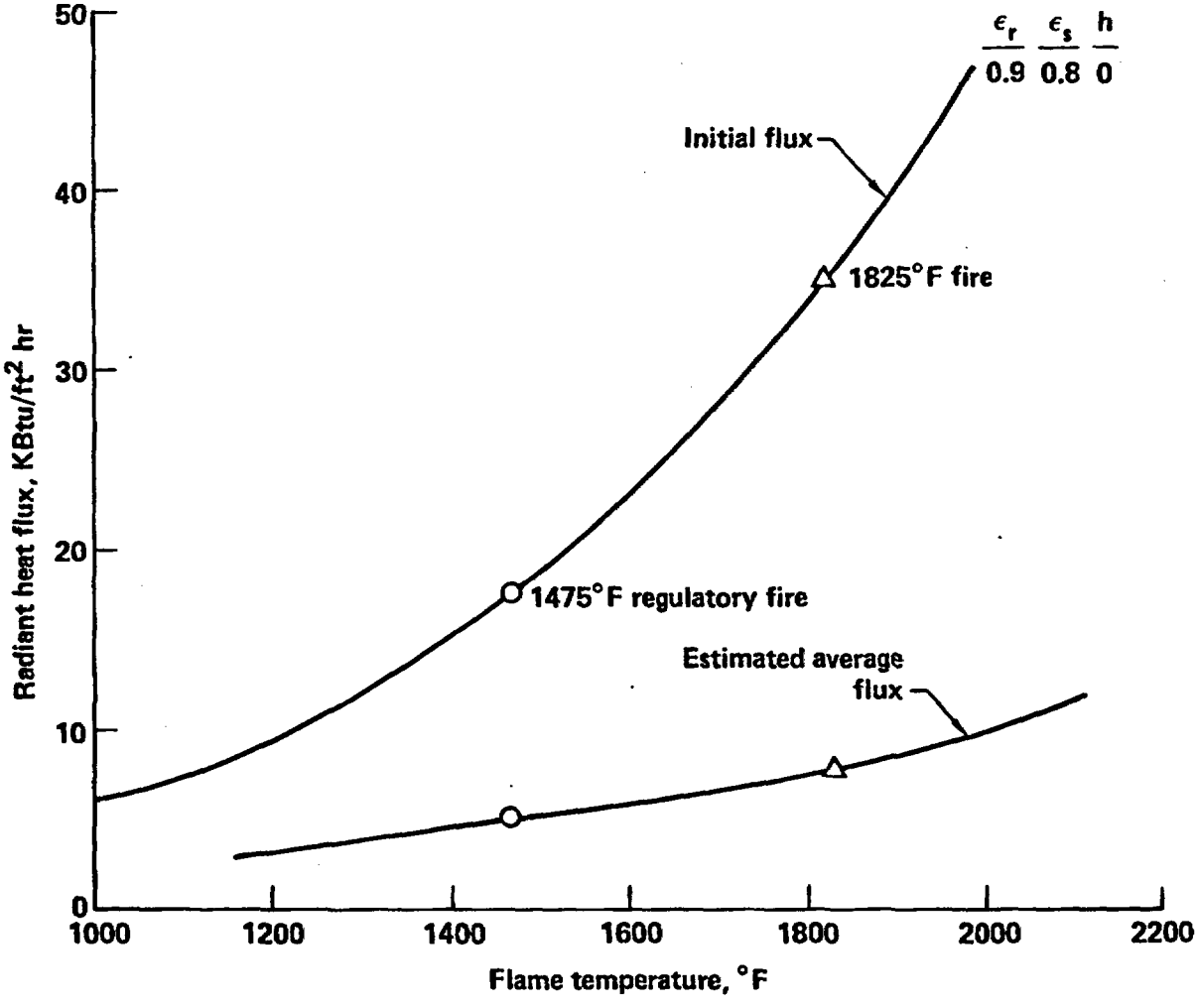

Figure F-11 Initial and average heat flux on truck and rail cask versus flame temperature.

The heat load to the cask also varies with the location of the fire with respect to the cask. For the case in which the flame front is just tangent to the cask, as shown in Fig. F-12, the geometric view factor to the part of the cask below the horizontal centerline is:[F.11]

$$A_s F_{s-f} = \frac{\pi r}{4} \text{ , } ft^2/ft \qquad (F.15)$$

The geometrical view factor to the upper portion of the cask is given by the relationship:

$$A_s F_{s-f} = \frac{r\delta}{2} \text{ , } ft^2/ft \qquad (F.16)$$

where

$\delta = \pi - 2 \tan^{-1}(\frac{r}{h-r})$, radians

h = flame height, ft

Finally, for the case in which the cask is removed a distance from the flame front as shown in Fig. F-13, the geometric view factor from the entire cask to the flame is given by:[F.11]

$$A_s F_{s-f} = r[\tan^{-1}(\frac{h-r}{x}) + \tan^{-1}(\frac{r}{x})] \text{ , } ft^2/ft \qquad (F.17)$$

where

x = separation distance, ft

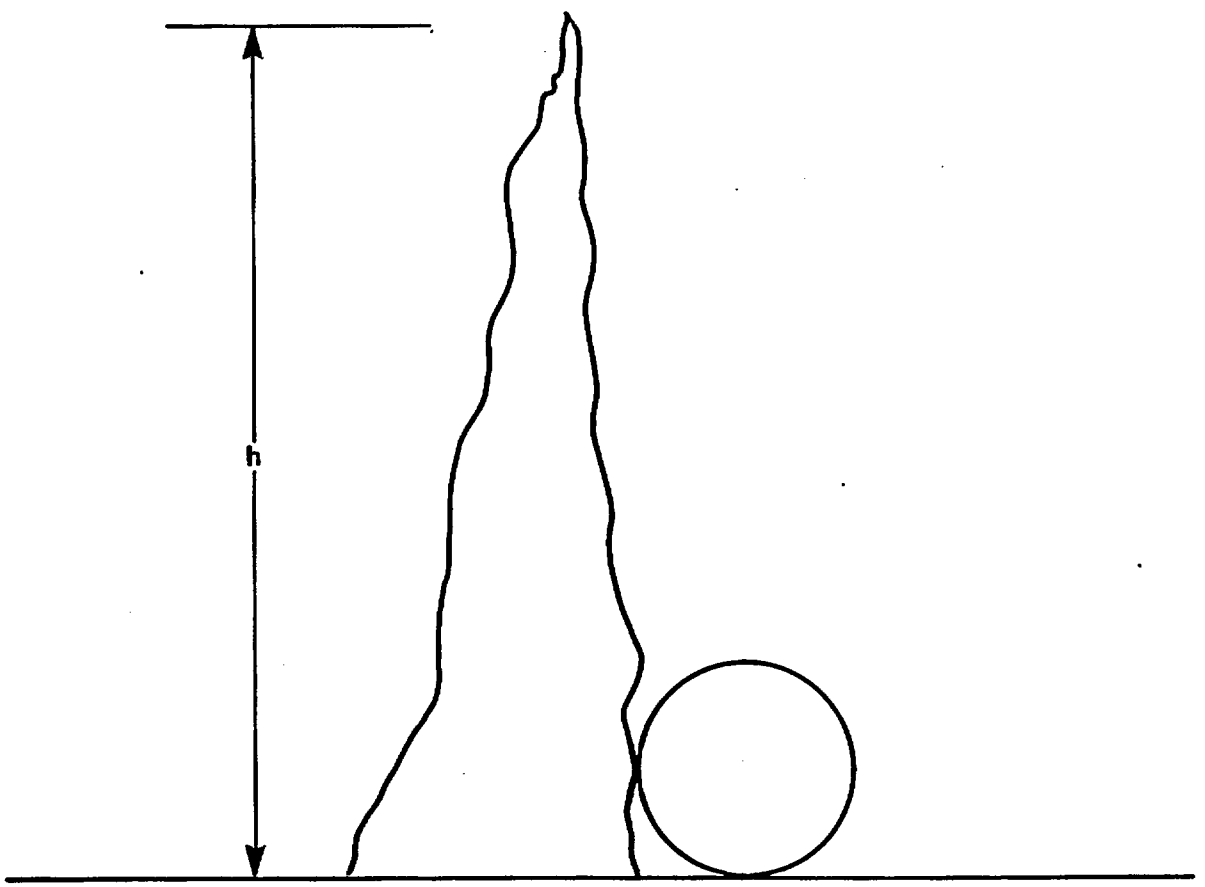

Figure F-12 Cask on ground with tangent flame front.

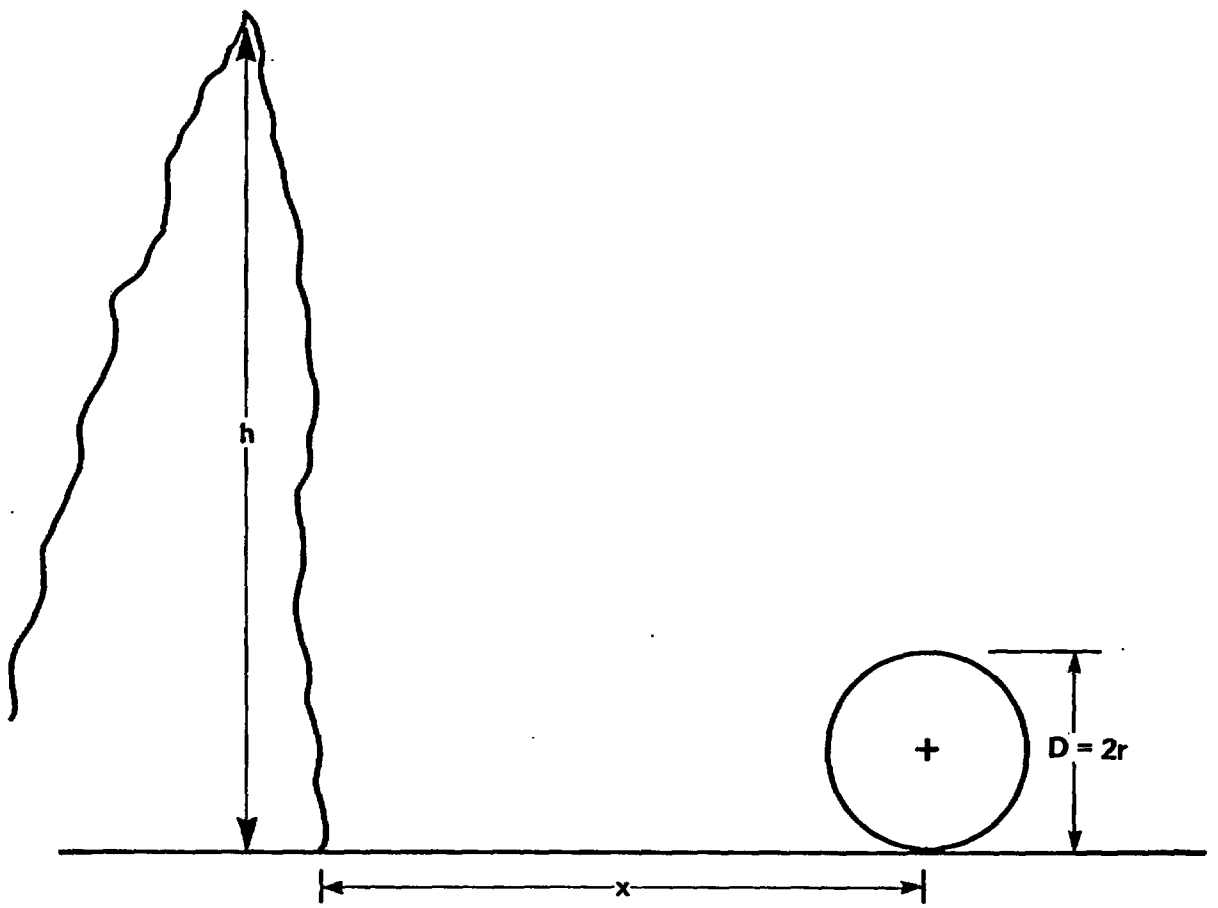

Figure F-13 Cask on ground--distant from flame front.

$$A_s = r(\pi + \psi) \text{ , } ft^2/ft$$

$$\psi = \tan^{-1}\left(\frac{h-4}{x}\right) - \tan^{-1}\left(\frac{r}{h^2 + x^2 - 2hr}\right) \text{ , radians}$$

and all other terms are as previously defined.

Evaluating these expressions over a range of distances relative to the cask diameter results in the family of curves for the heat load on the cask relative to the engulfing fire value versus the separation distance divided by the cask diameter as shown in Fig. F-14. The total heat load drops rapidly from the reference regulatory value as the distance from the fire increases. In addition at distances removed from the flame, a lower value of emissivity for the cask surface is likely since a blackening of the surface from soot in the flame is less probable, leading therefore to even lower heat loading. In addition to lower heat loading, the cask involved in a nonengulfing fire is able to reject heat by reradiation and natural convection to the environment.

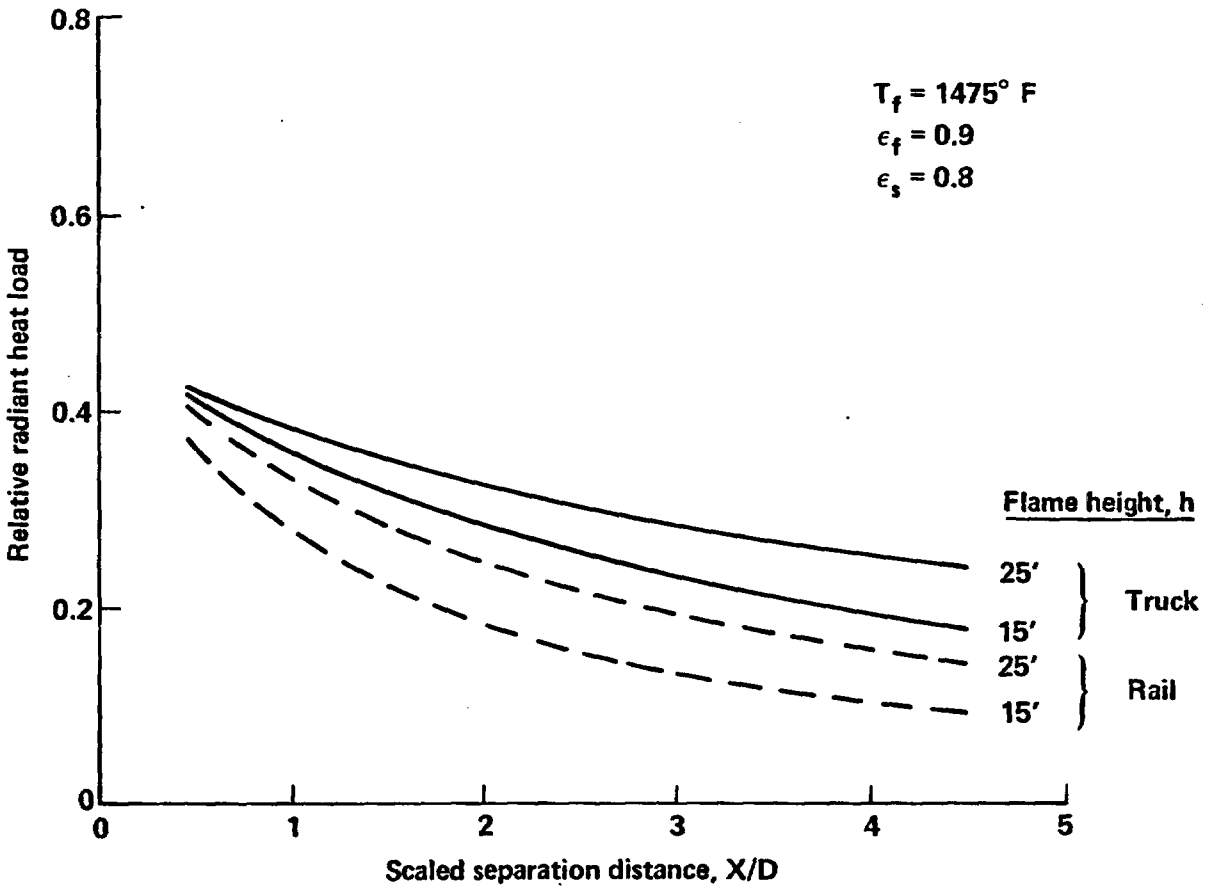

Figure F-14 Fraction of heat load from nonengulfing fires.

References

F.1 P. J. Burns, TACO-2D - A Finite Element Heat Transfer Code, Lawrence Livermore National Laboratory Report, Livermore, CA, UCID-17980, Rev. 2, January 1982.

F.2 M. G. Vigil, A. A. Trujillo, H. R. Yoshimura, HNPF Spent Fuel Cask Temperature Response; Torch Impinging on Water Filled Neutron Shield, Sandia National Laboratory, Albuquerque, NM, SAND82-0704, March 1982.

F.3 W. H. McAdams, Heat Transmission, McGraw-Hill, New York, NY, 1954.

F.4 J. P. Holman, Heat Transfer, McGraw-Hill, New York, NY, 1976.

F.5 R. K. Clarke, et. al., Severities of Transportation Accidents, Sandia National Laboratory, Albuquerque, NM, SLA-74-001, July 1976.

F.6 Final Report on Assessment of Rail Cask Performance in Railroad Accident Environments, Ridihalgh, Eggers and Associates, Columbus, OH, June 1977.

F.7 L. H. Russel, and J. A. Canfield, "Experimental Measurement of Heat Transfer to a Cylinder Immersed in a Large Aviation-Fuel Fire", Journal of Heat Transfer, August 1973.

F.8 B. E. Bader, "Heat Transfer in Liquid Hydrocarbon Fuel Fires", Proceedings-International Symposium for Packaging and Transportation of Radioactive Materials, January 1965.

F.9 B. Hagglund, and L. Persson, The Heat Radiation from Petroleum Fires, FOA Report C 20126-d6(A3), Forsvarets Forskningsanstalt, Huvudenhet 2, July 1976.

F.10 L. Orloff, and J. de Ris, Froude Modeling of Pool Fires, Technical Report FMRC J. I. OHON3.BU RC81-BT-9, Factory Mutual Research, October 1983.

F.11 R. Siegel, and J. R. Howell, Thermal Radiation Heat Transfer, McGraw-Hill, New York, NY, 1972.

APPENDIX G
Probability Estimation Techniques

G.1 Introduction

Assessment of the probability of the potential responses of a cask to various accident scenarios depends on (1) the description of the distributions of the accident parameters given an accident, and (2) integration of these probability distributions over the appropriate subranges of values of the accident parameters. An important accident parameter is the velocity of the transporting vehicle, either truck or train, at the time of the accident. The distribution of vehicle velocities at the point of an accident is unknown; however, there are data which can be used to estimate the distribution of velocities either subjectively, as in the case of trucks, or recorded, as for trains. In Section G.2, a method of estimation, called maximum entropy, is described for developing the distribution of vehicle velocities using observed velocities at past accidents. This method was applied to both trucks and trains to develop estimates of the appropriate probability distributions of velocity. Given descriptions of the distributions of vehicle velocities and other accident parameters, assessment of the probability of potential cask responses involves integrating several probability functions. The integration process is described in Section G.3. Specifically, Section G.3 describes an approximation, based on sums of discrete probabilities, to the integration of the continuous distributions.

G.2 Maximum Entropy Method of Estimation

Given the historical data on velocities of vehicles involved in accidents, there are several methods, such as least squares, maximum likelihood, and density estimation, which can be used to estimate the probability distribution of velocities. Most methods require some identification of the form (family) of the probability distributions. Several distributions and mixtures of distributions were fitted to the accident data but no one family consistently fit all the data.

Since a specific parametric family of distributions was not readily identifiable, a reasonable approach is to evaluate a nonparametric estimate of the probability distributions of velocity. Although not as powerful, i.e., it has a greater uncertainty, the nonparametric approach allows the data to determine the form of the distribution of velocities rather than forcing the distribution to be of some specific type, e.g., normal or lognormal. If a specific distribution is used and it is not correct, then estimates of probabilities derived from the incorrect distribution can be biased significantly. Thus, we chose to estimate the distributions of velocity nonparametrically.

To determine a nonparametric estimate of the distributions of velocity, we based the estimates on the maximum entropy method of estimation. This approach is based on information theory and provides a procedure for estimating a probability distribution, with maximum entropy, consistent with the information available about a random variable. Subject to certain conditions and the appropriate interpretation of probability,[G.1] it can be shown that the entropy function

$$H(p_1, \ldots, p_K) = - \sum_{k=1}^{K} p_i \log p_i \qquad (G.1)$$

measures the amount of "uncertainty" represented by a probability distribution $(p_1, \ldots, p_K)$ for a variable X (where it is assumed that X is discrete and has range $x_1, \ldots, x_K$). Given some information about the distribution of X, such as its expected value and variation or uncertainty, a reasonable criterion for estimating the probability distribution $p_1, \ldots, p_K$ is to maximize the entropy function, (G.1), consistent with the information available, i.e., if μ_o, σ_o^2 are the expected value and variance, to estimate $p_1, \ldots, p_k$ such that

$$\sum_{k=1}^{K} x_k p_k = \mu_o$$

$$\sum_{k=1}^{K} (x_k - \mu_o)^2 \, p_k = \sigma_o^2 \tag{G.2}$$

That is, an estimate of the probability distribution $p_1, \ldots, p_K$ is the set of values $\tilde{p}_1, \ldots, \tilde{p}_k$ such that

$$H(\tilde{p}_1, \ldots, \tilde{p}_k) = \max_{(p_1, \ldots)} H \; (p_1, \ldots, p_K) \tag{G.3}$$

subject to the constraints

$$\sum_{k=1}^{K} p_k = 1$$

$$\sum_{k=1}^{K} x_k \, p_k = \mu_o$$

$$\sum_{k=1}^{K} (x_k - \mu_o)^2 \, p_k = \sigma_o^2 \; .$$

Introducing Lagrangian multipliers $\lambda_0, \lambda_1, \lambda_2$ associated with the three constraints, the estimated probabilities are

$$\tilde{p}_i = e^{-[\lambda_0 + \lambda_1 x_i + \lambda_2 (x_i - \mu_o)^2]} \tag{G.4}$$

where

$$\lambda_0 = \log \sum_{k=1}^{K} e^{-[\lambda_1 x_k + \lambda_2 (x_k - \mu_o)^2]} \tag{G.5}$$

and λ_1, λ_2 are solutions to the equations

$$\eta^{-1} \sum_{k=1}^{K} x_k \, e^{-[\lambda_1 x_k + \lambda_2 (x_k - \mu_o)^2]} = \mu_o \tag{G.6}$$

$$\eta^{-1} \sum_{k=1}^{K} (x_k - \mu_o)^2 \, e^{-[\lambda_1 x_k + \lambda_2 (x_k - \mu_o)^2]} = \sigma_o^2 \tag{G.7}$$

where

$$\eta = \sum_{k=1}^{K} e^{-[\lambda_1 x_k + \lambda_2 (x_k - \mu_o)^2]} \tag{G.8}$$

Thus, a discrete probability distribution can be constructed which maximizes entropy and which equals the specified mean and variance. In our application of the methodology, we used the mean and the variance of the historical data on velocities as the available information.

If the variable X is considered to be a continuous variable, i.e., its probability distribution has a density function, the estimated density function f(x) can be approximated, based on maximizing entropy, using the identity

$$dp = f(x)dx \quad . \tag{G.9}$$

Approximating the density function by a discrete relative histogram $[(\Delta p_k, \Delta x_k) : k=1, \ldots, K]$,

$$f(x_k) \simeq \frac{\Delta p_k}{\Delta x_k} . \tag{G.10}$$

However, in our notation $\Delta p_k = p_k$ and, assuming a partition of the (finite) range R_x of X into N equal subintervals of length Δx,

$$\Delta x = R_x/N \tag{G.11}$$

the maximum entropy estimate of $f(x_k)$ is

$$\tilde{f}(x_k) = \lim_{\Delta \to 0} \frac{e^{-[\Delta\lambda_0 + \Delta\lambda_1 x_k + \Delta\lambda_2 (x_k - \mu_o)^2]}}{R_x/N} \tag{G.12}$$

$$\simeq \frac{e^{-[\lambda_0 + \lambda_1 x_k + \lambda_2 (x_k - \mu_o)^2]}}{R_x/N}$$

for sufficiently small Δ.

The estimated probability distribution, as described by the estimated cumulative distribution function, is based on cumulative sums of the $\tilde{f}(x_k)$'s, interpolating for $x = x_k$. This is the method used to estimate the probability distributions for vehicle velocities prior to and at the point of an accident. The uncertainty of using the sample information for specifying μ_o and σ_o^2 was not quantified, nor was the sensitivity investigated for the predicted probabilities of the various response states. Some parametric

estimates of the distributions of velocities were analyzed, and these would provide some basis for an investigation of sensitivity.

G.3 Discretized Probability Integration

Estimation of the probability that the response of a cask to an accident is a specific response state, e.g., R(2,3), between 0.2% (S_1) and 2% (S_2) strain and between 600°F (T_2) and 650°F (T_3) lead mid-thickness temperature, is based on evaluating a pair of double integrals of probability distribution and density functions (see Equation 5.23). Some of the probability distribution and density functions are known analytically, but some, for example the distributions of velocities estimated by the method of maximum entropy, are only known numerically. In either case, the integration is complex and cannot be done analytically. Instead, evaluation of the estimated probabilities is based on the identity, given the appropriate conditions,

$$\int_a^b H(t)dt = \lim_{\Delta \to 0} \sum_{k=1}^{K(\Delta)} [H(t_k + \Delta_u) - H(t_k - \Delta_\ell)]\Delta t_k \qquad (G.13)$$

$$= \sum_{k=1}^{K(\Delta)} [H(t_k + \Delta_u) - H(t_k - \Delta_\ell)]\Delta t_k$$

for sufficiently small Δ . In this application, the function H(t) itself involves the integral of probability distributions and density functions.

The computer code TASP was developed to perform the necessary summations to approximate the probability integrals (in addition, the code contains all the appropriate probabilities). In each case the code partitions the range of integration into an appropriate number of subintervals to integrate over a probability distribution. When appropriate, the code conservatively evaluates a function at the upper (lower) limit of a subinterval to assure that the estimated probability is conservative. However, the estimate is not overly

conservative because a reasonable number of subintervals are used for the approximation. Thus, in the context of the inputs, the estimated probabilities are considered good estimates.

G.4 References

G.1 E. T. Jaynes, "Information Theory and Statistical Mechanisms", Physical Review, Vol. 106, No. 4, May, 1957, pp. 620-630.

APPENDIX H

List of Figures

		Page
H-1	Impact of weighted steel cylinder into a rigid rail	H-5
H-2	Finite element mesh for one-quarter of the cylinders	H-6
H-3	Deformed shapes of the cylinder impacting a rail (DYNA 3-D analytical solutions)	H-7
H-4	Mesh of steel nose cone	H-8
H-5	Location of tied and sliding interfaces	H-9
H-6	Sequence of deformed configurations	H-10
H-7	Computed and experimental force-displacement curve. The steps in the curves correspond to void closures	H-11
H-8	Calculational mesh for the oblique rod impact problem	H-12
H-9	Deformed shapes of a rod impacting an oblique rigid wall	H-13
H-10	Another view of a rod at 300 μs	H-14
H-11	Final profiles at 3000 μs (a) experiment and (b) computed	H-15

APPENDIX H

Benchmarking for Computer Codes Used in Impact Analyses

H.1 Introduction

Several computer codes were used in the structural impact analyses to estimate cask responses for the various accidental impact loading conditions in this study. Impact is a governing loading condition in the cask structural evaluation. The results and conclusions stated in this report rely on the adequacy of these codes to estimate structural response. Impact is a loading condition which can generate large amounts of energy during a very short duration of impact. During the impact, energy changes form from potential into kinetic, and into strain energy. After the initial impact, the cask has a potential for bouncing back into the air depending on the target hardness and the property of impact limiters. Rigid body motion is involved during this process. In order to estimate the structural damage due to the second impact, i.e., the other end of the cask hitting the target after bouncing around in the air, the computer code needs to have a special capability of handling rigid body motion. Most of the finite element computer codes available today cannot handle the rigid body motion and, therefore, were not selected for this study. To assess cask response to the impact orientation, i.e., the angle between the cask longitudinal axis and the target surface, the selected computer codes need to have the capability of handling impact at an angle. Impact limiters play an important role in cask response. During impact, the limiter will enter a nonlinear region. The selected computer codes need to be capable of handling nonlinear impact-limiter responses.

The representative casks selected in this study use a lead layer for shielding. In order to model the lead behavior inside the inner and outer steel shells, the computer codes need to be capable of handling sliding between two surfaces of different materials. Not every computer code can satisfy all these specified requirements. Certain computer codes may be capable of meeting partial requirements. It is necessary that the user understands the limitations of the codes selected.

Three computer codes were selected to perform various types of impact analysis in this study. They are DYNA 2-D/3-D, NIKE 2-D/3-D (the 2D/3D designation indicating that either two-dimensional or three-dimensional modeling can be performed), and IMPASC (part of the SCAN system). All three codes were developed and maintained at Lawrence Livermore National Laboratory through other programs in the Laboratory. The limitations of each code are understood. During the course of calculating cask response, the analytical group worked very closely with the code development group. In many cases, the codes were modified to suit the specific needs of this study. There is high confidence that these codes were properly used within code capability in calculating cask response when subjected to impact loads. The qualifications of users is only part of the concerns in assuring adequate analytical solutions.

The next question is how can the selected computer codes simulate the impact conditions and the structural response. To answer this question, computer codes are generally benchmarked by comparing their results against one or more of the following: (1) results from closed form engineering solutions, (2) test data, and (3) other computer codes which have been benchmarked. This appendix presents benchmark codes for DYNA 3-D. The other codes, DYNA 2-D, NIKE 2D/3-D, and IMPASC have been benchmarked against DYNA 3-D, hence this benchmark test also generally applies to the other codes.

To date, these codes have not been benchmarked for predicting lead slump. Although at least one foreign country has performed impact tests with lead casks and used DYNA 2-D for benchmarking, these results are proprietary and cannot be disclosed. Therefore all of the calculations done in this study with DYNA and NIKE were performed assuming conservative lead properties and boundary conditions that over predict lead slump and the strain on the inner wall of the representative cask models.

H.2 Benchmark Calibrations for DYNA 3-D

H.2.1 Impact of Cylinder into Rail

The steel cylinder shown in Fig. H-1 is impacted into a long rigid rail at 1676 cm/sec. Attached to the ends of this cylinder are weights of 62.3 M dyne. An experimental test was conducted and the final configuration was measured.

One quarter of the cylinder was modeled by using DYNA 3-D with two planes of symmetry using the mesh illustrated in Fig. H-2. This mesh contains 3432 elements. Elastic-perfectly plastic behavior was assumed for the steel with a yield strength of 0.0131 Mbar.

Deformed shapes at approximately millisecond increments are shown in Fig. H-3. At 6.4 ms the cylinder can be seen to have completely rebounded with its final deformed shape. A maximum residual dent of 1.53 inches was calculated. A maximum dent of 1.44 inches was measured at the same location in an experimental test.

H.2.2 Nose Cone Analysis

Figure H-4 shows the DYNA 3-D mesh (6074 nodes, 4356 elements) used to model a steel (yield strength = 0.0048 Mbar, E_t = 0.0138 Mbar) nose cone that, on impact, has been designed by Sandia Laboratories in Livermore to limit the resultant force transmitted to the aft section.[H.1] The mass of the aft section is mocked with a high-density material, 131,477 gm/cm^3, in the top rows of elements.

This problem is interesting from a code development viewpoint because it exercises the sliding interface logic. Five interfaces are defined of which two are tied. The locations of these interfaces are depicted in Fig. H-5.

Deformed shapes at 3,000 μs intervals are shown in Fig. H-6. At 15,000 μs the peak deformation is reached and the nose cone begins to rebound.

Comparisons with experimental data from a static test showed excellent agreement with the calculation.[H.1] The final shape obtaining in the experiment was very close to the final computed shape. In Fig. H-7, the computed force deflection curve from DYNAP is compared to the experiment. Only minor discrepancies exist.

H.2.3 Oblique Impact of Rod

An aluminum rod 30.5 cm long and 0.638 cm in diameter impacts a rigid wall oriented at 10^{o} at a velocity of 20,170 cm/sec. The material behavior is simulated with material model 11 using the properties defined in UCRL-80465.[H.2] Fig. H-8 shows the DYNA 3-D calculational mesh.

The computed results showed good agreement with the experimental profiles up to 600 μs. At later times the experiments showed more curvature in the rod. Four factors probably contributed to these late time discrepancies.

- coarse zoning,
- inaccurate material properties,
- rigid wall approximation to armor plate,
- lack of interface friction.

Figure H-9 shows a sequence of deformed configurations. Figure. H-10 shows a view of 300 μs to illustrate the cross-sectional zoning. Figure H-11 shows the residual experimental profile for comparison to the computed result at 3,000 μs.

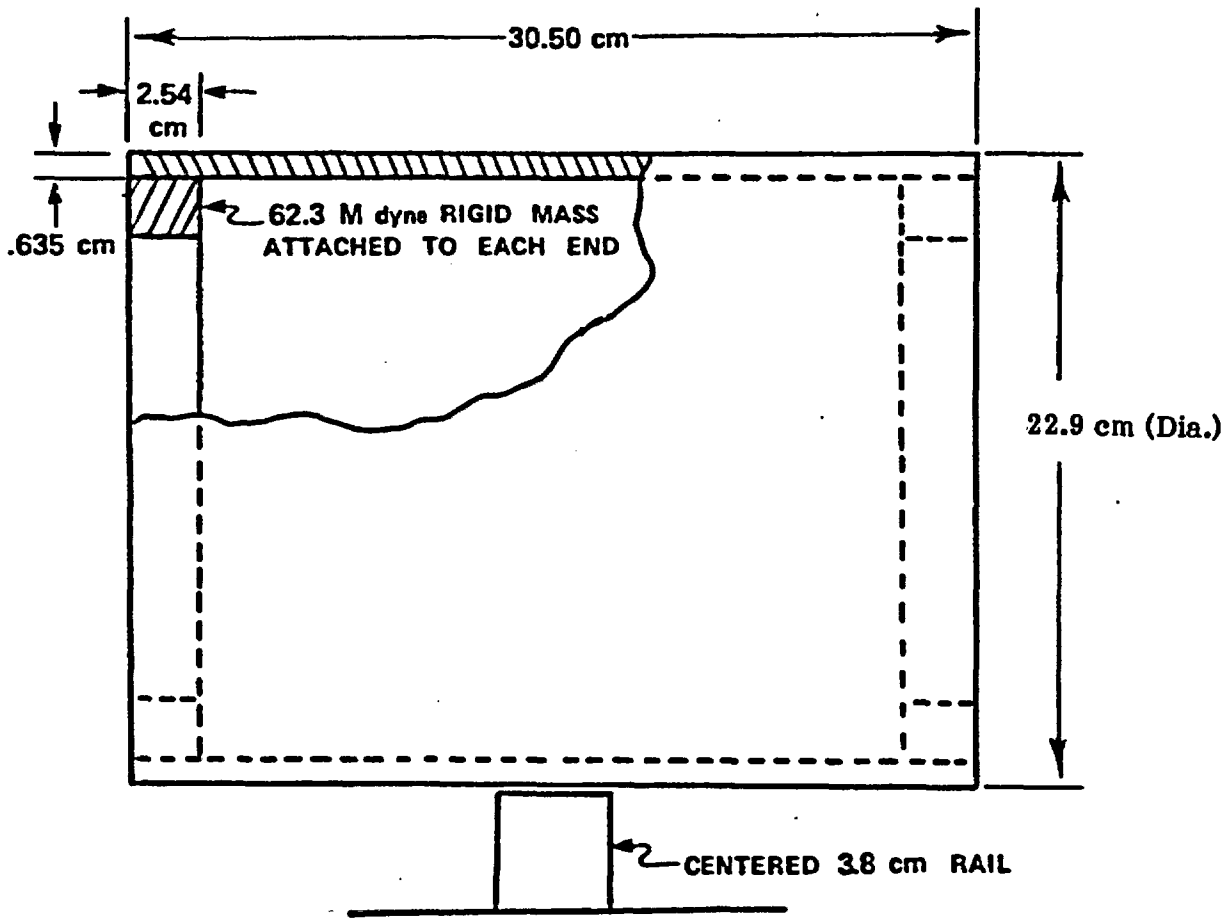

Figure H-1 Impact of weighted steel cylinder into a rigid rail.

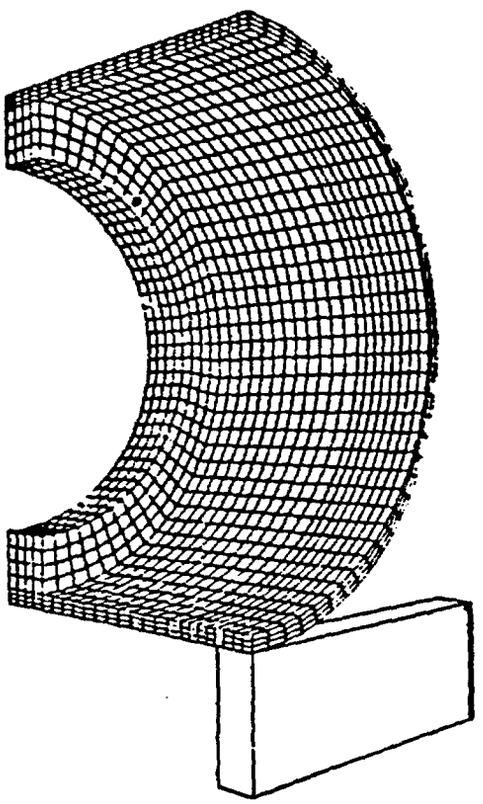

Figure H-2 Finite element mesh for one-quarter of the cylinders.

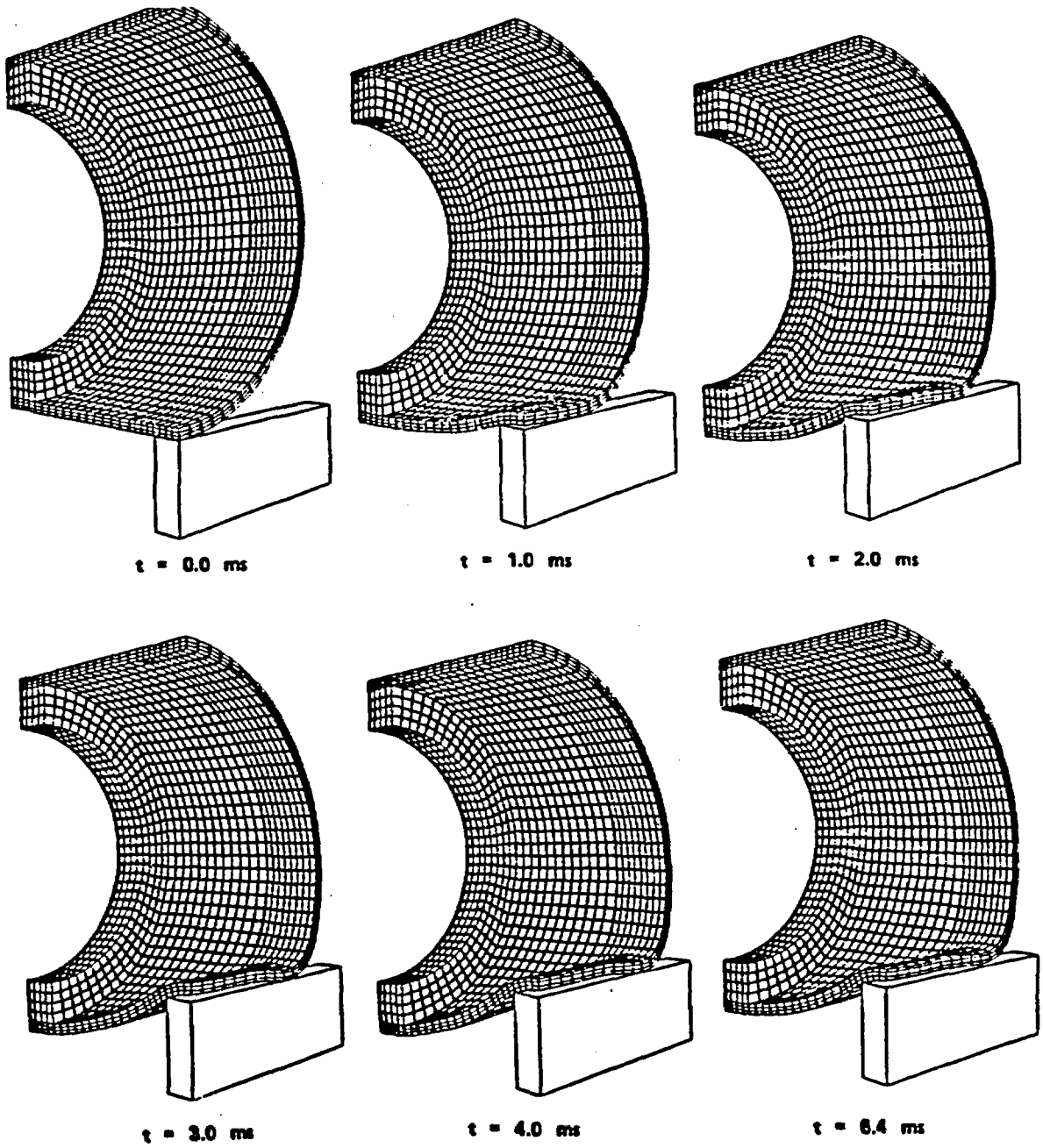

Figure H-3 Deformed shapes of the cylinder impacting a rail (DYNA 3-D analytical solutions).

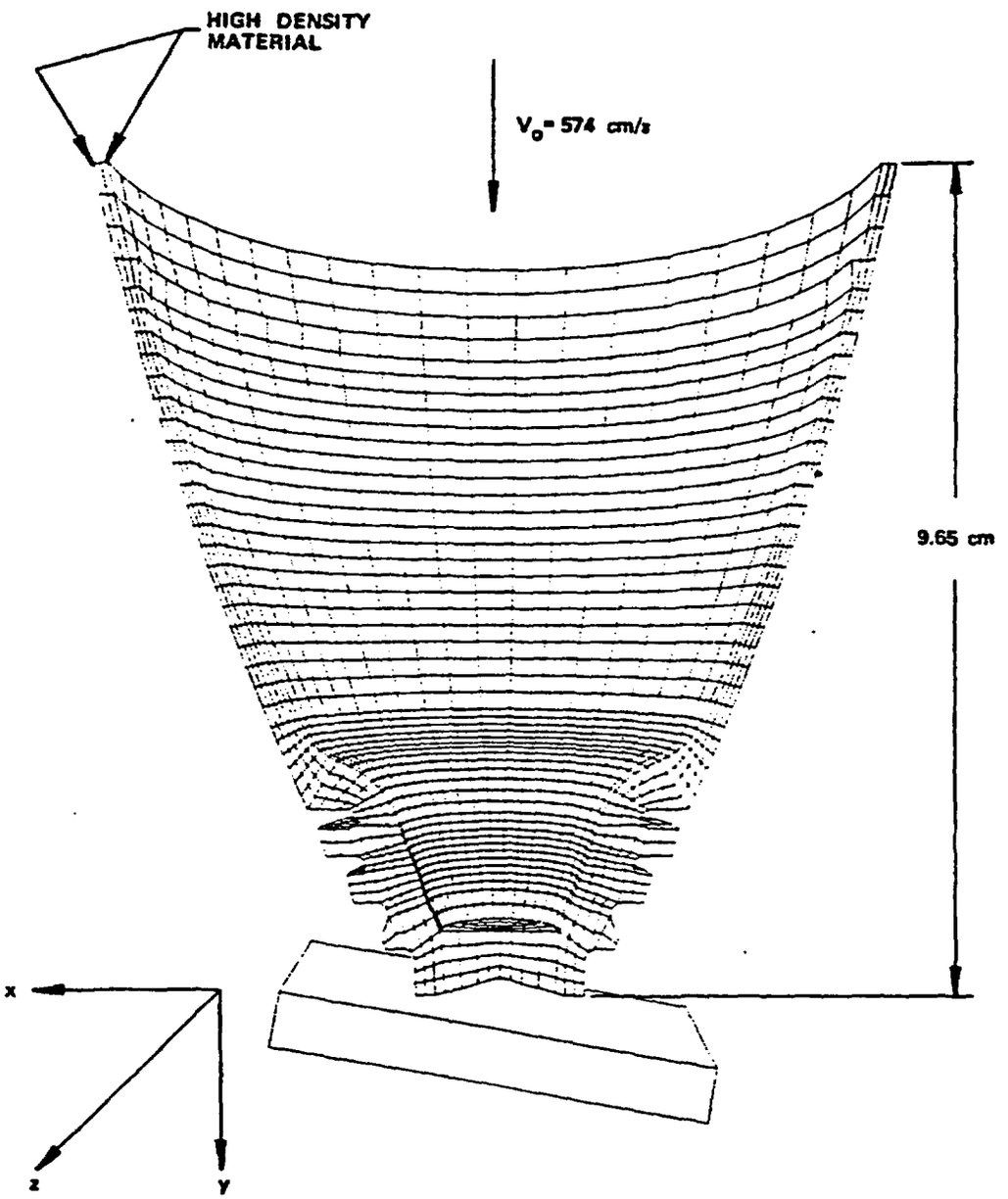

Figure H-4 Mesh of steel nose cone.

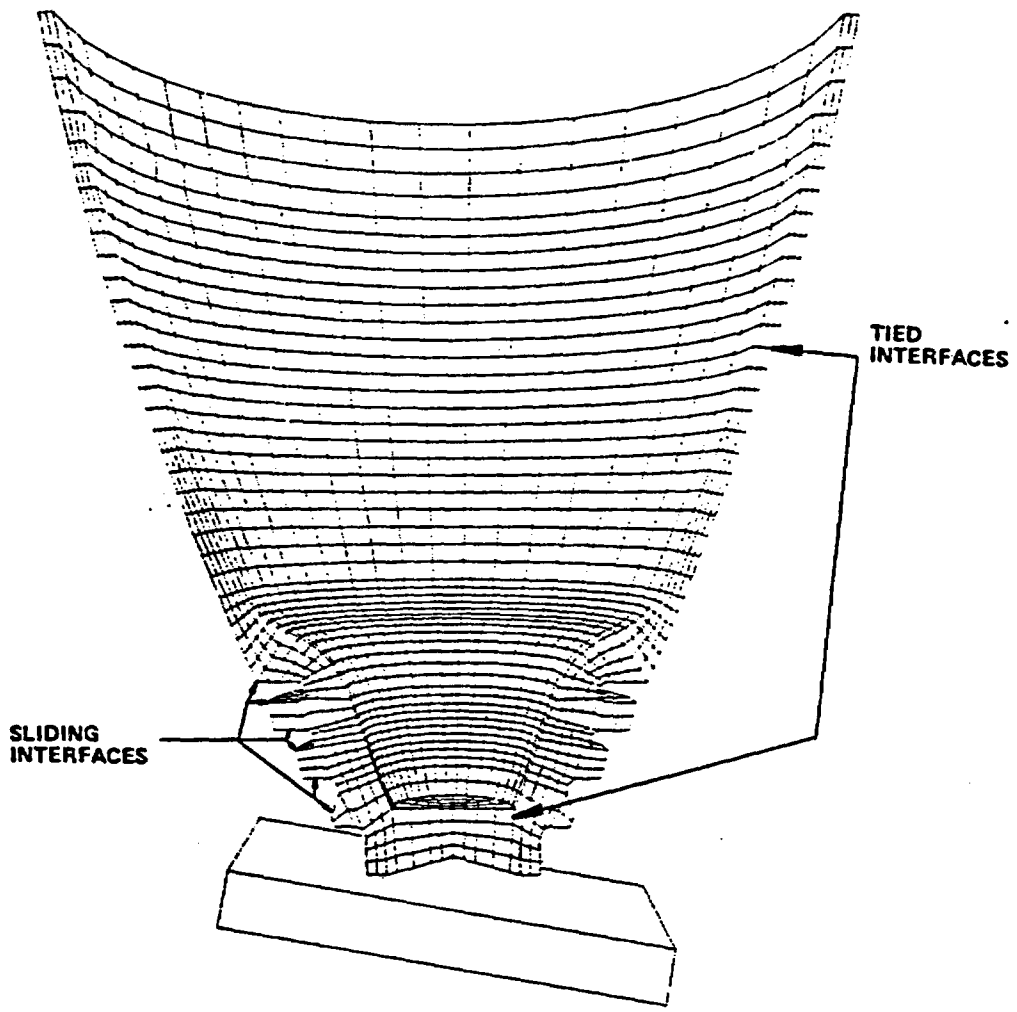

Figure H-5 Location of tied and sliding interfaces.

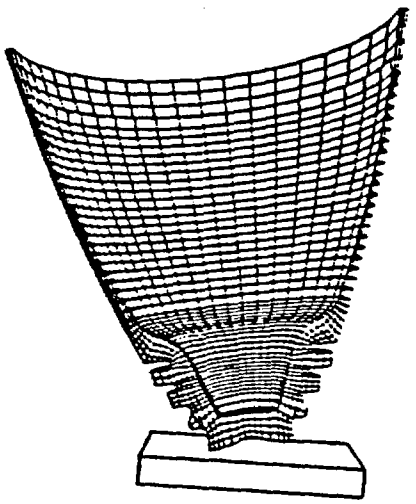

t = 0.0

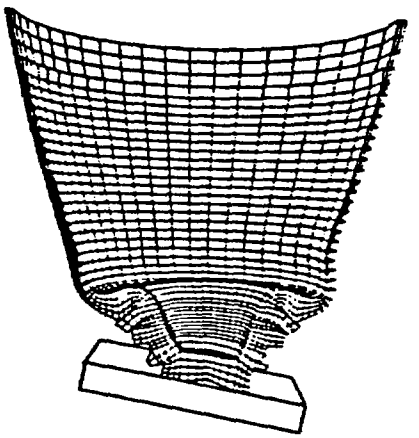

t = 3000 μs

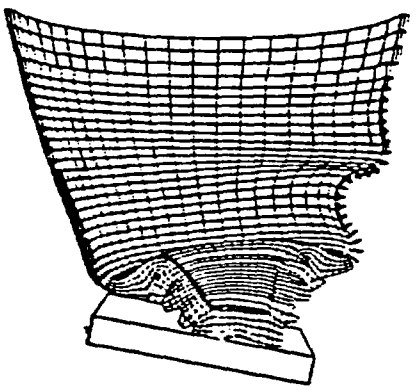

t = 6000 μs

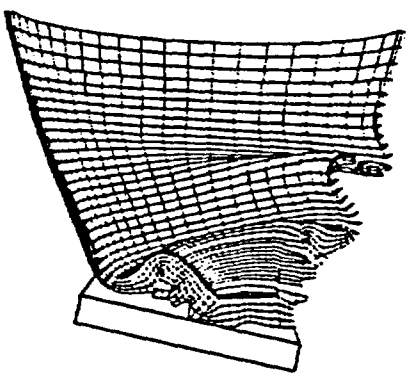

t = 9000 μs

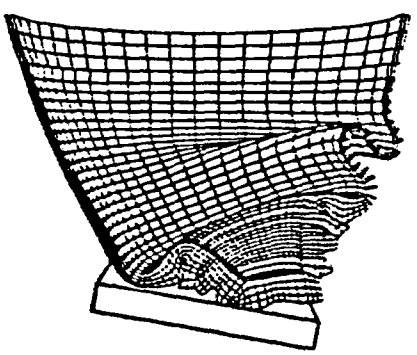

t = 12000 μs

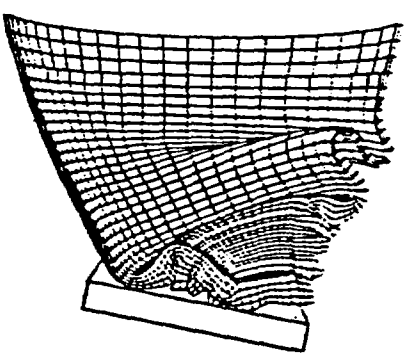

t = 15000 μs

Figure H-6 Sequence of deformed configurations.

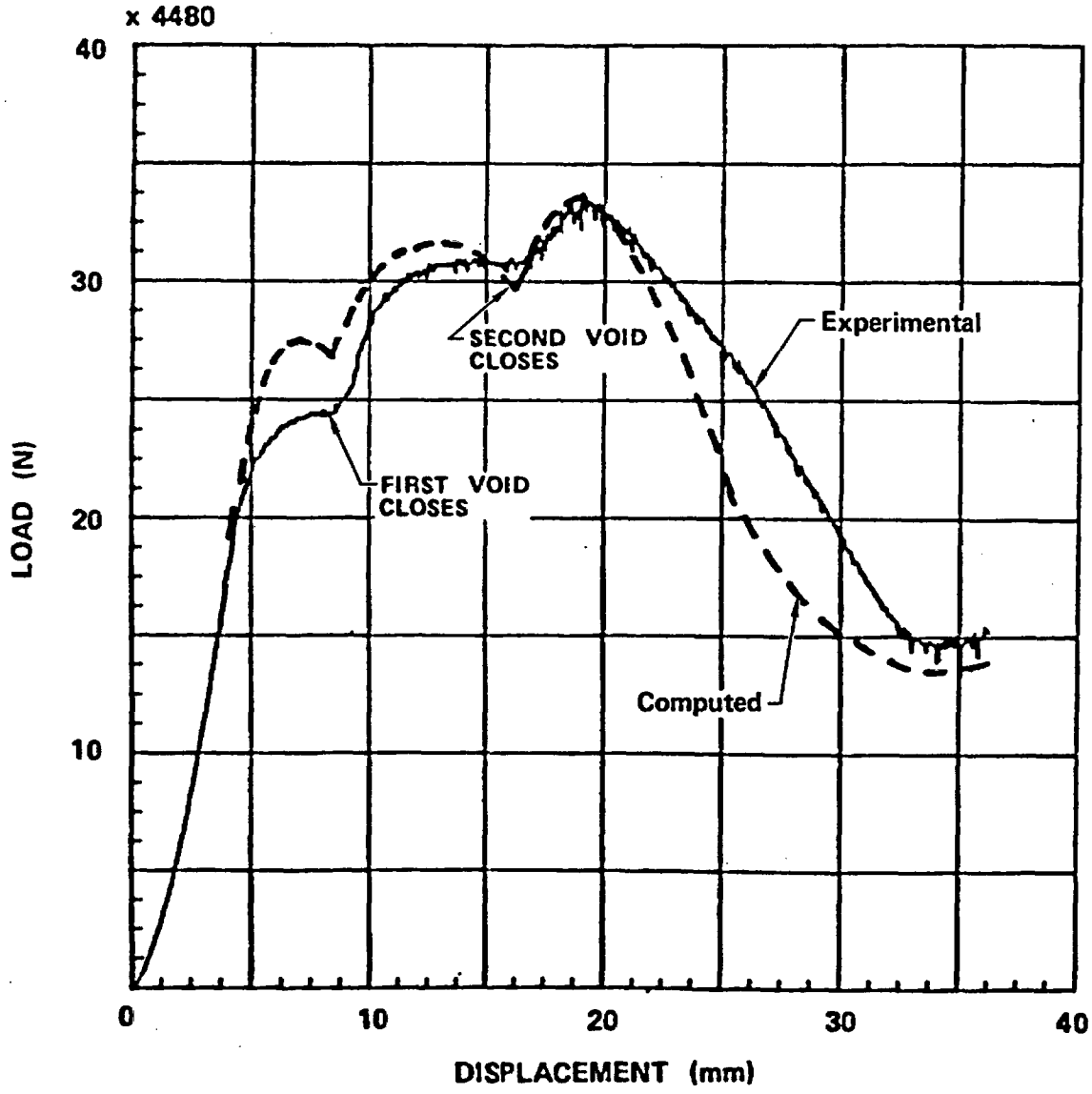

Figure H-7 Computed and experimental force-displacement curve. The steps in the curves correspond to void closures.

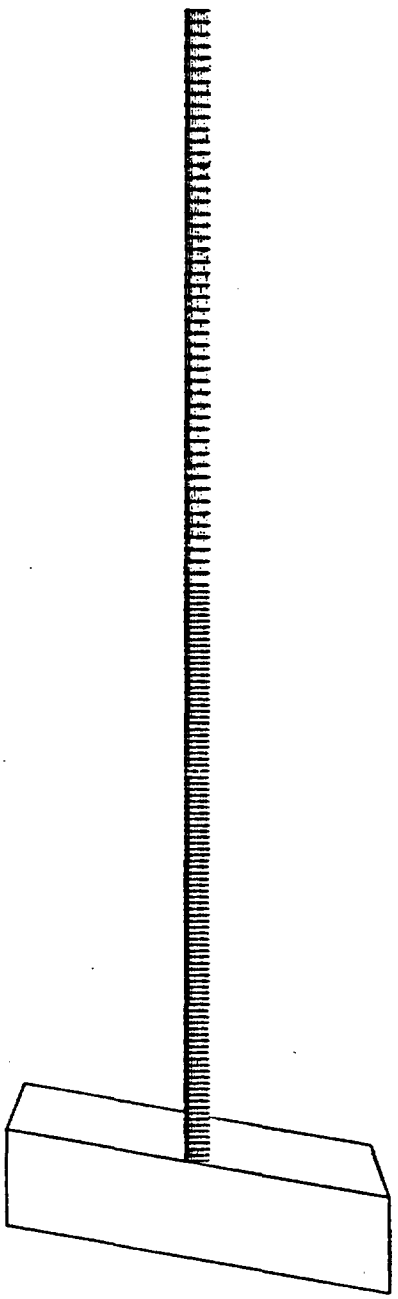

Figure H-8 Calculational mesh for the oblique rod impact problem.

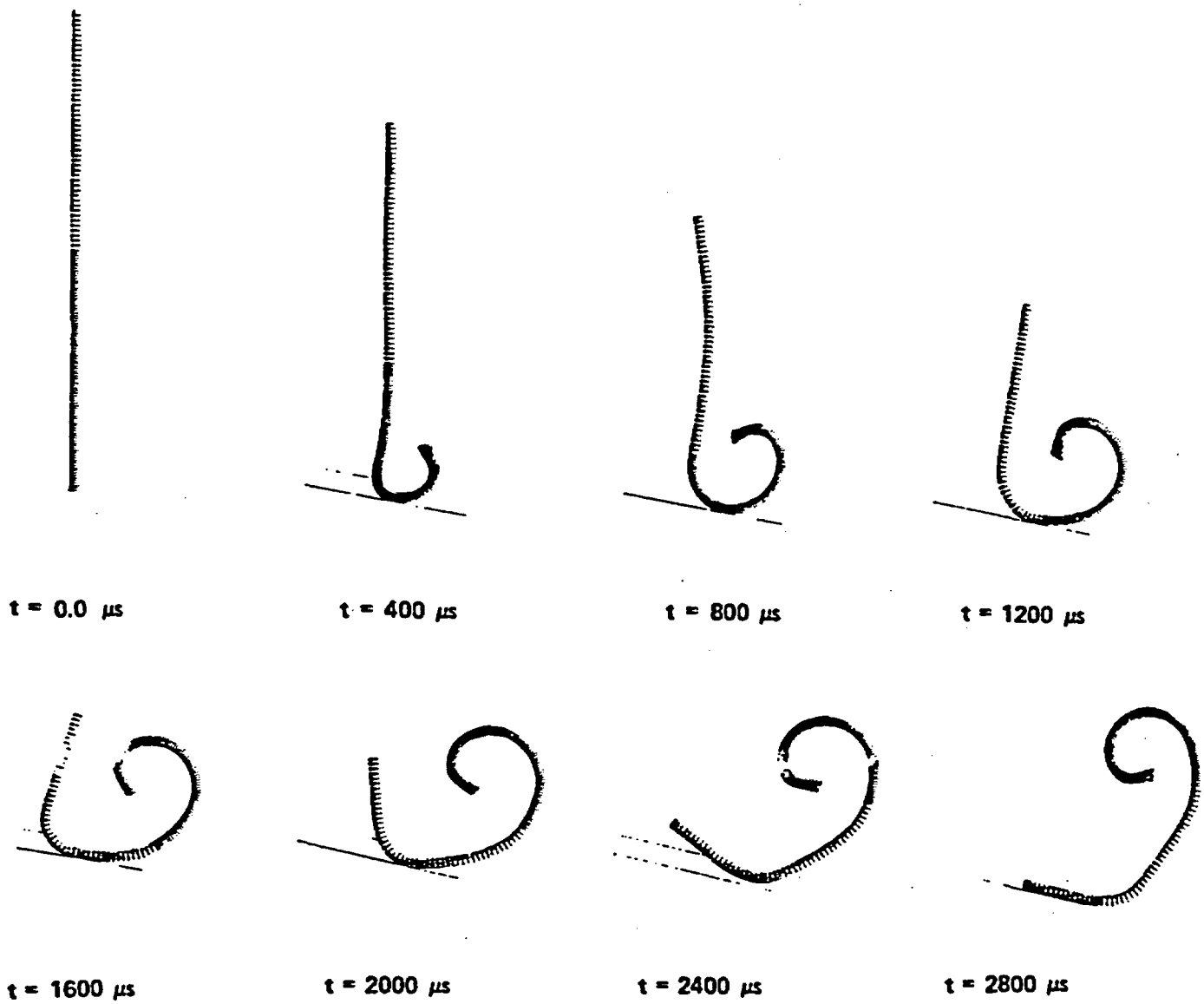

Figure H-9 Deformed shapes of a rod impacting an oblique rigid wall.

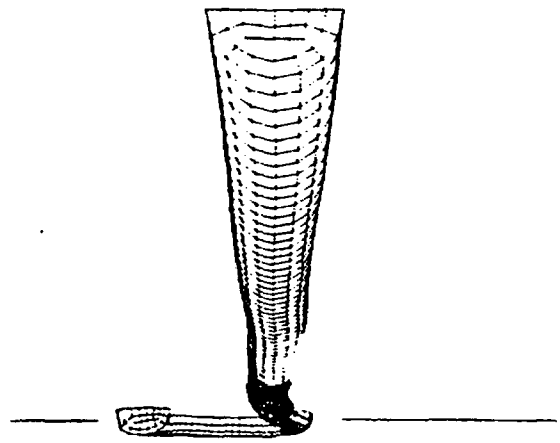

Figure H-10 Another view of a rod at 300 μs.

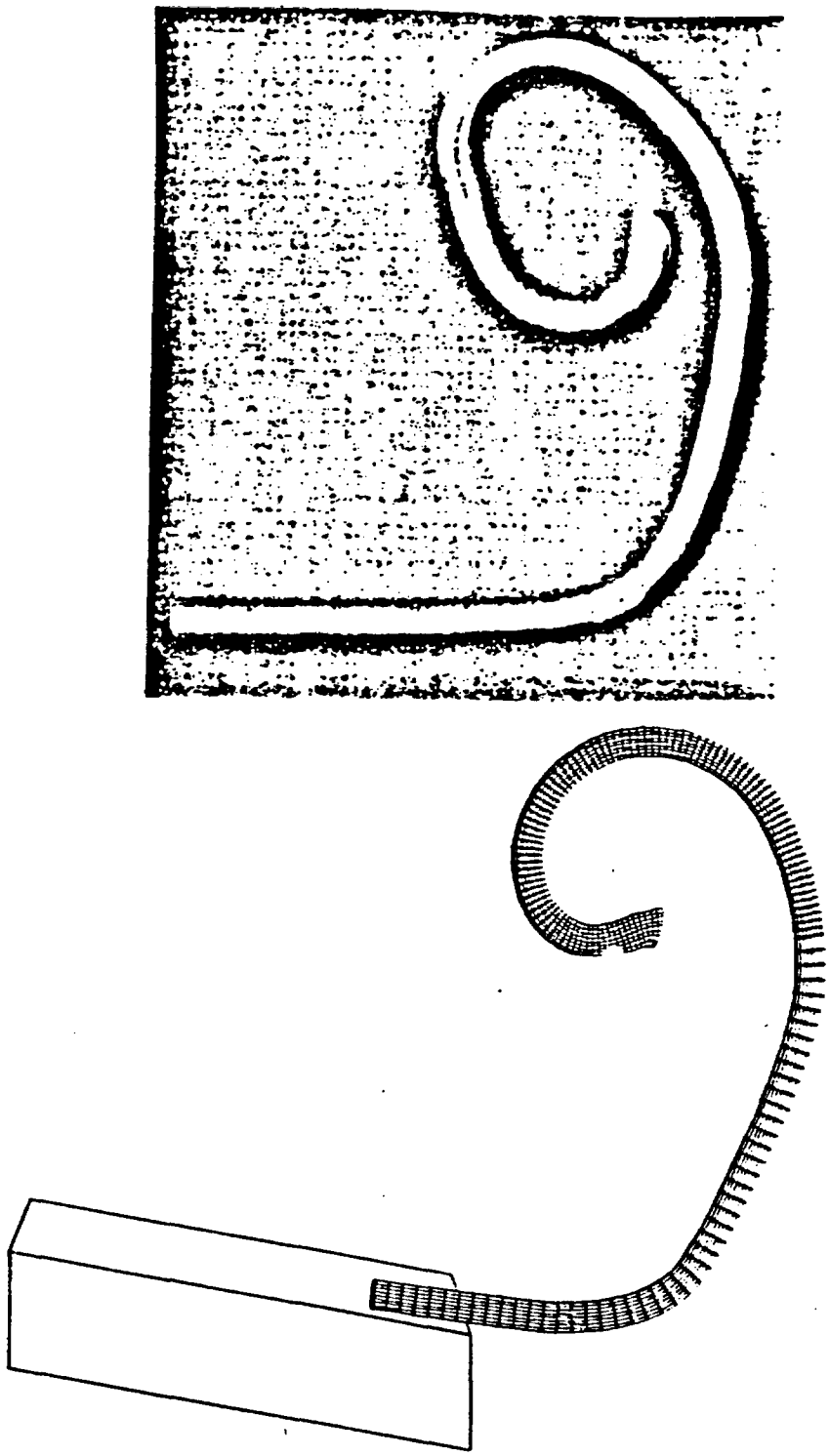

Figure H-11 Final profiles at 3000 μs (a) experiment and (b) computed.

References

H.1 M. Chiesa and M. Callabresi, "Nonlinear Analysis of a Mitigating Steel Nose Cone," Computers and Structures, Vol. 13, Sandia National Laboratories, Livermore, CA, 1981, p. 295.

H.2 D. J. Steinberg and M. W. Guinan, A High-Strain Constitutive Model for Metals, Lawrence Livermore National Laboratory, Livermore, CA, UCRL-80465, 1978.

NRC FORM 336 (2-84) NRCM 1102, 3201, 3202

U.S. NUCLEAR REGULATORY COMMISSION

BIBLIOGRAPHIC DATA SHEET

SEE INSTRUCTIONS ON THE REVERSE

1. REPORT NUMBER (Assigned by TIDC, add Vol. No., if any)
NUREG/CR-4829, Vol. 2
UCID-20733

2. TITLE AND SUBTITLE
Shipping Container Response to Severe Highway and Railway Accident Conditions

Appendices

3. LEAVE BLANK

4. DATE REPORT COMPLETED
MONTH: April YEAR: 1986

5. AUTHOR(S)
L.E. Fischer, C.K. Chou, M.A. Gerhard, C.Y. Kimura, R.W. Martin, R.W. Mensing, M.E. Mount, M.C. Witte

6. DATE REPORT ISSUED
MONTH: February YEAR: 1987

7. PERFORMING ORGANIZATION NAME AND MAILING ADDRESS (Include Zip Code)
Lawrence Livermore National Laboratory
P. O. Box 808, L-197
Livermore, California 94550

8. PROJECT/TASK/WORK UNIT NUMBER

9. FIN OR GRANT NUMBER
A0397

10. SPONSORING ORGANIZATION NAME AND MAILING ADDRESS (Include Zip Code)
Division of Reactor System Safety
Office of Nuclear Regulatory Research
U.S. Nuclear Regulatory Commission
Washington, D.C. 20555

11a. TYPE OF REPORT
Technical

b. PERIOD COVERED (Inclusive dates)

12. SUPPLEMENTARY NOTES

13. ABSTRACT (200 words or less)

This report describes a study performed by the Lawrence Livermore National Laboratory to evaluate the level of safety provided under severe accident conditions during the shipment of spent fuel from nuclear power reactors. The evaluation is performed using data from real accident histories and using representative truck and rail cask models that likely meet 10 CFR 71 regulations. The responses of the representative casks are calculated for structural and thermal loads generated by severe highway and railway accident conditions. The cask responses are compared with those responses calculated for the 10 CFR 71 hypothetical accident conditions. By comparing the responses it is determined that most highway and railway accident conditions fall within the 10 CFR 71 hypothetical accident conditions. For those accidents that have higher responses, the probabilities and potential radiation exposures of the accidents are compared with those identified by the assessments made in the "Final Environmental Statement on the Transportation of Radioactive Material by Air and other Modes," NUREG-0170. Based on this comparison, it is concluded that the radiological risks from spent fuel under severe highway and railway accident conditions as derived in this study are less than risks previously estimated in the NUREG-0170 document.

14. DOCUMENT ANALYSIS – a. KEYWORDS/DESCRIPTORS
spent fuel casks
Severe highway and railway accident conditions

b. IDENTIFIERS/OPEN-ENDED TERMS

15. AVAILABILITY STATEMENT
Unlimited

16. SECURITY CLASSIFICATION
(This page) Unclassified
(This report) Unclassified

17. NUMBER OF PAGES

18 PRICE

UNITED STATES
NUCLEAR REGULATORY COMMISSION
WASHINGTON, D.C. 20555